Self-propelled Motion and Collective Effect of Active Elements in Nonequilibrium Systems

January 2018

Department of Physics, Division of Fundamental Science,
Graduate School of Science, Chiba University

Yuki Koyano

(千葉大学審査学位論文)

Self-propelled Motion and Collective Effect of Active Elements in Nonequilibrium Systems

January 2018

Department of Physics, Division of Fundamental Science,
Graduate School of Science, Chiba University

Yuki Koyano

Abstract

Self-propelled motion realized in non-equilibrium systems is now growing to be an important topic of nonlinear physics. Not only motion of a single self-propelled particle (SPP) but also collective motion of them are important problems. For collective motion of SPPs, spatio-temporal patterns of the density profile and the mean velocity field are often discussed, whereas such pattern formation can be also induced by active elements which cannot move by themselves under an isolated condition. In this doctoral thesis, we consider two topics; one is motion of a single SPP and the other is collective phenomena induced by active elements without mobility.

In the first half of the thesis, we discuss spontaneous motion of a single camphor particle on water surface. We focus on motion through a spontaneous symmetry breaking; we consider motion emerging through instabilization of rest state. As actual systems, we investigated the motion of a camphor particle in a one-dimensional finite system with an inversion symmetry and that in the two-dimensional circular system with inversion and rotational symmetries. We also analyzed rotational motion of a symmetric camphor-driven rotor, which also emerges by the instabilization of rest state.

In the latter half, we discuss diffusion enhancement and drift flow inside cells or on biomembrane induced by active proteins, which change their shapes with energy supply. By conformational change of active proteins, cytoplasm or biomenbrane is stirred, and thus diffusion is enhanced. When the active proteins are distributed inhomogeneously, directional flow is also induced. By using a mathematical model where an active protein is approximately considered to be a force dipole, we discussed the collective effect of active proteins.

Contents

Chapter 1

Preface

The idea "dissipative structure" has been proposed by I. Prigogine, who got Nobel Prize in chemistry [1]. A dissipative system is defined as the system with continuous injections and drains of energy without detailed balances, and thus the dissipative system is classified into nonequilibrium systems. In such a dissipative system, spatio-temporal pattern can emerge through spontaneous symmetry breaking, i.e., a seemingly-lower-entropy structure can emerge. Belousov-Zhabotinsky reaction (BZ reaction) is a typical example exhibiting spatio-temporal pattern [2–4]. Commonly, chemical reaction is a monotonical relaxation process, but oscillatory relaxation process of reactants is observed in a batch system of BZ reaction. In an open system with injection of reactants and drain of products such as reaction in a continuous-flow stirred tank reactor (CSTR), the stable oscillation is observed instead of a stable steady state as shown in Fig. 1.0.1(a). Bénard convection is also a typical example that exhibits spatio-temporal pattern [5, 6]. When a layer of fluid in a shallow water chamber is heated from the below, rolled convection transferring the heat from the bottom to the top is induced when the heat flow is more than a threshold value, while below it only thermal diffusion without convective flow occurs. The rolled convection forms a spatial (or spatio-temporal) pattern as shown in Fig. 1.0.1(b).

Elements which show systematic motion under continuous energy gain and dissipation are called active matter [7–11]. From the definition mentioned in the previous paragraph, active matter is also classified into dissipative structures. In some active matter systems, directional motion can emerge through spontaneous symmetry breaking as shown in Fig. 1.0.1(c). Such directional motion is considered to be one of the spontaneous spatio-temporal pattern formation in a broad sense. For instance, a spot pattern and its motion is observed in a reaction-diffusion system [12–14]. Since reaction-diffusion systems are often used as a typical example of the dissipative systems and the spot shows the systematic motion, the motion of spots is considered to be both active matter and pattern formation. It is noted that in some cases the direction of motion is predetermined by asymmetry in the systems as shown in Fig. 1.0.1(d).

The significance of studying active matter is considered as follows: First of all, the self-propelled systems are common in the actual world; animals are one of the examples, and it is natural that one is motivated to understand the underlying mechanisms of the phenomena. The second point is that the self-propelled motion is one of the characteristic behaviors in nonequilibrium system. They consume free energy and convert it into kinetic energy, which is completely different from kinetic-energy-conserved systems. The third point is possibility of application, e.g., drag delivery systems [15] and soft actuators [16, 17].

There are many types of mechanisms for self-propulsion. Here we introduce several self-propelled systems. Janus particles, which are composed of semispheres having different surface properties,

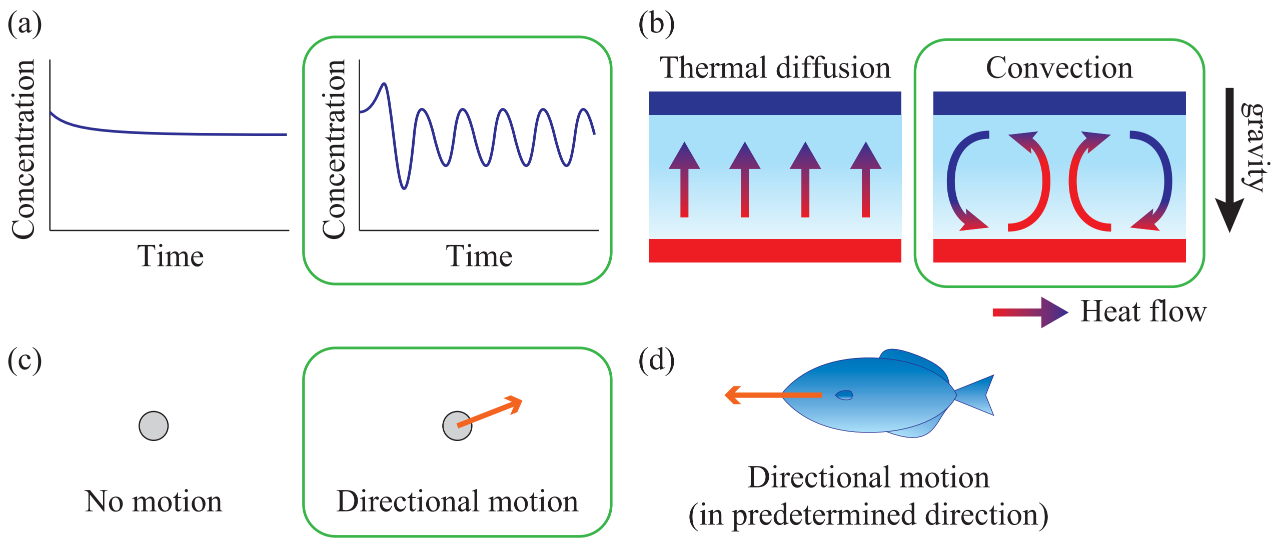

Figure 1.0.1: Schematic illustration of dissipative structures. (a) Time evolution of concentration of a component in BZ reaction. The stable oscillation is observed instead of a stable steady state in certain conditions. (b) Heat transfer in fluid from bottom to top. When the temperature difference is large enough, convective flow is induced. (c) Motion of an element through spontaneous symmetry breaking. (d) Motion of element whose direction of motion is predetermined.

are moving by using hydrodynamic effects [18, 19]. An oil droplet producing surfactants moves by Marangoni flow induced by surface tension difference [20, 21]. Camphor particles on water surface is moving using surface tension difference [22]. A pentanol droplet on water surface also moves with the same mechanism as a camphor particle, but it also shows deformation coupled with motion [23]. Cell crawling is the result of the action-reaction between the cell and substrate [24]. Collective motion of self-propelled particles is also an important one of the major topics [8, 25, 26]. Structures much greater than an element are observed, such as cluster [25, 26], band [11, 27, 28], or rolls [29].

It is true that actual systems are important, but its theoretical aspects are also important to understand generic physical insights of active matter. Equation of motion for self-propelled particles is often analyzed in terms of dynamical systems. This is because self-propelled motion is realized with the balance of energy gain and dissipation, which has nonlinearity in most cases [30–32].

A typical example of a theoretical study is performed by Ohta and Ohkuma [11, 33]. They studied the relationship between the velocity of a self-propelled particle and its shape by constructing a dynamical system:

$$\frac{d}{dt}v_\alpha = \gamma v_\alpha - |\boldsymbol{v}|^2 v_\alpha - a S_{\alpha\beta} v_\beta, \tag{1.0.1}$$

$$\frac{d}{dt}S_{\alpha\beta} = -\kappa S_{\alpha\beta} + b\left(v_\alpha v_\beta - \frac{1}{2}|\boldsymbol{v}|^2\right), \tag{1.0.2}$$

where $\boldsymbol{v}$ is the velocity and $S_{\alpha\beta}$ is the tensor which represents the degree of second-mode deformation as shown in Fig. 1.0.2(a). Here $S_{\alpha\beta} = n_\alpha n_\beta - \delta_{\alpha\beta}/2$ for a two-dimensional system. It is noted that only the system symmetry is considered to construct the model. They reported that when the rest state becomes unstable, the particle exhibits straight or rotational motion depending on the parameters, a, b, γ, and κ.

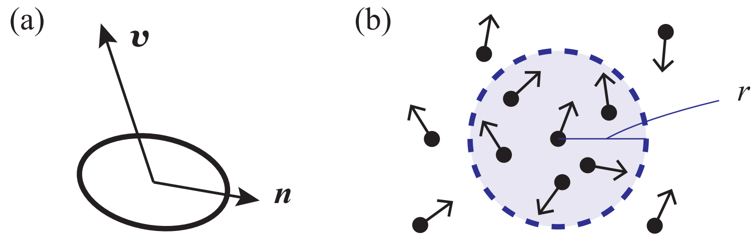

Figure 1.0.2: Schematic illustration of (a) Ohta-Ohkuma model for a deformable self-propelled particle [11, 33] and (b) Vicsek model [25, 26] for collective motion of self-propelled particles. (a) The velocity $\boldsymbol{v}$ and the characteristic direction of the second-mode deformation $\boldsymbol{n}$ is illustrated. Here, $\boldsymbol{n}$ directs along the major axis of the elliptic deformation. (b) The self-propelled particles with the same velocity and the radius for the interaction is illustrated. The self-propelled particle located at the center of the circle changes the direction of the motion into the average direction of the motion of self-propelled particles inside the circle.

Here we also introduce Vicsek model [25, 26], which is a simple model of collective motion. The velocities of the self-propelled particles are the same and constant:

$$v_i(t) = v\boldsymbol{e}_{\theta_i(t)}, \tag{1.0.3}$$

where i identifies the particle and $\boldsymbol{e}_\theta$ is a unit vector $\boldsymbol{e}_\theta = (\cos\theta, \sin\theta)$. The direction of the motion $\theta_i(t)$ is determined by the following equation:

$$\theta_i(t) = \frac{1}{N(t)} \sum_{j=1}^{N(t)} \theta_j(t), \tag{1.0.4}$$

where $\sum_{j=1}^{N(t)}$ is a summation over the particles which are located in the circle with a radius of r, whose center is the i-th particle. The schematic illustration is shown in Fig. 1.0.2(b). Each particle obeys the following equation of motion:

$$x_i(t+1) = x_i(t) + v_i(t)\Delta t. \tag{1.0.5}$$

In this model, the direction of the motion is globally ordered for small noise and high density of the self-propelled particles.

In this doctoral thesis, two topics are discussed. One is motion of a single self-propelled particle, and the other is collective effect by active elements.

As for a single self-propelled particle, we discuss the motion of a camphor particle on water surface. We investigate the motion emerging through spontaneous symmetry breaking. We consider three cases; motion of a camphor particle in a one-dimensional finite system [34] and a two-dimensional circular system [35], and motion of a camphor-driven rotor in a two-dimensional system [36], which are discussed in Secs. 2.2, 2.4, and 2.5, respectively. We reduce a mathematical model describing motion of a camphor particle around the rest state for each geometry, and analyze bifurcation structures of the reduced equation. The bifurcation structures correspond to instabilization of the rest state and indicate what kind of motion can occur. In Sec. 2.2, we consider motion of a camphor particle confined in a one-dimensional system. In Sec. 2.3, the generalized equation for motion of a self-propelled particle in a two-dimensional axisymmetric system is analyzed [37], and the results are applied to a two-dimensional circular system in Sec. 2.4. In Sec. 2.5, we consider motion of a camphor-driven rotor whose center of mass is fixed.

As for collective effect by active elements, we consider collective flow induced by active proteins inside cells or on biomembranes. Here we define an active protein to be a protein which shows conformational change in its shape with supply of substrates. It has been reported that the diffusion inside cells are greater than the normal diffusion under thermal equilibrium. Such diffusion enhancement is explained by the model where an active protein is considered to be a force dipole [38, 39]. The model was proposed by Mikhailov and Kapral, and it can be applied to various systems. In Sec. 3.3, we analyze the model to clarify the effect of inhomogeneous distribution of force dipoles, especially the effect of localization of them [40]. We also discuss the effect of alignment of force dipoles in Sec. 3.4 [41].

Chapter 2

Camphor Particle Moving Through Spontaneous Symmetry Breaking

2.1 Introduction

When a camphor particle is put on water surface, the camphor particle shows spontaneous motion at the water surface [22,42–45]. The camphor-water system was firstly reported in nineteenth century [42–44]. In recent decades, the camphor-water system has been attracting more and more interest, since it is regarded as a self-propelled system.

The detailed mechanism of self-propelled motion is as follows. A camphor particle diffuses camphor molecules on water surface and reduces the surface tension, since camphor molecules work as surfactants. When the surface tension around the camphor particle becomes anisotropic, the camphor particle is driven by the surface tension difference. Camphor molecules on water surface sublimate into the air. Thus the water surface is not perfectly covered with camphor molecules and the camphor particle can continue to move. The schematic illustration is shown in Fig. 2.1.1.

By attaching a plastic plate to the camphor particle asymmetrically, the diffusion of camphor molecules on the water surface also becomes asymmetric, and as a consequence, the self-propulsion is induced [22, 46]. On the other hand, a camphor particle with a symmetric shape, e.g., a disk-shaped camphor particle, diffuses camphor molecules in a symmetric manner, and the rest state with a symmetric profile of camphor molecules around the camphor particle can be considered. In this case, the stability of the rest state is important. If the rest state is unstable, the camphor particle exhibits the self-propulsion through spontaneous symmetry breaking [47, 48].

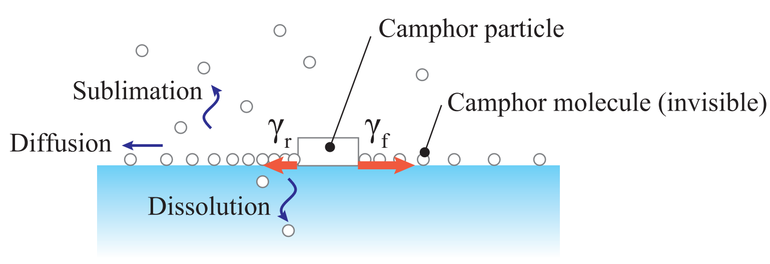

Figure 2.1.1: Schematic illustration of a camphor-water system. The camphor particle is driven when the surface tension of the front and rear sides, γ_f and γ_r, is different.

There are many systems in which a self-propelled particle moves by using surface tension [15,49–57]. The advantage of the camphor-water system is that the experimental system is simple and it is rather easy to construct complex systems that exhibit collective behaviour [58–60] and information processing [61, 62], and so on. Another advantage is that the mathematical model is rather simple and suitable for analytical investigations, which enables us to consider interaction with wall [63–65].

A camphor particle moves in the direction with the lower camphor concentration around the particle, and the motion of camphor particle can be considered as a negative chemotaxis [30]. As the other examples of chemotactic self-propelled motion, droplets detecting chemical gradient [66, 67] and self-propelled molecular machines [68, 69] are known.

In Sec. 2.2, we consider motion of a camphor particle in a one-dimensional finite region, which is the simplest case where a camphor particle is confined in a certain region [34, 48]. By reducing a mathematical model and analyzing a reduced equation in terms of dynamical systems, we revealed that a camphor particle shows oscillatory motion or rest state depending on the size of the finite region and also on the resistance coefficient exerting on the particle. As an extension of a one-dimensional finite region, we consider a motion of a camphor particle in a circular region. In this case, the analysis on the reduced equation is more complicated than that for the one-dimensional system. Thus, we begin with the analysis on an equation of motion for a self-propelled particle in an axisymmetric system, which is constructed only by considering the symmetric properties under the assumption that the system is close to the bifurcation point [37]. The results are described in Sec. 2.3. Then, in Sec. 2.4, we consider the motion of a camphor particle in a circular region, as a natural extension to the two-dimensional case [35]. The interesting point specific to the two-dimensional system is that there are several candidates of motion when the rest state becomes unstable such as rotational motion and oscillatory motion. In Sec. 2.5, we discussed the motion of a camphor-driven rotor, which is constructed with two camphor particles connected with a rigid bar [36]. By considering such geometry of self-propelled particle, we can investigate the spinning motion.

2.2 Camphor particle in a one-dimensional finite region

In this section, motion of a camphor particle in a one-dimensional system is analyzed [34]. First we introduce the mathematical model for the motion of a camphor particle, which is composed of an ordinary differential equation and a partial differential equation. Then we reduce it into a two-dimensional dynamical system and analyze the bifurcation structure of it.

2.2.1 Mathematical model

In this subsection, we introduce a mathematical model, and derive a dimensionless form of it.

Introduction of the mathematical model

Here we introduce the mathematical model based on the previous work by Nagayama *et al.* [47]. We assume a camphor particle is a point particle, whose position is denoted as $X = X(t)$. The time evolution equation for the position of the camphor particle is given by the following equation:

$$m\frac{d^2X}{dt^2} = -\eta\frac{dX}{dt} + F(X; c), \tag{2.2.1}$$

where m is a mass of the camphor particle, η is a resistance coefficient, and F is a driving force. The explicit expression of F is obtained as follows; the surface tension γ is a function of the concentration field c. Here we assume $\gamma(c) = -\Gamma c + \gamma_0$, where $\Gamma(> 0)$ is a constant and γ_0 is the surface tension of pure water. Since the driving force originates from the surface tension difference at the lefthand and righthand sides of the particle, we have

$$\begin{aligned} F(X; c) =& k \left\{ \gamma(c(X + \epsilon)) - \gamma(c(X - \epsilon)) \right\} \\ =& k\epsilon \left(\left. \frac{\partial \gamma(c(x,t))}{\partial x} \right|_{x=X+0} + \left. \frac{\partial \gamma(c(x,t))}{\partial x} \right|_{x=X-0} \right) \\ =& -K \left(\left. \frac{\partial c}{\partial x} \right|_{x=X+0} + \left. \frac{\partial c}{\partial x} \right|_{x=X-0} \right), \end{aligned} \tag{2.2.2}$$

where $k > 0$ and $K = k\epsilon\Gamma > 0$. Here we assume that we can take the limit where ϵ goes to zero but $K = k\epsilon\Gamma$ keeps its finite value.

The time evolution equation for the concentration field of camphor molecules c at water surface is described as:

$$\frac{\partial c}{\partial t} = D \frac{\partial^2 c}{\partial x^2} - \alpha c + f(x; X), \tag{2.2.3}$$

where D is a diffusion constant and α is a dissipation rate of camphor molecules from water surface by sublimation into the air and dissolution into aqueous phase. It is noted that the diffusion constant should be considered as effective one, since the diffusion is enhanced by the Marangoni flow [70]. The Marangoni flow is the flow induced by the shear stress at free surface originating the surface tension difference [71]. The function f is a supply from the camphor particle, and has a form:

$$f(x; X) = c_0 \delta(x - X), \tag{2.2.4}$$

where c_0 is a supply rate from the camphor particle per unit time and $\delta(x)$ is the Dirac's delta function. The Neumann condition:

$$\left. \frac{\partial c}{\partial x} \right|_{x=0,R} = 0 \tag{2.2.5}$$

is imposed to Eq. (2.2.3), which means no diffusional flux at the boundaries.

Dimensionless form of the mathematical model

The evolution equation for the concentration field in Eq. (2.2.3) is nondimensionalized. Hereafter, dimensionless variables are denoted by adding tildes ($\tilde{}$). The dimensionless time, $\tilde{t}$, length, $\tilde{x}$, and concentration field, $\tilde{c}$, are set as $\tilde{t} = \alpha t$, $\tilde{x} = \sqrt{\alpha/D}x$, and $\tilde{c}(\tilde{x}, \tilde{t}) = c(x,t)/c_0$, respectively. By substituting these dimensionless variables into Eq. (2.2.3), we obtain

$$\frac{\partial \tilde{c}(\tilde{x}, \tilde{t})}{\partial \tilde{t}} = \frac{\partial^2 \tilde{c}(\tilde{x}, \tilde{t})}{\partial \tilde{x}^2} - \tilde{c}(\tilde{x}, \tilde{t}) + \frac{1}{c_0 \alpha} f\left(\sqrt{\frac{D}{\alpha}} \tilde{x}; X\left(\frac{\tilde{t}}{\alpha} \right) \right). \tag{2.2.6}$$

Here, the source term in Eq. (2.2.6), f, is rewritten as

$$\tilde{f}(\tilde{x}; \tilde{X}(\tilde{t})) = \frac{1}{c_0 \alpha} f\left(\sqrt{\frac{D}{\alpha}} \tilde{x}; X\left(\frac{\tilde{t}}{\alpha} \right) \right) = \frac{1}{\sqrt{\alpha D}} \delta\left(\tilde{x} - \tilde{X}\left(\tilde{t}\right) \right), \tag{2.2.7}$$

where $\tilde{X}(\tilde{t}) = \sqrt{\alpha/D}X(\tilde{t}/\alpha)$. Here we use $\delta(ax) = \delta(x)/|a|$. Then we obtain the dimensionless equation for the concentration field as

$$\frac{\partial \tilde{c}(\tilde{x}, \tilde{t})}{\partial \tilde{t}} = \frac{\partial^2 \tilde{c}(\tilde{x}, \tilde{t})}{\partial \tilde{x}^2} - \tilde{c}(\tilde{x}, \tilde{t}) + \tilde{f}\left(\tilde{x}; \tilde{X}(\tilde{t}) \right), \tag{2.2.8}$$

where

$$\tilde{f}(\tilde{x};\tilde{X}(\tilde{t})) = \frac{1}{\sqrt{\alpha D}}\delta\left(\tilde{x}-\tilde{X}(\tilde{t})\right). \tag{2.2.9}$$

Then, we show the manner of the nondimensionalization on the equation of motion, Eq. (2.2.1). The driving force is represented as

$$F\left(\sqrt{\frac{D}{\alpha}};\tilde{X}(\tilde{t})c_0\tilde{c}\left(\tilde{x},\tilde{t}\right)\right) = -Kc_0\sqrt{\frac{\alpha}{D}}\left(\left.\frac{\partial\tilde{c}(\tilde{x},\tilde{t})}{\partial\tilde{x}}\right|_{\tilde{x}=\tilde{X}(\tilde{t})+0}+\left.\frac{\partial\tilde{c}(\tilde{x},\tilde{t})}{\partial\tilde{x}}\right|_{\tilde{x}=\tilde{X}(\tilde{t})-0}\right). \tag{2.2.10}$$

The variables, t, x, X, c, and F, in the equation of motion, Eq. (2.2.1), are replaced with $\tilde{t}$, $\tilde{x}$, $\tilde{X}$, $\tilde{c}$, and $\tilde{F}$, respectively. Then we obtain

$$\tilde{m}\frac{d^2\tilde{X}(\tilde{t})}{d\tilde{t}^2} = -\tilde{\eta}\frac{d\tilde{X}(\tilde{t})}{d\tilde{t}} + \tilde{F}\left(\tilde{X}(\tilde{t});\tilde{c}\left(\tilde{x},\tilde{t}\right)\right), \tag{2.2.11}$$

where

$$\tilde{F}(\tilde{X}(\tilde{t});\tilde{c}\left(\tilde{x},\tilde{t}\right)) = -\left(\left.\frac{\partial\tilde{c}(\tilde{x},\tilde{t})}{\partial\tilde{x}}\right|_{\tilde{x}=\tilde{X}(\tilde{t})+0}+\left.\frac{\partial\tilde{c}(\tilde{x},\tilde{t})}{\partial\tilde{x}}\right|_{\tilde{x}=\tilde{X}(\tilde{t})-0}\right). \tag{2.2.12}$$

Here we define $\tilde{m} = m\alpha D/(Kc_0)$ and $\tilde{\eta} = \eta D/(Kc_0)$.

Hereafter, we use the dimensionless model and omit tildes ($\tilde{}$).

2.2.2 Reduction of the mathematical model

In this section, we derive a reduced equation for the dynamics of the camphor particle position through the expansion of the mathematical model around the solution for the rest state. First, we expand the concentration field c with regard to trigonometric function, i.e., $\cos(k\pi/R)$ for $k = 0, 1, 2, \cdots$,

$$\frac{d}{dt}c_k = \left(i\frac{k\pi}{R}\right)^2 c_k - c_k + f_k(X), \tag{2.2.13}$$

where c_k and f_k are the concentration field and the source term in wavenumber space, respectively. Here f_k is given by $f_0 = 1$ and $f_k = 2\cos(k\pi X/R)$ for $k \geq 1$. The Green's function g_k for Eq. (2.2.13) satisfies the following equation:

$$\left(\frac{d}{dt}+\left(\frac{k\pi}{R}\right)^2+1\right)g_k(t) = \delta(t), \tag{2.2.14}$$

and is solved as:

$$g_k(t) = \exp\left(-\left(\frac{k^2\pi^2}{R^2}+1\right)t\right)\Theta(t), \tag{2.2.15}$$

where $\Theta(t)$ is the Heaviside's step function, i.e., $\Theta(t) = 1$ for $t \geq 0$ and $\Theta(t) = 0$ otherwise. By using $g_k(t)$, the concentration field $c_k(t)$ in wavenumber space is expressed as:

$$c_k(t) = \int_{-\infty}^{t} dt' 2\cos\left(\frac{k\pi}{R}X(t')\right)\exp\left(-\left(\frac{k^2\pi^2}{R^2}+1\right)(t-t')\right). \tag{2.2.16}$$

We expand Eq. (2.2.16) with regard to the position X, the velocity $\dot{X}$, and the acceleration $\ddot{X}$ following the procedure in the previous work on the spot dynamics in a reaction-diffusion system [72].

$$\begin{aligned}
c_k =& 2e^{-At}\int_{-\infty}^{t} dt' \cos\left(\kappa X(t')\right) e^{At'} \\
=& \frac{2e^{-At}}{A}\cos\left(\kappa X(t)\right)\exp\left(At\right) - \frac{2e^{-At}}{A}\int_{-\infty}^{t} dt' \left(-\kappa \frac{dX(t')}{dt'}\sin\left(\kappa X(t')\right)\right) e^{At'} \\
=& \frac{2e^{-At}}{A}\cos\left(\kappa X(t)\right) e^{-At} + \frac{2\kappa e^{-At}}{A^2}\frac{dX(t)}{dt}\sin\left(\kappa X(t)\right)\exp\left(At\right) \\
& - \frac{2\kappa\exp(-At)}{A^2}\int_{-\infty}^{t} dt' \left\{\frac{d^2X(t')}{dt'^2}\sin\left(\kappa X(t')\right) + \kappa\left(\frac{dX(t')}{dt'}\right)^2 \cos\left(\kappa X(t')\right)\right\} e^{At'} \\
=& \cdots ,
\end{aligned} \tag{2.2.17}$$

where $A = k^2\pi^2/R^2 + 1$ and $\kappa = k\pi/R$. The expanded concentration field is obtained by converting c_k into the real space.

$$\begin{aligned}
c(x,t) =& c_0(x,X) \\
& + \dot{X}c_1(x,X) + \dot{X}^2 c_2(x,X) + \dot{X}^3 c_3(x,X) + \cdots \\
& + \ddot{X}c_4(x,X) + \cdots \\
& + (\text{higher order terms \& cross terms}).
\end{aligned} \tag{2.2.18}$$

Here we neglect the higher-order terms of X and the higher-order derivatives with regard to time. Then we calculate the driving force from Eq. (2.2.18), and expand it around $X = R/2$ as $X = R/2 + \delta X$:

$$m\delta\ddot{X} = -\eta\delta\dot{X} + F(\delta X, \delta\dot{X}, \delta\ddot{X}), \tag{2.2.19}$$

where

$$\begin{aligned}
F =& -\frac{2}{\sinh R}\delta X - \frac{4}{3\sinh R}(\delta X)^3 + \frac{(\cosh R - 1)(\sinh R + R)}{2(\sinh R)^2}\delta\dot{X} \\
& + \frac{-3\sinh R + R\cosh R}{4(\sinh R)^2}(\delta X)^2\delta\dot{X} \\
& - \frac{\left(\sinh R(\sinh R - R) + R^2(\cosh R - 1)\right)(\cosh R - 1)}{8(\sinh R)^3}\delta\ddot{X} \\
& - \frac{\sinh R(3\sinh R - 5R\cosh R) + R^2(2 + (\sinh R)^2)}{8(\sinh R)^3}\delta X\left(\delta\dot{X}\right)^2 \\
& - \frac{\left((2 - \cosh R)R^3 + 6R^2\sinh R + 3(\cosh R + 1)(\sinh R - R)\right)(\cosh R - 1)^2}{48(\sinh R)^4}\left(\delta\dot{X}\right)^3 \\
\equiv& A(R)\delta X + B(R)(\delta X)^3 + C(R)\delta\dot{X} \\
& + E(R)(\delta X)^2\delta\dot{X} + G(R)\delta\ddot{X} + H(R)\delta X\left(\delta\dot{X}\right)^2 + I(R)\left(\delta\dot{X}\right)^3.
\end{aligned} \tag{2.2.20}$$

The detailed calculation is shown in Appendix A.1.1. The coefficients of terms in the driving force F are the function of R. $C(R)$ is positive for all $R > 0$ and $A(R)$, $B(R)$, $G(R)$, and $I(R)$ are negative for all $R > 0$. The dependence of the coefficients on R is shown in Fig. A.1.1 in Appendix A.1.2.

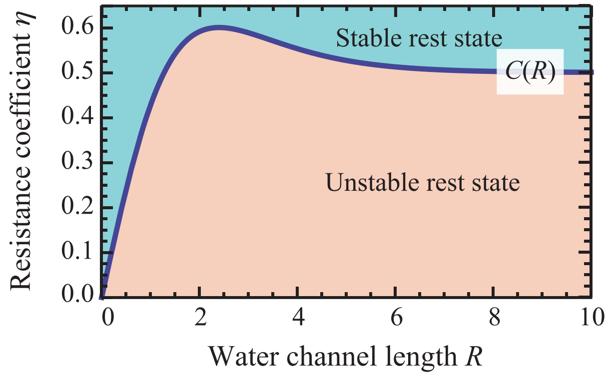

Figure 2.2.1: Phase diagram of the bifurcation structure obtained by the theoretical analysis. The curve in the diagram is $\eta = C(R)$. Reproduced from Ref. [34].

2.2.3 Analysis on bifurcation structure

The second-order ordinary differential equation Eq. (2.2.19) with Eq. (2.2.20) is regarded as a two-dimensional dynamical system on $(\delta X, \delta\dot{X})$. The phase point $(\delta X, \delta\dot{X}) = (0, 0)$ is a fixed point which corresponds to the steady state, i.e., a camphor particle is settled at the center of the water channel. The linearized equation around the fixed point is derived as follows:

$$\frac{d}{dt}\begin{pmatrix}\delta X\\ \delta\dot{X}\end{pmatrix} = \begin{pmatrix}0 & 1\\ -\omega^2 & 2\beta\end{pmatrix}\begin{pmatrix}\delta X\\ \delta\dot{X}\end{pmatrix} \equiv M\begin{pmatrix}\delta X\\ \delta\dot{X}\end{pmatrix}, \tag{2.2.21}$$

where $\omega = \sqrt{-A(R)/(m - G(R))}$ and $\beta = (C(R) - \eta)/(2m - 2G(R))$. The eigenvalue of the matrix M is $\lambda_\pm = \beta \pm i\sqrt{-\beta^2 + \omega^2}$, and thus the Hopf bifurcation occurs where the bifurcation parameter $\beta = C(R) - \eta$ is 0. The value of β depends on the water channel length R and the resistance coefficient η, so that R and η are considered to be the bifurcation parameters in experiments. The phase diagram of the bifurcation structure is shown in Fig. 2.2.1. When η is smaller and larger than $C(R)$, then the rest state is stable and unstable, respectively.

From the weakly nonlinear analysis [74], when $3I(R)\omega^2 + E(R)$ is positive or negative, then the bifurcation type is supercritical or subcritical Hopf bifurcation. $E(R)$, $I(R)$, and ω include $A(R)$ and $G(R)$, which depend on the water channel length R, and ω also depends on m. In Fig. 2.2.2, the border between supercritical and subcritical Hopf bifurcation, $3I(R)\omega^2 + E(R) = 0$, is shown on R-m plane.

We numerically calculated Eqs. (2.2.19) and (2.2.20) for $R = 1$ and 8, and plotted the amplitudes for the stable and unstable oscillation in Fig. 2.2.3. The branch of unstable amplitude, which is characteristic for subcritical Hopf bifurcation, appears only in a narrow range of η for $R = 8$.

2.2.4 Comparison with a one-dimensional infinite system

The same analysis can be adopted for the motion of a camphor particle in a one-dimensional infinite system. Based on the same equation as in Eqs. (2.2.9) and (2.2.11) but without the boundaries, the driving force F is calculated as

$$F = \frac{1}{2}\dot{X}(t) - \frac{1}{8}\ddot{X}(t) - \frac{1}{16}(\dot{X}(t))^3. \tag{2.2.22}$$

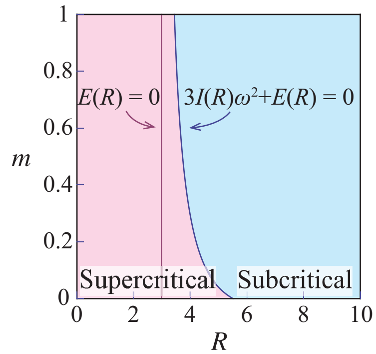

Figure 2.2.2: Plot of $3I(R)\omega^2 + E(R) = 0$ on R-m plane. The curve $3I(R)\omega^2 + E(R) = 0$ approaches $E(R) = 0$ for $m \to \infty$. Reproduced from Ref. [34].

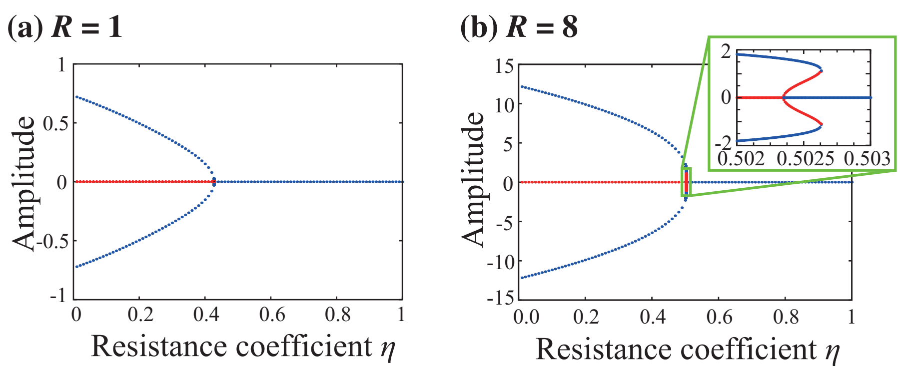

Figure 2.2.3: Bifurcation diagram for (a) $R = 1$ and (b) $R = 8$, numerically obtained based on Eqs. (2.2.19) and (2.2.20). The blue and red dots show the stable and unstable amplitudes, respectively. It is noted that the dots on the zero amplitude indicate the rest state. We see supercritical and subcritical Hopf bifurcations for $R = 1$ and $R = 8$, respectively. The mass m is set to be $m = 0.01$. Reproduced from Ref. [34].

The detailed calculation is provided in Appendix A.1.3. The driving force does not depend on the position but on the velocity and acceleration of the camphor particle, since the system has a translational symmetry. It is noted that the limit of Eq. (2.2.20) where R goes to infinity corresponds to Eq. (2.2.22).

In the reduced equation:

$$\left(m + \frac{1}{8}\right)\ddot{X} = \left(\frac{1}{2} - \eta\right)\dot{X} - \frac{1}{16}(\dot{X}(t))^3, \tag{2.2.23}$$

the supercritical pitchfork bifurcation occurs, where the resistance coefficient η is the bifurcation parameter. Nagayama *et al.* investigated the motion of a camphor particle with a finite size in a one-dimensional infinite system [47]. They found that the supercritical and subcritical pitchfork bifurcation occurs for the small and large size of a camphor particle, respectively. In the present study, the size of a camphor particle is set to be infinitesimally small, and thus the present analysis is consistent with the results by Nagayama *et al.*

2.2.5 Water channel length where the rest state is unstable

As shown in Fig. 2.2.1, the function $C(R)$ has a peak around $R \sim 2$. This peak indicates that the rest state is easiest to become unstable at the water channel length where $C(R)$ takes a maximum value. Here we explain why there is a certain water channel length where the rest state is easiest to become unstable by considering a semi-infinite system with a boundary.

First, we consider the translational motion with a constant velocity without boundaries. We set the velocity of the particle to be v. Then the position of the camphor particle X and the concentration field c is denoted as $X = vt + \text{const.}$ and $c(x - X; v)$. By setting $z = x - X$, Eq. (2.2.9) is expressed as

$$-v\frac{dc}{dz} = \frac{d^2c}{dz^2} - c + \delta(z). \tag{2.2.24}$$

By substituting $c = e^{\lambda z}$, we obtain $\lambda = -v/2 \pm \sqrt{v^2/4 + 1} \equiv \lambda_{\pm}$. From the boundary condition $c(z \to \pm\infty) = 0$, the continuity at $z = 0$, and the discontinuity of the first derivative due to the Dirac's delta function, the coefficients of the general solutions $c = e^{\lambda_{\pm} z}$ is determined as follows:

$$c(z; v) = \begin{cases} \dfrac{1}{\sqrt{v^2 + 4}} e^{\lambda_+ z}, & (z < 0), \\ \dfrac{1}{\sqrt{v^2 + 4}} e^{\lambda_- z}, & (z > 0). \end{cases} \tag{2.2.25}$$

The Taylor expansion of the concentration field c around $v = 0$ is given as

$$c(z; v) = \frac{1}{2}\left(1 - v\frac{z}{2}\right) e^{-|z|}, \tag{2.2.26}$$

where the more-than-second-order terms of v are truncated. By subtracting the steady state:

$$c_0 = c(z; v = 0) = \frac{1}{2} e^{-|z|} \tag{2.2.27}$$

from Eq. (2.2.26), the effect of the motion on the concentration field c_1 is obtained as

$$c_1(z; v) = -\frac{1}{4} v z e^{-|z|}, \tag{2.2.28}$$

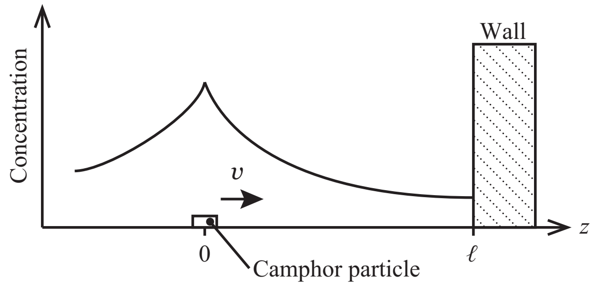

Figure 2.2.4: Schematic illustration of a semi-infinite system with a boundary. A camphor particle moves with a constant velocity v. The camphor particle and the boundary are located at $x = 0$ and $x = \ell$, respectively. Reproduced from Ref. [34].

where Eq. (2.2.26) is the summation of c_0 and c_1. Since the concentration field with zero velocity, c_0, has a symmetric profile with regard to the particle position, the driving force F_0 originating from c_0 is zero. Thus the driving force working on the camphor particle is $F_1(v) = v/2$ originating from c_1, which directs in the moving direction.

Then we consider the effect by the boundary. Here we assume that the particle is located at the left side of the boundary as shown in Fig. 2.2.4. The distance between the particle and the boundary is set to be ℓ. To satisfy the Neumann boundary condition, we add the concentration field by the virtual camphor particle, which is located at the right side of the boundary and has a velocity $-v$. The distance between the virtual particle and the boundary is also ℓ. We denote the concentration field by the virtual particle as ${c_0}^* + {c_1}^*$, where ${c_0}^*$ and ${c_1}^*$ are the concentration field for the steady state and the proportional to the velocity, respectively. The explicit forms of them are ${c_0}^*(z;\ell) = c_0(z - 2\ell)$ and ${c_1}^*(z;\ell, v) = c_1(z - 2\ell; -v)$, where 2ℓ is the distance between the real and virtual camphor particles. Thus the concentration field for the system with the camphor particle and the boundary is given by

$$c(z; v, \ell) = c_0(z) + {c_0}^*(z;\ell) + c_1(z; v) + {c_1}^*(z;\ell, v). \tag{2.2.29}$$

The driving forces ${F_0}^*(\ell)$ and ${F_1}^*(\ell, v)$ originating from ${c_0}^*$ and ${c_1}^*$ are described as $-e^{-2\ell}$ and $-v(1/4 - \ell/2)e^{-2\ell}$, respectively. Thus we have

$$\begin{aligned} F(v, \ell) =& F_0 + {F_0}^*(\ell) + F_1(v) + {F_1}^*(\ell, v) \\ =& -e^{-2\ell} + \frac{v}{2} - \frac{v}{4}(1 - 2\ell)e^{-2\ell} \\ \equiv& g_0(\ell) + g_1(\ell)v + \mathcal{O}(v^2), \end{aligned} \tag{2.2.30}$$

where $g_0(\ell) = -e^{-2\ell}$ and $g_1(\ell) = 1/2 - (1/4 - \ell/2)e^{-2\ell}$. The coefficient $g_1(\ell)$ of the first order of v is plotted against ℓ in Fig. 2.2.5. In Fig. 2.2.5, $g_1(\ell)$ has a peak around $\ell = 1$, which indicates that the camphor particle is greatly accelerated around $\ell = 1$. The function $C(R)$ in Eq. (2.2.20) is the coefficient of the first order of v. When the water channel length R is 2, the distance between the camphor particle and the boundaries is 1. Thus the fact that $C(R)$ has a maximum value around $R \sim 2$ is consistent with the fact that $g_1(\ell)$ has a maximum value around $\ell \sim 1$. In other words, the peak of $C(R)$ is qualitatively reproduced by considering the effect of a boundary.

By the way, the concentration field by the camphor particle resting at $z = 0$ is given in Eq. (2.2.27) and its width is about 2. Thus the result indicates that the rest state is easiest to

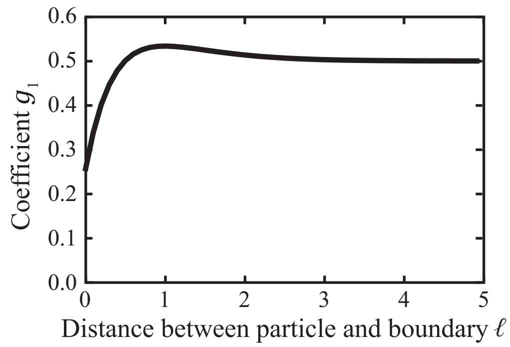

Figure 2.2.5: Coefficient $g_1(\ell)$ of the first order of v in $F_1(v) + F_1{}^*(\ell, v)$. Reproduced from Ref. [34].

be unstable when the water channel length and the width of the profile of concentration field is comparable.

2.2.6 Comparison with the numerical results

To confirm the theoretical results, we performed numerical calculations based on Eqs. (2.2.9) and (2.2.11). We used the Euler method for Eq. (2.2.11) and the implicit method for Eq. (2.2.9). The time and spatial steps were 10^{-5} and 10^{-3}, respectively. The mass m was fixed to $m = 10^{-2}$.

The typical trajectories are shown in Fig. 2.2.6. Figure 2.2.6(a) shows a trajectory approaching a limit-cycle orbit and Fig. 2.2.6(b) shows a damped oscillation approaching the rest state. We numerically obtained the stable amplitudes and maximum and minimum velocities for two parameters, i.e., the water channel length R and the resistance coefficient η. The results are shown in Fig. 2.2.7. We confirmed that the bifurcation occurred at certain pairs of R and η.

The phase diagram obtained by numerical results is shown in Fig. 2.2.8. The qualitative features were the same as the theoretical results though the numerical results slightly differed from the theoretical ones quantitatively. It is expected that the difference between the numerical and theoretical results mainly comes from the discretization of the Dirac's delta function.

We also checked the validity of the reduction of our model in Subsection 2.2.2. Here we compared the driving force obtained by numerical calculation with that obtained by reduction of the model. The results for $R = 1$ and $R = 8$ are shown in Figs. 2.2.9 and 2.2.10, respectively. The driving force obtained by the reduction of the model matched well for the water channel length $R = 1$, but did not for $R = 8$. For smaller water channel, the confinement by the system boundary was greater, and the amplitude of oscillation was smaller. Thus we conclude that the reduction is valid moderately for a smaller water channel even though the bifurcation parameters, R and η, are not close to the bifurcation point.

2.2.7 Comparison with the experimental results

The oscillatory motion of a camphor particle was reported by Hayashima *et al.* and observed an oscillatory motion [48]. However, the oscillatory motion lasted within 1 min., since the aqueous phase was too small (1.0 ml) and saturated with camphor molecules in short time.

In our experiments, we succeeded in observation of stable oscillations by increasing the volume of the aqueous phase. We experimentally determined the bifurcation points between the rest and

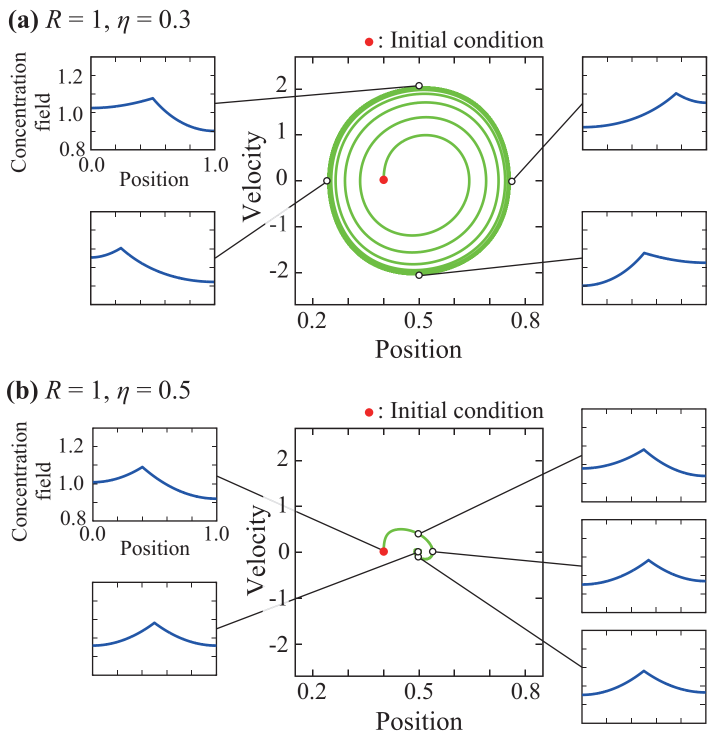

Figure 2.2.6: Trajectories on X-$\dot{X}$ plane and the concentration field. The water channel length R was $R = 1$ for both (a) and (b), and the resistance coefficient η was set to be (a) $\eta = 0.3$ and (b) $\eta = 0.5$. Reproduced from Ref. [34].

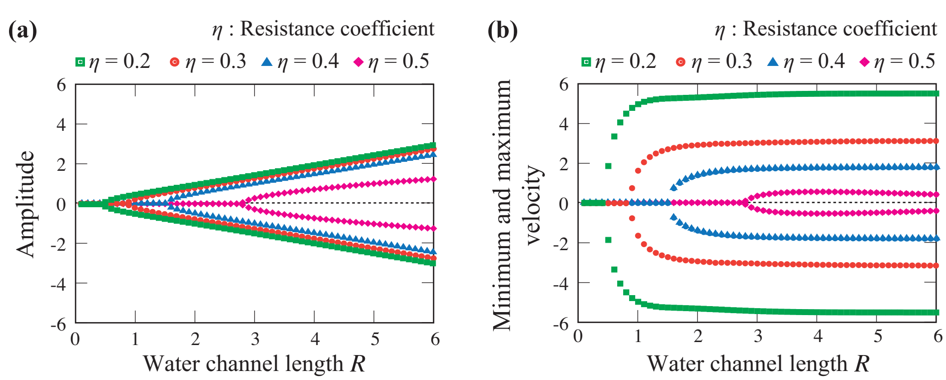

Figure 2.2.7: Stable (a) amplitude and (b) maximum and minimum velocities for each viscosity η depending on R. Reproduced from Ref. [34].

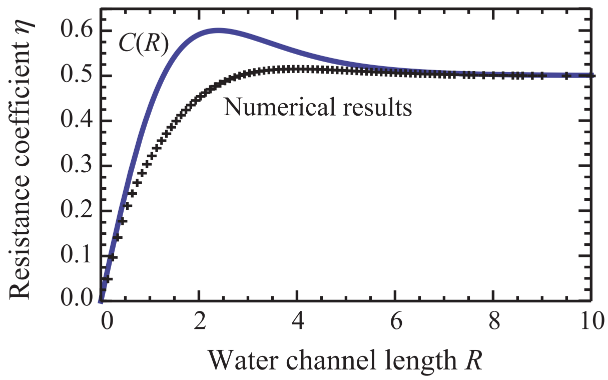

Figure 2.2.8: Phase diagram for the comparison of the theoretical results with numerical ones. The marks "+" show the bifurcation points obtained by numerical calculations, and the solid line is the bifurcation curve $C(R)$ obtained by the theoretical analysis. Reproduced from Ref. [34].

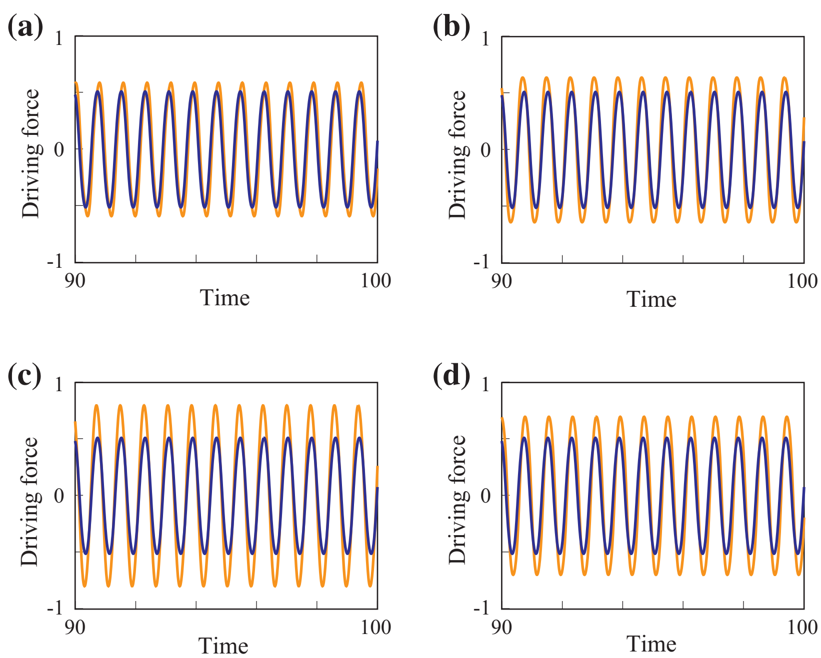

Figure 2.2.9: Comparison between the numerical and analytical results for the water channel length $R = 1$. The dark blue curves in (a-d) show the numerical result using the model equations (2.2.9) and (2.2.11) and are all the same for (a-d). The orange curves show the driving force obtained by the theoretical analysis: We substitute the values X, $\dot{X}$, and $\ddot{X}$ obtained by numerical calculation into (a) the result in Eq. (2.2.20), $AX + BX^3 + C\dot{X} + EX^2\dot{X} + HX\dot{X}^2 + I\dot{X}^3 + G\ddot{X}$, (b) the result in Eq. (2.2.20) without $G\ddot{X}$, $AX + BX^3 + C\dot{X} + EX^2\dot{X} + HX\dot{X}^2 + I\dot{X}^3$, (c) the first order terms of position and velocity, $AX + C\dot{X}$, and (d) the first order terms of position, velocity, and acceleration, $\ddot{X}AX + C\dot{X} + G\ddot{X}$. The resistance coefficient was $\eta = 0.3$. Reproduced from Ref. [34].

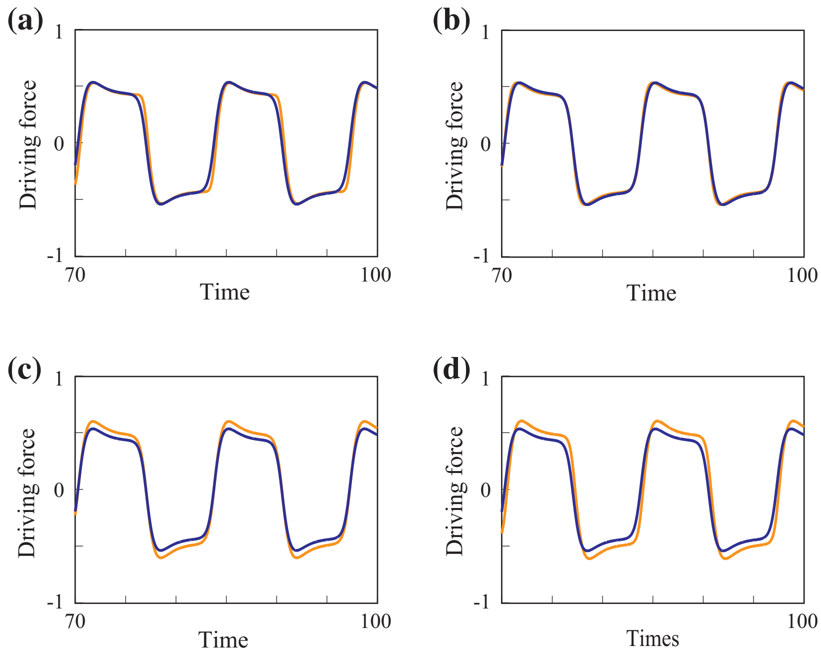

Figure 2.2.10: Comparison between the numerical and analytical results for the water channel length $R = 8$. The caption for these plots is the same as Fig. 2.2.9 except for the value of the water channel length and the resistance coefficient; $R = 8$ and $\eta = 0.45$. Reproduced from Ref. [34].

oscillatory states, and then quantitatively compared the experimental results with the theoretical results.

Experimental setup and methods

The water chamber was filled with pure water or glycerol aqueous solution (Wako, Japan), whose volume was 250 ml. Pure water was prepared with the Millipore water purifying system (UV3, Merck, Germany). A water channel was floated on the aqueous phase. The water channels were prepared by making a rectangle hole in the Teflon sheet with thickness of 1 mm. The size of rectangular holes was 4 mm for the short side and 15, 20, 25, 30, 35, 40, 45, and 50 mm for the long side. Camphor particles were made of camphor powder (Wako, Japan) using a pill maker (Kyoto Pastec, Japan). The camphor particles had cylinderical shapes, whose diamater and height were 3 and 1 mm, respectively. The camphor particle motion was captured by HD video camera (iVIS HV30, CANON, Japan). The size of a frame of the movie was 720×480 pixels and the time resolution was 1/30 s. By controlling the concentration of glycerol aqueous solution, the viscosities of solutions were changed, which resulted in the change in the resistant force exerting on a camphor particle. The viscosity was measured by vibrational viscometer (SV-10A, A&D, Japan). The experimental setup is shown in Fig. 2.2.11. The experiments were performed at room temperature.

The movies were analyzed using ImageJ (NIH, USA). The characteristic period of oscillation was 1-2 s and the oscillation seemed to settle to the stable oscillation sufficiently ca. 1 min. after the camphor particle was floated. The camphor particle became smaller and they began to move not only along but also perpendicular to the water channel ca. 10 min. after a camphor particle was floated. Thus the movies were used from 1 to 6 min. after a camphor particle was floated for

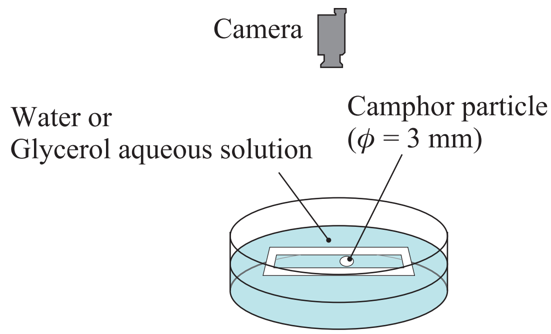

Figure 2.2.11: Schematic illustration of the experimental setup. Reproduced from Ref. [34].

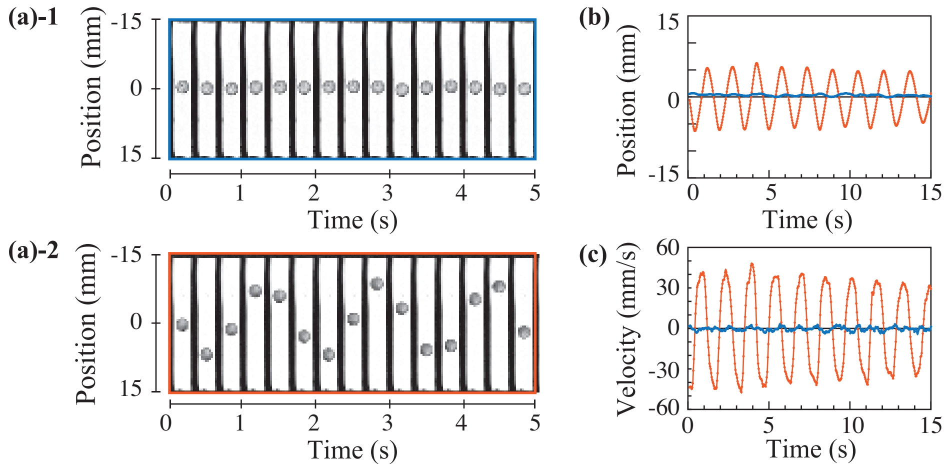

Figure 2.2.12: (a) Snapshots of a camphor particle and water channel every 1/3 s. We used 3.5 mol/L and 2.5 mol/L glycerol aqueous solution as an aqueous phase for (a)-1 and -2, respectively. Time evolution of (b) the positions and (c) the velocities of camphor particles. The blue and orange curves corresponding to (a)-1 and -2, respectively. Reproduced from Ref. [34].

the image processing. The experiments were made at least four times for each water channel length and viscosity of the aqueous phase.

Experimental results

We observed the rest state and oscillatory motion of a camphor particle in a one-dimensional water channel. The snapshots of the system and the time change in the position and velocity are shown in Fig. 2.2.12. As shown in Fig. 2.2.12(a), two types of behavior, i.e., rest state ((a)-1) and stable oscillation ((a)-2), were observed. We analyzed the amplitude of the oscillation and local maximum and minimum of the velocity, which were detected by averaging the amplitude of the oscillation and local maximum and minimum for every 5-s term. The results are shown in Fig. 2.2.13. Near the bifurcation point, the standard deviations tended to be larger, since the stability was close to neutral. The oscillatory motion was observed with smaller viscosity and larger water channel. We classified the behavior into oscillation and rest state, and summarized as a phase

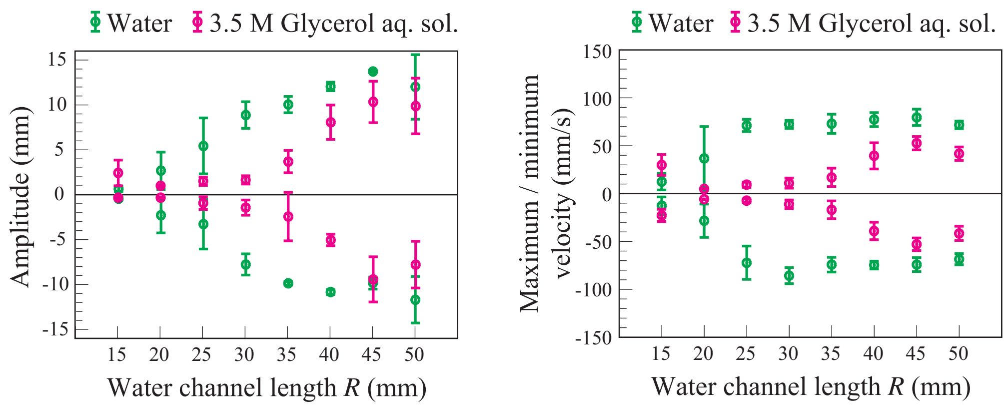

Figure 2.2.13: Dependence of amplitudes and maximum and minimum velocities on the water channel length R. The plots colored with green and magenta show the results for water and 3.5 M glycerol aqueous solution, respectively. The bifurcation structures were observed around 15-20 mm for water and 35 mm for 3.5 M glycerol aqueous solution. The error bars show the standard deviations. Reproduced from Ref. [34].

diagram in Fig. 2.2.14.

Discussion on experimental results

Here, we discuss the physical meaning of the bifurcation structure in the motion of the camphor particle in a one-dimensional finite region, as schematically shown in Fig. 2.2.15. For a small system size, the camphor particle does not move since the camphor molecules are quickly saturated at the water surface and do not produce sufficient driving force. Thus, the camphor particle stops at the center position as in Fig. 2.2.15(b), where the driving force balances. By increasing the system size, the saturation of the camphor molecules becomes slower and the camphor particle begins to move. The particle does not exhibit translational motion owing to the confinement by the boundaries, but it exhibits oscillation around the system center, as shown in Fig. 2.2.15(c). For the greater system size, the amplitude of the position increases almost linearly and the amplitude of the velocity is saturated, as shown in Figs. 2.2.7 and 2.2.13. This behavior can be understood by considering the effect of the boundaries, which affect the motion of a camphor particle through the concentration field. The characteristic length of the effect of the boundaries is considered to be the diffusion length of the concentration field. For the system size greater than the diffusion length, the effect of the boundaries is negligible except for the boundaries' neighborhood. Therefore, a camphor particle exhibits translational motion with an almost constant velocity that is determined only by the viscosity of the aqueous phase, and it is reflected by a boundary when the camphor particle is within the distance of the diffusion length from the boundaries, as shown in Fig. 2.2.15(d).

Quantitative comparison of the experimental results with the theoretical ones

We examine whether the order of bifurcation points obtained by theoretical analysis quantitatively matches with the experiments. In the theoretical analysis, the bifurcation structure is observed for $R = \mathcal{O}(1)$ and $\eta = \mathcal{O}(0.1 \sim 1)$.

First, we estimate the order of R. The order of the water channel used in the experiments

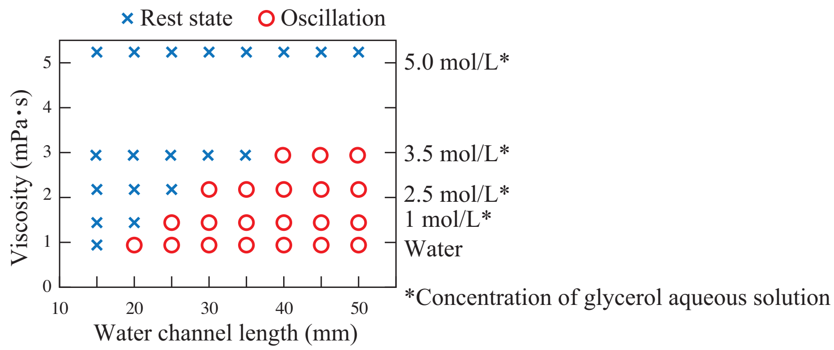

Figure 2.2.14: Phase diagram obtained by experiments. Here we define the rest state as the state where the averages of local maximum and minimum velocity is less than 30 mm/s. Reproduced from Ref. [34].

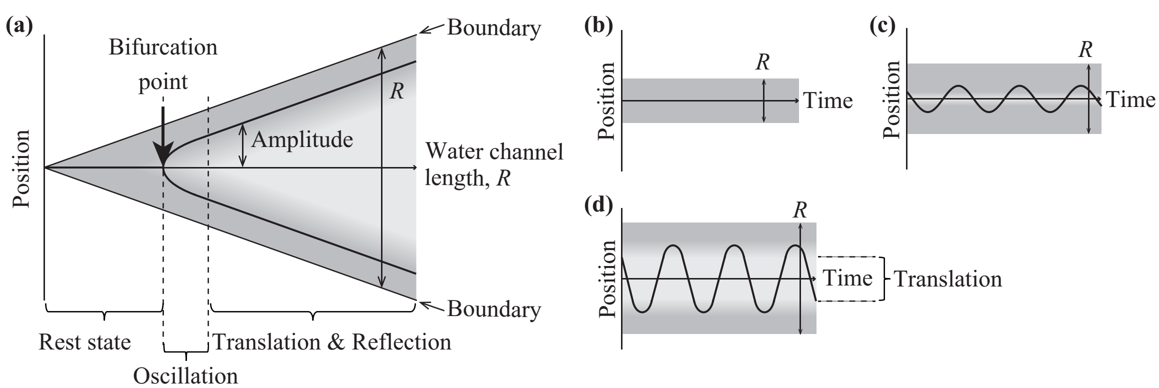

Figure 2.2.15: Schematic illustration for (a) the bifurcation diagram and (b)-(d) the typical behavior of motion of a camphor particle for each water channel length: (b) rest state, (c) oscillatory motion, and (d) translation and reflection. It is noted that there is no clear boundary between (c) and (d).

was 10 mm. The diffusion length $\sqrt{D/\alpha}$ is estimated as $\sqrt{D/\alpha} \sim 10$ mm, which is the length within which the particle is affected by the boundary through the concentration field. Here we do not use the diffusion constant obtained by fluctuation-dissipation theorem, since the diffusion is enhanced by the Marangoni flow [?]. The water channel length $\tilde{R}$ is $R = \sqrt{\alpha/D}\tilde{R}$. Thus we have $R = 10$ mm/10 mm $= 1$.

The order of resistance coefficient η is estimated as follows. For the relation between the resistance coefficient $\tilde{\eta}$ and the viscosity ν, we assume the Stokes' law, $\tilde{\eta} = 6\pi\nu a \sim 10^{-5}$ kg/s, where a is a radius of the particle. In the experiments, we used the particle with a radius of 1.5 mm. The viscosity of pure water and glycerol aqueous solution were 1 mPa·s and 50 mPa·s, respectively.

The order of the driving force is estimated by the concentration field of the steady state. The solution for the equation:

$$\frac{\partial c}{\partial t} = D\frac{\partial^2 c}{\partial x^2} - \alpha c + c_0\delta(x) \tag{2.2.31}$$

is $c_0 e^{-\sqrt{\alpha/D}|x|}/(2\sqrt{\alpha D})$. The gradient of the concentration near the camphor particle is $\pm c_0/(2D)$, and thus the driving force F is $F \sim Kc_0/D$. The driving force F and sublimation rate α were experimentally measured as $F \sim 1$ μN and $\alpha \sim (1.8 \pm 0.4) \times 10^{-2}$ s^{-1} in the previous work by Suematsu *et al.* [75]. The resistance coefficient $\tilde{\eta}$ is $\eta = D\sqrt{\alpha D}/(Kc_0)\tilde{\eta}$. Thus we have

$$\begin{aligned}\eta =& \frac{D\sqrt{\alpha D}}{Kc_0}\tilde{\eta} = \frac{D}{Kc_0}\sqrt{\frac{D}{\alpha}}\alpha \times 6\pi\hat{\eta}a \\ =& \frac{1}{1\ \mu\mathrm{N}} \times (10\ \mathrm{mm}) \times (1.8 \times 10^{-2}\ \mathrm{s}^{-1}) \times 6\pi\hat{\eta} \times (1.5\ \mathrm{mm}) \\ \sim& 6\hat{\eta}\ (\mathrm{Pa}\cdot\mathrm{s})^{-1}.\end{aligned} \tag{2.2.32}$$

The resistance coefficient η is $\eta \sim 10^{-2}$ and $\eta \sim 10^{-1}$ for water and glycerol aqueous solution. Thus the bifurcation point obtained by theoretical analysis is in good correspondence with that of experiments.

2.2.8 Summary for Section 2.2

The motion of a camphor particle in a one-dimensional system is investigated [34]. A camphor particle exhibits the rest state at the center of the system or oscillatory motion depending on the physical parameters, the water channel length and the resistance coefficient. Oscillatory motion emerges from the rest state through Hopf bifurcation. The theoretical results qualitatively correspond to the numerical and experimental results.

2.3 Motion of a self-propelled particle in an axisymmetric system

In this section, we discuss motion of a symmetric self-propelled particle (SPP) in a system with axial symmetry [37]. Here, we use the word "an axisymmetric system" as a system with inversion and rotational symmetry. The considered self-propelled systems have symmetry, and therefore the rest state at the center of the system should exist. It is noted that the stability of the steady state depends on the physical parameters of the system. In some cases, the stability of the steady state changes with the change in the physical parameter, i.e., a bifurcation occurs.

Here, we especially focus on the motion which emerges through a bifurcation from the rest state at the system center position. Due to the dimensionality and symmetric property of the system,

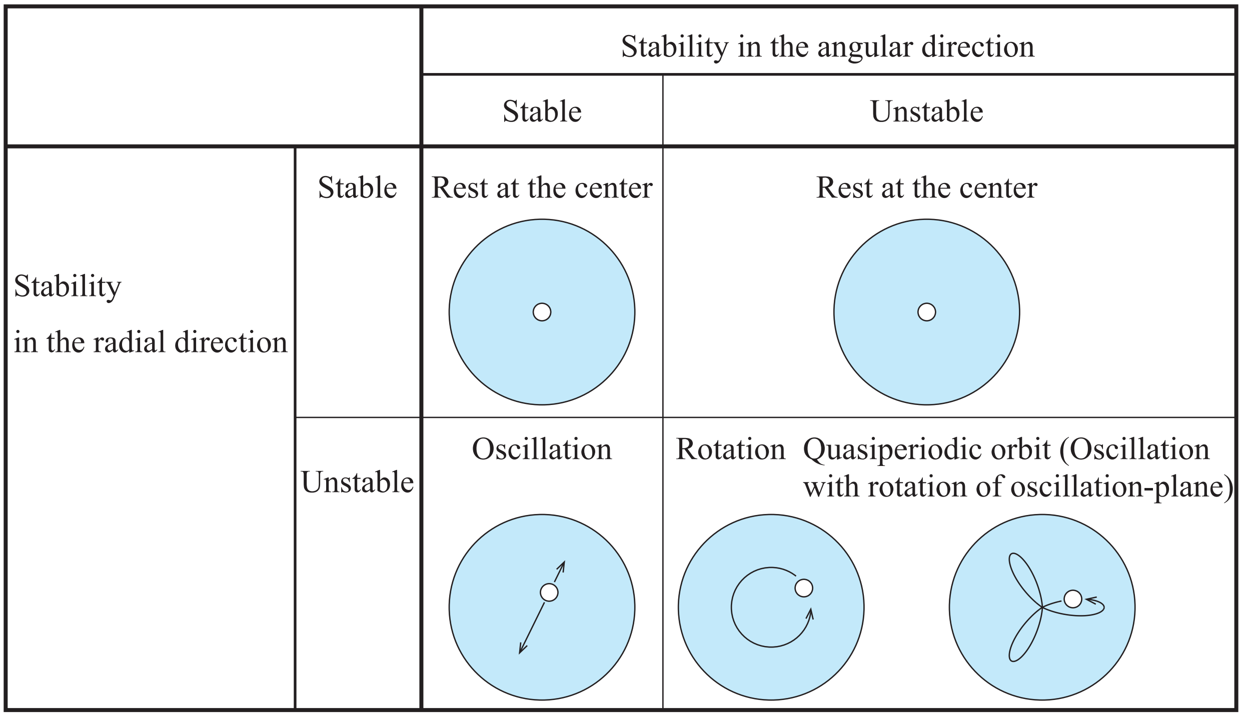

Figure 2.3.1: Relation between the instabilized direction and possible motion.

there are several candidates of motion when the rest state becomes unstable. The relation between the instabilized direction and the possible motion is summarized in Fig. 2.3.1.

We first construct a dynamical system only considering the symmetric property of the original system under the assumption that the system is close to the bifurcation point, and then analyze the dynamical system using a weakly nonlinear analysis.

2.3.1 Construction of the dynamical system

The center of mass and velocity of a SPP are set to be $\boldsymbol{x} = (x_1, x_2)$, and $\boldsymbol{v} = \dot{\boldsymbol{x}} = (v_1, v_2)$, respectively. Here the dot $(\dot{\ })$ denotes time derivative. We assume that the time change in the position of the SPP, $\boldsymbol{x}$, is represented by the equation of motion, which has the inversion and rotational symmetries. Here, inversion and rotational symmetries indicate that the equation of motion is invariant even though the coordinates are inverted and rotated with respect to the origin. We also assume that the SPP moves around the origin with a sufficiently small velocity, i.e., $|\boldsymbol{x}(t)| \ll 1$ and $|\boldsymbol{v}(t)| \ll 1$. The general form of the equation of motion under the above assumptions is represented as:

$$\begin{cases} \dot{\boldsymbol{x}} = \boldsymbol{v}, & \text{(2.3.1a)} \\ \dot{\boldsymbol{v}} = a\boldsymbol{x} + b\boldsymbol{v} + c|\boldsymbol{x}|^2\boldsymbol{x} + k|\boldsymbol{v}|^2\boldsymbol{v} + h|\boldsymbol{v}|^2\boldsymbol{x} + n|\boldsymbol{x}|^2\boldsymbol{v} + j(\boldsymbol{x}\cdot\boldsymbol{v})\boldsymbol{x} + p(\boldsymbol{x}\cdot\boldsymbol{v})\boldsymbol{v}, & \text{(2.3.1b)} \end{cases}$$

where a, b, c, k, h, n, j, and p are parameters. Equation (2.3.1) is a four-dimensional dynamical system. In addition, we also assume a linear restoring force $a\boldsymbol{x}$ $(a < 0)$ to discuss the motion around the origin.

We set the time scale of harmonic oscillation to be 1 by setting the coefficient for the linear restoring force to be $a = -1$. The dimensionless time $\tilde{t}$ is $\tilde{t} = \sqrt{-a}t$. Then the dynamical system becomes

$$\dot{\boldsymbol{v}} = -\boldsymbol{x} + \frac{b}{\sqrt{-a}}\boldsymbol{v} - \frac{c}{a}|\boldsymbol{x}|^2\boldsymbol{x} + k\sqrt{-a}|\boldsymbol{v}|^2\boldsymbol{v} + h|\boldsymbol{v}|^2\boldsymbol{x} + \frac{n}{\sqrt{-a}}|\boldsymbol{x}|^2\boldsymbol{v} + \frac{j}{\sqrt{-a}}(\boldsymbol{x}\cdot\boldsymbol{v})\boldsymbol{x} + p(\boldsymbol{x}\cdot\boldsymbol{v})\boldsymbol{v}. \tag{2.3.2}$$

Hereafter, we redefine the variable for time $\tilde{t} \to t$, and the parameters $b/\sqrt{-a} \to b$, $-c/a \to c$, $k\sqrt{-a} \to k$, $n/\sqrt{-a} \to n$, $j/\sqrt{-a} \to j$, and analyze the following equation:

$$\begin{cases} \dot{\boldsymbol{x}} = \boldsymbol{v}, & (2.3.3\text{a}) \\ \dot{\boldsymbol{v}} = -\boldsymbol{x} + b\boldsymbol{v} + c|\boldsymbol{x}|^2\boldsymbol{x} + k|\boldsymbol{v}|^2\boldsymbol{v} + h|\boldsymbol{v}|^2\boldsymbol{x} + n|\boldsymbol{x}|^2\boldsymbol{v} + j(\boldsymbol{x}\cdot\boldsymbol{v})\boldsymbol{x} + p(\boldsymbol{x}\cdot\boldsymbol{v})\boldsymbol{v}. & (2.3.3\text{b}) \end{cases}$$

2.3.2 Weakly nonlinear analysis

In this subsection, we assume that there are two time scales of dynamics in Eq. (2.3.3); one is that for the periodic motion by linear restoring force and the other is the slower one for perturbative dynamics. First, the dynamical system for the perturbative dynamics is derived by separating the time scales. Then the existence and linear stability of rotational and oscillatory motions are analyzed.

Separation of time scales

Here we assume that the first term in the righthand side in Eq. (2.3.3), $-\boldsymbol{x}$, is the main term, and the others are perturbative terms. We separate the time scale of the harmonic oscillation by the term $-\boldsymbol{x}$ from those of changes in the amplitude and phase of the oscillation. We assume that the perturbative terms in Eq. (2.3.3) are at the order of ε. Then the time scales for the harmonic oscillation and perturbation are set to be $\tau = t$ and $T = \varepsilon t$ $(0 < \varepsilon \ll 1)$, respectively [73]. The time derivative is expressed as follows:

$$\frac{d}{dt} = \frac{\partial \tau}{\partial t}\frac{\partial}{\partial \tau} + \frac{\partial T}{\partial t}\frac{\partial}{\partial T} \equiv \partial_\tau + \varepsilon\partial_T. \tag{2.3.4}$$

Since we separate the time scales of the oscillation and the change of amplitude and phase, we set $\boldsymbol{x} = (x_1, x_2)$ as

$$\begin{cases} x_1 = r_1(T)\cos(\tau + \phi_1(T)), & (2.3.5\text{a}) \\ x_2 = r_2(T)\cos(\tau + \phi_2(T)). & (2.3.5\text{b}) \end{cases}$$

Then the velocity $\boldsymbol{v}$ and the time derivative of it $\dot{\boldsymbol{v}}$ are explicitly expressed as

$$\begin{cases} v_1 = (\partial_\tau + \varepsilon\partial_T)x_1 = -r_1\sin(\tau+\phi_1) + \varepsilon\{r_1{}'\cos(\tau+\phi_1) - r_1\phi_1{}'\sin(\tau+\phi_1)\}, & (2.3.6\text{a}) \\ v_2 = (\partial_\tau + \varepsilon\partial_T)x_2 = -r_2\sin(\tau+\phi_2) + \varepsilon\{r_2{}'\cos(\tau+\phi_2) - r_1\phi_2{}'\sin(\tau+\phi_2)\}, & (2.3.6\text{b}) \end{cases}$$

$$\begin{cases} \dot{v}_1 = (\partial_\tau + \varepsilon\partial_T)^2 x_1 = (\partial_\tau{}^2 + 2\varepsilon\partial_\tau\partial_T + \varepsilon^2\partial_T{}^2)x_1 & \\ \quad = -r_1\cos(\tau+\phi_1) - 2\varepsilon\{r_1{}'\sin(\tau+\phi_1) + r_1\phi_1{}'\cos(\tau+\phi_1)\} + \mathcal{O}(\varepsilon^2), & (2.3.7\text{a}) \\ \dot{v}_2 = (\partial_\tau + \varepsilon\partial_T)^2 x_2 = (\partial_\tau{}^2 + 2\varepsilon\partial_\tau\partial_T + \varepsilon^2\partial_T{}^2)x_2 & \\ \quad = -r_2\cos(\tau+\phi_2) - 2\varepsilon\{r_2{}'\sin(\tau+\phi_2) + r_2\phi_2{}'\cos(\tau+\phi_2)\} + \mathcal{O}(\varepsilon^2), & (2.3.7\text{b}) \end{cases}$$

where the prime ($'$) denotes the differential by T. By substituting Eqs. (2.3.5), (2.3.6), and (2.3.7) into (2.3.3) and comparing the both sides of the equation as an identity with regard to ε, we have the following equations; From the equation for $\dot{v}_1$, we have

$$
\begin{aligned}
\mathcal{O}(1): &\quad -r_1\cos\theta_1 = -r_1\cos\theta_1, && (2.3.8)\\
\mathcal{O}(\varepsilon): &\quad -2\varepsilon\{{r_1}'\sin\theta_1 + r_1{\phi_1}'\cos\theta_1\}\\
&= -br_1\sin\theta_1 + cr_1({r_1}^2\cos^2\theta_1 + {r_2}^2\cos^2\theta_2)\cos\theta_1 - kr_1({r_1}^2\sin^2\theta_1 + {r_2}^2\sin^2\theta_2)\sin\theta_1\\
&\quad + hr_1({r_1}^2\sin^2\theta_1 + {r_2}^2\sin^2\theta_2)\cos\theta_1 - nr_1({r_1}^2\cos^2\theta_1 + {r_2}^2\cos^2\theta_2)\sin\theta_1,\\
&\quad - jr_1({r_1}^2\sin\theta_1\cos\theta_1 + {r_2}^2\sin\theta_2\cos\theta_2)\cos\theta_1 + pr_1({r_1}^2\sin\theta_1\cos\theta_1 + {r_2}^2\sin\theta_2\cos\theta_2)\sin\theta_1,\\
&\equiv H(r_1, r_2, \theta_1, \theta_2),
\end{aligned}
\tag{2.3.9}
$$

and from the equation for $\dot{v}_2$, we also have

$$
\begin{aligned}
\mathcal{O}(1): &\quad -r_2\cos\theta_2 = -r_2\cos\theta_2, && (2.3.10)\\
\mathcal{O}(\varepsilon): &\quad -2\varepsilon\{{r_2}'\sin\theta_2 + r_2{\phi_1}'\cos\theta_2\}\\
&= -br_2\sin\theta_2 + cr_2({r_1}^2\cos^2\theta_1 + {r_2}^2\cos^2\theta_2)\cos\theta_2 - kr_2({r_1}^2\sin^2\theta_1 + {r_2}^2\sin^2\theta_2)\sin\theta_2,\\
&\quad + hr_2({r_1}^2\sin^2\theta_1 + {r_2}^2\sin^2\theta_2)\cos\theta_2 - nr_2({r_1}^2\cos^2\theta_1 + {r_2}^2\cos^2\theta_2)\sin\theta_2,\\
&\quad - jr_2({r_1}^2\sin\theta_1\cos\theta_1 + {r_2}^2\sin\theta_2\cos\theta_2)\cos\theta_2 + pr_2({r_1}^2\sin\theta_1\cos\theta_1 + {r_2}^2\sin\theta_2\cos\theta_2)\sin\theta_2\\
&= H(r_2, r_1, \theta_2, \theta_1),
\end{aligned}
\tag{2.3.11}
$$

where we define $\theta_1 = \tau + \phi_1$ and $\theta_2 = \tau + \phi_2$.

To discuss the effect by the perturbative terms, we derive the equations for ${r_1}'$, ${r_2}'$, ${\phi_1}'$, and ${\phi_2}'$. The time average of ${r_1}'\sin^2\theta_1$ over a period of oscillation, 2π, is approximately calculated as

$$
\frac{1}{2\pi}\int_0^{2\pi} {r_1}'\sin^2\theta_1\, d\theta_1 = \frac{1}{2\pi}{r_1}'\int_0^{2\pi}\sin^2\theta_1\, d\theta_1 = \frac{1}{2}{r_1}'. \tag{2.3.12}
$$

Here we assume that ${r_1}'$ is a constant during one period. For the same reason, the amplitudes (r_1 and r_2), phases (ϕ_1 and ϕ_2), and their derivatives (${r_2}'$, ${\phi_1}'$, ${\phi_2}'$) are also considered to be constants during one period.

By using the equation for $\dot{v}$ at the order of ε:

$$
\begin{cases}
-2\varepsilon\{{r_1}'\sin\theta_1 + r_1{\phi_1}'\cos\theta_1\} = H(r_1, r_2, \theta_1, \theta_2), & (2.3.13a)\\
-2\varepsilon\{{r_2}'\sin\theta_2 + r_2{\phi_1}'\cos\theta_2\} = H(r_2, r_1, \theta_2, \theta_1), & (2.3.13b)
\end{cases}
$$

we have

$$
\begin{cases}
\varepsilon{r_1}' = \dfrac{dr_1}{dt} = -\dfrac{1}{2\pi}\displaystyle\int_0^{2\pi} H(r_1, r_2, \theta_1, \theta_2)\sin\theta_1\, d\theta_1, & (2.3.14a)\\
\varepsilon r_1{\phi_1}' = r_1\dfrac{d\phi_1}{dt} = -\dfrac{1}{2\pi}\displaystyle\int_0^{2\pi} H(r_1, r_2, \theta_1, \theta_2)\cos\theta_1\, d\theta_1, & (2.3.14b)\\
\varepsilon{r_2}' = \dfrac{dr_2}{dt} = -\dfrac{1}{2\pi}\displaystyle\int_0^{2\pi} H(r_2, r_1, \theta_2, \theta_1)\sin\theta_2\, d\theta_2, & (2.3.14c)\\
\varepsilon r_2{\phi_2}' = r_2\dfrac{d\phi_2}{dt} = -\dfrac{1}{2\pi}\displaystyle\int_0^{2\pi} H(r_2, r_1, \theta_2, \theta_1)\cos\theta_2\, d\theta_2. & (2.3.14d)
\end{cases}
$$

We integrate them to obtain

$$\frac{dr_1}{dt} = \frac{1}{2}br_1 + \frac{1}{8}(3k+n+j){r_1}^3 + \left(\frac{1}{4}(k+n) + \frac{1}{8}(k-n+j)\cos 2\phi - \frac{1}{8}(c-h+p)\sin 2\phi\right) r_1{r_2}^2, \tag{2.3.15}$$

$$\frac{d\phi_1}{dt} = -\frac{1}{8}(3c+h+p){r_1}^2 + \left(-\frac{1}{4}(c+h) - \frac{1}{8}(c-h+p)\cos 2\phi - \frac{1}{8}(k-n+j)\sin 2\phi\right) {r_2}^2, \tag{2.3.16}$$

$$\frac{dr_2}{dt} = \frac{1}{2}br_2 + \frac{1}{8}(3k+n+j){r_2}^3 + \left(\frac{1}{4}(k+n) + \frac{1}{8}(k-n+j)\cos 2\phi + \frac{1}{8}(c-h+p)\sin 2\phi\right) {r_1}^2 r_2, \tag{2.3.17}$$

$$\frac{d\phi_2}{dt} = -\frac{1}{8}(3c+h+p){r_2}^2 + \left(-\frac{1}{4}(c+h) - \frac{1}{8}(c-h+p)\cos 2\phi + \frac{1}{8}(k-n+j)\sin 2\phi\right) {r_1}^2, \tag{2.3.18}$$

where we set ϕ to be $\phi = \theta_1 - \theta_2$.

Here, we adopt the summation of phases $\phi_+ = \phi_1 + \phi_2$ and the phase difference $\phi = \phi_1 - \phi_2$ instead of ϕ_1 and ϕ_2. Then we have

$$\frac{d\phi}{dt} = -\frac{1}{8}(c-h+p)({r_1}^2 - {r_2}^2)(1-\cos 2\phi) - \frac{1}{8}(k-n+j)({r_1}^2 + {r_2}^2)\sin 2\phi, \tag{2.3.19}$$

$$\begin{aligned}\frac{d\phi_+}{dt} =& -\frac{1}{8}(5c+3h+p)({r_1}^2 + {r_2}^2) - \frac{1}{8}(c-h+p)({r_1}^2 + {r_2}^2)\cos 2\phi \\ &+ \frac{1}{8}(k-n+j)({r_1}^2 - {r_2}^2)\sin 2\phi.\end{aligned} \tag{2.3.20}$$

In the righthand side of the time evolution equations for r_1, r_2, ϕ, and ϕ_+ in Eqs. (2.3.15), (2.3.17), (2.3.19), and (2.3.20), only r_1, r_2, and ϕ appear, while ϕ_+ does not appear. Thus, the system is intrinsically a three-variable system on r_1, r_2, and ϕ, and ϕ_+ is a slave variable.

Existence and linear stability of rotational motion

In this subsection, a solution for rotational motion is constructed, and then its linear stability is analyzed. Here, we define rotational motion as the motion with a constant distance from the origin having a constant velocity.

Firstly, we construct a solution for rotational motion. The solution for rotational motion should satisfy $r_1 = r_2 =$ const. and $\phi = \pm\pi/2 =$ const. It is noted that $\phi = \pi/2$ and $\phi = -\pi/2$ correspond to counterclockwise and clockwise rotation on x_1-x_2 plane, respectively. Thus we set

$$r_1 = r_2 = r_{\mathrm{rot}} > 0, \qquad (r_{\mathrm{rot}} = \mathrm{const.}) \tag{2.3.21}$$

$$\phi = \pm\frac{\pi}{2}, \tag{2.3.22}$$

and derive r_{rot}. By substituting $(r_1,\ r_2,\ \phi) = (r_{\mathrm{rot}},\ r_{\mathrm{rot}},\ \pm\pi/2)$ into Eq. (2.3.15), we have

$$\dot{r}_1 = \frac{1}{2}br_{\mathrm{rot}} + \frac{1}{2}(k+n){r_{\mathrm{rot}}}^3. \tag{2.3.23}$$

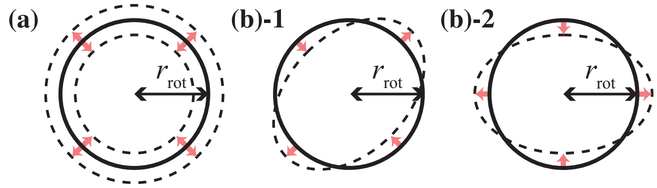

Figure 2.3.2: Schematic illustration of the mode of perturbation represented on x_1-x_2 plane, corresponding to each eigenvector. (a) Extension or contraction of the radius and (b,c) deformation to an elliptic orbit. The corresponding eigenvalues are (a) $-b$, (b,c) $(k-n+j){r_{\rm rot}}^2/2$. Here we consider the case that $c=h=p=0$. Reproduced from Ref. [37].

$\dot{r}_1$ should be zero when $(r_1, r_2, \phi) = (r_{\rm rot}, r_{\rm rot}, \pm\pi/2)$ is a fixed point. From a viewpoint of physics, $r_{\rm rot}$ should be positive. Thus, we obtain $r_{\rm rot} = \sqrt{-b/(k+n)}$ for $k+n<0$, since b is set to be a positive value. By substituting $(r_1, r_2, \phi) = (r_{\rm rot}, r_{\rm rot}, \pm\pi/2)$ into Eq. (2.3.19), we also have $\dot{\phi}=0$, and thus it is shown that $(r_1, r_2, \phi) = (r_{\rm rot}, r_{\rm rot}, \pm\pi/2)$ is a fixed point corresponding to rotational motion.

Then we investigate the linear stability of the fixed point $(r_1, r_2, \phi) = (r_{\rm rot}, r_{\rm rot}, \pm\pi/2)$. Here we set the perturbations for r_1, r_2, and ϕ, which are denoted as Δr_1, Δr_2, and $\Delta\phi$, respectively. The linearized equation around the fixed point is obtained as:

$$\begin{aligned}\begin{pmatrix} \Delta\dot{r}_1 \\ \Delta\dot{r}_2 \\ \Delta\dot{\phi} \end{pmatrix} &= \begin{pmatrix} \dfrac{b}{2} + \dfrac{1}{4}(5k+3n+j){r_{\rm rot}}^2 & \dfrac{1}{4}(k+3n-j)\,{r_{\rm rot}}^2 & \dfrac{1}{4}(c-h+p){r_{\rm rot}}^3 \\ \dfrac{1}{4}(k+3n-j)\,{r_{\rm rot}}^2 & \dfrac{b}{2} + \dfrac{1}{4}(5k+3n+j){r_{\rm rot}}^2 & -\dfrac{1}{4}(c-h+p){r_{\rm rot}}^3 \\ -\dfrac{1}{2}(c-h+p)r_{\rm rot} & \dfrac{1}{2}(c-h+p)r_{\rm rot} & \dfrac{1}{2}(k-n+j){r_{\rm rot}}^2 \end{pmatrix} \begin{pmatrix} \Delta r_1 \\ \Delta r_2 \\ \Delta\phi \end{pmatrix} \\ &\equiv \begin{pmatrix} \alpha & \beta & \gamma \\ \beta & \alpha & -\gamma \\ \delta & -\delta & \varepsilon \end{pmatrix} \begin{pmatrix} \Delta r_1 \\ \Delta r_2 \\ \Delta\phi \end{pmatrix}. \end{aligned} \tag{2.3.24}$$

The eigenvalues of the matrix in Eq. (2.3.24) are $\alpha+\beta$ and $(\alpha-\beta+\varepsilon)/2 \pm \sqrt{(\alpha-\beta-\varepsilon)^2 + 8\gamma\delta}/2$. The eigenvalues rewritten by b, c, h, j, k, n, and p instead of α, β, γ, δ, and ε are $-b$ and $(k-n+j){r_{\rm rot}}^2/2 \pm i|c-h+p|{r_{\rm rot}}^2/2$. The condition $k-n+j<0$ is required for the linear stability of the fixed point. When c, h, and p are zero, the corresponding eigenvector for $-b$ is $(1/\sqrt{2}, 1/\sqrt{2}, 0)$, and the corresponding eigenvectors for $(k-n+j){r_{\rm rot}}^2/2$ are $(1/\sqrt{2}, -1/\sqrt{2}, 0)$ and $(0,0,1)$. Here the eigenvalue $(k-n+j){r_{\rm rot}}^2/2$ is degenerated.

In Fig. 2.3.2, the schematic illustration of the deformations of the orbit for the rotational motion by the perturbations in the directions of eigenvectors is shown.

Therefore, we have the conditions for the linearly stable rotation as follows:

$$\begin{cases} k+n<0, & \text{(Condition for the existence of the radius)}, \quad (2.3.25\text{a}) \\ k-n+j<0, & \text{(Condition for the linear stability for the phase difference)}. \quad (2.3.25\text{b}) \end{cases}$$

Existence and linear stability of oscillatory motion

In this subsection, a solution for oscillatory motion is constructed, and then its linear stability is analyzed. Here, we define oscillatory motion as the reciprocal motion whose center is the origin of x_1-x_2 plane.

First, we construct a solution for stable oscillatory motion. Here we set the amplitude of oscillation to be $r_{\mathrm{osc}} = \text{const.}$ and the direction of oscillation in x_1-x_2 plane to be ψ. The domain of definition for ψ is $0 \leq \psi < \pi$. Thus, the fixed point in (r_1, r_2, ϕ) for oscillatory motion should be $r_1 = r_{\mathrm{osc}} \cos\psi$, $r_2 = r_{\mathrm{osc}} \sin\psi$, and $\phi = 0$. By substituting the fixed point into Eqs. (2.3.15), (2.3.17), and (2.3.19), we have

$$\dot{r}_1 = \frac{1}{2} b r_{\mathrm{osc}} \cos\psi + \frac{1}{8}(3k + n + j) {r_{\mathrm{osc}}}^3 \cos\psi, \tag{2.3.26}$$

$$\dot{r}_2 = \frac{1}{2} b r_{\mathrm{osc}} \sin\psi + \frac{1}{8}(3k + n + j) {r_{\mathrm{osc}}}^3 \sin\psi, \tag{2.3.27}$$

$$\dot{\phi} = 0. \tag{2.3.28}$$

The fixed point $(r_{\mathrm{osc}} \cos\psi, r_{\mathrm{osc}} \sin\psi, 0)$ satisfies $\dot{r}_1 = 0$, $\dot{r}_2 = 0$, and $\dot{\phi} = 0$. Thus we have $r_{\mathrm{osc}} = 2\sqrt{-b/(3k + n + j)}$, where the condition $3k + n + j < 0$ is required for $r_{\mathrm{osc}} > 0$.

Then we investigate the linear stability of the fixed point $(r_{\mathrm{osc}} \cos\psi, r_{\mathrm{osc}} \sin\psi, 0)$, in the same manner as in the case of rotational motion. We set the perturbations for r_1, r_2, and ϕ to be Δr_1, Δr_2, and $\Delta\phi$, respectively. The linearized equation around the fixed point is obtained as:

$$\begin{pmatrix} \dot{\Delta r_1} \\ \dot{\Delta r_2} \\ \dot{\Delta \phi} \end{pmatrix} = \begin{pmatrix} -b\cos^2\psi & -b\sin\psi\cos\psi & -\frac{1}{4}(c - h + p){r_{\mathrm{osc}}}^3 \sin^2\psi\cos\psi \\ -b\sin\psi\cos\psi & -b\sin^2\psi & \frac{1}{4}(c - h + p){r_{\mathrm{osc}}}^3 \sin\psi\cos^2\psi \\ 0 & 0 & -\frac{1}{4}(k - n + j){r_{\mathrm{osc}}}^2 \end{pmatrix} \begin{pmatrix} \Delta r_1 \\ \Delta r_2 \\ \Delta\phi \end{pmatrix}. \tag{2.3.29}$$

The eigenvalues of the matrix in Eq. (2.3.29) are $-b$, 0, and $\tilde{\varepsilon} = -(k - n + j){r_{\mathrm{osc}}}^2/4$. The condition $k - n + j > 0$ is required for the linear stability of the fixed point. The corresponding eigenvector for $-b$, 0, and $-(k - n + j){r_{\mathrm{osc}}}^2/4$ are $(\cos\psi, \sin\psi, 0)$, $(-\sin\psi, \cos\psi, 0)$, and $(0, 0, 1)$, respectively.

In Fig. 2.3.3, the schematic illustration of the deformations of the orbit for the oscillatory motion by the perturbations in the directions of eigenvectors is shown. The eigenvalue 0 means that the solution for oscillatory motion is neutral for the perturbation in the direction $(0, 0, 1)$, reflecting the symmetric property of the system.

Therefore, we have the conditions for the linearly stable oscillation as follow:

$$\begin{cases} 3k + n + j < 0, & \text{(Condition for the existence of the amplitude)}, \quad (2.3.30\text{a}) \\ k - n + j > 0, & \text{(Condition for the linear stability of the phase difference)}. \quad (2.3.30\text{b}) \end{cases}$$

2.3.3 Discussion on the results of weakly nonlinear analysis

We obtained the conditions for stable rotational motion:

$$\begin{cases} k + n < 0, & \text{(Condition for the existence of the radius)}, \quad (2.3.31\text{a}) \\ k - n + j < 0, & \text{(Condition for the linear stability for the phase difference)}, \quad (2.3.31\text{b}) \end{cases}$$

and those for oscillatory motion:

$$\begin{cases} 3k + n + j < 0, & \text{(Condition for the existence of the amplitude)}, \quad (2.3.32\text{a}) \\ k - n + j > 0, & \text{(Condition for the linear stability of the phase difference)}, \quad (2.3.32\text{b}) \end{cases}$$

by the weakly nonlinear analysis. From these conditions (2.3.31) and (2.3.32), only three coefficients of the third-order terms, k, n, and j, appear and the other coefficients of them, c, h, and p, do

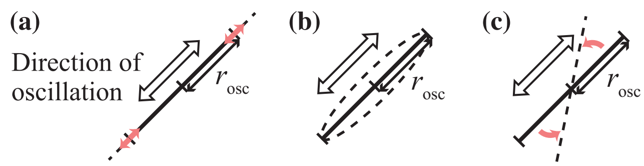

Figure 2.3.3: Schematic illustration of the mode of perturbation represented on x_1-x_2 plane, corresponding to each eigenvector. (a) Extension or contraction of the amplitude, (b) deformation to an elliptic orbit, and (c) rotation of oscillatory direction. The corresponding eigenvalues are (a) $-b$, (b) $-(k-n+j){r_{\mathrm{osc}}}^2/4$, and (c) 0. Here we consider the case that $c=h=p=0$. Reproduced from Ref. [37].

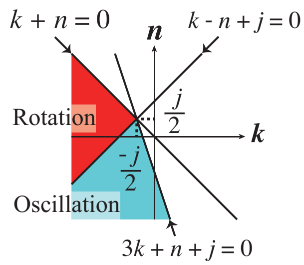

Figure 2.3.4: Phase diagram for the stable motion. The diagram is plotted on k-n plane based on the result of the weakly nonlinear analysis. Here the parameter j is fixed. The parameter set for stable rotational and oscillatory motion are indicated red and cyan.

not appear. It is also said that the parameter region where rotational and oscillatory motion are bistable does not exist within the regime of the weakly nonlinear analysis. The results (2.3.31) and (2.3.32) are summarized in Fig. 2.3.4.

Here we consider the physical meaning of the terms $k|\boldsymbol{v}|^2\boldsymbol{v}$, $n|\boldsymbol{x}|^2\boldsymbol{v}$, and $j(\boldsymbol{x}\cdot\boldsymbol{v})\boldsymbol{x}$, which determine the type of stable motion. In the case of $k<0$, $n<0$, and $j<0$, the term $k|\boldsymbol{v}|^2\boldsymbol{v}$ is a velocity-dependent energy dissipation and $n|\boldsymbol{x}|^2\boldsymbol{v}$ and $j(\boldsymbol{x}\cdot\boldsymbol{v})\boldsymbol{x}$ are position-dependent energy dissipations. In particular, the position-dependent energy dissipations depend on not only the position but also the direction of the velocity. The terms $n|\boldsymbol{x}|^2\boldsymbol{v}$ and $j(\boldsymbol{x}\cdot\boldsymbol{v})\boldsymbol{x}$ are decomposed in the radial direction $\boldsymbol{e}^r$ and angular direction $\boldsymbol{e}^\theta$ as follows:

$$\begin{aligned} n|\boldsymbol{x}|^2\boldsymbol{v}+j(\boldsymbol{x}\cdot\boldsymbol{v})\boldsymbol{x} =& \left(\Gamma^{\parallel}_{ij}+\Gamma^{\perp}_{ij}\right)(nx_kx_kv_j+j(x_kv_k)x_j) \\ =&(n+j)|\boldsymbol{x}|(\boldsymbol{x}\cdot\boldsymbol{v})\boldsymbol{e}^r+n|\boldsymbol{x}|(xv_y-yv_x)\boldsymbol{e}^\theta, \end{aligned} \tag{2.3.33}$$

where $\Gamma^{\parallel}_{ij}=x_ix_j/|\boldsymbol{x}|^2$ and $\Gamma^{\perp}_{ij}=\delta_{ij}-x_ix_j/|\boldsymbol{x}|^2$. To simplify the coefficients of $\boldsymbol{e}^r$ and $\boldsymbol{e}^\theta$, they are expressed v_r and v_θ, where $\boldsymbol{v}=v_r\boldsymbol{e}^r+v_\theta\boldsymbol{e}^\theta$. Since v_r and v_θ are given by $v_r=x_iv_i/|\boldsymbol{x}|$ and $v_\theta=E_{ij}x_iv_j/|\boldsymbol{x}|$, we have

$$v_r\boldsymbol{e}^r =\Gamma^{\parallel}_{ij}v_j=\frac{x_kv_kx_i}{x_kx_k}=\frac{\boldsymbol{x}\cdot\boldsymbol{v}}{|\boldsymbol{x}|}\frac{\boldsymbol{x}}{|\boldsymbol{x}|}, \tag{2.3.34}$$

$$v_\theta\boldsymbol{e}^\theta =\Gamma^{\perp}_{ij}v_j=\frac{E_{kl}x_kv_lE_{ij}x_j}{x_kx_k}=\frac{x_1v_2-x_2v_1}{|\boldsymbol{x}|}\frac{\boldsymbol{x}^\perp}{|\boldsymbol{x}|}. \tag{2.3.35}$$

Here E is a 2 by 2 matrix, where $E_{11} = E_{22} = 0$, $E_{12} = -1$, and $E_{21} = 1$. Here $\boldsymbol{x}^{\perp}$ is defined as $\boldsymbol{x}^{\perp} = |\boldsymbol{x}|\boldsymbol{e}^{\theta}$ Then Eq. (A.3.33) is expressed as

$$\begin{aligned} n|\boldsymbol{x}|^2\boldsymbol{v} + j(\boldsymbol{x}\cdot\boldsymbol{v})\boldsymbol{x} = &\left(\Gamma^{\parallel}_{ij} + \Gamma^{\perp}_{ij}\right)(nx_kx_kv_j + j(x_kv_k)x_j) \\ =&(n+j)x_kx_kv_r{e^r}_i + nx_kx_kv_\theta {e^\theta}_i \\ =&(n+j)|\boldsymbol{x}|^2 v_r\boldsymbol{e}^r + n|\boldsymbol{x}|^2 v_\theta \boldsymbol{e}^\theta. \end{aligned} \tag{2.3.36}$$

Thus, it is concluded that the force $n|\boldsymbol{x}|^2\boldsymbol{v}$ is isotropic, but $j(\boldsymbol{x}\cdot\boldsymbol{v})\boldsymbol{x}$ is anisotropic with regard to the position of a considered self-propelled particle. Here ${e^r}_i = x_i/(x_kx_k)$ and ${e^\theta}_i = E_{ij}x_j/(x_kx_k)$.

As for the mathematical model exhibiting limit-cycle oscillation, van der Pol equation [76]:

$$\ddot{x} + (p_1 + q_1x^2)\dot{x} + x = 0, \qquad (p_1 < 0, q_1 > 0) \tag{2.3.37}$$

and Rayleigh equation [77]:

$$\ddot{x} + (p_2 + q_2\dot{x}^2)\dot{x} + x = 0, \qquad (p_2 < 0, q_2 > 0) \tag{2.3.38}$$

are familiar. Since these two equations converted into the same form, there is no qualitative difference in terms of bifurcation structure. By extending van der Pol equation (2.3.37) and Rayleigh equation (2.3.38) into the two-dimensional axisymmetric system, we have

$$\ddot{\boldsymbol{x}} + (P_1 + Q_1|\boldsymbol{x}|^2)\dot{\boldsymbol{x}} + \boldsymbol{x} = 0, \qquad (P_1 < 0, Q_1 > 0), \tag{2.3.39}$$

$$\ddot{\boldsymbol{x}} + (P_2 + Q_2|\dot{\boldsymbol{x}}|^2)\dot{\boldsymbol{x}} + \boldsymbol{x} = 0, \qquad (P_2 < 0, Q_2 > 0). \tag{2.3.40}$$

By comparing with our model in Eq. (2.3.3), van der Pol-like equation (2.3.39) and Rayleigh-like equation (2.3.40) exhibit stable rotational and oscillatory motion, respectively.

The both Rayleigh and van der Pol equations in Eqs. (2.3.37) and (2.3.38) show qualitatively the same limit-cycle oscillation, i.e., the forms of third order of dissipative terms do not affect so much. However, the forms of third order terms in Eqs. (2.3.39) and (2.3.40) play an important role to determine the stable orbit.

2.3.4 Conserved quantity for the model equation

In this subsection, the third order terms $c|\boldsymbol{x}|^2\boldsymbol{x}$, $h|\boldsymbol{v}|^2\boldsymbol{x}$, and $p(\boldsymbol{x}\cdot\boldsymbol{v})\boldsymbol{v}$ in Eq. (2.3.3), which do not affect the results of the weakly nonlinear analysis, are discussed. Here we consider a conserved quantity F for the dynamical system in Eq. (2.3.3) with $b = k = n = j = 0$:

$$\begin{cases} \dot{\boldsymbol{x}} = \boldsymbol{v}, & (2.3.41\text{a}) \\ \dot{\boldsymbol{v}} = a\boldsymbol{x} + c|\boldsymbol{x}|^2\boldsymbol{x} + h|\boldsymbol{v}|^2\boldsymbol{x} + p(\boldsymbol{x}\cdot\boldsymbol{v})\boldsymbol{v}. & (2.3.41\text{b}) \end{cases}$$

The conserved quantity $F = F(\boldsymbol{x}, \boldsymbol{v})$ should satisfy the following equation:

$$\frac{dF}{dt} = \frac{\partial F}{\partial x_i}\dot{x}_i + \frac{\partial F}{\partial v_i}\dot{v}_i = 0. \tag{2.3.42}$$

From Eq. (2.3.42), the conserved quantity F is explicitly derived as follows:

$$F(\boldsymbol{x}, \boldsymbol{v}) = f\left(\exp(-(h+p)|\boldsymbol{x}|^2)\left(\frac{c}{(h+p)^2} + \frac{a}{h+p} + |\boldsymbol{v}|^2 + \frac{c}{h+p}|\boldsymbol{x}|^2\right)\right), \tag{2.3.43}$$

where $f(\cdot) \in C^1(\mathbb{R})$ is an arbitrary function. Since we heuristically found the form of conserved quantity in Eq. (2.3.43), we can confirm that F is a conserved quantity by the following calculation:

$$\begin{aligned}\frac{dF}{dt} =& \frac{df}{dY}\frac{\partial Y}{\partial x_i}\dot{x}_i + \frac{df}{dY}\frac{\partial Y}{\partial v_i}\dot{v}_i \\ =& \frac{df}{dY}\left[-2(h+p)\exp(-(h+p)|\boldsymbol{x}|^2)\left(\frac{c}{(h+p)^2} + \frac{a}{h+p} + |\boldsymbol{v}|^2 + \frac{c}{h+p}|\boldsymbol{x}|^2\right)x_i v_i\right. \\ &+ 2\exp(-(h+p)|\boldsymbol{x}|^2)\frac{c}{h+p}x_i v_i \\ &\left. +2\exp(-(h+p)|\boldsymbol{x}|^2)(ax_i + cx^2 x_i + hv^2 x_i + px_j v_j v_i)v_i\right] \\ =& 2\frac{df}{dY}\exp(-(h+p)|\boldsymbol{x}|^2)\left[-\left(\frac{c}{h+p} + a + (h+p)|\boldsymbol{v}|^2 + c|\boldsymbol{x}|^2\right)x_i v_i\right. \\ &\left. + \frac{c}{h+p}x_i v_i + (ax_i + c|\boldsymbol{x}|^2 x_i + h|\boldsymbol{v}|^2 x_i + px_j v_j v_i)v_i\right] \\ =& 0, \end{aligned} \tag{2.3.44}$$

where Y is the argument of f in Eq. (2.3.43), i.e.,

$$Y = \exp(-(h+p)|\boldsymbol{x}|^2)\left(\frac{c}{(h+p)^2} + \frac{a}{h+p} + |\boldsymbol{v}|^2 + \frac{c}{h+p}|\boldsymbol{x}|^2\right). \tag{2.3.45}$$

It is noted that F is not energy for arbitrary f. If F was energy, the dynamical system (2.3.41) should be derived from the Hamiltonian equation:

$$\dot{x}_i = \frac{\partial F}{\partial v_i} = \frac{df}{dY}\frac{\partial X}{\partial v_i}, \tag{2.3.46}$$

$$\dot{v}_i = -\frac{\partial F}{\partial x_i} = -\frac{df}{dY}\frac{\partial X}{\partial x_i}. \tag{2.3.47}$$

Since $\partial Y/\partial x_i$ and $\partial Y/\partial v_i$ are calculated as

$$\frac{\partial Y}{\partial x_i} = -2\exp\left((h+p)|\boldsymbol{x}|^2\right)\left(a + (h+p)|\boldsymbol{v}|^2 + c|\boldsymbol{x}|^2\right), \tag{2.3.48}$$

$$\frac{\partial Y}{\partial v_i} = 2\exp\left((h+p)|\boldsymbol{x}|^2\right)v_i, \tag{2.3.49}$$

the function $f(Y)$ which holds Eqs. (2.3.46) and (2.3.47) should satisfy

$$\frac{df}{dY} = \frac{1}{2}\exp\left((h+p)|\boldsymbol{x}|^2\right). \tag{2.3.50}$$

When the coefficients h and p are zero, Y is not defined. The potential energy $U(\boldsymbol{x})$ is however defined instead of F:

$$U(\boldsymbol{x}) = -\frac{a|\boldsymbol{x}|^2}{2} - \frac{c|\boldsymbol{x}|^4}{4}, \tag{2.3.51}$$

and mechanical energy $E = K + U$ is also where $K = |\boldsymbol{v}|^2/2$.

By setting $f(Y) = Y/2$ and $w = h + p$, and expanding F around $w = 0$, we have

$$\begin{aligned}
F =& \frac{1}{2}\exp(-w|\boldsymbol{x}|^2)\left(\frac{c}{w^2} + \frac{a}{w} + |\boldsymbol{v}|^2 + \frac{c}{w}|\boldsymbol{x}|^2\right) \\
\simeq& \frac{1}{2}\left(1 - w|\boldsymbol{x}|^2 + \frac{1}{2}w^2|\boldsymbol{x}|^4\right)\left(\frac{c}{w^2} + \frac{a}{w} + |\boldsymbol{v}|^2 + \frac{c}{w}|\boldsymbol{x}|^2\right) \\
=& \frac{c}{2w^2} + \frac{a}{2w} + \frac{|\boldsymbol{v}|^2}{2} - \frac{a}{2}|\boldsymbol{x}|^2 - \frac{c}{2}|\boldsymbol{x}|^4 + \frac{c}{4}|\boldsymbol{x}|^4 + \mathcal{O}(w) \\
=& \frac{|\boldsymbol{v}|^2}{2} - \frac{a}{2}|\boldsymbol{x}|^2 - \frac{c}{4}|\boldsymbol{x}|^4 + \text{const.} + \mathcal{O}(w) \\
=& E + \text{const.} + \mathcal{O}(w). \qquad (2.3.52)
\end{aligned}$$

Thus F can be considered to be mechanical energy in the limit of $w \to 0$, though it is not mechanical energy for finite w ($w \neq 0$).

2.3.5 Stable motion in the region beyond the weakly nonlinear analysis

So far we discuss the stable motion with an infinitesimally small $b > 0$. In this subsection, we consider the case with a finite value of b.

For rotational motion, we succeed to construct a solution for rotational motion even though b is not infinitesimally small. We also analyze the linear stability of the solution for rotational motion.

By transforming the variables x_1, x_2, v_1, and v_2 in Eq. (2.3.3) to $r = \sqrt{{x_1}^2 + {x_2}^2}$, $v = \sqrt{{v_1}^2 + {v_2}^2}$, and $\Theta = \cos^{-1}((\boldsymbol{x}\cdot\boldsymbol{v})/(rv))$, we have the following dynamical system:

$$\begin{cases}
\dot{r} = v\cos\Theta, & (2.3.53\text{a}) \\
\dot{v} = -r\cos\Theta + bv + cr^3\cos\Theta + (h+p)rv^2\cos\Theta & \\
\qquad + \left(n + \dfrac{j}{2}\right)r^2 v + \dfrac{j}{2}r^2 v\cos 2\Theta + kv^3, & (2.3.53\text{b}) \\
v\dot{\Theta} = -\dfrac{v^2}{r}\sin\Theta + r\sin\Theta - cr^3\sin\Theta - hrv^2\sin\Theta - \dfrac{j}{2}r^2 v\sin 2\Theta. & (2.3.53\text{c})
\end{cases}$$

In this dynamical system, the fixed point for rotational motion is expressed as $(r_0, v_0, \pm\pi/2)$, where r_0 and v_0 are both positive.

Here we assume $c = h = p = 0$, i.e., the terms which do not affect the results of weakly nonlinear analysis are neglected. First, the fixed point is determined. By substituting $(r_0, v_0, \pm\pi/2)$ to the dynamical system (2.3.53), we have

$$\begin{cases}
\dot{r} = 0, & (2.3.54\text{a}) \\
\dot{v} = bv_0 + n{r_0}^2 v_0 + k{v_0}^3, & (2.3.54\text{b}) \\
\dot{\Theta} = -\dfrac{v_0}{r_0} + \dfrac{r_0}{v_0}. & (2.3.54\text{c})
\end{cases}$$

Since the fixed point satisfies $\dot{r} = \dot{v} = \dot{\Theta} = 0$, we have ${r_0}^2 = {v_0}^2$ and ${v_0}^2 = -b/(k+n)$. Since $r_0 > 0$ and $b > 0$ hold, $k + n < 0$ is required for the existence of the fixed point corresponding to rotational motion.

Then the linear stability of the fixed point is discussed. The perturbation terms Δr, Δv, and $\Delta\Theta$ are introduced as $r = r_0 + \Delta r$, $v = v_0 + \Delta v$, and $\Theta = \pi/2 + \Delta\Theta$, respectively. By substituting them into Eq. (2.3.54), we have the following equations for the time evolution equation for Δr, Δv, and $\Delta\Theta$:

$$\begin{pmatrix} \dot{\Delta r} \\ \dot{\Delta v} \\ \dot{\Delta\Theta} \end{pmatrix} = \begin{pmatrix} 0 & 0 & -r_0 \\ 2n{r_0}^2 & 2k{r_0}^2 & r_0 \\ \dfrac{2}{r_0} & -\dfrac{2}{r_0} & j{r_0}^2 \end{pmatrix} \begin{pmatrix} \Delta r \\ \Delta v \\ \Delta\Theta \end{pmatrix}. \tag{2.3.55}$$

Here we neglect the square and higher-order terms of Δr, Δv, and $\Delta\Theta$. The characteristic polynomial of the matrix is given by

$$\lambda^3 - (2k+j){r_0}^2\lambda^2 + 2(kj{r_0}^4 + 2)\lambda + 4b = 0. \tag{2.3.56}$$

Here we define $V(\lambda)$ as $V(\lambda) = \lambda^3 - (2k+j){r_0}^2\lambda^2 + 2(kj{r_0}^4 + 2)\lambda + 4b$. Considering $4b > 0$, the one of the solutions of $V(\lambda) = 0$ has a negative real value. There are two possible cases for the rest two solutions of $V(\lambda) = 0$ as follows.

- Case I: All solutions are real.
  As shown before, one of the solutions is negative. The signs of the other two solutions are unknown, but they are the same and unchanged by changing the parameters k, n, and j, since the intercept is always positive.

- Case II: One of the solutions is negative and two of them are complex conjugates.
  The signs of the real parts of the complex conjugates are the same, and may be changed by changing the parameters k, n, and j.

Thus, any bifurcation does not occur for the former case but it does for the latter case. Here, we assume that the solution of $V(\lambda) = 0$ has negative real value and complex conjugates, and examine that the real parts of complex conjugates can be zero for a certain parameter set of b, k, n, and j. If we obtain a relation among b, k, n, and j where the sign of the complex conjugates changes, a bifurcation occurs at where the parameter set satisfies the relation. We set two complex conjugates solutions to be $\lambda_\pm = \xi \pm i\zeta$ ($\xi, \zeta \in \mathbb{R}$, $\zeta > 0$) and the real solution to be λ_r, and then we have

$$\begin{cases} \lambda_r + \lambda_+ + \lambda_- = \lambda_r + 2\xi = (2k+j){r_0}^2, & \text{(2.3.57a)} \\ \lambda_r\lambda_+ + \lambda_+\lambda_- + \lambda_-\lambda_r = 2\lambda_r\xi + \xi^2 + \zeta^2 = 2(kj{r_0}^4 + 2), & \text{(2.3.57b)} \\ \lambda_r\lambda_+\lambda_- = \lambda_r(\xi^2 + \zeta^2) = -4b. & \text{(2.3.57c)} \end{cases}$$

When $\xi = 0$, Eqs. (2.3.57) become

$$\begin{cases} \lambda_r = (2k+j){r_0}^2, & \text{(2.3.58a)} \\ \zeta^2 = 2(kj{r_0}^4 + 2), & \text{(2.3.58b)} \\ \lambda_r\zeta^2 = -4b. & \text{(2.3.58c)} \end{cases}$$

By eliminating λ_r and ζ from Eqs. (2.3.58), we have

$$(2k+j)kjb^2 = -2(k-n+j)(k+n)^2. \tag{2.3.59}$$

Thus a bifurcation occurs and the stability of the fixed point corresponding to rotational motion changes at the surface expressed in Eq. (2.3.59) in the parameter space. The result is shown in Fig. 2.3.5. For $b = 0$, Eq. (2.3.59) becomes $k - n + j = 0$ and the result is consistent with the result by weakly nonlinear analysis in Eq. (2.3.25).

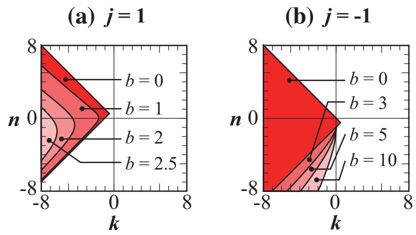

Figure 2.3.5: Phase diagram on k-n plane showing the parameter region for various b where the rotational motion is stable. The parameter j is set to be (a) $j = 1$ and (b) $j = -1$. For $b = 0$, the result obtained here corresponds to the result obtained by weakly nonlinear analysis as shown in Fig. 2.3.4.

For the oscillatory motion, on the other hand, we have not succeeded to construct a solution for finite $b > 0$.

Here we introduce a related previous work by Keith and Rand [78]. They analyzed the dynamical system:

$$\ddot{x} = -x + \epsilon\dot{x}\left(1 - \alpha x^2 - \beta\dot{x}^2\right), \tag{2.3.60}$$

and analytically obtained the condition for the stable limit-cycle oscillation,

$$\alpha + 3\beta > 0, \tag{2.3.61}$$

when ϵ is infinitesimally small. Since the third-order terms $|\boldsymbol{x}|^2\boldsymbol{v}$ and $(\boldsymbol{x}\cdot\boldsymbol{v})\boldsymbol{v}$ in Eq. (2.3.3) are the same when the motion is limited to the line through the center of the system, b, $n + j$, and k in Eq. (2.3.3) correspond to ϵ, α, and β, respectively. Thus the condition for the existence of the amplitude in Eq. (2.3.30)(a) is the same as the condition in Eq. (2.3.61).

They also performed the numerical simulations with finite ϵ, and found that the line corresponding to the threshold in Eq. (2.3.61) bends at the origin on the α-β plane. The degree of bending becomes greater with an increase in ϵ, and the threshold approaches a combination of two half-lines, $\alpha = 0$ for $\beta < 0$ and $\beta = 0$ for $\alpha < 0$, when $\epsilon \to +\infty$.

2.3.6 Comparison with the numerical results

To confirm the validity of the theoretical results, we numerically calculated the time evolution of $\boldsymbol{x}$ and $\boldsymbol{v}$ based on Eq. (2.3.3) using the Euler method. We also checked whether there were quasi-periodic orbits or not. We used adaptive mesh method for the time step. The adaptive mesh was set for each time step so that the changes in x_1, x_2, v_1, and v_2 did not exceed the thresholds for them.

First, we show typical examples of stable rotational and oscillatory motion in Fig. 2.3.6. The stable motion depended on the parameter sets in Eq. (2.3.3). The parameter sets used in the calculation and the stable motion were consistent with the theoretical results.

Next, by scanning the parameter sets, we made phase diagrams which show the kinds of stable motion as shown in Fig. 2.3.7. The detailed manner is shown in Appendix A.2.1. The results were compared with the theoretical results by the weakly nonlinear analysis in Eqs. (2.3.25) and (2.3.30) and also that for finite b in Eq. (2.3.59). The theoretical results matched well with the numerical results.

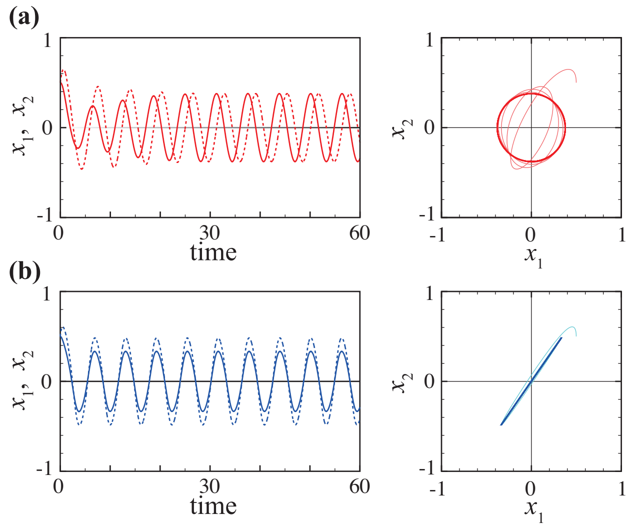

Figure 2.3.6: Time evolutions of x_1 and x_2 and trajectories on the x_1-x_2 plane for stable (a) rotational and (b) oscillatory motion, respectively. The lighter- and darker-colored curves show the transient trajectory and the trajectory after sufficiently long time. The parameters were set to be $b = 1$ and $j = c = h = p = 0$ for both (a) and (b), and the other parameters were (a) $k = -5$, $n = -2$, (b) $k = -2$, $n = -5$. The initial conditions were set to be $x_1 = 0.5$, $x_2 = 0.5$, $v_1 = 0$, and $v_2 = 0.5$ for both cases. Reproduced from Ref. [37].

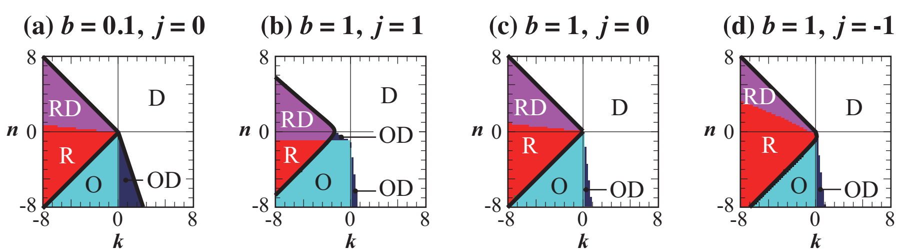

Figure 2.3.7: Comparison of the theoretical results with the numerical ones. The parameter b was set to be (a) 0.1 and (b-d) 1. The symbols R, O, D, RD, and OD indicate stable rotational motion, stable oscillatory motion, divergence to the infinity, coexistence of stable rotational motion and divergence, and coexistence of stable oscillatory motion and divergence. The black line in (a) shows the conditions for stable rotation and oscillation obtained by the weakly nonlinear analysis in Eqs. (2.3.25) and (2.3.30). Those in (b-d) show the conditions for stable rotation for finite $b > 0$ in Eq. (2.3.59). Reproduced from Ref. [37].

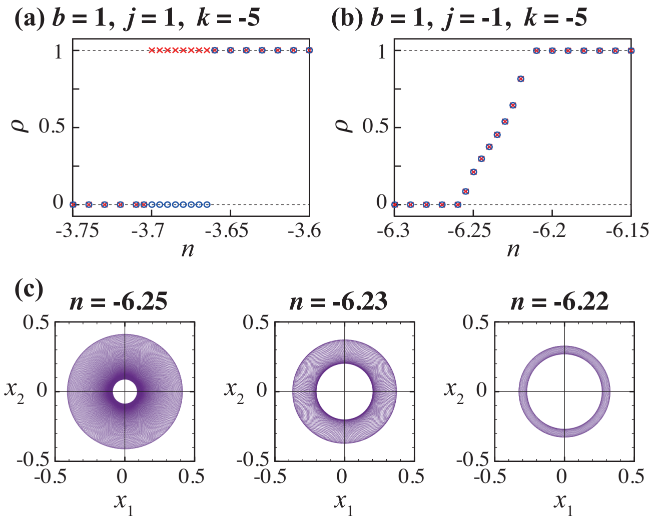

Figure 2.3.8: Dependence of $\rho(= r_{\min}/r_{\max})$ on n after sufficiently long time evolution (after time interval 100000). The parameters were set to be $b = 1$, $k = -5$, $c = h = p = 0$, (a) $j = 1$, and (b) $j = -1$. Between the region where rotational and oscillatory motion was stable, the region where rotational and oscillatory motion were bistable and the region where quasiperiodic orbits were stable were seen in the plots (a) and (b), respectively. The initial conditions in (i) and (ii) in Table A.1 in Appendix A.2.1 were adopted, and the obtained ρ is shown as cross and circle, respectively. (c) Quasiperiodic orbit on x_1-x_2 plane. The parameters were the same as in (b) and the values of n are indicated in the figure. Reproduced from Ref. [37].

We performed numerical calculation precisely near the boundaries on the parameter space between the regions where the rotational and oscillatory motions were observed. We found that the bistable region of rotational and oscillatory motions and also the motion with quasiperiodic orbits. We introduced $\rho = r_{\min}/r_{\max}$, where $r_{\min}$ and $r_{\max}$ are the minimun and maximun of $r = \sqrt{x_1{}^2 + x_2{}^2}$, and detected ρ as shown in Fig. 2.3.8. The variable ρ characterizes the motion: In this case, $\rho = 1$, $\rho = 0$, and $0 < \rho < 1$ correspond to rotational, oscillatory, and quasiperiodic motion, respectively.

To see the quasiperiodic orbit, we calculated the trajectories with a larger b, i.e. with more energy injection. In Fig. 2.3.9, we show the obtained quasiperiodic orbits for $b = 2$. The quasiperiodic orbit was something like an elliptic orbit whose major (minor) axis was slowly rotating.

2.3.7 Summary for Section 2.3

The general equation for motion of a self-propelled particle in a two-dimensional axisymmetric system is derived. By the weakly nonlinear analysis, the conditions for stable rotational and oscillatory motion are obtained. We confirmed the validity of the results of the weakly nonlinear analysis by numerical calculations. We also found the parameter region where quasi-periodic orbits are stably observed [37]. As future work, we expect that the quasiperiodic orbit can be analyzed in detail by considering the stable manifold where the quasi-periodic orbits are stable [79].

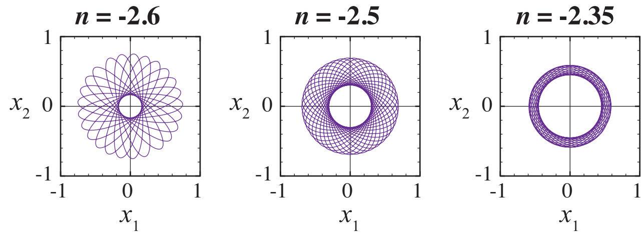

Figure 2.3.9: Quasiperiodic orbits on the x_1-x_2 plane. The parameters were set to be $b = 2$, $k = -5$, $c = h = p = 0$, $j = 1$, and the values of n are shown in the figure. Reproduced from Ref. [37].

2.4 Camphor particle in a circular region

As an extension of the one-dimensional system in Sec. 2.2, we consider a system where a camphor particle is confined in the two-dimensional circular region [35]. By reducing a proposed model shown below, we derive a dynamical system which has a form in Eq. (2.3.3), and then determine whether a camphor particle shows stable rotation or oscillation, by applying the results in Sec. 2.3.

2.4.1 Mathematical model

In this subsection, we introduce a mathematical model, and derive a dimensionless form of it.

Introduction of the mathematical model

The center position of a camphor particle is represented by $\boldsymbol{\rho} = \boldsymbol{\rho}(t) = (\rho(t), \phi(t))$ in the two-dimensional polar coordinates. The equation of motion with regard to the center position of a camphor particle is described as:

$$\sigma S \frac{d^2\boldsymbol{\rho}}{dt^2} = -\xi S \frac{d\boldsymbol{\rho}}{dt} + \boldsymbol{F}_d(c; \boldsymbol{\rho}), \tag{2.4.1}$$

where σ and ξ are the mass and resistance coefficient per unit area, $S(= \pi\epsilon^2)$ is the surface area of a camphor particle, and $\boldsymbol{F}_d$ denotes the driving force originating from the surface tension difference. Here, we set the radius of the camphor particle as ϵ.

The driving force $\boldsymbol{F}_d$ originates from the surface tension difference around the camphor particle. We assume that the driving force is obtained by summing up the force originating from surface tension working on the periphery of the camphor particle. To avoid the dependence of ϵ, we divide the both sides of Eq. (2.4.1) with S, and then we take the limit that ϵ goes to $+0$.

$$\begin{aligned} \boldsymbol{F} &= \lim_{\epsilon \to +0} \frac{1}{S} \boldsymbol{F}_d \\ &= \lim_{\epsilon \to +0} \frac{1}{S} \int_{\partial\Omega} \gamma \left(c(\boldsymbol{\rho} + \epsilon \boldsymbol{n}) \right) \boldsymbol{n} dl, \end{aligned} \tag{2.4.2}$$

where $\Omega = \left\{ \boldsymbol{r} \,\middle|\, |\boldsymbol{r} - \boldsymbol{\rho}| < \epsilon \right\}$ is the circular region around the camphor particle with a radius of ϵ, and $\boldsymbol{n}$ is a unit vector represented as $\boldsymbol{n} = \boldsymbol{n}(\theta) = (\cos\theta, \sin\theta)$ in the Cartesian coordinates. Here, we assume that the surface tension γ is a linear decreasing function with regard to c, i.e., $\gamma = -\Gamma c + \gamma_0$,

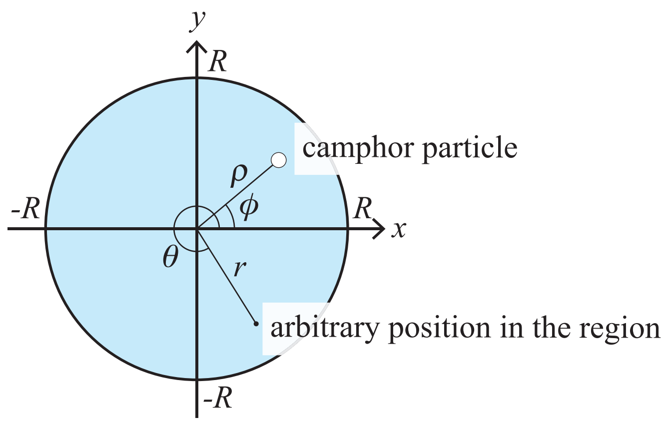

Figure 2.4.1: Schematic illustration of the considered system. The position of the camphor particle and an arbitrary position are denoted as $\boldsymbol{\rho} = (\rho, \phi)$ and $\boldsymbol{r} = (r, \theta)$ in the two-dimensional polar coordinates.

where Γ is a positive constant and γ_0 is surface tension of pure water as in Sec. 2.2. When the gradient of concentration field c is continuous at $\boldsymbol{r} = \boldsymbol{\rho}$, we have

$$\boldsymbol{F} = \lim_{\epsilon \to +0} \frac{-\Gamma}{\pi \epsilon^2} \int_0^{2\pi} \left[c(\boldsymbol{\rho}) + \epsilon \boldsymbol{n}(\theta) \cdot \nabla c(\boldsymbol{\rho}) \right] \boldsymbol{n}(\theta) \epsilon d\theta \tag{2.4.3}$$

$$= - \Gamma \left. \nabla c \right|_{\boldsymbol{r}=\boldsymbol{\rho}} . \tag{2.4.4}$$

In this case, the driving force is proportional to the gradient of concentration field. Hereafter, we consider the following equation for the motion of a camphor particle:

$$\sigma \frac{d^2 \boldsymbol{\rho}}{dt^2} = -\xi \frac{d\boldsymbol{\rho}}{dt} + \boldsymbol{F}(\boldsymbol{\rho}; c). \tag{2.4.5}$$

The time evolution for concentration field is described by the following equation:

$$\frac{\partial c(\boldsymbol{r}, t)}{\partial t} = D \nabla^2 c(\boldsymbol{r}, t) - \alpha c(\boldsymbol{r}, t) + f(\boldsymbol{r}; \boldsymbol{\rho}), \tag{2.4.6}$$

where $\boldsymbol{r}$ is an arbitrary position in the circular region, D is the diffusion constant including the effect of the Marangoni flow [70], α is the dissipation rate by sublimation and dissolution, and f denotes the dissolution of camphor molecules from the camphor particle. Here, the domain of definition for radial and angular components are given by $\rho, r \in [0, R]$, $\phi, \theta \in [0, 2\pi)$, which is shown in Fig. 2.4.1. The camphor molecules are dissolved constantly at the position of the camphor particle, $\boldsymbol{\rho} = (\rho(t), \phi(t))$, and thus the source term f is considered as follows:

$$f(\boldsymbol{r}; \boldsymbol{\rho}) = c_0 \delta(\boldsymbol{r} - \boldsymbol{\rho}) = \begin{cases} \dfrac{c_0}{r} \delta(r - \rho) \delta(\theta - \phi), & (\rho > 0), \\[2ex] \dfrac{c_0}{\pi r} \delta(r - \rho), & (\rho = 0), \end{cases} \tag{2.4.7}$$

where c_0 is the amount of dissolved camphor molecules per unit time. The concentration field satisfies the Neumann condition at the boundary:

$$\left. \frac{\partial c(r, \theta, t)}{\partial r} \right|_{r=R} = 0. \tag{2.4.8}$$

Dimensionless form of mathematical model

First, we consider the nondimensionalization of Eq. (2.4.6). The dimensions of α, D, and c_0 are [1/T], [L^2/T], and [C/L^2], respectively. Here, T, L, and C represent the dimensions of time, length, and concentration, respectively. Thus, we introduce the dimensionless time, position, and concentration as $\tilde{t} = \alpha t$, $\tilde{r} = \sqrt{\alpha/D}\ r$, and $\tilde{c} = \alpha c/c_0$, respectively. By substituting the three dimensionless variables into Eq. (2.4.6) and dividing the both sides of the above equation with c_0, we obtain

$$\frac{\partial \tilde{c}\left(\tilde{r},\theta,\tilde{t}\right)}{\partial \tilde{t}} = \left(\frac{\partial^2}{\partial \tilde{r}^2} + \frac{1}{\tilde{r}}\frac{\partial}{\partial \tilde{r}} + \frac{1}{\tilde{r}^2}\frac{\partial^2}{\partial \theta^2}\right)\tilde{c}\left(\tilde{r},\theta,\tilde{t}\right) - \tilde{c}\left(\tilde{r},\theta,\tilde{t}\right) + \frac{1}{c_0} f\left(\sqrt{\frac{D}{\alpha}}\tilde{r},\theta;\sqrt{\frac{D}{\alpha}}\tilde{\rho}\left(\tilde{t}\right),\phi\left(\tilde{t}\right)\right). \tag{2.4.9}$$

The source term is considered as follows:

$$\begin{aligned}\frac{1}{c_0} f\left(\sqrt{\frac{D}{\alpha}}\tilde{r},\theta;\sqrt{\frac{D}{\alpha}}\rho\left(\tilde{t}\right),\phi\left(\tilde{t}\right)\right) =& \sqrt{\frac{\alpha}{D}}\frac{1}{\tilde{r}}\delta\left(\sqrt{\frac{D}{\alpha}}\tilde{r} - \sqrt{\frac{D}{\alpha}}\rho\left(\tilde{t}\right)\right)\delta\left(\theta - \phi\left(\tilde{t}\right)\right)\\ =& \frac{1}{\tilde{r}}\delta\left(\tilde{r} - \rho\left(\tilde{t}\right)\right)\delta\left(\theta - \phi\left(\tilde{t}\right)\right)\\ \equiv& \tilde{f}\left(\tilde{r},\theta;\tilde{\rho},\phi\right).\end{aligned} \tag{2.4.10}$$

Here we use $\delta(ax) = \delta(x)/|a|$. Then, we have

$$\frac{\partial \tilde{c}\left(\tilde{r},\theta,\tilde{t}\right)}{\partial \tilde{t}} = \left(\frac{\partial^2}{\partial \tilde{r}^2} + \frac{1}{\tilde{r}}\frac{\partial}{\partial \tilde{r}} + \frac{1}{\tilde{r}^2}\frac{\partial^2}{\partial \theta^2}\right)\tilde{c}\left(\tilde{r},\theta,\tilde{t}\right) - \tilde{c}\left(\tilde{r},\theta,\tilde{t}\right) + \tilde{f}\left(\tilde{r},\theta;\tilde{\rho},\phi\right), \tag{2.4.11}$$

where $\tilde{\rho} = \sqrt{\alpha/D}\rho$.

Next, Eq. (2.4.5) is nondimensionalized. The variables t, $\boldsymbol{r}$, $\boldsymbol{\rho}$, c are replaced with $\tilde{t}$, $\tilde{\boldsymbol{r}}$, $\tilde{\boldsymbol{\rho}}$, $\tilde{c}$, and then we have

$$\sigma D\alpha \frac{d^2\tilde{\boldsymbol{\rho}}(\tilde{t})}{d\tilde{t}} = -\xi\sqrt{D\alpha}\frac{d\tilde{\boldsymbol{\rho}}(\tilde{t})}{d\tilde{t}} + \boldsymbol{F}\left(\frac{c_0}{\alpha}\tilde{c}\left(\sqrt{\frac{D}{\alpha}}\tilde{\boldsymbol{\rho}}(\tilde{t});\sqrt{\frac{D}{\alpha}}\tilde{\boldsymbol{r}},\frac{\tilde{t}}{\alpha}\right)\right). \tag{2.4.12}$$

In Eq. (2.4.12), we cannot eliminate all coefficients but one. Here, we adopt the dimensionless driving force,

$$\begin{aligned}\boldsymbol{F}(\boldsymbol{\rho};c) =& \lim_{\epsilon\to+0}\frac{-\Gamma}{\pi\epsilon^2}\int_0^{2\pi}\left[c(\boldsymbol{\rho}) + \epsilon\boldsymbol{n}(\theta)\cdot\nabla c(\boldsymbol{\rho})\right]\epsilon d\theta\\ =& \lim_{\tilde{\epsilon}\to+0}\frac{\alpha}{D}\frac{-\Gamma}{\pi\tilde{\epsilon}^2}\int_0^{2\pi}\left[\frac{c_0}{\alpha}\tilde{c}\left(\sqrt{\frac{D}{\alpha}}\tilde{\boldsymbol{\rho}}\right) + \tilde{\epsilon}\boldsymbol{n}(\theta)\cdot\tilde{\nabla}\frac{c_0}{\alpha}\tilde{c}\left(\sqrt{\frac{D}{\alpha}}\tilde{\boldsymbol{\rho}}\right)\right]\sqrt{\frac{D}{\alpha}}\tilde{\epsilon}d\theta\\ =& \frac{c_0}{\sqrt{\alpha D}}\lim_{\tilde{\epsilon}\to+0}\frac{-\Gamma}{\pi\tilde{\epsilon}^2}\int_0^{2\pi}\left[\tilde{c}\left(\sqrt{\frac{D}{\alpha}}\tilde{\boldsymbol{\rho}}\right) + \tilde{\epsilon}\boldsymbol{n}(\theta)\cdot\nabla\tilde{c}\left(\sqrt{\frac{D}{\alpha}}\tilde{\boldsymbol{\rho}}\right)\right]\tilde{\epsilon}d\theta\\ \equiv& \frac{c_0\Gamma}{\sqrt{\alpha D}}\tilde{\boldsymbol{F}}\left(\tilde{\boldsymbol{\rho}};\tilde{c}\right).\end{aligned} \tag{2.4.13}$$

Here, $\tilde{\boldsymbol{F}}$ is a dimensionless driving force. Then we obtain

$$\frac{\sigma\alpha^2 D}{\Gamma c_0}\frac{d^2\tilde{\boldsymbol{\rho}}}{d\tilde{t}^2} = -\frac{\xi\alpha D}{\Gamma c_0}\frac{d\tilde{\boldsymbol{\rho}}}{d\tilde{t}} + \tilde{\boldsymbol{F}}\left(\tilde{\boldsymbol{\rho}};\tilde{c}\right), \tag{2.4.14}$$

where

$$\tilde{\sigma} \equiv \frac{\sigma\alpha^2 D}{\Gamma c_0}, \quad \tilde{\xi} \equiv \frac{\xi\alpha D}{\Gamma c_0}. \tag{2.4.15}$$

For the simplicity, we omit tilde (˜), and the dimensionless evolution equations are described as

$$\sigma\frac{d^2\boldsymbol{\rho}}{dt^2} = -\xi\frac{d\boldsymbol{\rho}}{dt} + \boldsymbol{F}(\boldsymbol{\rho}; c), \tag{2.4.16}$$

$$\boldsymbol{F}(\boldsymbol{\rho}; c) = \lim_{\tilde{\epsilon}\to+0}\int_0^{2\pi}\left[c\left(\boldsymbol{\rho}\right) + \boldsymbol{n}(\theta)\cdot\nabla c\left(\boldsymbol{\rho}\right)\right]d\theta \tag{2.4.17}$$

$$\frac{\partial c(r,\theta,t)}{\partial t} = \left(\frac{\partial^2}{\partial r^2} + \frac{1}{r}\frac{\partial}{\partial r} + \frac{1}{r^2}\frac{\partial^2}{\partial\theta^2}\right)c(r,\theta,t) - c(r,\theta,t) + f(r,\theta;\rho,\phi). \tag{2.4.18}$$

$$f(\boldsymbol{r};\boldsymbol{\rho}) = \delta(\boldsymbol{r}-\boldsymbol{\rho}) = \begin{cases} \dfrac{c_0}{r}\delta(r-\rho)\delta(\theta-\phi), & (\rho > 0), \\ \dfrac{c_0}{\pi r}\delta(r-\rho), & (\rho = 0), \end{cases} \tag{2.4.19}$$

Hereafter, we proceed the analysis using Eqs. (2.4.16) and (2.4.18).

2.4.2 Steady state in an infinite system

In this section, the steady concentration field when a camphor particle stops at $\boldsymbol{\rho} = (\rho, \phi)$ in the two-dimensional polar coordinates is obtained. The concentration field satisfies Eq. (2.4.18) without time derivative term:

$$\left(\frac{\partial^2}{\partial r^2} + \frac{1}{r}\frac{\partial}{\partial r} + \frac{1}{r^2}\frac{\partial^2}{\partial\theta^2}\right)c(r,\theta) - c(r,\theta) + f(r,\theta;\rho,\phi) = 0. \tag{2.4.20}$$

The expansions of $c(r,\theta)$ and $f(r,\theta;\rho,\phi)$ in wavenumber space are represented as

$$g(r,\theta) = \frac{1}{2\pi}\sum_{m=-\infty}^{\infty}\int_0^{\infty} g_m(k)\mathcal{J}_m(kr)e^{im\theta}kdk, \tag{2.4.21}$$

$$f(r,\theta;\rho,\phi) = \frac{1}{2\pi}\sum_{m=-\infty}^{\infty}\int_0^{\infty} f_m(k)\mathcal{J}_m(kr)e^{im\theta}kdk, \tag{2.4.22}$$

where $\mathcal{J}_m$ is the first-kind Bessel function of m-th order. Here we use Hankel transform and Fourier expansion for the in radial and angular direction, respectively. The details of Hankel transform is expressed in Appendix A.3.1. We calculate $f_m(k)$ as follows:

$$f_m(k) = \int_0^{2\pi}\int_0^{\infty}\frac{1}{r}\delta(r-\rho)\delta(\theta-\phi)\mathcal{J}_m(kr)e^{-im\theta}rdrd\theta = \mathcal{J}_m(k\rho)e^{-im\phi}. \tag{2.4.23}$$

Therefore, we have

$$f(r,\theta;\rho,\phi) = \frac{1}{2\pi}\sum_{m=-\infty}^{\infty}\int_0^{\infty}\mathcal{J}_m(kr)\mathcal{J}_m(k\rho)e^{im(\theta-\phi)}kdk. \tag{2.4.24}$$

By substituting the above expansions into Eq. (2.4.20), and solving with regard to $g_m(k)$, we have

$$g_m(k) = \frac{\mathcal{J}_m(k\rho)e^{-im\phi}}{k^2+1}. \tag{2.4.25}$$

Thus, the steady state is calculated as:

$$\begin{aligned} g(r,\theta) =& \frac{1}{2\pi}\sum_{m=-\infty}^{\infty}\int_0^{\infty}\frac{\mathcal{J}_m(k\rho)}{k^2+1}\mathcal{J}_m(kr)e^{im(\theta-\phi)}kdk & (2.4.26)\\ =& \frac{1}{2\pi}\int_0^{\infty}\frac{1}{k^2+1}\mathcal{J}_0\left(k\sqrt{r^2+\rho^2-2r\rho\cos(\theta-\phi)}\right)kdk & (2.4.27)\\ =& \frac{1}{2\pi}\mathcal{K}_0\left(\sqrt{r^2+\rho^2-2r\rho\cos(\theta-\phi)}\right), & (2.4.28)\end{aligned}$$

where $\mathcal{K}_n$ is the second-kind modified Bessel function of the n-th order. Here we use the formulae in Ref. [81] (Eq. (4) in p.361 and Eq. (5) in p.425).

2.4.3 Reduction of the driving force for a camphor particle in an infinite system

The driving force is calculated as follows:

$$\begin{aligned} \boldsymbol{F} =& \frac{k}{4\pi}\left(-\gamma_{\text{Euler}}+\log\frac{2}{\epsilon}\right)\left(\dot{\rho}\boldsymbol{e}_\rho+\rho\dot{\phi}\boldsymbol{e}_\phi\right)-\frac{k}{16\pi}\left\{\left(\ddot{\rho}-\rho\dot{\phi}^2\right)\boldsymbol{e}_\rho+\left(\rho\ddot{\phi}+2\dot{\rho}\dot{\phi}\right)\boldsymbol{e}_\phi\right\}\\ &-\frac{k}{32\pi}\left\{\dot{\rho}\left(\dot{\rho}^2+\rho^2\dot{\phi}^2\right)\boldsymbol{e}_\rho+\rho\dot{\phi}\left(\dot{\rho}^2+\rho^2\dot{\phi}^2\right)\boldsymbol{e}_\phi\right\}+\frac{k}{48\pi}\left\{-3\dot{\rho}\dot{\phi}^2\boldsymbol{e}_\rho+\rho\dot{\phi}^3\boldsymbol{e}_\phi\right\}. \end{aligned} \tag{2.4.29}$$

Since the position, velocity, acceleration, jerk (time derivative of acceleration) are represented as $\rho\boldsymbol{e}_\rho$, $\dot{\rho}\boldsymbol{e}_\rho+\rho\dot{\phi}\boldsymbol{e}_\phi$, $\left(\ddot{\rho}-\rho\dot{\phi}^2\right)\boldsymbol{e}_\rho+\left(\rho\ddot{\phi}+2\dot{\rho}\dot{\phi}\right)\boldsymbol{e}_\phi$, and $\left(\dddot{\rho}-3\dot{\rho}\dot{\phi}^2-3\rho\dot{\phi}\ddot{\phi}\right)\boldsymbol{e}_\rho+\left(\rho\dddot{\phi}+3\ddot{\rho}\dot{\phi}+3\dot{\rho}\ddot{\phi}-\rho\dot{\phi}^3\right)\boldsymbol{e}_\phi$, the vector form of the driving force is expressed as:

$$\boldsymbol{F} = \frac{k}{4\pi}\left(-\gamma_{\text{Euler}}+\log\frac{2}{\epsilon}\right)\dot{\boldsymbol{\rho}}-\frac{k}{16\pi}\ddot{\boldsymbol{\rho}}-\frac{k}{32\pi}\left|\dot{\boldsymbol{\rho}}\right|^2\dot{\boldsymbol{\rho}}, \tag{2.4.30}$$

where the terms which related to the jerk are neglected. Here the detailed calculation is provided in Appendix A.3.2.

2.4.4 Steady state in a circular region

The steady state $g(r,\theta)$ with the source term $f(r,\theta) = \frac{1}{r}\delta(r-\rho)\delta(\theta-\phi)$ satisfies the following equation:

$$\left(\frac{\partial^2}{\partial r^2}+\frac{1}{r}\frac{\partial}{\partial r}+\frac{1}{r^2}\frac{\partial^2}{\partial\theta^2}\right)g(r,\theta)-g(r,\theta)+f(r,\theta)=0. \tag{2.4.31}$$

The steady state $g(r,\theta)$ and the source term $f(r,\theta)$ are expanded using Hankel expansion [80] for r-direction and Fourier series for θ-direction.

$$g(r,\theta) = \frac{1}{2\pi}\sum_{m=-\infty}^{\infty}\sum_{n=0}^{\infty}a_{mn}g_{mn}\mathcal{J}_{|m|}(k_{mn}r)e^{im\theta}, \tag{2.4.32}$$

$$f(r,\theta) = \frac{1}{2\pi}\sum_{m=-\infty}^{\infty}\sum_{n=0}^{\infty}a_{mn}\mathcal{J}_m(k_{mn}\rho)\mathcal{J}_{|m|}(k_{mn}r)e^{im(\theta-\phi)}. \tag{2.4.33}$$

By substituting Eqs. (2.4.32) and (2.4.33) into Eq. (2.4.31), we have

$$\begin{aligned}&\left\{-\left(\frac{\partial^2}{\partial r^2}+\frac{1}{r}\frac{\partial}{\partial r}+\frac{1}{r^2}\frac{\partial^2}{\partial \theta^2}\right)+1\right\}g(r,\theta)\\&=\left\{-\left(\frac{\partial^2}{\partial r^2}+\frac{1}{r}\frac{\partial}{\partial r}+\frac{1}{r^2}\frac{\partial^2}{\partial \theta^2}\right)+1\right\}\frac{1}{2\pi}\sum_{m=-\infty}^{\infty}\sum_{n=0}^{\infty}a_{mn}g_{mn}\mathcal{J}_{|m|}(k_{mn}r)\,e^{im\theta}\\&=\frac{1}{2\pi}\sum_{m=-\infty}^{\infty}\sum_{n=0}^{\infty}a_{mn}({k_{mn}}^2+1)g_{mn}\mathcal{J}_{|m|}(k_{mn}r)\,e^{im\theta}\\&=\frac{1}{2\pi}\sum_{m=-\infty}^{\infty}\sum_{n=0}^{\infty}a_{mn}\mathcal{J}_{|m|}(k_{mn}\rho)\mathcal{J}_{|m|}(k_{mn}r)e^{im(\theta-\phi)}.\end{aligned}\tag{2.4.34}$$

By solving with regard to g_{mn}, we have

$$g_{mn}=\frac{\mathcal{J}_{|m|}(k_{mn}\rho)e^{-im\phi}}{2\pi({k_{mn}}^2+1)}.\tag{2.4.35}$$

Thus, the steady state $g(r,\theta)$ in real space is written as

$$g(r,\theta)=\frac{1}{2\pi}\sum_{m=-\infty}^{\infty}\sum_{n=0}^{\infty}\frac{a_{mn}}{2\pi({k_{mn}}^2+1)}\mathcal{J}_{|m|}(k_{mn}\rho)\mathcal{J}_{|m|}(k_{mn}r)e^{im(\theta-\phi)}.\tag{2.4.36}$$

In Subsection 2.4.2, we obtain the steady state in an infinite region as follows:

$$c(r,\theta)=\frac{1}{2\pi}\mathcal{K}_0\left(\sqrt{r^2+\rho^2-2r\rho\cos(\theta-\phi)}\right),\tag{2.4.37}$$

where $\boldsymbol{\rho}=(\rho,\phi)$ is the position of the camphor particle in the two-dimensional polar coordinates. To satisfy the Neumann boundary condition, we adequately add the general solution for Eq. (2.4.31) without the source term, i.e., the homogeneous form of Eq. (2.4.31):

$$\left(\frac{\partial^2}{\partial r^2}+\frac{1}{r}\frac{\partial}{\partial r}+\frac{1}{r^2}\frac{\partial^2}{\partial \theta^2}\right)g(r,\theta)-g(r,\theta)=0,\tag{2.4.38}$$

as correction terms. From the definition of the modified Bessel functions, the general solution of Eq. (2.4.38) is expressed as

$$\begin{aligned}c(r,\theta)=&A_0\mathcal{K}_0(r)+B_0\mathcal{I}_0(r)\\&+\sum_{m=1}^{\infty}\left(A_m\mathcal{K}_m(r)+B_m\mathcal{I}_m(r)\right)\cos m(\theta-\phi)+\sum_{m=1}^{\infty}\left(C_m\mathcal{K}_m(r)+D_m\mathcal{I}_m(r)\right)\sin m(\theta-\phi).\end{aligned}\tag{2.4.39}$$

By considering the symmetric property of the system, the m-th mode term should be expressed only by $\cos m(\theta-\phi)$, i.e., C_m and D_m should be zero. Furthermore, $\mathcal{K}_n(r)$ $(n\geq 1)$ is not suitable for representing the concentration field of camphor, since $\int_0^{2\pi}\int_0^R \mathcal{K}_n(r)rdrd\theta$ diverges for $n\geq 1$. $\mathcal{K}_0(r)$ diverges at $r=0$ and is not suitable when a camphor particle is off the origin. When a camphor particle is located at the origin, $\mathcal{K}_0(r)$ is already included as the steady state without the

Neumann boundary. Thus, for the both cases, the concentration field with the correction terms should be given by the following form:

$$c(r,\theta) = \frac{1}{2\pi}\mathcal{K}_0\left(\sqrt{r^2+\rho^2-2r\rho\cos(\theta-\phi)}\right) + \sum_{m=0}^{\infty} B_m \mathcal{I}_m(r)\cos m(\theta-\phi). \tag{2.4.40}$$

Then, the coefficients B_m are determined by the boundary condition

$$\left.\frac{\partial}{\partial r}c(r,\theta)\right|_{r=R} = 0, \tag{2.4.41}$$

that is

$$\left.\frac{1}{2\pi}\frac{\partial}{\partial r}\mathcal{K}_0\left(\sqrt{r^2+\rho^2-2r\rho\cos(\theta-\phi)}\right)\right|_{r=R} = -\sum_{m=0}^{\infty} B_m \left.\frac{\partial \mathcal{I}_m(r)}{\partial r}\cos m(\theta-\phi)\right|_{r=R}. \tag{2.4.42}$$

If $\partial\mathcal{K}_0\left(\sqrt{r^2+\rho^2-2r\rho\cos(\theta-\phi)}\right)/\partial r$ at $r=R$ is expanded with regard to $\cos m(\theta-\phi)$, we can determine B_m. By using the formula represented in Eq. (8) in p.361 of Ref. [81]:

$$\mathcal{K}_0\left(\sqrt{R^2+r^2-2Rr\cos\theta}\right) = \sum_{n=-\infty}^{\infty}\mathcal{K}_n(R)\mathcal{I}_n(r)\cos n\theta, \qquad (\text{for } R>r), \tag{2.4.43}$$

we have

$$\begin{aligned}
&\frac{\partial}{\partial R}\int_0^{2\pi}\mathcal{K}_0\left(\sqrt{R^2+\rho^2-2R\rho\cos(\theta-\phi)}\right)\cos n(\theta-\phi)d\theta \\
&= \frac{\partial}{\partial R}\sum_{m=-\infty}^{\infty}\mathcal{K}_m(R)\mathcal{I}_m(\rho)\int_0^{2\pi}\cos m(\theta-\phi)\cos n(\theta-\phi)d\theta \\
&= \frac{\partial}{\partial R}\sum_{m=-\infty}^{\infty}\mathcal{K}_m(R)\mathcal{I}_m(\rho)\left\{\begin{array}{ll} 2\pi\delta_{mn} & (n=0) \\ \pi\delta_{mn} & (n\neq 0)\end{array}\right. \\
&= \left\{\begin{array}{ll} 2\pi\dfrac{\partial\mathcal{K}_0(R)}{\partial R}\mathcal{I}_0(\rho) & (n=0) \\ \pi\left(\dfrac{\partial\mathcal{K}_n(R)}{\partial R}\mathcal{I}_n(\rho)+\dfrac{\partial\mathcal{K}_{-n}(R)}{\partial R}\mathcal{I}_{-n}(\rho)\right) & (n\neq 0)\end{array}\right. \\
&= 2\pi\frac{\partial\mathcal{K}_n(R)}{\partial R}\mathcal{I}_n(\rho) \quad (n=0,1,2,\cdots).
\end{aligned} \tag{2.4.44}$$

Here we use $\mathcal{K}_{-m}(r)=\mathcal{K}_m(r)$ and $\mathcal{I}_{-m}(r)=\mathcal{I}_m(r)$. As a consequence, we have

$$B_0 = \frac{1}{2\pi}\frac{\mathcal{K}_0'(R)}{\mathcal{I}_0'(R)}\mathcal{I}_0(\rho), \tag{2.4.45}$$

$$B_m = \frac{1}{\pi}\frac{\mathcal{K}_m'(R)}{\mathcal{I}_m'(R)}\mathcal{I}_m(\rho). \tag{2.4.46}$$

Thus, we have

$$\begin{aligned}
c(r,\theta) =& \frac{1}{2\pi}\mathcal{K}_0\left(\sqrt{r^2+\rho^2-2r\rho\cos(\theta-\phi)}\right) \\
&- \frac{1}{2\pi}\frac{\mathcal{K}_0{}'(R)}{\mathcal{I}_0{}'(R)}\mathcal{I}_0(\rho)\mathcal{I}_0(r) - \frac{1}{\pi}\sum_{m=1}^{\infty}\frac{\mathcal{K}_m{}'(R)}{\mathcal{I}_m{}'(R)}\mathcal{I}_m(\rho)\mathcal{I}_m(r)\cos m(\theta-\phi).
\end{aligned} \tag{2.4.47}$$

Next, the conservation of integration of concentration over the circular region,

$$\int_0^R \int_0^{2\pi} c(r,\theta) r dr d\theta = 1, \tag{2.4.48}$$

is checked. We directly integrate as follows:

$$\begin{aligned}
&\int_0^R \int_0^{2\pi} c(r,\theta) r dr d\theta \\
&= \frac{1}{2\pi} \int_0^R \int_0^{2\pi} \mathcal{K}_0\left(\sqrt{r^2+\rho^2-2r\rho\cos(\theta-\phi)}\right) r dr d\theta + \sum_{m=0}^{\infty} B_m \int_0^R \int_0^{2\pi} \mathcal{I}_m(r)\cos m(\theta-\phi) r dr d\theta \\
&= \frac{1}{2\pi} \sum_{m=-\infty}^{\infty} \int_0^{2\pi} \left\{ \int_0^{\rho} \mathcal{K}_m(\rho)\mathcal{I}_m(r) r dr + \int_{\rho}^{R} \mathcal{K}_m(r)\mathcal{I}_m(\rho) r dr \right\} \cos m(\theta-\phi) d\theta \\
&\quad + \sum_{m=0}^{\infty} B_m \int_0^R \int_0^{2\pi} \mathcal{I}_m(r)\cos m(\theta-\phi) r dr d\theta,
\end{aligned} \tag{2.4.49}$$

where we use the formula (Eq. (8) in p.361 of Ref. [81]):

$$\mathcal{K}_0\left(\sqrt{r^2+\rho^2-2r\rho\cos(\theta-\phi)}\right) = \begin{cases} \displaystyle\sum_{n=-\infty}^{\infty} \mathcal{K}_n(\rho)\mathcal{I}_n(r)\cos n\theta, & \text{(for } R > r\text{)}, \\ \displaystyle\sum_{n=-\infty}^{\infty} \mathcal{K}_n(r)\mathcal{I}_n(\rho)\cos n\theta, & \text{(for } R < r\text{)}. \end{cases} \tag{2.4.50}$$

By integrating the both sides of Eq. (2.4.49) with regard to θ, the integration is zero except for $m = 0$, and we have

$$\begin{aligned}
&\left\{ \int_0^{\rho} \mathcal{K}_0(\rho)\mathcal{I}_0(r) r dr + \int_{\rho}^{R} \mathcal{K}_0(r)\mathcal{I}_0(\rho) r dr \right\} + 2\pi B_0 \int_0^R \mathcal{I}_0(r) r dr \\
&\quad = \{\mathcal{K}_0(\rho)\rho\mathcal{I}_1(\rho) + \mathcal{I}_0(\rho)(\rho\mathcal{K}_1(\rho) - R\mathcal{K}_1(R))\} + 2\pi B_0 R\mathcal{I}_1(R) \\
&\quad = (1 - R\mathcal{I}_0(\rho)\mathcal{K}_1(R)) + 2\pi B_0 R\mathcal{I}_1(R) \\
&\quad = 1.
\end{aligned} \tag{2.4.51}$$

Here we use $\mathcal{K}_0(r)\mathcal{I}_1(r) + \mathcal{I}_0(r)\mathcal{K}_1(r) = 1/r$ (cited by Eq. (20) in p.80 of Ref. [81]). We also use formulae $(r\mathcal{K}_1(r))' = \mathcal{K}_1(r) + r\mathcal{K}_1'(r) = -\mathcal{K}_0(r)$ and $(r\mathcal{I}_1(r))' = \mathcal{I}_1(r) + r\mathcal{I}_1'(r) = \mathcal{I}_0(r)$, which are represented in Eq. (4) in p.79 of Ref. [81].

2.4.5 Reduction of the driving force for a camphor particle in a circular region

The concentration field c is expanded with the Bessel functions so-called "discrete Hankel transform" and Fourier series on radial and angular directions, respectively.

$$c(r,\theta,t) = \frac{1}{2\pi} \sum_{m=-\infty}^{\infty} \sum_{n=0}^{\infty} a_{mn} c_{mn}(t) \mathcal{J}_{|m|}(k_{mn} r) e^{im\theta}. \tag{2.4.52}$$

The details of "discrete Hankel transform" is expressed in Appendix A.3.1. The source term in Eq. (2.4.7) is also expanded as

$$\begin{aligned} f(r,\theta;\rho,\phi) =& \frac{1}{r}\delta(r-\rho(t))\delta(\theta-\phi(t)) \\ =& \frac{1}{2\pi}\sum_{m=-\infty}^{\infty}\sum_{n=0}^{\infty} a_{mn}\mathcal{J}_{|m|}(k_{mn}\rho(t))e^{-im\phi(t)}\mathcal{J}_{|m|}(k_{mn}r)e^{im\theta}. \end{aligned} \tag{2.4.53}$$

Thus we have the equation for concentration in wavenumber space:

$$\frac{\partial c_{mn}(t)}{\partial t} = -({k_{mn}}^2+1)c_{mn}(t) + \mathcal{J}_{|m|}(k_{mn}\rho(t))e^{-im\phi(t)}. \tag{2.4.54}$$

First, the Green's function $g_{mn}(t)$ is calculated. The Green's function satisfies the following equation:

$$\frac{\partial g_{mn}(t)}{\partial t} = -({k_{mn}}^2+1)g_{mn}(t) + \delta(t). \tag{2.4.55}$$

By solving the above equation, we have

$$g_{mn}(t) = e^{-({k_{mn}}^2+1)t}\Theta(t), \tag{2.4.56}$$

where $\Theta(t)$ is the Heaviside's step function.

Using the Green's function g_{mn}, the concentration field c_{mn} in wavenumber space is described as

$$c_{mn}(t) = \int_{-\infty}^{t} \mathcal{J}_{|m|}(k_{mn}\rho(t'))e^{-im\phi(t')}e^{-({k_{mn}}^2+1)(t-t')}dt'. \tag{2.4.57}$$

By adopting partial integration on Eq. (2.4.57), we have the following expression:

$$\begin{aligned} &c_{mn} \\ &= \frac{1}{A}\mathcal{J}_{|m|}(k_{mn}\rho(t))e^{-im\phi(t)} + \frac{1}{A^2}\left\{-k_{mn}\dot{\rho}(t)\mathcal{J}'_{|m|}(k_{mn}\rho(t)) + im\dot{\phi}(t)\mathcal{J}_{|m|}(k_{mn}\rho(t))\right\}e^{-im\phi(t)} \\ &\quad + \frac{1}{A^3}\left\{k_{mn}\ddot{\rho}(t)\mathcal{J}'_{|m|}(k_{mn}\rho(t)) + {k_{mn}}^2(\dot{\rho}(t))^2\mathcal{J}''_{|m|}(k_{mn}\rho(t)) - 2ik_{mn}m\dot{\rho}(t)\dot{\phi}(t)\mathcal{J}'_{|m|}(k_{mn}\rho(t))\right. \\ &\qquad\qquad \left. -im\ddot{\phi}(t)\mathcal{J}_{|m|}(k_{mn}\rho(t)) - m^2(\dot{\phi}(t))^2\mathcal{J}_{|m|}(k_{mn}\rho(t))\right\}e^{-im\phi(t)} \\ &\quad + \frac{1}{A^4}\left\{-k_{mn}\dddot{\rho}(t)\mathcal{J}'_{|m|}(k_{mn}\rho(t)) - 3{k_{mn}}^2\dot{\rho}(t)\ddot{\rho}(t)\mathcal{J}''_{|m|}(k_{mn}\rho(t)) + 3ik_{mn}m\ddot{\rho}(t)\dot{\phi}(t)\mathcal{J}'_{|m|}(k_{mn}\rho(t))\right. \\ &\qquad - {k_{mn}}^3(\dot{\rho}(t))^3\mathcal{J}'''_{|m|}(k\rho(t)) + 3i{k_{mn}}^2m(\dot{\rho}(t))^2\dot{\phi}(t)\mathcal{J}''_{|m|}(k_{mn}\rho(t)) + 3ik_{mn}m\dot{\rho}(t)\ddot{\phi}(t)\mathcal{J}'_{|m|}(k_{mn}\rho(t)) \\ &\qquad + 3k_{mn}m^2\dot{\rho}(t)(\dot{\phi}(t))^2\mathcal{J}'_{|m|}(k_{mn}\rho(t)) + im\dddot{\phi}(t)\mathcal{J}_{|m|}(k_{mn}\rho(t)) + 3m^2\dot{\phi}(t)\ddot{\phi}(t)\mathcal{J}_{|m|}(k_{mn}\rho(t)) \\ &\qquad \left. -im^3(\dot{\phi}(t))^3\mathcal{J}_{|m|}(k_{mn}\rho(t))\right\}e^{-im\phi(t)} \\ &\quad + \cdots. \end{aligned} \tag{2.4.58}$$

The detailed calculation is provided in Appendix A.3.3. Thus we have

$$
\begin{aligned}
&c(r,\theta,t)\\
&=\frac{1}{2\pi}\sum_{m=-\infty}^{\infty}\sum_{n=0}^{\infty}\frac{a_{mn}}{k_{mn}^2+1}\mathcal{J}_{|m|}(k_{mn}\rho(t))\mathcal{J}_{|m|}(k_{mn}r)e^{im(\theta-\phi(t))}\\
&\quad+\frac{1}{2\pi}\sum_{m=-\infty}^{\infty}\sum_{n=0}^{\infty}\frac{a_{mn}}{(k_{mn}^2+1)^2}\left\{-k_{mn}\dot{\rho}(t)\mathcal{J}'_{|m|}(k\rho(t))+im\dot{\phi}(t)\mathcal{J}_{|m|}(k_{mn}\rho(t))\right\}\mathcal{J}_{|m|}(k_{mn}r)e^{im(\theta-\phi(t))}\\
&\quad+\frac{1}{2\pi}\sum_{m=-\infty}^{\infty}\sum_{n=0}^{\infty}\frac{a_{mn}}{(k_{mn}^2+1)^3}\left\{k_{mn}\ddot{\rho}(t)\mathcal{J}'_{|m|}(k_{mn}\rho(t))+{k_{mn}}^2(\dot{\rho}(t))^2\mathcal{J}''_{|m|}(k\rho(t))\right.\\
&\qquad-2ik_{mn}m\dot{\rho}(t)\dot{\phi}(t)\mathcal{J}'_{|m|}(k_{mn}\rho(t))-im\ddot{\phi}(t)\mathcal{J}_{|m|}(k_{mn}\rho(t))\\
&\qquad\left.-m^2(\dot{\phi}(t))^2\mathcal{J}_{|m|}(k_{mn}\rho(t))\right\}\mathcal{J}_{|m|}(k_{mn}r)e^{im(\theta-\phi(t))}\\
&\qquad+\frac{1}{2\pi}\sum_{m=-\infty}^{\infty}\sum_{n=0}^{\infty}\frac{a_{mn}}{(k_{mn}^2+1)^4}\left\{-k_{mn}\dddot{\rho}(t)\mathcal{J}'_{|m|}(k_{mn}\rho(t))-3k_{mn}^2\dot{\rho}(t)\ddot{\rho}(t)\mathcal{J}''_{|m|}(k_{mn}\rho(t))\right.\\
&\qquad\quad+3ik_{mn}m\ddot{\rho}(t)\dot{\phi}(t)\mathcal{J}'_{|m|}(k_{mn}\rho(t))-k_{mn}^3(\dot{\rho}(t))^3\mathcal{J}'''_{|m|}(k_{mn}\rho(t))\\
&\qquad\quad+3ik_{mn}^2m(\dot{\rho}(t))^2\dot{\phi}(t)\mathcal{J}''_{|m|}(k_{mn}\rho(t))+3ik_{mn}m\dot{\rho}(t)\ddot{\phi}(t)\mathcal{J}'_{|m|}(k_{mn}\rho(t))\\
&\qquad\quad+3k_{mn}m^2\dot{\rho}(t)(\dot{\phi}(t))^2\mathcal{J}'_{|m|}(k_{mn}\rho(t))+im\dddot{\phi}(t)\mathcal{J}_{|m|}(k_{mn}\rho(t))\\
&\qquad\quad\left.+3m^2\dot{\phi}(t)\ddot{\phi}(t)\mathcal{J}_{|m|}(k_{mn}\rho(t))-im^3(\dot{\phi}(t))^3\mathcal{J}_{|m|}(k_{mn}\rho(t))\right\}\mathcal{J}_{|m|}(k_{mn}r)e^{im(\theta-\phi(t))}.
\end{aligned}
\tag{2.4.59}
$$

By taking the summation of Eq. (2.4.59), we have the concentration field as follows:

$$
\begin{aligned}
&c(\boldsymbol{r};\boldsymbol{\rho})\\
&\quad=c_0^{00}(R,r)+c_0^{10}(R,r)(\boldsymbol{r}\cdot\boldsymbol{\rho})+c_0^{20}(R,r)(\boldsymbol{r}\cdot\boldsymbol{\rho})^2+c_1^{20}(R,r)|\boldsymbol{\rho}|^2\\
&\qquad+c_0^{11}(R,r)\left(\boldsymbol{r}\cdot\dot{\boldsymbol{\rho}}\right)\\
&\qquad+c_0^{30}(R,r)(\boldsymbol{r}\cdot\boldsymbol{\rho})^3+c_1^{30}(R,r)|\boldsymbol{\rho}|^2(\boldsymbol{r}\cdot\boldsymbol{\rho})\\
&\qquad+c_0^{21}(R,r)\left(\boldsymbol{\rho}\cdot\dot{\boldsymbol{\rho}}\right)+c_1^{21}(R,r)\left(\boldsymbol{r}\cdot\boldsymbol{\rho}\right)\left(\boldsymbol{r}\cdot\dot{\boldsymbol{\rho}}\right)+c_0^{12}(R,r)\left(\boldsymbol{r}\cdot\ddot{\boldsymbol{\rho}}\right)\\
&\qquad+c_0^{31}(R,r)|\boldsymbol{\rho}|^2\left(\boldsymbol{r}\cdot\dot{\boldsymbol{\rho}}\right)+c_1^{31}(R,r)\left(\boldsymbol{r}\cdot\boldsymbol{\rho}\right)\left(\boldsymbol{\rho}\cdot\dot{\boldsymbol{\rho}}\right)+c_2^{31}(R,r)\left(\boldsymbol{r}\cdot\boldsymbol{\rho}\right)^2\left(\boldsymbol{r}\cdot\dot{\boldsymbol{\rho}}\right)\\
&\qquad+c_0^{22}(R,r)\left(\boldsymbol{\rho}\cdot\ddot{\boldsymbol{\rho}}\right)+c_1^{22}(R,r)\left|\dot{\boldsymbol{\rho}}\right|^2+c_2^{22}(R,r)\left(\boldsymbol{r}\cdot\boldsymbol{\rho}\right)\left(\boldsymbol{r}\cdot\ddot{\boldsymbol{\rho}}\right)+c_3^{22}(R,r)\left(\boldsymbol{r}\cdot\dot{\boldsymbol{\rho}}\right)^2+c_0^{13}(R,r)\left(\boldsymbol{r}\cdot\dddot{\boldsymbol{\rho}}\right)\\
&\qquad+c_0^{32}(R,r)\left|\dot{\boldsymbol{\rho}}\right|^2\left(\boldsymbol{r}\cdot\boldsymbol{\rho}\right)+c_1^{32}(R,r)\left(\boldsymbol{r}\cdot\dot{\boldsymbol{\rho}}\right)\left(\boldsymbol{\rho}\cdot\dot{\boldsymbol{\rho}}\right)+c_2^{32}(R,r)\left(\boldsymbol{r}\cdot\boldsymbol{\rho}\right)\left(\boldsymbol{r}\cdot\dot{\boldsymbol{\rho}}\right)^2+c_3^{32}(R,r)\left(\boldsymbol{r}\cdot\boldsymbol{\rho}\right)\left(\boldsymbol{\rho}\cdot\ddot{\boldsymbol{\rho}}\right)\\
&\qquad+c_4^{32}(R,r)\left|\boldsymbol{\rho}\right|^2\left(\boldsymbol{r}\cdot\ddot{\boldsymbol{\rho}}\right)+c_5^{32}(R,r)\left(\boldsymbol{r}\cdot\boldsymbol{\rho}\right)^2\left(\boldsymbol{r}\cdot\ddot{\boldsymbol{\rho}}\right)\\
&\qquad+c_0^{23}(R,r)\left(\boldsymbol{\rho}\cdot\dddot{\boldsymbol{\rho}}\right)+c_1^{23}(R,r)\left(\dot{\boldsymbol{\rho}}\cdot\ddot{\boldsymbol{\rho}}\right)+c_2^{23}(R,r)\left(\boldsymbol{r}\cdot\dot{\boldsymbol{\rho}}\right)\left(\boldsymbol{r}\cdot\ddot{\boldsymbol{\rho}}\right)+c_3^{23}(R,r)\left(\boldsymbol{r}\cdot\boldsymbol{\rho}\right)\left(\boldsymbol{r}\cdot\dddot{\boldsymbol{\rho}}\right)\\
&\qquad+c_0^{33}(R,r)\left|\boldsymbol{\rho}\right|^2\left(\boldsymbol{r}\cdot\dddot{\boldsymbol{\rho}}\right)+c_1^{33}(R,r)\left|\dot{\boldsymbol{\rho}}\right|^2\left(\boldsymbol{r}\cdot\dot{\boldsymbol{\rho}}\right)+c_2^{33}(R,r)\left(\boldsymbol{r}\cdot\boldsymbol{\rho}\right)\left(\boldsymbol{\rho}\cdot\dddot{\boldsymbol{\rho}}\right)+c_3^{33}(R,r)\left(\boldsymbol{r}\cdot\dot{\boldsymbol{\rho}}\right)^3\\
&\qquad+c_4^{33}(R,r)\left(\boldsymbol{r}\cdot\boldsymbol{\rho}\right)\left(\dot{\boldsymbol{\rho}}\cdot\ddot{\boldsymbol{\rho}}\right)+c_5^{33}(R,r)\left(\boldsymbol{r}\cdot\boldsymbol{\rho}\right)^2\left(\boldsymbol{r}\cdot\dddot{\boldsymbol{\rho}}\right)+c_6^{33}(R,r)\left(\boldsymbol{r}\cdot\dot{\boldsymbol{\rho}}\right)\left(\boldsymbol{\rho}\cdot\ddot{\boldsymbol{\rho}}\right)\\
&\qquad+c_7^{33}(R,r)\left(\boldsymbol{r}\cdot\ddot{\boldsymbol{\rho}}\right)\left(\boldsymbol{\rho}\cdot\dot{\boldsymbol{\rho}}\right)+c_8^{33}(R,r)\left(\boldsymbol{r}\cdot\boldsymbol{\rho}\right)\left(\boldsymbol{r}\cdot\dot{\boldsymbol{\rho}}\right)\left(\boldsymbol{r}\cdot\ddot{\boldsymbol{\rho}}\right).
\end{aligned}
\tag{2.4.60}
$$

where we truncate the higher-order terms of ρ and ϕ. The detailed calculation, the explicit forms of c_k^{ij}, and their plots are provided in Appendix A.3.4.

By calculating the gradient of Eq. (2.4.60) at $\boldsymbol{r} = \boldsymbol{\rho}$, we have the reduced driving force as follows:

$$\begin{aligned}\boldsymbol{F}(\boldsymbol{\rho}, \dot{\boldsymbol{\rho}}, \ddot{\boldsymbol{\rho}}) =& - \left.\nabla c(\boldsymbol{r}; \boldsymbol{\rho})\right|_{\boldsymbol{r}=\boldsymbol{\rho}} \\ =& a(R)\boldsymbol{\rho} + b(R)\dot{\boldsymbol{\rho}} + c(R)|\boldsymbol{\rho}|^2\boldsymbol{\rho} + g(R)\ddot{\boldsymbol{\rho}} + h(R)|\dot{\boldsymbol{\rho}}|^2\boldsymbol{\rho} + j(R)(\boldsymbol{\rho}\cdot\dot{\boldsymbol{\rho}})\boldsymbol{\rho} \\ &+ k(R)|\dot{\boldsymbol{\rho}}|^2\dot{\boldsymbol{\rho}} + h(R)|\boldsymbol{\rho}|^2\dot{\boldsymbol{\rho}} + p(R)(\boldsymbol{\rho}\cdot\dot{\boldsymbol{\rho}})\dot{\boldsymbol{\rho}},\end{aligned} \tag{2.4.61}$$

where

$$a(R) = \frac{1}{4\pi}\left(\frac{\mathcal{K}_0'(R)}{\mathcal{I}_0'(R)} + \frac{\mathcal{K}_1'(R)}{\mathcal{I}_1'(R)}\right), \tag{2.4.62}$$

$$b(R) = \frac{1}{4\pi}\left(-\gamma_{\mathrm{Euler}} + \log\frac{2}{\epsilon}\right) + \frac{1}{8\pi}\left(2\frac{\mathcal{K}_1'(R)}{\mathcal{I}_1'(R)} + \left(1 + \frac{1}{R^2}\right)\frac{1}{(\mathcal{I}_1'(R))^2}\right), \tag{2.4.63}$$

$$c(R) = \frac{1}{32\pi}\left(3\frac{\mathcal{K}_0'(R)}{\mathcal{I}_0'(R)} + 4\frac{\mathcal{K}_1'(R)}{\mathcal{I}_1'(R)} + \frac{\mathcal{K}_2'(R)}{\mathcal{I}_2'(R)}\right), \tag{2.4.64}$$

$$g(R) = -\frac{1}{16\pi} + \frac{1}{16\pi}\left(-\left(R + \frac{1}{R}\right)\frac{\mathcal{I}_1''(R)}{(\mathcal{I}_1'(R))^3} + \frac{1}{(\mathcal{I}_1'(R))^2}\right), \tag{2.4.65}$$

$$\begin{aligned}h(R) =& \frac{1}{64\pi}\left(8\frac{\mathcal{K}_0'(R)}{\mathcal{I}_0'(R)} + 4\frac{\mathcal{K}_1'(R)}{\mathcal{I}_1'(R)} - 4\frac{\mathcal{K}_2'(R)}{\mathcal{I}_2'(R)} - 2R\frac{\mathcal{I}_0''(R)}{(\mathcal{I}_0'(R))^3} - \left(R + \frac{1}{R}\right)\frac{\mathcal{I}_1''(R)}{(\mathcal{I}_1'(R))^3}\right. \\ &\left. + \left(R + \frac{4}{R}\right)\frac{\mathcal{I}_2''(R)}{(\mathcal{I}_2'(R))^3} + \frac{6}{(\mathcal{I}_0'(R))^2} + \left(\frac{2}{R^2} + 3\right)\frac{1}{(\mathcal{I}_1'(R))^2} - \left(\frac{8}{R^2} + 3\right)\frac{1}{(\mathcal{I}_2'(R))^2}\right),\end{aligned} \tag{2.4.66}$$

$$j(R) = \frac{1}{16\pi}\left(4\frac{\mathcal{K}_0'(R)}{\mathcal{I}_0'(R)} + 4\frac{\mathcal{K}_1'(R)}{\mathcal{I}_1'(R)} + \frac{1}{(\mathcal{I}_0'(R))^2} + \left(1 + \frac{1}{R^2}\right)\frac{1}{(\mathcal{I}_1'(R))^2}\right), \tag{2.4.67}$$

$$\begin{aligned}k(R) =& -\frac{1}{32\pi} \\ &+ \frac{1}{128\pi}\left(3\left(1 + R^2\right)\frac{(\mathcal{I}_1''(R))^2}{(\mathcal{I}_1'(R))^4} - \left(\frac{3}{R} + 7R\right)\frac{\mathcal{I}_1''(R)}{(\mathcal{I}_1'(R))^3} - \left(1 + R^2\right)\frac{\mathcal{I}_1'''(R)}{(\mathcal{I}_1'(R))^3} + 4\frac{1}{(\mathcal{I}_1'(R))^2}\right),\end{aligned} \tag{2.4.68}$$

$$n(R) = \frac{1}{32\pi}\left(\left(1 + \frac{1}{R^2}\right)\frac{1}{(\mathcal{I}_1'(R))^2} + \left(1 + \frac{4}{R^2}\right)\frac{1}{(\mathcal{I}_2'(R))^2} + 4\frac{\mathcal{K}_2'(R)}{\mathcal{I}_2'(R)} + 4\frac{\mathcal{K}_1'(R)}{\mathcal{I}_1'(R)}\right), \tag{2.4.69}$$

$$\begin{aligned}p(R) =& \frac{1}{32\pi}\left(4\frac{\mathcal{K}_1'(R)}{\mathcal{I}_1'(R)} + 4\frac{\mathcal{K}_2'(R)}{\mathcal{I}_2'(R)} - \left(\frac{1}{R} + R\right)\frac{\mathcal{I}_1''(R)}{(\mathcal{I}_1'(R))^3} - \left(\frac{4}{R} + R\right)\frac{\mathcal{I}_2''(R)}{(\mathcal{I}_2'(R))^3}\right. \\ &\left. + \left(\frac{2}{R^2} + 3\right)\frac{1}{(\mathcal{I}_1'(R))^2} + \left(\frac{8}{R^2} + 3\right)\frac{1}{(\mathcal{I}_2'(R))^2}\right).\end{aligned} \tag{2.4.70}$$

Here γ_{Euler} denotes the Euler's constant ($\gamma_{\mathrm{Euler}} \simeq 0.577$). We confirm that, when R goes to infinity, the coefficients $a(R)$, $b(R)$, $c(R)$, $h(R)$, $j(R)$, $k(R)$, $n(R)$, and $p(R)$ correspond to the ones for the infinite system shown in Eq. (2.4.30). The dependence of the coefficients on the radius of water chamber R is shown in Appendix A.3.5.

Since we have the reduced driving force, the dynamical system becomes:

$$\begin{aligned}(\sigma - g(R))\ddot{\boldsymbol{\rho}} =& a(R)\boldsymbol{\rho} + (b(R) - \xi)\dot{\boldsymbol{\rho}} + c(R)|\boldsymbol{\rho}|^2\boldsymbol{\rho} + h(R)|\dot{\boldsymbol{\rho}}|^2\boldsymbol{\rho} + j(R)(\boldsymbol{\rho}\cdot\dot{\boldsymbol{\rho}})\boldsymbol{\rho} \\ &+ k(R)|\dot{\boldsymbol{\rho}}|^2\dot{\boldsymbol{\rho}} + n(R)|\boldsymbol{\rho}|^2\dot{\boldsymbol{\rho}} + p(R)(\boldsymbol{\rho}\cdot\dot{\boldsymbol{\rho}})\dot{\boldsymbol{\rho}}.\end{aligned} \tag{2.4.71}$$

Then we investigate the bifurcation structure of Eq. (2.4.71). We check the stable motion by using the conditions for stable rotation and oscillation in Eqs. (2.3.25) and (2.3.30), respectively. To apply

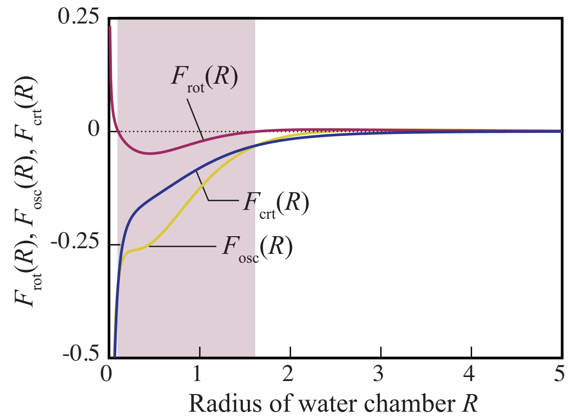

Figure 2.4.2: Plots of $F_{\rm osc}(R) = K(R) + N(R)$, $F_{\rm rot}(R) = 3K(R) + N(R) + J(R)$, and $F_{\rm crt}(R) = K(R) - N(R) + J(R)$ against the radius of the water chamber R. Rotational motion is linearly stable in a certain range of R, which is indicated by coloring with magenta.

the conditions, we convert time t into $\tau = \omega t$, where $\omega(R,\sigma) = \sqrt{-a(R)/(\sigma - g(R))}$, and have

$$\begin{aligned}\ddot{\boldsymbol{\rho}} = &-\boldsymbol{\rho} + (B(R,\sigma) - \Xi)\dot{\boldsymbol{\rho}} + C(R,\sigma)|\boldsymbol{\rho}|^2\boldsymbol{\rho} + H(R)|\dot{\boldsymbol{\rho}}|^2\boldsymbol{\rho} + J(R,\sigma)(\boldsymbol{\rho}\cdot\dot{\boldsymbol{\rho}})\boldsymbol{\rho} \\ &+ K(R,\sigma)|\dot{\boldsymbol{\rho}}|^2\dot{\boldsymbol{\rho}} + N(R,\sigma)|\boldsymbol{\rho}|^2\dot{\boldsymbol{\rho}} + P(R)(\boldsymbol{\rho}\cdot\dot{\boldsymbol{\rho}})\dot{\boldsymbol{\rho}},\end{aligned} \tag{2.4.72}$$

where $B(R,\sigma) = b(R)/\omega(R,\sigma)$, $\Xi = \xi/\omega(R,\sigma)$, $C(R,\sigma) = c(R)/\omega(R,\sigma)^2$, $H(R) = h(R)$, $J(R,\sigma) = j(R)/\omega(R,\sigma)$, $K(R,\sigma) = k(R)\omega(R,\sigma)$, $N(R,\sigma) = n(R)/\omega(R,\sigma)$, and $P(R) = p(R)$. The stability of the rest state at the center of the circular region is determined by the sign of $B(R,\sigma) - \Xi$. For negative $B(R,\sigma) - \Xi$, the rest state is linearly stable. When we fix the radius of the circular region R, the bifurcation parameter is the (dimensionless) resistance coefficient Ξ. By decreasing Ξ, $B(R,\sigma) - \Xi$ becomes negative, then Hopf bifurcation occurs, and the rest state becomes unstable. The stable motion is determined by the conditions in Eqs. (2.3.25) and (2.3.30). Here we show them again below; For stable rotation,

$$\begin{cases} K(R) + N(R) < 0, \\ K(R) - N(R) + J(R) < 0, \end{cases} \tag{2.4.73}$$

and for stable oscillation,

$$\begin{cases} 3K(R) + N(R) + J(R) < 0, \\ K(R) - N(R) + J(R) > 0, \end{cases} \tag{2.4.74}$$

should be satisfied. We show the R-dependence of functions $F_{\rm osc}(R) = K(R) + N(R)$, $F_{\rm rot}(R) = 3K(R)+N(R)+J(R)$, and $F_{\rm crt}(R) = K(R)-N(R)+J(R)$ in Fig. 2.4.2. As in Fig. 2.4.2, rotational motion of a camphor particle in the two-dimensional circular region is linearly stable for a certain range around $R = 1$, and oscillatory motion of it is unstable. When the radius of the water chamber is around $R = 1$, the camphor particle near the center position is affected by the boundary through the concentration field, since the length is normalized by the diffusion length. Thus the rotational motion is stable when the boundary effect is sufficiently large.

It is noted that the conditions in Eqs. (2.4.73) and (2.4.74) are valid for large $|a(R)|$, i.e., for small R. The coefficients $a(R)$, $c(R)$, $h(R)$, $j(R)$, $n(R)$, and $p(R)$, which are the coefficients of position-related terms, go to zero for $R \to \infty$. Thus for sufficiently large R, the position-independent force

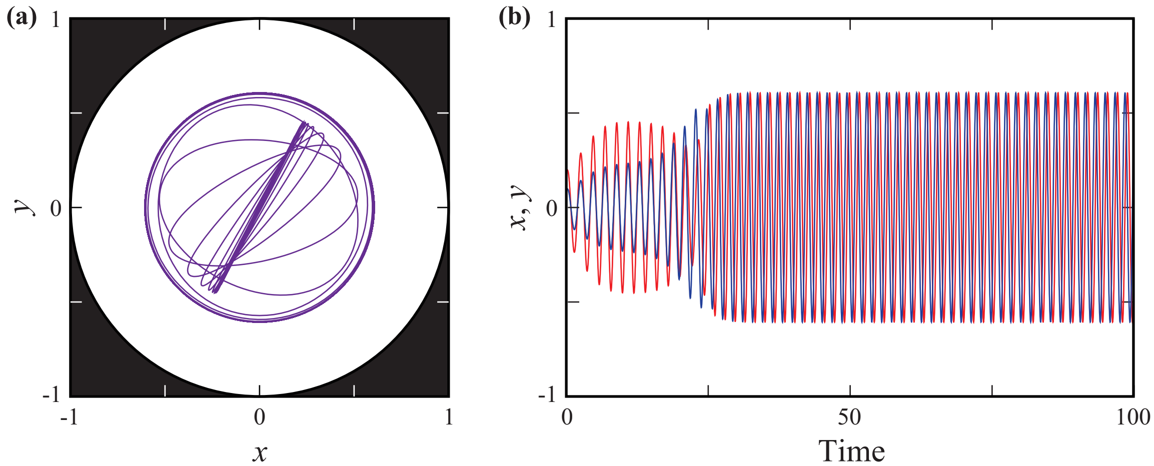

Figure 2.4.3: Numerical results on the trajectories of a camphor particle for the resistance coefficient $\xi = 0.18$. The camphor particle exhibited rotational motion. (a) The trajectory on the x-y plane. (b) Time evolutions of $x(t)$ and $y(t)$ shown in blue- and red-colored curves, respectively. The initial conditions for the position and velocity of the camphor particle were $x = 0.1$, $y = 0.2$, $v_x = -0.01$, and $v_y = 0$, respectively. The concentration field c was zero at every point in the region.

exerted on the camphor particle becomes smaller, and straight motion should be observed at least near the center position of the circular region.

2.4.6 Comparison with the numerical results

To confirm the theoretical results, we performed numerical calculations based on Eqs. (2.4.16) and (2.4.18). We used the Euler method for Eq. (2.4.16) and the explicit method for Eq. (2.4.18). The time and spatial steps were 10^{-5} and 10^{-2}, respectively. The mass per unit area σ was fixed to $sigma = 10^{-2}$. In order to calculate the force acting on the camphor particle in Eq. (2.4.17), we adopted the summation over 40 arc elements as the integration in Eq. (2.4.17).

Here we show the results for the radius of the circular region $R = 1$. The results for the resistance coefficient per unit area $\xi = 0.18$ and $\xi = 0.2$ are shown in Figs. 2.4.3 and 2.4.4, respectively. The initial conditions were the same. We obtained the trajectories toward the circular orbit whose center corresponds to the center of the circular chamber for $\xi = 0.18$ and toward the rest state at the center of the circular chamber for $\xi = 0.2$. Thus it is expected that the bifurcation point exists between $\xi = 0.18$ and $\xi = 0.2$. The bifurcation point for $R = 1$ expected by the theoretical analysis is *ca.* 0.218 and the order of the bifurcation point is the same as that by the numerical results. The comparison of the bifurcation structure obtained by numerical calculation with the theoretical analysis remains as future work.

2.4.7 Comparison with the experimental results

We also made experiments to confiem the theoretical results. Here we observed motion of a camphor particle in the water chamber whose radius was continuously controlled.

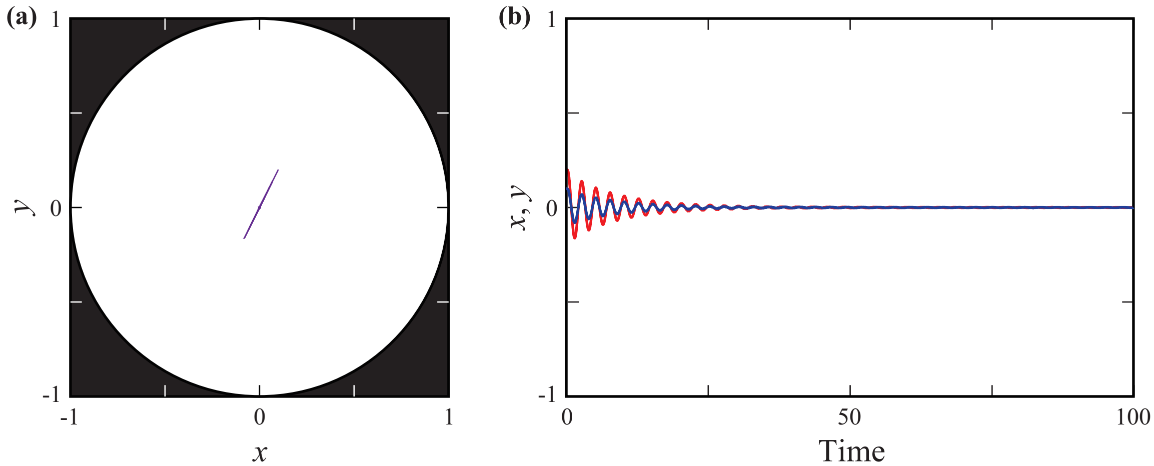

Figure 2.4.4: Numerical results on the trajectories of a camphor particle for the resistance coefficient $\xi = 0.2$. The camphor particle finally stopped at the center of the circular region. (a) The trajectory on the x-y plane. (b) Time evolutions of $x(t)$ and $y(t)$ shown in blue- and red-colored curves, respectively. The initial conditions for the position and velocity of the camphor particle were $x = 0.1$, $y = 0.2$, $v_x = -0.01$, and $v_y = 0$, respectively. The concentration field c was zero at every point in the region.

Experimental setup

A camphor gel disk, whose diameter was 4.0 mm and thickness was 0.5 mm, was made of agar gel in which water was replaced with camphor methanol solution. After the methanol dried up, a camphor particle was floated on a water phase (15 mm in the depth). To achieve a variable-sized water phase, an optical focus (IDC-025, Sigma-koki) was placed on the water phase whose radius R could be changed. As the initial state, a camphor particle was placed on a small sized water phase ($R = 5.0$ mm) where the disk was in the rest state. Then, the radius was increased to 13.0 mm and the motion of the camphor particle was monitored.

Experimental results

At the initial stage with small size of water phase ($R = 5.0$ mm), the disk was in the rest state. With an increase in the radius of the water chamber R, the disk started to move and finally showed rotational motion as shown in Fig. 2.4.5(a). For rotational motion, both the moving speed v and the position of the disk r were almost constant in time as shown in Fig. 2.4.5(b). The theoretical results qualitatively explain the transition from the rest state at the center position of the circular chamber to the rotational motion with an increase in the radius of the water chamber R.

2.4.8 Summary for Section 2.4

The motion of a camphor particle confined in the two-dimensional circular system is investigated [35]. By reducing the model, we analyzed the bifurcation structure. The theoretical results suggest that the rotational motion occurs when the rest state becomes unstable for a water chamber whose radius is comparable with or smaller than the difusion length. The theoretical results correspond to the numerical and experimental results.

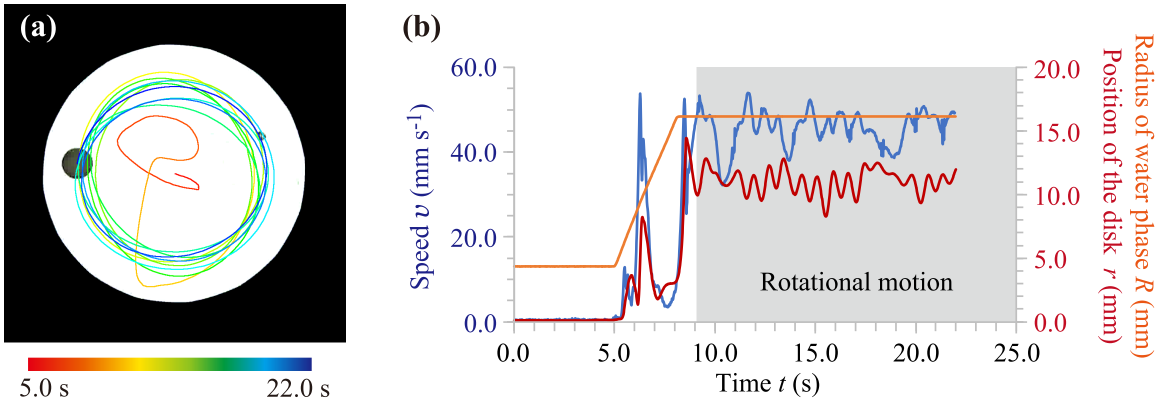

Figure 2.4.5: Motion of a camphor particle obtained in experiments. (a) Trajectory of the moving camphor particle. (b) Time series of speed v, the position of the disk r, and the radius of the water chamber R. The radius of the water chamber was gradually changed from 5.0 mm to 13.0 mm.

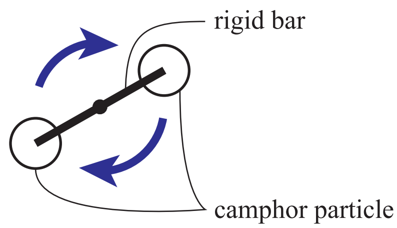

Figure 2.5.1: Schematic illustration of a camphor-driven rotor seen from the top. A camphor-driven rotor is composed of two camphor particles and a rigid bar connecting these camphor particles. The center position of a camphor-driven rotor is fixed.

2.5 Symmetric camphor rotor

In this section, we discuss motion of a camphor-driven rotor, which is constructed with two camphor particles connected with a rigid bar. As shown in Fig. 2.5.1, the considered camphor-driven rotor has mirror symmetry, and therefore either clockwise and counterclockwise rotation is possible.

2.5.1 Mathematical model

In order to discuss the mechanisms of the motion of the camphor-driven rotor, we consider a mathematical model presented below. We define the center position of the i-th camphor particle ($i = 1, 2$) as $\boldsymbol{\ell}_i(t)$. The center of mass of both camphor particles is fixed to the origin of the coordinate system $((\boldsymbol{\ell}_1(t) + \boldsymbol{\ell}_2(t))/2 = \mathbf{0})$. Thus, the center position of the i-th camphor particle is defined only using a single angle $\theta(t)$, i.e.,

$$\boldsymbol{\ell}_1(t) = \ell \boldsymbol{e}(\theta(t)), \quad \boldsymbol{\ell}_2(t) = -\ell \boldsymbol{e}(\theta(t)), \tag{2.5.1}$$

where we set a unit vector $\boldsymbol{e}(\theta(t))$ as $\boldsymbol{e}(\theta) = \boldsymbol{e}_x \cos\theta + \boldsymbol{e}_y \sin\theta$, and $\boldsymbol{e}_x$ and $\boldsymbol{e}_y$ are the unit vectors along the x- and y-axes, respectively.

The time evolution of the surface concentration field of camphor molecules $c(\boldsymbol{r}, t)$ is described as [22, 47]

$$\frac{\partial c}{\partial t} = \nabla^2 c - c + f, \tag{2.5.2}$$

where $-c$ describes sublimation into the air phase and $f = f(\boldsymbol{r}; \boldsymbol{\ell}_1, \boldsymbol{\ell}_2)$ is a function representing the supply of camphor molecules from the camphor particles. Equation (2.5.2) is written using dimensionless variables. In the same manner in Secs. 2.2 and 2.4, the real length, time, and concentration are normalized with the diffusion length $\sqrt{D/\alpha}$, the characteristic time of dissipation of camphor molecules by sublimation and dissipation $1/\alpha$, and the ratio between the supply and dissipation rates of camphor, f_0/α, where D is the diffusion constant of camphor molecules, α is the sublimation rate of camphor, and f_0 is the total supply of camphor from a single particle per unit of real time.

Time evolution of $\theta(t)$ is described as

$$I(\ell)\frac{d^2\theta}{dt^2} = -\eta(\ell)\frac{d\theta}{dt} + \mathcal{T}, \tag{2.5.3}$$

where I and η are the moment of inertia and the resistance coefficient for rotational motion of the camphor particles, respectively, and they depend on ℓ as follows:

$$I(\ell) = 2\pi\epsilon^2\sigma\ell^2, \tag{2.5.4}$$

$$\eta(\ell) = 2\pi\epsilon^2\kappa\ell^2, \tag{2.5.5}$$

where σ and κ are dimensionless parameters corresponding to the mass and the resistance coefficient per unit area for the camphor particles, respectively. The variable ϵ is the radius of the camphor particle. Here, the friction force working on the i-th camphor particle is described as $-(\pi\epsilon^2\kappa)\dot{\boldsymbol{\ell}}_i$.

In Eq. (2.5.3), $\mathcal{T}$ is the torque with respect to the origin acting on the rotor:

$$\mathcal{T} = \sum_{i=1}^{2} \boldsymbol{\ell}_i \times \left[\int_0^{2\pi} \gamma\left(c\left(\boldsymbol{\ell}_i + \epsilon\boldsymbol{e}(\phi)\right)\right)\boldsymbol{e}(\phi)\epsilon d\phi\right], \tag{2.5.6}$$

where $\gamma(c)$ is a function that represents the dependence of the surface tension on the surface concentration of camphor molecules. Here, the vector product "$\times$" describes the operation

$$\boldsymbol{a} \times \boldsymbol{b} = a_1 b_2 - a_2 b_1, \tag{2.5.7}$$

for $\boldsymbol{a} = a_1\boldsymbol{e}_x + a_2\boldsymbol{e}_y$, and $\boldsymbol{b} = b_1\boldsymbol{e}_x + b_2\boldsymbol{e}_y$. If we assume that the surface tension γ is a linear decreasing function of c in the same way as in Secs. 2.2 and 2.4:

$$\gamma(c) = \gamma_0 - \Gamma c, \tag{2.5.8}$$

where γ_0 is the surface tension of pure water, and Γ is a positive constant. Then Eq. (2.5.6) can be rewritten as

$$\mathcal{T} = -\Gamma\ell\boldsymbol{e}(\theta) \times \left[\int_0^{2\pi} c\left(\boldsymbol{\ell}_1 + \epsilon\boldsymbol{e}(\phi)\right)\boldsymbol{e}(\phi)\epsilon d\phi - \int_0^{2\pi} c\left(\boldsymbol{\ell}_2 + \epsilon\boldsymbol{e}(\phi)\right)\boldsymbol{e}(\phi)\epsilon d\phi\right]. \tag{2.5.9}$$

Hereafter, we set $\Gamma = 1$ without losing generality.

2.5.2 Analysis on the angular velocity depending on the rotor size

In this section, the dynamical system for the angular velocity of a single rotor is derived by the reduction of the model equations and its bifurcation structure is revealed. We consider the limit of $\epsilon \to +0$, i.e., the case where the radius of camphor particles is sufficiently small compared with the diffusion length ($= 1$) and the radius of the rotor ($= \ell$).

By dividing the both sides of Eq. (2.5.3) with $\pi\epsilon^2\ell^2$, we obtain

$$\sigma \frac{d^2\theta}{dt^2} = -\kappa \frac{d\theta}{dt} + \frac{1}{2\pi\epsilon^2\ell^2}\mathcal{T}. \tag{2.5.10}$$

Here, we take the limit of $\epsilon \to +0$, and we obtain

$$\frac{1}{\pi\epsilon^2}\mathcal{T} \ \to \lim_{\epsilon\to+0} \frac{1}{\pi\epsilon^2}\mathcal{T} = -\sum_{i=1,2} \boldsymbol{\ell}_i \times \nabla c(\boldsymbol{r})|_{\boldsymbol{r}=\boldsymbol{\ell}_i}, \tag{2.5.11}$$

from the simple calculation for the concentration $c(\boldsymbol{r})$ with no divergence at $\boldsymbol{r} = \boldsymbol{\ell}_i$.

The equation for the concentration field is represented in Eq. (2.5.2). The source term f in Eq. (2.5.2) is given by

$$f(\boldsymbol{r}; \boldsymbol{\ell}_1, \boldsymbol{\ell}_2) = \sum_{i=1,2} \delta(\boldsymbol{r} - \boldsymbol{\ell}_i) = \sum_{i=1,2} \frac{1}{r}\delta(r-\ell)\delta(\phi - \theta_i), \tag{2.5.12}$$

since we consider that the size of the camphor particles is infinitesimally small. Here, $\boldsymbol{r}$ is represented as $\boldsymbol{r} = (r, \phi)$ in the two-dimensional polar coordinates.

The concentration field is the summation of the concentration field made by each camphor particle since the equation for the concentration field is linear. Thus, the concentration field made by a rotor is given by

$$c(\boldsymbol{r}) = c_s(\boldsymbol{r}; \boldsymbol{\ell}_1) + c_s(\boldsymbol{r}; \boldsymbol{\ell}_2), \tag{2.5.13}$$

where $c_s(\boldsymbol{r}; \boldsymbol{\ell})$ is the concentration field made by a single camphor particle located at $\boldsymbol{\ell}$, i.e., the solution of Eq. (2.5.2) with the source term $\delta(\boldsymbol{r} - \boldsymbol{\ell})$. When the velocity of the camphor particle is sufficiently small, the concentration field made by a single particle $c_s(\boldsymbol{r}; \boldsymbol{\ell})$ is analytically expressed as

$$\begin{aligned} c_s(\boldsymbol{r}; \boldsymbol{\ell}) =& c_{00}(\lambda) + c_{10}(\lambda)(\boldsymbol{r} - \boldsymbol{\ell}) \cdot \dot{\boldsymbol{\ell}} + c_{20}(\lambda)(\boldsymbol{r} - \boldsymbol{\ell}) \cdot \ddot{\boldsymbol{\ell}} + c_{21}(\lambda)\left|\dot{\boldsymbol{\ell}}\right|^2 + c_{22}(\lambda)\left[(\boldsymbol{r} - \boldsymbol{\ell}) \cdot \dot{\boldsymbol{\ell}}\right]^2 \\ &+ c_{30}(\lambda)(\boldsymbol{r} - \boldsymbol{\ell}) \cdot \dddot{\boldsymbol{\ell}} + c_{31}(\lambda)\left|\dot{\boldsymbol{\ell}}\right|^2 (\boldsymbol{r} - \boldsymbol{\ell}) \cdot \dot{\boldsymbol{\ell}} + c_{32}(\lambda)\left[(\boldsymbol{r} - \boldsymbol{\ell}) \cdot \dot{\boldsymbol{\ell}}\right]^3 + c_{33}(\lambda)\dot{\boldsymbol{\ell}} \cdot \ddot{\boldsymbol{\ell}} \\ &+ c_{34}(\lambda)\left[(\boldsymbol{r} - \boldsymbol{\ell}) \cdot \dot{\boldsymbol{\ell}}\right]\left[(\boldsymbol{r} - \boldsymbol{\ell}) \cdot \ddot{\boldsymbol{\ell}}\right], \end{aligned} \tag{2.5.14}$$

where $\lambda = |\boldsymbol{r} - \boldsymbol{\ell}|$, the dot over variables ($\dot{}$) represents the time derivative, and the dot between vectors ($\cdot$) represents inner product. Here,

$$\begin{aligned} c_{00}(\lambda) &= \frac{1}{2\pi}\mathcal{K}_0(\lambda), & c_{10}(\lambda) &= -\frac{1}{4\pi}\mathcal{K}_0(\lambda), \\ c_{20}(\lambda) &= \frac{1}{16\pi}\lambda\mathcal{K}_1(\lambda), & c_{21}(\lambda) &= -\frac{1}{16\pi}\lambda\mathcal{K}_1(\lambda), \\ c_{22}(\lambda) &= \frac{1}{16\pi}\mathcal{K}_0(\lambda), & c_{30}(\lambda) &= -\frac{1}{96\pi}\lambda^2\mathcal{K}_2(\lambda), \\ c_{31}(\lambda) &= \frac{1}{32\pi}\lambda\mathcal{K}_1(\lambda), & c_{32}(\lambda) &= -\frac{1}{96\pi}\mathcal{K}_0(\lambda), \\ c_{33}(\lambda) &= \frac{1}{32\pi}\lambda^2\mathcal{K}_2(\lambda), & c_{34}(\lambda) &= -\frac{1}{32\pi}\lambda\mathcal{K}_1(\lambda), \end{aligned} \tag{2.5.15}$$

where $\mathcal{K}_n$ is the second-kind modified Bessel function of the n-th order. It is noted that the term composed of variables with totally more-than-three-time derivatives is neglected. The derivation is shown in Appendix A.3.2.

From Eq. (2.5.13), the torque per contact area (2.5.11) is represented as

$$\lim_{\epsilon\to+0}\frac{1}{\pi\epsilon^2}\mathcal{T}=\sum_{i,j=1,2}\tau_{ij}. \tag{2.5.16}$$

τ_{ii} is the torque per contact area working on a camphor particle originating from self-made concentration field, and calculated as

$$\begin{aligned}\tau_{ii}=&\boldsymbol{\ell}_i\times\lim_{\epsilon\to+0}\frac{-1}{\pi\epsilon^2}\int_0^{2\pi}c_s\left(\boldsymbol{\ell}_i+\epsilon\boldsymbol{e}(\phi);\boldsymbol{\ell}_j\right)\boldsymbol{e}(\phi)\epsilon d\phi\\ =&\frac{1}{4\pi}\left(-\gamma_{\mathrm{Euler}}+\log\frac{2}{\epsilon}\right)\ell^2\dot{\theta}-\frac{1}{16\pi}\ell^2\ddot{\theta}-\frac{1}{32\pi}\ell^4\dot{\theta}^3+\frac{1}{48\pi}\ell^2\left(\dddot{\theta}-\dot{\theta}^3\right),\end{aligned} \tag{2.5.17}$$

where γ_{Euler} is the Euler's constant ($\gamma_{\mathrm{Euler}}\simeq 0.577$). Here we calculated the torque τ_{ii} by taking the vector product of $\boldsymbol{\ell}_i$ with Eq. (2.4.30). Here we used $\boldsymbol{\ell}\times\dot{\boldsymbol{\ell}}=\ell^2\dot{\theta}$, $\boldsymbol{\ell}\times\ddot{\boldsymbol{\ell}}=\ell^2\ddot{\theta}$, and $\boldsymbol{\ell}\times\dddot{\boldsymbol{\ell}}=\ell^2\left(\dddot{\theta}-\dot{\theta}^3\right)$.

Then, we consider the torque working on one camphor particle by the other camphor particle. Since the concentration field $c_s(\boldsymbol{r};\boldsymbol{\ell})$ does not diverge except at $\boldsymbol{r}=\boldsymbol{\ell}$, the torque per contact area by the other camphor particle, τ_{ij} $(i\neq j)$, is calculated as

$$\tau_{ij}=-\frac{1}{4\pi}\mathcal{K}_0\left(2\ell\right)\ell^2\dot{\theta}+\frac{1}{8\pi}\mathcal{K}_1\left(2\ell\right)\ell^3\ddot{\theta}-\frac{1}{16\pi}\mathcal{K}_1\left(2\ell\right)\ell^5\dot{\theta}^3-\frac{1}{24\pi}\mathcal{K}_2(2\ell)\ell^4\left(\dddot{\theta}-\dot{\theta}^3\right), \tag{2.5.18}$$

by using Eq. (2.5.11).

From Eqs. (2.5.10), (2.5.17), and (2.5.18), we have the reduced equation:

$$\sigma\ddot{\theta}=-\kappa\dot{\theta}+\frac{1}{2\ell^2}\sum_{i,j=1,2}\tau_{ij} \tag{2.5.19}$$

$$\begin{aligned}=&-\kappa\dot{\theta}+\frac{1}{4\pi}\left(-\gamma_{\mathrm{Euler}}+\log\frac{2}{\epsilon}-\mathcal{K}_0\left(2\ell\right)\right)\dot{\theta}\\ &-\frac{1}{16\pi}\left(1-2\ell\mathcal{K}_1\left(2\ell\right)\right)\ddot{\theta}-\frac{1}{32\pi}\left(1+2\ell\mathcal{K}_1\left(2\ell\right)\right)\ell^2\dot{\theta}^3+\frac{1}{48\pi}\left(1-2\ell^2\mathcal{K}_2(2\ell)\right)\left(\dddot{\theta}-\dot{\theta}^3\right).\end{aligned} \tag{2.5.20}$$

Based on the description, we discuss a bifurcation structure. We consider the stable solution of $\dot{\theta}=\text{const.}\equiv\omega$. When the rotor rotates with a constant angular velocity, $\dot{\omega}$ and $\ddot{\omega}$ should be zero. Thus we have

$$\left[\frac{1}{4\pi}\left(-\gamma_{\mathrm{Euler}}+\log\frac{2}{\epsilon}-\mathcal{K}_0\left(2\ell\right)\right)-\kappa\right]\omega-\frac{1}{96\pi}\left[3\left(1+2\ell\mathcal{K}_1\left(2\ell\right)\right)\ell^2+2\left(1-2\ell^2\mathcal{K}_2(2\ell)\right)\right]\omega^3=0. \tag{2.5.21}$$

Here, we define the coefficients of ω and ω^3 as $G(\ell)=\left[-\gamma_{\mathrm{Euler}}+\log(2/\epsilon)-\mathcal{K}_0\left(2\ell\right)\right]/(4\pi)-\kappa$ and $H(\ell)=-\left[3\left(1+2\ell\mathcal{K}_1\left(2\ell\right)\right)\ell^2+2\left(1-2\ell^2\mathcal{K}_2(2\ell)\right)\right]/(96\pi)$, respectively. The dependence of $G(\ell)$ and $H(\ell)$ on ℓ is displayed in Fig. 2.5.2. The stable angular velocity is realized when $G(\ell)$ is positive and $H(\ell)$ is negative, and thus the bifurcation point is $\ell=\ell_c$, where $G(\ell_c)=0$.

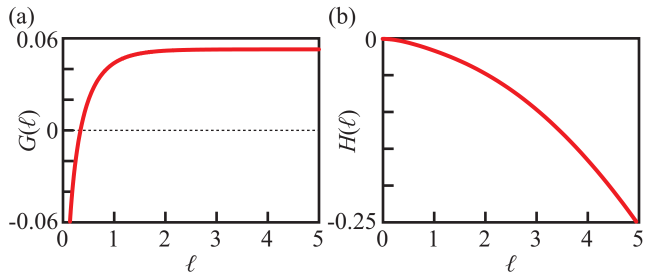

Figure 2.5.2: Plots of the coefficients $G(\ell)$ and $H(\ell)$. The parameters are set to be $\kappa = 1.2$ and $\epsilon = 0.1e^{1/4}$. Reproduced from Ref. [36].

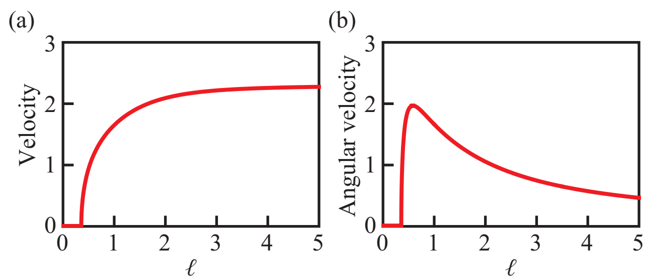

Figure 2.5.3: Velocity and angular velocity depending on ℓ. Parameters are $\kappa = 1.2$ and $\epsilon = 0.1e^{1/4}$. Reproduced from Ref. [36].

The stable angular velocity ω is given by $\sqrt{-G(\ell)/H(\ell)}$ for $G(\ell) > 0$ and 0 for $G(\ell) < 0$, and its dependence on ℓ is shown in Fig. 2.5.3. At $\ell \simeq 0.35$, pitchfork bifurcation occurs when we set the parameters as $\kappa = 1.2$ and $\epsilon = 0.1e^{1/4}$.[1] Over the bifurcation point, the rest state becomes unstable and rotational motion occurs with a constant angular velocity either clockwise or counterclockwise. The asymptotic form of the stable angular velocity for $\ell \to \infty$ is given by $\omega = \sqrt{8\left(-\gamma_{\text{Euler}} + \log(2/\epsilon)\right) - 32\pi\kappa}/\ell \propto \ell^{-1}$. The dependence $\omega \propto \ell^{-1}$ for sufficiently large ℓ is trivial, since the interaction of camphor particles becomes small with an increase of ℓ and each camphor particle moves with a constant velocity independently.

2.5.3 Comparison with the numerical results

We performed numerical calculations of the rotor dynamics according to Eqs. (2.5.2) and (2.5.3). The supply rate from the camphor particle in Eq. (2.5.2) was given as

$$f(\boldsymbol{r}; \boldsymbol{\ell}_1, \boldsymbol{\ell}_2) = \sum_{i=1,2} \frac{1}{\pi\epsilon^2} \left[\frac{1}{2} \left(1 + \tanh \frac{\epsilon - |\boldsymbol{r} - \boldsymbol{\ell}_i|}{\delta} \right) \right], \tag{2.5.22}$$

[1] We used $\epsilon = 0.1e^{1/4}$ to compare with the numerical results by the following reason: In the analytical framework in which the source term is the Dirac's delta function, the force originating from a camphor particle moving at a constant velocity $v\boldsymbol{e}_x$ is written as $\boldsymbol{F} = [(-\gamma_{\text{Euler}} + \log(2/\epsilon))v/(4\pi) - (1/(32\pi))v^3 + \mathcal{O}(v^5)]\boldsymbol{e}_x$. On the while, in the framework that camphor molecules are dissolved inside a circular region with a radius of R, it can be written as $\boldsymbol{F} = [(-\gamma_{\text{Euler}} + \log(2/R) - 1/4)v/(4\pi) - (1/(32\pi))v^3 + \mathcal{O}(v^5)]\boldsymbol{e}_x$ [82]. Therefore, these two situations correspond to each other by setting $\epsilon = R\exp(1/4)$.

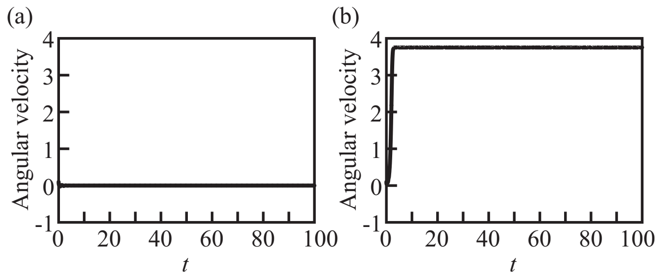

Figure 2.5.4: Numerical results on the angular velocity as a function of time for a small and a large rotor: (a) $\ell = 0.3$ and (b) $\ell = 0.5$. The initial conditions were $\theta = 1$, $d\theta/dt = 0.1$, and $c = 0$ at all space points. Reproduced from Ref. [36].

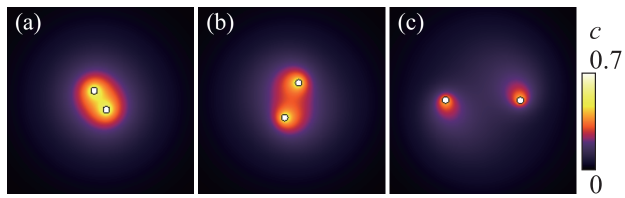

Figure 2.5.5: Profiles of camphor concentration at $t = 100$ for (a) $\ell = 0.3$, (b) $\ell = 0.5$, and (c) $\ell = 1.0$, obtained by numerical calculation. The rotor did not move in (a) and it rotated clockwise in (b) and (c). The initial conditions were all the same as those in Fig. 2.5.4. Reproduced from Ref. [36].

where δ is a smoothing parameter set to be $\delta = 0.025$. The total supply from a single camphor particle was approximately equal to 1. We used the Euler method to calculate the reaction terms, and explicit method for the diffusion term. The time and spatial steps were 10^{-4} and 0.025, respectively. The parameters were set as $\epsilon = 0.1$, $\sigma = 0.004$, and $\kappa = 0.12$. As for the concentration field, we considered a circular outer boundary with a radius of 10, which hardly affects the motion of the rotor for $\ell \leq 5$. In order to calculate the force acting on each camphor particle in Eq. (2.5.9), we adopted the summation over 32 arc elements as the integration in Eq. (2.5.9). We performed numerical calculations and obtained the time evolution of the angle $\theta(t)$ and the angular velocity $d\theta/dt$. We investigated the behavior of a rotor depending on the distance between two camphor particles 2ℓ. For larger ℓ, the rotor moved stationarily, whereas for smaller ℓ, it stopped as shown in Fig. 2.5.4. The snapshots of the camphor concentration for various ℓ are shown in Fig. 2.5.5. In the case when the rotor did not move, the camphor concentration profile was symmetric with respect to the axis connecting the centers of two camphor particles as in Fig. 2.5.5(a). In contrast, if it rotated, the profile had chiral asymmetry as shown in Fig. 2.5.5(b,c).

In Fig. 2.5.6, we present the stationary speed of the center position of each camphor particle and the stationary angular velocity of the rotor as a function of rotor radius ℓ. For large ℓ, we expect that the interaction between the two camphor particles becomes negligible. In such a case, the both camphor particles should move at the speed equal to that for a single camphor particle without any constraints. Then, the angular velocity should be inversely proportional to ℓ. For small ℓ, we can see the transition-like behaviour between static and moving rotor around $\ell \simeq 0.33$ in Fig. 2.5.6, and thus the theoretical results were confirmed. We consider the numerical error comes from the size

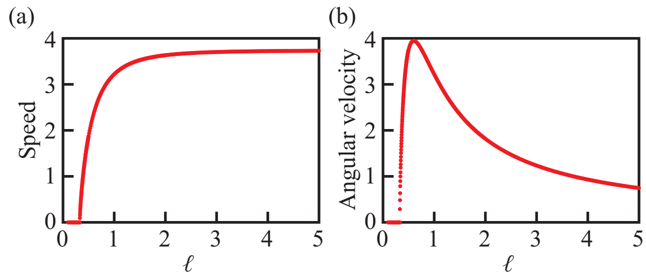

Figure 2.5.6: Numerical results on stationary speed (a) and stationary angular velocity (b) as a function of the rotor radius ℓ. Reproduced from Ref. [36].

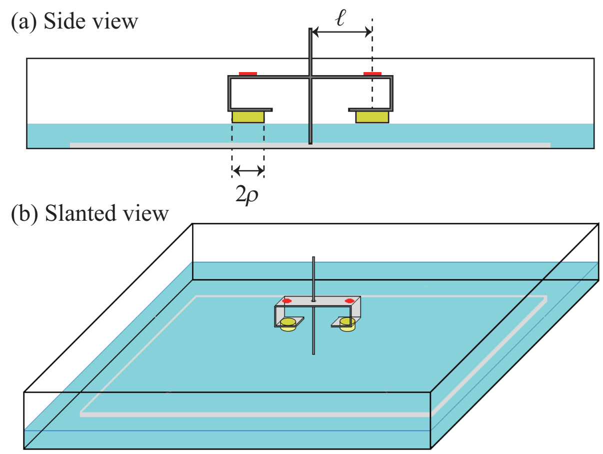

Figure 2.5.7: Schematic illustration of the experimental setup. The side view (a) and the slanted view (b) of the rotor are shown. Reproduced from Ref. [36].

effect of the camphor particle. We expect this transition originates from pitchfork bifurcation, at which the stable rest state becomes unstable.

2.5.4 Comparison with the experimental results

In order to confirm the theoretical results, we also performed the experiments. We studied the motion of a simple rotor driven by two camphor particles glued below the ends of a plastic stripe as illustrated in Fig. 2.5.7. The system could rotate around a vertical axis located at the center of the stripe. The particles were made by pressing camphor (Sigma-Aldrich) in a pill maker. The radius of each camphor particle was 1.5 mm and it was 1 mm high. The rotor was floating on a water surface in the square tank (tank side 120 mm) and the water level was 10 mm. In order to reduce the hydrodynamic flows, the central part of the plastic stripe was elevated above the water level so that only the bottom surface of camphor particles had contact with water surface and the stripe did not touch it. The time evolution of rotor was recorded using a digital camera (NEX VG20EH, SONY) and the coordinates of red dots (cf. Fig. 2.5.8(b)) located over the centers of camphor particles were obtained using the ImageJ (NIH, USA). A typical time of experiment was in the range from 5 to 10 min.

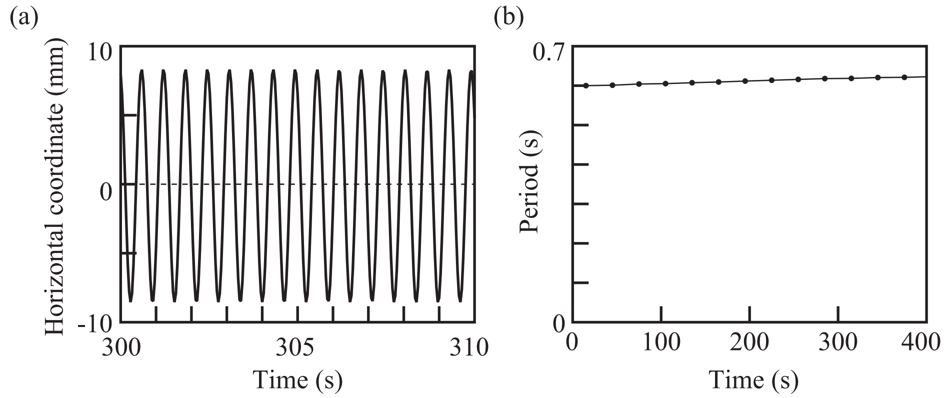

Figure 2.5.8: Experimental results on rotor motion. (a) Time evolution of a horizontal coordinate of one of marking dots for a rotor with $\ell = 8.5$ mm in the time interval from 300 s to 310 s. (b) Period for the rotor with $\ell = 8.5$ mm as a function of time. Reproduced from Ref. [36].

The distance between the axis and the particle center ℓ was controlled as the parameter. Periodic changes in the horizontal coordinate of one of the dots of the rotor with $\ell = 8.5$ mm are shown in Fig. 2.5.8(a). During the time of all experiments we observed highly regular rotations without any significant perturbations of rotor motion. The period of oscillations was measured as the time between the successive maxima separately in each 30-s interval. Typically the period slowly increased with time as illustrated in Fig. 2.5.8(b). The changes were not significant and for the subsequent analysis we considered the values obtained in the time interval from 300 s to 400 s.

Figure 2.5.9 illustrates the speed of center position of the particle (a) and the angular velocity (b) as the function of ℓ. The speed grew monotonically with an increase in ℓ. It can be expected that for a large ℓ the speed saturates to be the one for a separated camphor particle. By considering the angular velocity instead of the velocity, we observed a single peak of angular velocity around $\ell = 2.5$ mm as a function of ℓ. For large ℓ, it was a decreasing function. Such features well correspond to the theoretical results. It is noted that the rest state was not observed in our experiments. We expect that the rest state can be observed for larger resistance, and it can be realized by using the glycerol aqueous solution whose viscosity is greater than that of pure water as the aqueous phase [34, 47].

2.5.5 Summary for Section 2.5

The motion of a symmetric camphor-driven rotor is investigated [36]. A camphor-driven rotor stops or rotates depending on the size of the rotor (the length of the bar). We analyzed the stable angular velocity for a camphor-driven rotor, and clarified that there is a bifurcation point where the zero angular velocity corresponding to the rest state becomes unstable. The theoretical results were confirmed by the numerical calculations and the experiments.

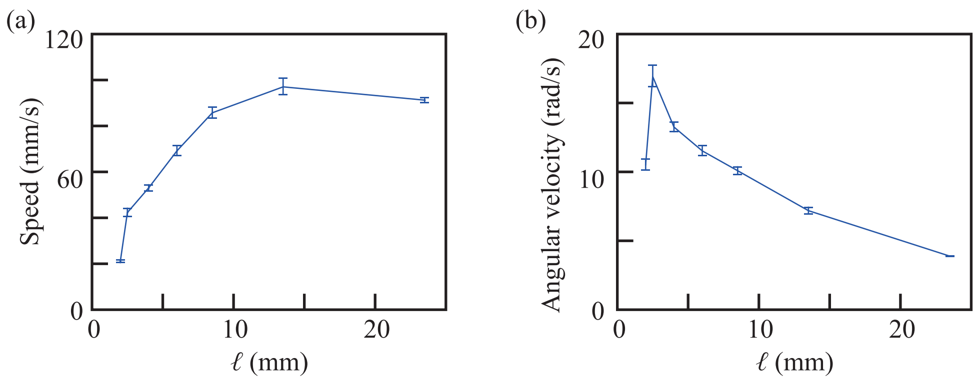

Figure 2.5.9: Experimental results on rotor motion as a function of rotor radius ℓ. (a) Speed of the camphor particle. (b) Angular velocity of a rotor. The green and red points indicate the experimental errors. Reproduced from Ref. [36].

Chapter 3

Hydrodynamic Collective Effect of Active Elements

3.1 Introduction

In biological cells, there are many proteins which have functions, e.g., pumps, channels, actuators, and so on. They recursively change their shapes and act by consuming chemical energy which is typically supplied from adenosine triphosphate (ATP). We call such proteins as "active proteins" in this thesis.

Recently, the direct observation of particles inside a cell have been available, and it was reported that diffusion was enhanced compared with normal diffusion under thermal equilibrium [83, 84]. Parry *et al.* reported that cellular metabolism fluidizes the cytoplasm though it is viscous enough to be a glass state without cellular metabolism. Guo *et al.* embedded tracer particles in a Meranoma cell (skin cancer cell), and observed trajectories of the tracer particles [84]. The tracer particles showed random motion similar to Brownian motion, but its mean square displacement was much greater than that of the Brownian motion under thermal fluctuations. Such an effect was also reported *in vitro* [85], as well as in a cell. They observed the diffusion at biphase fluid in a microchannel; one fluid included substrates and the other breakdown enzymes. Here enzymes and substrates are comparable to active proteins and source of chemical energy, respectively. The diffusion of enzymes to the substrate phase is greater than that in the case when the substrates were not included. Thus, micro-scale active elements immersed in a fluid seem to enhance the diffusion.

To explain the diffusion enhancement in a system with active elements such as active proteins, Mikhailov and Kapral proposed a model with an assumption that active proteins are considered to be force dipoles immersed in fluid [38]. The assumption is valid for a dilute system of active proteins, since dipole approximation is appropriate in the regime of far field. It is also supported by the fact that an elastic network mimicking a conformation of an active protein has a slow relaxation dynamics [86]. For arbitrary deformations, the rapid relaxation dynamics takes place in the first stage, followed by the slow dynamics toward to the original configuration with the lowest energy. Such a lowest-energy state depends on the chemical circumstance of substrate, and the deformation process to the new stable configuration of the protein caused by the switching of the stable configurations is considered to be slow dynamics along a one-dimensional orbit. This model can be applied not only to cytoplasm (a three-dimensional system) but also to biomembrane (a two-dimensional system).

In this chapter, we first summarize the previous results by Mikhailov and Kapral in Sec. 3.2.

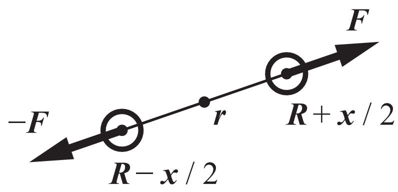

Figure 3.2.1: Schematic illustration on a force dipole. A protein in cytoplasm and biomembrane is modeled as a force dipole immersed in a three- and two-dimensional fluid.

They explained the diffusion enhancement by active force dipoles. In Sec. 3.3, we consider a localized effect of force dipoles, as an example of an inhomogeneous system [40]. In the previous study and in Sec. 3.3, we assumed that the orientation of force dipoles is randomly distributed. We also discussed the effect of nematic order of force dipoles in Sec. 3.4. We consider the case that the force dipoles are perfectly aligned in a one direction, and compare the results in the case of randomly directed force dipoles [41].

3.2 Mathematical model and previous results

In this section, we show the derivation of the model for the motion of particles induced by active elements through hydrodynamic interaction and the explanation of diffusion enhancement by them, which was proposed by Mikhailov and Kapral [38].

3.2.1 Derivation of equation for the distribution of tracer particles

In the model, the cytoplasm and biomembrane around active proteins are considered to be three- and two-dimensional fluid, respectively. It is assumed that active proteins induce flow when they change their shape. An active protein acts as a force dipole under far-field approximation.

A force dipole is composed of a pair of point forces $\boldsymbol{F}$ and $-\boldsymbol{F}$, which act on different two points as shown in Fig. 3.2.1. The directions of forces are opposite to each other and parallel to the line connecting the two points on which the forces are exerted. The flow $\boldsymbol{v}$ induced by a force dipole located at $\boldsymbol{R}(t)$ is described as

$$v_\alpha(\boldsymbol{r}) = \left[G_{\alpha\beta}\left(\boldsymbol{r}-\boldsymbol{R}+\frac{\boldsymbol{x}(t)}{2}\right) - G_{\alpha\beta}\left(\boldsymbol{r}-\boldsymbol{R}-\frac{\boldsymbol{x}(t)}{2}\right)\right]F_\beta \tag{3.2.1}$$

$$\simeq \frac{\partial G_{\alpha\beta}(\boldsymbol{r}-\boldsymbol{R})}{\partial R_\gamma} e_\beta(t) e_\gamma(t) m(\boldsymbol{R},t), \tag{3.2.2}$$

where $\boldsymbol{x}$ is a vector directing from one point to the other, $\boldsymbol{e}$ is a unit vector proportional to $\boldsymbol{x}$ and $\boldsymbol{F}$, and $m(\boldsymbol{r},t) = |\boldsymbol{x}(t)||\boldsymbol{F}(\boldsymbol{r},t)|$ is the strength of the force dipole located at $\boldsymbol{r}$ at time t. Here we adopt the Einstein summation convention, i.e., the summation symbols are omitted for doubled subscripts. The function G is the Oseen tensor, which is the Green's function of Stokesian equation, and has a form:

$$G_{\alpha\beta} = \frac{1}{4\pi\eta}\left(-(1+\ln(\kappa r))\delta_{\alpha\beta} + \frac{r_\alpha r_\beta}{r^2}\right) \tag{3.2.3}$$

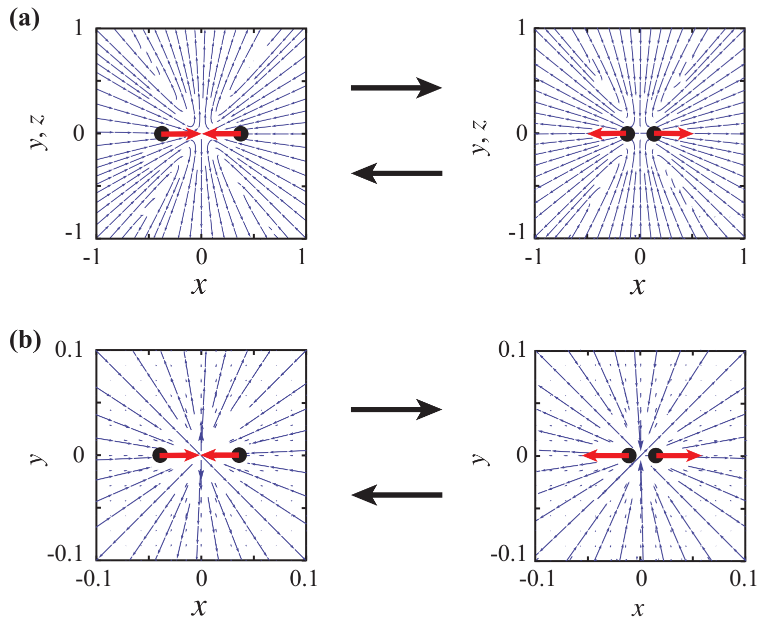

Figure 3.2.2: Flow induced by a force dipole. A force dipole is immersed in (a) a three-dimensional and (b) a two-dimensional systems, respectively.

for a two-dimensional system [87] and

$$G_{\alpha\beta} = \frac{1}{8\pi\eta}\left(\frac{1}{r}\delta_{\alpha\beta} + \frac{r_\alpha r_\beta}{r^3}\right) \tag{3.2.4}$$

for a three-dimensional system. It is noted that κ in Eq. (3.2.3) is the characteristic inverse length, which related to Saffman-Delbrück length [88], $\kappa^{-1} = \eta h/(2\eta_s)$, where h is the thickness of the membrane and η and η_s are the viscosity of the membrane and solvent, respectively. Here, $\delta_{\alpha\beta}$ is the Kronecker's detla, i.e., $\delta_{\alpha\beta}$ is 1 for $\alpha = \beta$ and 0 otherwise. The derivation of the Oseen tensor is provided in Appendix B.1. The flow induced by a single protein in a three- and two-dimensional fluid is shown in Fig. 3.2.2.

Here we consider the situation with many active proteins as shown in Fig. 3.2.3. Since the Stokesian equation is linear, the flow induced by multiple force dipoles is the summation of the flow induced by each force dipole. Tracer particles are carried by flow with the same velocity of the fluid itself, and also affected by thermal noise. Thus, the velocity of a tracer particle is represented as follows:

$$\frac{dr_\alpha}{dt} = \sum_i \frac{\partial G_{\alpha\beta}(\boldsymbol{r}(t) - \boldsymbol{R}_i)}{\partial R_{i,\gamma}} e_{i,\beta}(t) e_{i,\gamma}(t) m_i(\boldsymbol{R}_i, t) + f_\alpha(t), \tag{3.2.5}$$

where the variable with subscript i represents that it is for the i-th force dipole and $f_\alpha(t)$ denotes thermal fluctuation, which satisfies $\langle f_\alpha(t)\rangle = 0$ and $\langle f_\alpha(t) f_{\alpha'}(t')\rangle = 2k_B T\gamma\delta_{\alpha\alpha'}\delta(t-t')$ where γ is the mobility coefficient of the tracer particle. Here k_B and T are the Boltzmann constant and the temperature, respectively. Since the identity $\delta_{\beta\gamma}\partial G_{\alpha\beta}/\partial R_\gamma = 0$ holds, $e_{i,\beta}e_{i,\gamma}$ can be replaced with $N^{(d)}_{i,\beta\gamma}(t)$:

$$\frac{dr_\alpha}{dt} = \sum_i \frac{\partial G_{\alpha\beta}(\boldsymbol{r} - \boldsymbol{R}_i(t))}{\partial R_{i,\gamma}} N^{(d)}_{i,\beta\gamma}(t) m_i(\boldsymbol{R}_i, t) + f_\alpha(t). \tag{3.2.6}$$

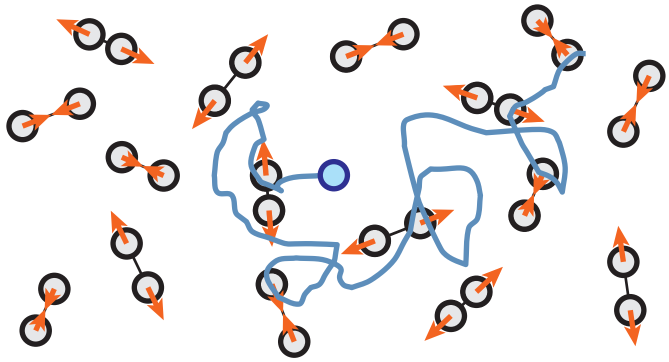

Figure 3.2.3: Schematic illustration of the considered situtation. There are many active proteins and a tracer particle is driven by the flow induced by active proteins.

Here $N^{(d)}_{i,\beta\gamma}(t)$ is defined as:

$$N^{(d)}_{i,\beta\gamma}(t) = e_{i,\beta}(t)e_{i,\gamma}(t) - \frac{1}{d}\delta_{\beta\gamma}, \tag{3.2.7}$$

where d is a spatial dimension. If the dynamics for the orientation of the force dipoles is sufficiently slower than that for the expansion and contraction of the force dipoles, the time dependence of $N^{(d)}_{i,\beta\gamma}(t)$ can be neglected.

The Kramers-Moyal coefficient of first order $V_\alpha(\boldsymbol{r})$ is calculated as follows:

$$V_\alpha(\boldsymbol{r}) = \lim_{\Delta t\to 0}\frac{1}{\Delta t}\left\langle \int_t^{t+\Delta t}\sum_i \frac{\partial G_{\alpha\beta}(\boldsymbol{r}(t_1)-\boldsymbol{R}_i)}{\partial R_{i,\gamma}} N^{(d)}_{i,\beta\gamma} m_i(\boldsymbol{R}_i,t_1)dt_1\right\rangle. \tag{3.2.8}$$

Here we adopt the Stratonovich interpretation and use $\langle f_\alpha(t)\rangle = 0$. Since the position of the tracer particle $\boldsymbol{r}$ does not change in small time period $[t, t+\Delta t]$, Eq. (3.2.8) is expanded as follows:

$$\begin{aligned}
&V_\alpha(\boldsymbol{r})\\
&= \lim_{\Delta t\to 0}\frac{1}{\Delta t}\Bigg\langle \int_t^{t+\Delta t}\sum_i \frac{\partial G_{\alpha\beta}(\boldsymbol{r}(t)-\boldsymbol{R}_i)}{\partial R_{i,\gamma}} N^{(d)}_{i,\beta\gamma} m_i(\boldsymbol{R}_i,t_1)dt_1\\
&\quad + \int_t^{t+\Delta t}\int_t^{t_1}\sum_{i,j}\frac{\partial^2 G_{\alpha\beta}(\boldsymbol{r}(t)-\boldsymbol{R}_i)}{\partial r_\delta \partial R_{i,\gamma}}\frac{\partial G_{\delta\beta'}(\boldsymbol{r}(t_2)-\boldsymbol{R}_j)}{\partial R_{j,\gamma'}} N^{(d)}_{i,\beta\gamma}N^{(d)}_{j,\beta'\gamma'} m_i(\boldsymbol{R}_i,t_1)m_j(\boldsymbol{R}_j,t_2)dt_2dt_1\Bigg\rangle\\
&= \lim_{\Delta t\to 0}\frac{1}{\Delta t}\Bigg\langle \int_t^{t+\Delta t}\sum_i \frac{\partial G_{\alpha\beta}(\boldsymbol{r}(t)-\boldsymbol{R}_i)}{\partial R_{i,\gamma}} N^{(d)}_{i,\beta\gamma} m_i(\boldsymbol{R}_i,t_1)dt_1\\
&\quad + \int_t^{t+\Delta t}\int_t^{t_1}\sum_{i,j}\frac{\partial^2 G_{\alpha\beta}(\boldsymbol{r}(t)-\boldsymbol{R}_i)}{\partial r_\delta \partial R_{i,\gamma}}\frac{\partial G_{\delta\beta'}(\boldsymbol{r}(t_2)-\boldsymbol{R}_j)}{\partial R_{j,\gamma'}} N^{(d)}_{i,\beta\gamma}N^{(d)}_{j,\beta'\gamma'} m_i(\boldsymbol{R}_i,t_1)m_j(\boldsymbol{R}_j,t_2)dt_2dt_1\\
&\quad + \int_t^{t+\Delta t}\int_t^{t_1}\int_t^{t_2}\sum_{i,j,k}\frac{\partial^2 G_{\alpha\beta}(\boldsymbol{r}(t)-\boldsymbol{R}_i)}{\partial r_\delta \partial R_{i,\gamma}}\frac{\partial^2 G_{\delta\beta'}(\boldsymbol{r}(t)-\boldsymbol{R}_j)}{\partial r_{\delta'} \partial R_{j,\gamma'}}\frac{\partial G_{\delta'\beta''}(\boldsymbol{r}(t_3)-\boldsymbol{R}_k)}{\partial R_{k,\gamma''}}\\
&\qquad\qquad \times N^{(d)}_{i,\beta\gamma}N^{(d)}_{j,\beta'\gamma'}N^{(d)}_{k,\beta''\gamma''} m_i(\boldsymbol{R}_i,t_1)m_j(\boldsymbol{R}_j,t_2)m_k(\boldsymbol{R}_k,t_3)dt_3dt_2dt_1\Bigg\rangle.
\end{aligned} \tag{3.2.9}$$

Here we use the integration of Eq. (3.2.6) with regard to time:

$$\begin{aligned} r_\alpha(t_1) =& r_\alpha(t) + \int_t^{t_1} \sum_i \frac{\partial G_{\alpha\beta}(\boldsymbol{r} - \boldsymbol{R}_i(t_2))}{\partial R_{i,\gamma}} N^{(d)}_{i,\beta\gamma}(t_2) m_i(\boldsymbol{R}_i, t_2) dt_2 + \int_t^{t_1} f_\alpha(t_2) dt_2 && (3.2.10) \\ \equiv& r_\alpha(t) + \Delta r_\alpha(t, t_1), && (3.2.11) \end{aligned}$$

the relation $\langle f_\alpha(t)\rangle = 0$, and expansion of $(\partial G_{\alpha\beta}(\boldsymbol{r}(t) + \Delta r_\alpha(t,t_1) - \boldsymbol{R}_i))/(\partial R_{i,\gamma})$ with regard to $\Delta r_\alpha(t,t_1)$. From the assumption $\langle m_i(\boldsymbol{R}_i, t_1)\rangle = 0$, the first term in Eq. (3.2.9) vanishes. The third term in Eq. (3.2.9) also vanishes since the following equations hold for the Gaussian distribution:

$$\begin{aligned} \langle m_i(\boldsymbol{R}_i, t_1) m_j(\boldsymbol{R}_j, t_2) m_k(\boldsymbol{R}_k, t_3)\rangle =& \langle m_i(\boldsymbol{R}_i, t_1) m_j(\boldsymbol{R}_j, t_2)\rangle \langle m_k(\boldsymbol{R}_k, t_3)\rangle \\ &+ \langle m_i(\boldsymbol{R}_i, t_1)\rangle \langle m_j(\boldsymbol{R}_j, t_2) m_k(\boldsymbol{R}_k, t_3)\rangle \\ &+ \langle m_j(\boldsymbol{R}_j, t_2)\rangle \langle m_i(\boldsymbol{R}_i, t_1) m_k(\boldsymbol{R}_k, t_3)\rangle \\ =& 0. && (3.2.12) \end{aligned}$$

The derivative with regard to the position of tracer particle $\partial/\partial r_\delta$ is replaced with that with regard to the position of a force dipole $-\partial/\partial R_{i,\delta}$.

$$\begin{aligned} V_\alpha(\boldsymbol{r}) =& -\lim_{\Delta t\to 0} \frac{1}{\Delta t} \int_t^{t+\Delta t}\int_t^{t_1} \sum_{i,j} \frac{\partial^2 G_{\alpha\beta}(\boldsymbol{r}(t) - \boldsymbol{R}_i)}{\partial R_{i,\delta}\partial R_{i,\gamma}} \frac{\partial G_{\delta\beta'}(\boldsymbol{r}(t) - \boldsymbol{R}_j)}{\partial R_{j,\gamma'}} \\ &\times \left\langle N^{(d)}_{i,\beta\gamma} N^{(d)}_{j,\beta'\gamma'}\right\rangle \langle m_i(\boldsymbol{R}_i, t) m_j(\boldsymbol{R}_j, t_2)\rangle dt_2 dt_1 \\ =& -\lim_{\Delta t\to 0} \frac{1}{\Delta t} \int_t^{t+\Delta t}\int_t^{t_1} \sum_{i,j} \frac{\partial^2 G_{\alpha\beta}(\boldsymbol{r}(t) - \boldsymbol{R}_i)}{\partial R_{i,\delta}\partial R_{i,\gamma}} \frac{\partial G_{\delta\beta'}(\boldsymbol{r}(t) - \boldsymbol{R}_j)}{\partial R_{j,\gamma'}} \\ &\times \left\langle N^{(d)}_{i,\beta\gamma} N^{(d)}_{j,\beta'\gamma'}\right\rangle 2S(\boldsymbol{R}_i)\delta_{ij}\delta(t_1 - t_2) dt_2 dt_1 \\ =& -\lim_{\Delta t\to 0} \frac{1}{\Delta t} \int_t^{t+\Delta t} \sum_i \frac{\partial^2 G_{\alpha\beta}(\boldsymbol{r}(t) - \boldsymbol{R}_i)}{\partial R_{i,\delta}\partial R_{i,\gamma}} \frac{\partial G_{\delta\beta'}(\boldsymbol{r}(t) - \boldsymbol{R}_i)}{\partial R_{i,\gamma'}} \left\langle N^{(d)}_{i,\beta\gamma} N^{(d)}_{i,\beta'\gamma'}\right\rangle S(\boldsymbol{R}_i) dt_1. \end{aligned} \quad (3.2.13)$$

Here we assume $\langle m_i(\boldsymbol{R}_i, t_1) m_j(\boldsymbol{R}_j, t_2)\rangle = 2S(\boldsymbol{R}_i)\delta_{ij}\delta(t_1 - t_2)$, which means that the considered time scale for the dynamics of the tracer particle is sufficiently longer than that for the characteristic correlation time of the activity force dipoles, and the activities of the force dipoles have no correlation. It is noted that we explicitly consider the spatial dependence of the correlation function $S(\boldsymbol{R}_i)$. Using $f(\boldsymbol{R}) = \int f(\boldsymbol{r}')\delta(\boldsymbol{r}' - \boldsymbol{R}) d\boldsymbol{r}'$ and $c(\boldsymbol{r}) = \sum_i \delta(\boldsymbol{r} - \boldsymbol{R}_i)$ where $c(\boldsymbol{r})$ is the number density of the force dipoles, we have

$$\begin{aligned} &V_\alpha(\boldsymbol{r}) \\ &= -\lim_{\Delta t\to 0} \frac{1}{\Delta t} \int_t^{t+\Delta t}\int \sum_i \frac{\partial^2 G_{\alpha\beta}(\boldsymbol{r}(t) - \boldsymbol{r}')}{\partial r'_\delta \partial r'_\gamma} \frac{\partial G_{\delta\beta'}(\boldsymbol{r}(t) - \boldsymbol{r}')}{\partial r'_{\gamma'}} \left\langle N^{(d)}_{i,\beta\gamma} N^{(d)}_{i,\beta'\gamma'}\right\rangle S(\boldsymbol{r}')\delta(\boldsymbol{r}' - \boldsymbol{R}_i) d\boldsymbol{r}' dt_1 \\ &= -\int \frac{\partial^2 G_{\alpha\beta}(\boldsymbol{r}(t) - \boldsymbol{r}')}{\partial r'_\delta \partial r'_\gamma} \frac{\partial G_{\delta\beta'}(\boldsymbol{r}(t) - \boldsymbol{r}')}{\partial r'_{\gamma'}} \left\langle N^{(d)}_{i,\beta\gamma} N^{(d)}_{i,\beta'\gamma'}\right\rangle S(\boldsymbol{r}') c(\boldsymbol{r}') d\boldsymbol{r}' \\ &= -\int \frac{\partial^2 G_{\alpha\beta}(\boldsymbol{r} - \boldsymbol{r}')}{\partial r'_\delta \partial r'_\gamma} \frac{\partial G_{\delta\beta'}(\boldsymbol{r} - \boldsymbol{r}')}{\partial r'_{\gamma'}} \left\langle N^{(d)}_{i,\beta\gamma} N^{(d)}_{i,\beta'\gamma'}\right\rangle S(\boldsymbol{r}') c(\boldsymbol{r}') d\boldsymbol{r}'. && (3.2.14) \end{aligned}$$

We assume that the property of orientational order of force dipoles is independent of the particles. We define $N^{(d)}_{i,\beta\gamma} = \bar{N}^{(d)}_{\beta\gamma} + n^{(d)}_{i,\beta\gamma}$, where $\bar{N}^{(d)}_{\beta\gamma} = \left\langle N^{(d)}_{i,\beta\gamma} \right\rangle$, and then we have

$$\begin{aligned}\left\langle N^{(d)}_{i,\beta\gamma} N^{(d)}_{i,\beta'\gamma'} \right\rangle =& \bar{N}^{(d)}_{\beta\gamma}\bar{N}^{(d)}_{\beta'\gamma'} + \bar{N}^{(d)}_{\beta\gamma}\left\langle n^{(d)}_{j,\beta'\gamma'} \right\rangle + \left\langle n^{(d)}_{i,\beta\gamma} \right\rangle \bar{N}^{(d)}_{\beta'\gamma'} + \left\langle n^{(d)}_{i,\beta\gamma} n^{(d)}_{i,\beta'\gamma'} \right\rangle \\ =& \bar{N}^{(d)}_{\beta\gamma}\bar{N}^{(d)}_{\beta'\gamma'} + \Lambda^{(d)}_{\beta\gamma\beta'\gamma'},\end{aligned} \tag{3.2.15}$$

where $\Lambda^{(d)}_{\beta\gamma\beta'\gamma'}$ is defined as $\Lambda^{(d)}_{\beta\gamma\beta'\gamma'} \equiv \left\langle n^{(d)}_{\beta\gamma} n^{(d)}_{\beta'\gamma'} \right\rangle$. Thus we have

$$V_\alpha(\boldsymbol{r}) = -\left(\bar{N}^{(d)}_{\beta\gamma}\bar{N}^{(d)}_{\beta'\gamma'} + \Lambda^{(d)}_{\beta\gamma\beta'\gamma'}\right)\int \frac{\partial^2 G_{\alpha\beta}(\boldsymbol{r}-\boldsymbol{r'})}{\partial r'_\delta \partial r'_\gamma}\frac{\partial G_{\delta\beta'}(\boldsymbol{r}-\boldsymbol{r'})}{\partial r'_{\gamma'}} S(\boldsymbol{r'})c(\boldsymbol{r'})d\boldsymbol{r'}. \tag{3.2.16}$$

The Kramers-Moyal coefficient of second order $D_{\alpha\alpha'}(\boldsymbol{r})$ is calculated as follows:

$$\begin{aligned}D_{\alpha\alpha'}(\boldsymbol{r}) =& \lim_{\Delta t\to 0}\frac{1}{2\Delta t}\left\langle \int_t^{t+\Delta t}\int_t^{t+\Delta t}\sum_{i,j}\frac{\partial G_{\alpha\beta}(\boldsymbol{r}(t_1)-\boldsymbol{R}_i)}{\partial R_{i,\gamma}}\frac{\partial G_{\alpha'\beta'}(\boldsymbol{r}(t_2)-\boldsymbol{R}_j)}{\partial R_{j,\gamma'}}\right. \\ &\left.\times N^{(d)}_{i,\beta\gamma}N^{(d)}_{j,\beta\gamma} m_i(\boldsymbol{R}_i,t_1)m_j(\boldsymbol{R}_j,t_2)dt_1dt_2\right\rangle + \lim_{\Delta t\to 0}\frac{1}{2\Delta t}\left\langle \int_t^{t+\Delta t}\int_t^{t+\Delta t} f_\alpha(t_1)f_{\alpha'}(t_2)dt_1dt_2\right\rangle.\end{aligned} \tag{3.2.17}$$

The second term is calculated as $k_BT\gamma\delta_{\alpha\alpha'} \equiv D^T\delta_{\alpha\alpha'}$. The first term is calculated as follows:

$$\begin{aligned}&D_{\alpha\alpha'}(\boldsymbol{r}) - D^T\delta_{\alpha\alpha'} \\ &= \lim_{\Delta t\to 0}\frac{1}{2\Delta t}\left\langle \int_t^{t+\Delta t}\int_t^{t+\Delta t}\sum_{i,j}\left[\frac{\partial G_{\alpha\beta}(\boldsymbol{r}(t)-\boldsymbol{R}_i)}{\partial R_{i,\gamma}}\frac{\partial G_{\alpha'\beta'}(\boldsymbol{r}(t)-\boldsymbol{R}_j)}{\partial R_{j,\gamma'}}\right.\right. \\ &+ \int_t^{t+\Delta t}\sum_k \frac{\partial^2 G_{\alpha\beta}(\boldsymbol{r}(t)-\boldsymbol{R}_i)}{\partial r_\delta \partial R_{i,\gamma}}\frac{\partial G_{\alpha'\beta'}(\boldsymbol{r}(t)-\boldsymbol{R}_j)}{\partial R_{j,\gamma'}}\frac{\partial G_{\delta\beta''}(\boldsymbol{r}(t_3)-\boldsymbol{R}_i)}{\partial R_{i,\gamma''}} N^{(d)}_{k,\beta''\gamma''}m_k(\boldsymbol{R}_k,t_3)dt_3 \\ &+ \int_t^{t+\Delta t}\sum_k \frac{\partial G_{\alpha\beta}(\boldsymbol{r}(t)-\boldsymbol{R}_i)}{\partial R_{i,\gamma}}\frac{\partial^2 G_{\alpha'\beta'}(\boldsymbol{r}(t)-\boldsymbol{R}_j)}{\partial r_\delta \partial R_{j,\gamma'}}\frac{\partial G_{\delta\beta''}(\boldsymbol{r}(t_3)-\boldsymbol{R}_j)}{\partial R_{j,\gamma''}} N^{(d)}_{k,\beta''\gamma''}m_k(\boldsymbol{R}_k,t_3)dt_3 \\ &+ \int_t^{t+\Delta t}\int_t^{t+\Delta t}\sum_{k,l} \frac{\partial^2 G_{\alpha\beta}(\boldsymbol{r}(t)-\boldsymbol{R}_i)}{\partial \delta \partial R_{i,\gamma}}\frac{\partial^2 G_{\alpha'\beta'}(\boldsymbol{r}(t)-\boldsymbol{R}_j)}{\partial r_{\delta'} \partial R_{j,\gamma'}}\frac{\partial G_{\delta\beta''}(\boldsymbol{r}(t_3)-\boldsymbol{R}_i)}{\partial R_{i,\gamma''}}\frac{\partial G_{\delta'\beta'''}(\boldsymbol{r}(t_4)-\boldsymbol{R}_j)}{\partial R_{j,\gamma'''}} \\ &\left.\left.\times N^{(d)}_{k,\beta''\gamma''}N^{(d)}_{l,\beta'''\gamma'''}m_k(\boldsymbol{R}_k,t_3)m_l(\boldsymbol{R}_l,t_4)dt_3dt_4\right] N^{(d)}_{i,\beta\gamma}N^{(d)}_{j,\beta\gamma}m_i(\boldsymbol{R}_i,t_1)m_j(\boldsymbol{R}_j,t_2)dt_1dt_2\right\rangle.\end{aligned} \tag{3.2.18}$$

From Eq. (3.2.12) and the following equation for the Gaussian distribution:

$$\begin{aligned}\langle m_i(\boldsymbol{R}_i,t_1)m_j(\boldsymbol{R}_j,t_2)m_k(\boldsymbol{R}_k,t_3)m_l(\boldsymbol{R}_l,t_4)\rangle =& \langle m_i(\boldsymbol{R}_i,t_1)m_j(\boldsymbol{R}_j,t_2)\rangle\langle m_k(\boldsymbol{R}_k,t_3)m_l(\boldsymbol{R}_l,t_4)\rangle \\ &+ \langle m_i(\boldsymbol{R}_i,t_1)m_k(\boldsymbol{R}_k,t_3)\rangle\langle m_j(\boldsymbol{R}_j,t_2)m_l(\boldsymbol{R}_l,t_4)\rangle \\ &+ \langle m_i(\boldsymbol{R}_i,t_1)m_l(\boldsymbol{R}_l,t_4)\rangle\langle m_j(\boldsymbol{R}_j,t_2)m_k(\boldsymbol{R}_k,t_3)\rangle,\end{aligned} \tag{3.2.19}$$

the second and third terms in Eq. (3.2.18) vanish, and the fourth term in Eq. (3.2.18) is the order of Δt and goes to zero for the limit of $\Delta t \to 0$. Thus we have

$$\begin{aligned}
&D_{\alpha\alpha'}(\boldsymbol{r}) - D^T \delta_{\alpha\alpha'} \\
&= \lim_{\Delta t \to 0} \frac{1}{2\Delta t} \int_t^{t+\Delta t} \int_t^{t+\Delta t} \sum_{i,j} \frac{\partial G_{\alpha\beta}(\boldsymbol{r}(t) - \boldsymbol{R}_i)}{\partial R_{i,\gamma}} \frac{\partial G_{\alpha'\beta'}(\boldsymbol{r}(t) - \boldsymbol{R}_j)}{\partial R_{j,\gamma'}} \\
&\quad \times \left\langle N^{(d)}_{i,\beta\gamma} N^{(d)}_{j,\beta\gamma} \right\rangle \langle m_i(\boldsymbol{R}_i, t_1) m_j(\boldsymbol{R}_j, t_2) \rangle \, dt_1 dt_2 \\
&= \lim_{\Delta t \to 0} \frac{1}{\Delta t} \int_t^{t+\Delta t} \sum_i \frac{\partial G_{\alpha\beta}(\boldsymbol{r}(t) - \boldsymbol{R}_i)}{\partial R_{i,\gamma}} \frac{\partial G_{\alpha'\beta'}(\boldsymbol{r}(t) - \boldsymbol{R}_i)}{\partial R_{i,\gamma'}} \left\langle N^{(d)}_{i,\beta\gamma} N^{(d)}_{i,\beta\gamma} \right\rangle S(\boldsymbol{R}_i) dt_2 \\
&= \left(\bar{N}^{(d)}_{\beta\gamma} \bar{N}^{(d)}_{\beta'\gamma'} + \Lambda^{(d)}_{\beta\gamma\beta'\gamma'} \right) \int \frac{\partial G_{\alpha\beta}(\boldsymbol{r}(t) - \boldsymbol{r}')}{\partial r'_\gamma} \frac{\partial G_{\alpha'\beta'}(\boldsymbol{r}(t) - \boldsymbol{r}')}{\partial r'_{\gamma'}} S(\boldsymbol{r}') c(\boldsymbol{r}') d\boldsymbol{r}' \\
&= \left(\bar{N}^{(d)}_{\beta\gamma} \bar{N}^{(d)}_{\beta'\gamma'} + \Lambda^{(d)}_{\beta\gamma\beta'\gamma'} \right) \int \frac{\partial G_{\alpha\beta}(\boldsymbol{r} - \boldsymbol{r}')}{\partial r'_\gamma} \frac{\partial G_{\alpha'\beta'}(\boldsymbol{r} - \boldsymbol{r}')}{\partial r'_{\gamma'}} S(\boldsymbol{r}') c(\boldsymbol{r}') d\boldsymbol{r}'.
\end{aligned} \tag{3.2.20}$$

When the number density of the active proteins and its activity depend on the position, V_α and $D_{\alpha\alpha'}$ are the Kramers-Moyal coefficients of the first and second orders, respectively. Thus the Fokker-Planck equation [89] for the dynamics of the distribution of tracer particles, $n(\boldsymbol{r}, t)$, is described as:

$$\frac{\partial n(\boldsymbol{r}, t)}{\partial t} = -\frac{\partial}{\partial r_\alpha} \left(V_\alpha(\boldsymbol{r}) n(\boldsymbol{r}, t) \right) + \frac{\partial^2}{\partial r_\alpha \partial r_{\alpha'}} \left(D_{\alpha\alpha'}(\boldsymbol{r}) n(\boldsymbol{r}, t) \right), \tag{3.2.21}$$

where

$$V_\alpha(\boldsymbol{r}) = -\left(\bar{N}^{(d)}_{\beta\gamma} \bar{N}^{(d)}_{\beta'\gamma'} + \Lambda^{(d)}_{\beta\gamma\beta'\gamma'} \right) \int \frac{\partial^2 G_{\alpha\beta}(\boldsymbol{r} - \boldsymbol{r}')}{\partial r'_\delta \partial r'_\gamma} \frac{\partial G_{\delta\beta'}(\boldsymbol{r} - \boldsymbol{r}')}{\partial r'_{\gamma'}} S(\boldsymbol{r}') c(\boldsymbol{r}') d\boldsymbol{r}', \tag{3.2.22}$$

$$\begin{aligned}
D_{\alpha\alpha'} =& D^T \delta_{\alpha\alpha'} + D^A_{\alpha\alpha'}(\boldsymbol{r}) \\
=& D^T \delta_{\alpha\alpha'} + \left(\bar{N}^{(d)}_{\beta\gamma} \bar{N}^{(d)}_{\beta'\gamma'} + \Lambda^{(d)}_{\beta\gamma\beta'\gamma'} \right) \int \frac{\partial G_{\alpha\beta}(\boldsymbol{r} - \boldsymbol{r}')}{\partial r'_\gamma} \frac{\partial G_{\alpha'\beta'}(\boldsymbol{r} - \boldsymbol{r}')}{\partial r'_{\gamma'}} S(\boldsymbol{r}') c(\boldsymbol{r}') d\boldsymbol{r}',
\end{aligned} \tag{3.2.23}$$

Here D^T is normal diffusion coefficient for a thermal equilibrium system.

Hereafter, we consider the two situations, one is the orientational order is absent, i.e., $\bar{N}^{(d)}_{\beta\gamma} = 0$, and the other is that the force dipoles are completely aligned in a certain direction. For the latter case, the main term in Eq. (3.2.15) is the first term, and thus here we neglect the second term.

3.2.2 Diffusion enhancement by force dipoles

First we consider a system where force dipoles are uniformly distributed and the activity of each force dipole is the same. Here we set $c(\boldsymbol{r}) = c_0$ and $S(\boldsymbol{r}) = S_0$. In this case, the Kramers-Moyal coefficient of the first order should be 0 from the viewpoint of the symmetric property.

For the two-dimensional case with an infinite system size, we have

$$D_{\alpha\alpha'} = \left(D^T + \frac{c_0 S_0}{32\pi\eta^2} \log \frac{\ell_0}{\ell_c} \right) \delta_{\alpha\alpha'}, \tag{3.2.24}$$

where we introduce a characteristic system size ℓ_0 and a cut-off length ℓ_c [38]. For the three-dimensional case with an infinite system size, we have

$$D_{\alpha\alpha'} = \left(D^T + \frac{c_0 S_0}{60\pi\eta^2 \ell_c} \right) \delta_{\alpha\alpha'}. \tag{3.2.25}$$

Equation (3.2.25) indicates that the diffusion is enhanced compared with the normal diffusion under the thermal equilibrium [38]. We cannot take a limit that ℓ_c goes to 0 from the viewpoint of physics. The cut-off length has a value whose order is the distance between the tracer particle and the nearest force dipole. Thus the cut-off length ℓ_c is greater than $\ell_t + \ell_p$, where ℓ_t and ℓ_p are the radii of a tracer particle and an active protein (force dipole), respectively.

When the force dipoles distribute with a constant gradient, the Kramers-Moyal coefficient of the first order also take place. Here we assume the activity of each force dipole is the same. For the two-dimensional case with an infinite system size, we have

$$V_\alpha = \frac{S_0}{32\pi\eta^2} (\nabla c)_\alpha \log \frac{\ell_0}{\ell_c}. \tag{3.2.26}$$

For the three-dimensional case with an infinite system size, we have

$$V_\alpha = \frac{S_0}{60\pi\eta^2 \ell_c} (\nabla c)_\alpha. \tag{3.2.27}$$

As we can see in Eqs. (3.2.24) and (3.2.26), the effect of force dipoles is long-ranged, i.e., its dependence on distance is proportional to $1/r$. Thus, to apply this model to an actual system, it is more natural to consider the system with a finite system size.

3.3 Localized effect of force dipoles

As shown in the previous section, the diffusion enhancement in a two-dimensional system with a constant number density of force dipoles logarithmically diverges with regard to the system size. However, we can discuss with a cluster of force dipoles in the proposed model. In fact, a localized structure of active proteins on biomembrane is known and referred to as a "lipid raft". We also discuss the localized effect of force dipoles in the three-dimensional case.

3.3.1 Fokker-Planck equation and convection-diffusion equation

In contrast to the case of the homogeneous number density of force dipoles, the directional drift velocity is induced, i.e., the Kramers-Moyal coefficient of the first order has a nonzero value. The Fokker-Planck equation (3.2.21) is transformed into in the following form

$$\frac{\partial n(\boldsymbol{r},t)}{\partial t} = -\frac{\partial}{\partial r_\alpha} \left(U_\alpha(\boldsymbol{r}) n(\boldsymbol{r},t) \right) + \frac{\partial}{\partial r_\alpha} \left(D_{\alpha\alpha'}(\boldsymbol{r},t) \frac{\partial n(\boldsymbol{r})}{\partial r_{\alpha'}} \right), \tag{3.3.1}$$

where $\boldsymbol{U}$ is the drift velocity of the flow of tracer particles defined as:

$$U_\alpha(\boldsymbol{r}) = V_\alpha(\boldsymbol{r}) - \frac{\partial D_{\alpha\alpha'}(\boldsymbol{r})}{\partial r_{\alpha'}}. \tag{3.3.2}$$

Since the diffusional flow is the product of diffusion coefficient and the gradient of the number density of tracer particles, Eq. (3.3.1) is the convection-diffusion equation. Hereafter, we basically discuss using $\boldsymbol{U}$ instead of $\boldsymbol{V}$.

3.3.2 Two-dimensional system

The expressions of V_α and $D_{\alpha\alpha'}$ shown in Eqs. (3.2.22) and (3.2.23) can be transformed into more simple ones as shown below [40, 41].

$$V_\alpha(\boldsymbol{r}) = -\frac{1}{32\pi^2\eta^2}\int d\boldsymbol{r}'\frac{r'_\alpha}{r'^4}S(\boldsymbol{r}+\boldsymbol{r}')c(\boldsymbol{r}+\boldsymbol{r}'), \tag{3.3.3}$$

$$D_{\alpha\alpha'} = D^T\delta_{\alpha\alpha'} + \frac{1}{32\pi^2\eta^2}\int d\boldsymbol{r}'\frac{r'_\alpha r'_{\alpha'}}{r'^4}S(\boldsymbol{r}+\boldsymbol{r}')c(\boldsymbol{r}+\boldsymbol{r}'). \tag{3.3.4}$$

The detailed calculations are provided in Appendix B.2.1.

Then, we consider the general form of the drift velocity $\boldsymbol{U}$ for the two-dimensional case. By substituting the general expression for $\boldsymbol{V}$ and D for the two-dimensional case with disordered force dipoles (Eqs. (3.3.3) and (3.3.4)) into the definition of $\boldsymbol{U}$ in Eq. (3.3.2), we have

$$U_\alpha(\boldsymbol{r}) = \frac{1}{32\pi\eta^2}\frac{\partial(S(\boldsymbol{r})c(\boldsymbol{r}))}{\partial r_\alpha} + \mathcal{O}(\ell_c), \tag{3.3.5}$$

The detailed calculation is provided in Appendix B.3.1. The drift velocity $\boldsymbol{U}$ is determined by the local profile of the number density of force dipoles $S(\boldsymbol{r})$ and its activity $c(\boldsymbol{r})$, in contrast with $\boldsymbol{V}$ and D which are determined by the global information of $S(\boldsymbol{r})c(\boldsymbol{r})$. Here we consider a circular region with force dipoles, i.e.,

$$c(r) = \frac{1}{2}\left[1 + \tanh\left(\frac{|R-r|}{\delta}\right)\right], \tag{3.3.6}$$

where r is a distance from the origin and R is the radius of the disk occupied by force dipoles. Since the tracer particles are swept up by the drift velocity at the periphery of the disk, the tracer particles are accumulated into the disk. Figure 3.3.2 shows numerical results on the accumulation of tracer particles inside the circular raft. The number density of the tracer particles n initially had uniform distribution ($n = 1$). Based on the Fokker-Planck equation in Eq. (3.2.21) with the Kramers-Moyal coefficients in Eqs. (3.3.3) and (3.3.4), the time evolution of the number density of the tracer particles n was calculated. The distribution of active proteins was given by Eq. (3.4.2). Finally, the distribution of tracer particles became steady, since the drift flow and diffusional flow was balanced.

So far we qualitatively explain the accumulation of tracer particles into a circular raft occupied by active proteins. Here we show the steady state for the distribution of tracer particles when there exists a circular raft. We set the radius of the circular raft is R and the center of the raft is corresponding to the origin of the coordinates. The distribution of tracer particles is defined as $n = n(r,\theta)$ in the polar coordinates.

The drift velocity is defined as $\boldsymbol{U} = (U_x(x,y), U_y(x,y))$. Here, we consider the situation that $\boldsymbol{U}$ depends on only the distance from the center of the circular raft, r, and define $U_\parallel(r)$ as $U_\parallel(r) = U_x(r,0)$.

The equation for the distribution of the tracer particles is represented as follows:

$$\frac{\partial n}{\partial t} = -\frac{1}{r}\frac{\partial}{\partial r}(rU_\parallel(r)n) + \frac{1}{r}\frac{\partial}{\partial r}\left(rD_\parallel(r)\frac{\partial n}{\partial r}\right), \tag{3.3.7}$$

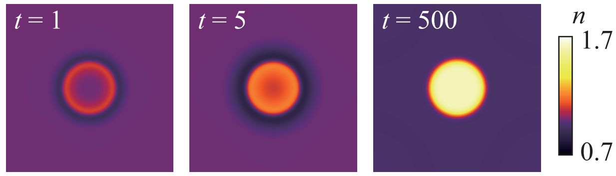

Figure 3.3.1: Numerical results on the accumulation of tracer particles to a circular region occupied with active force dipoles in the two-dimensional system. Consequent snapshots of the number density distribution are shown. The parameters were $R = 16\ell_c$, $\delta = 0.5\ell_c$, $S = 1$, and $D_0/D^T = 1$, where $D_0 = D^A(\mathbf{0})$. The time unit was ℓ_c^2/D^T; the tracer particles were uniformly distributed with $n = 1$ at $t = 0$. The spatial and time steps were $0.4\ell_c$ and 10^{-7}, respectively. Reproduced from Ref. [41].

where $D_\parallel$ is given by $D_\parallel(r) = D_{xx}(r, 0)$. For the steady state of n, $\partial n/\partial t$ should be zero.

$$0 = \frac{1}{r}\frac{\partial}{\partial r}(rU_\parallel(r)n) + \frac{1}{r}\frac{\partial}{\partial r}\left(rD_\parallel(r)\frac{\partial n}{\partial r}\right). \tag{3.3.8}$$

By solving Eq. (3.3.8) with regard to $n(r)$, we have

$$n(r) = n_0 \exp\left(\int_0^r \frac{U_\parallel(r')}{D_\parallel(r')}dr'\right), \tag{3.3.9}$$

where n_0 is a value of $n(r)$ at $r = 0$. Here we use the boundary conditions, $\partial n/\partial t = 0$ and $U_r = 0$ at $r \to \infty$. When the cut-off length is small enough, the drift velocity is approximately represented as $U_\parallel(r) = -U_0\delta(R - r)$, where $U_0 > 0$. In this case, we obtain

$$\int_0^r \frac{U_\parallel(r')}{D_\parallel(r')}dr' = \begin{cases} 0, & (r < R), \\ -U_0/D_\parallel(R), & (r > R), \end{cases} \tag{3.3.10}$$

and n is written as

$$n = \begin{cases} n_0, & (r < R), \\ n_0 \exp(-U_0/D_\parallel(R)), & (r > R). \end{cases} \tag{3.3.11}$$

The theoretical results was confirmed by comparing the numerical results as shown in Fig. 3.3.2.

The accumulation of tracer particles in the region occupied by active proteins were observed for other shape of the raft in numerical calculation. Here we show the numerical results on the time evolution of the number density field of tracer particles with an elliptic raft and two circular rafts in Fig. 3.3.3.

For a single circular raft, whose profile is given by

$$c(r) = \begin{cases} c_0, & (r < R), \\ 0, & (r > R), \end{cases} \tag{3.3.12}$$

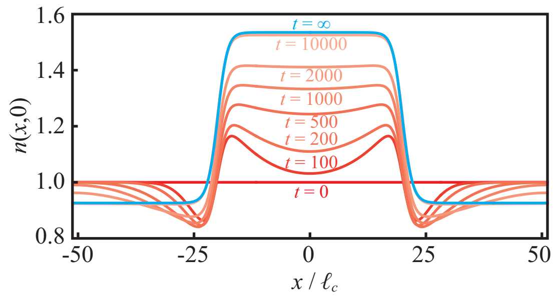

Figure 3.3.2: Accumulation of tracer particles by a raft occupied with active proteins. Radial profiles at different time moments are displayed. The final profile ($t = \infty$) is determined by integrating the analytical solution (3.3.9). The parameters are set to be $R = 20\ell_c$, $\delta = 2\ell_c$, $S = 1$, and $Sc/(32\pi^2\eta^2 D^T) = 1$. Reproduced from Ref. [40].

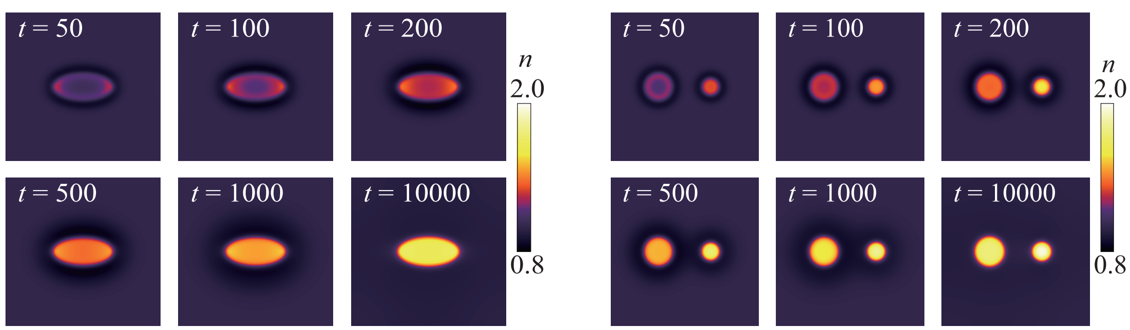

Figure 3.3.3: Numerical results on the accumulation of tracer particles to (a) an elliptic region and (b) two circular regions occupied with active force dipoles in the two-dimensional system. Consequent snapshots of the number density distribution are shown. (a) The major and minor axes of the elliptic raft were $20\ell_c$ and $10\ell_c$, respectively. (b) The radii of the circular rafts were $10\ell_c$ and $6\ell_c$. The other parameters were set to be $\delta = 2\ell_c$, $S = 1$, and $D_0/D^T = 1$, where $D_0 = D^A(\mathbf{0})$. The time unit was ℓ_c^2/D^T; the particles were uniformly distributed with $n = 1$ at $t = 0$. Reproduced from Ref. [40].

we have explicit forms of V and D except for the periphery of the raft as follows.

$$\boldsymbol{V}(\boldsymbol{r}) = -\frac{Sc_0}{32\pi\eta^2}\begin{cases} \begin{pmatrix} \dfrac{r}{R^2-r^2} \\ 0 \end{pmatrix}, & (r < R-\ell_c), \\ \begin{pmatrix} \dfrac{R^2}{r(r^2-R^2)} \\ 0 \end{pmatrix}, & (r > R+\ell_c), \end{cases} \tag{3.3.13}$$

$$\equiv \begin{pmatrix} V_\parallel \\ 0 \end{pmatrix}, \tag{3.3.14}$$

$$D^A(\boldsymbol{r}) = \frac{Sc_0}{32\pi\eta^2}\begin{cases} \ln\left(\dfrac{\sqrt{R^2-r^2}}{\ell_c}\right)\mathbb{1}, & (r < R-\ell_c), \\ \ln\left(\dfrac{r}{\sqrt{r^2-R^2}}\right)\mathbb{1} + \dfrac{R^2}{2r^2}\begin{pmatrix} 1 & 0 \\ 0 & -1 \end{pmatrix}, & (r > R+\ell_c), \end{cases} \tag{3.3.15}$$

$$\equiv \begin{pmatrix} D_\parallel & 0 \\ 0 & D_\perp \end{pmatrix}, \tag{3.3.16}$$

where

$$D_\parallel = \ln\left(\frac{r}{\sqrt{r^2-R^2}}\right) + \frac{R^2}{2r^2}, \tag{3.3.17}$$

$$D_\perp = \ln\left(\frac{r}{\sqrt{r^2-R^2}}\right) - \frac{R^2}{2r^2}. \tag{3.3.18}$$

The profiles of V, $D_\parallel$, and $D_\perp$ are shown in Fig. 3.3.4. It is noted that for $r \gg R$, $D_\parallel$ and $D_\perp$ are asymptotically expressed as

$$D_\parallel = \frac{Sc_0}{32\pi\eta^2}\frac{R^2}{r^2}, \tag{3.3.19}$$

$$D_\perp = \frac{Sc_0}{128\pi\eta^2}\frac{R^4}{r^4}. \tag{3.3.20}$$

Thus the diffusion in the radial direction $D_\parallel$ remains further compared with that in the angular direction at the point far from the raft.

We also numerically calculated the profile of the diffusion enhancement in the case of an elliptic raft as shown in Fig. 3.3.5. Note that, in contrast to the case with a circular raft, the anisotropy of the diffusion enhancement, i.e., $(D^A_{11}-D^A_{22})/\xi$, is present also inside the raft, where $\xi = Sc/(32\pi^2\eta^2)$.

3.3.3 Three-dimensional system

For a three-dimensional case with no orientational order, V_α and $D_{\alpha\alpha'}$ are simplified in the same manner as in the two-dimensional case:

$$V_\alpha(\boldsymbol{r}) = -\frac{1}{40\pi^2\eta^2}\int d\boldsymbol{r}'\frac{r'_\alpha}{r'^6}S(\boldsymbol{r}+\boldsymbol{r}')c(\boldsymbol{r}+\boldsymbol{r}'), \tag{3.3.21}$$

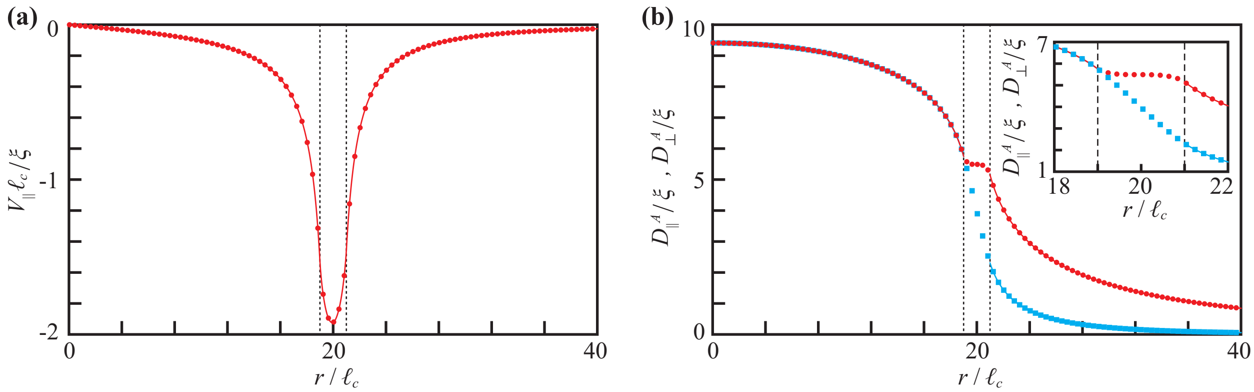

Figure 3.3.4: Profiles of the radial component of the velocity, $V_{\parallel}$ obtained by the numerical integration (closed circles) and analytical calculation (solid curves) in the case with a circular raft of a radius R, in which the number density of active proteins is c_0. We set $R/\ell_c = 20$ and $S = 1$. The parameter ξ is the set of the parameters $\xi = Sc/(32\pi^2\eta^2)$. Reproduced from Ref. [40].

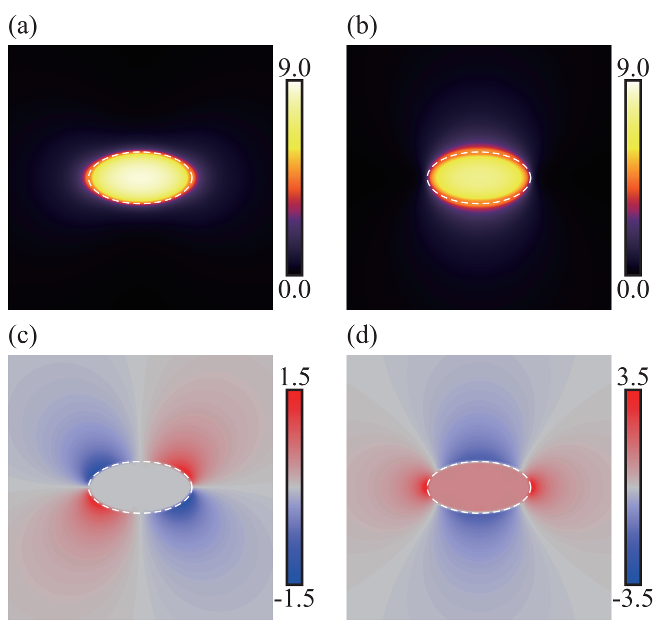

Figure 3.3.5: Diffusion enhancement for an elliptic raft with the semiaxes $20\ell_c$ and $10\ell_c$ and the sharp boundary. The diffusion enhancement components (a) D_{11}^A/ξ, (b) D_{22}^A/ξ, and (c) D_{12}^A/ξ are displayed, where $\xi = Sc/(32\pi^2\eta^2)$. The diffusion anisotropy $(D_{11}^A - D_{22}^A)/\xi$ is additionally shown in panel (d). Reproduced from Ref. [40].

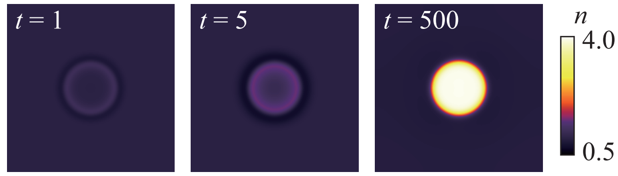

Figure 3.3.6: Numerical results on the accumulation of tracer particles to a sphere occupied with active force dipoles in a three-dimensional system. Consequent snapshots of the number density distribution are shown. The parameters were $R = 16\ell_c$, $\delta = 0.5\ell_c$, $S = 1$, and $D_0/D^T = 1$, where $D_0 = D^A(\mathbf{0})$. The time unit was ℓ_c^2/D^T; the particles were uniformly distributed with $n = 1$ at $t = 0$. The spatial and time steps were $0.4\ell_c$ and 10^{-7}, respectively. Reproduced from Ref. [41].

$$D_{\alpha\alpha'} = D^T \delta_{\alpha\alpha'} + \frac{1}{80\pi^2\eta^2} \int d\boldsymbol{r}' \frac{r'_\alpha r'_{\alpha'}}{r'^6} S(\boldsymbol{r}+\boldsymbol{r}')c(\boldsymbol{r}+\boldsymbol{r}'). \tag{3.3.22}$$

The detailed calculations are provided in Appendix B.2.2.

Then, we consider the general form of the drift velocity $\boldsymbol{U}$ for the three-dimensional case. By substituting the general expression for $\boldsymbol{V}$ and D for three-dimensional case with disordered force dipoles (Eqs. (3.3.21) and (3.3.22)) into the definition of $\boldsymbol{U}$ in Eq. (3.3.2), we have

$$U_\alpha(\boldsymbol{r}) = \frac{1}{60\pi\eta^2\ell_c} \frac{\partial(c(\boldsymbol{r})S(\boldsymbol{r}))}{\partial r_\alpha} + \mathcal{O}({\ell_c}^0). \tag{3.3.23}$$

The detailed calculation is provided in Appendix B.3.2. The drift velocity $\boldsymbol{U}$ is determined by the local gradient of the number density of force dipoles and its activity.

Here we consider a spherical region with force dipoles, i.e.,

$$c(r) = \frac{1}{2}\left[1 + \tanh\left(\frac{|R-r|}{\delta}\right)\right], \tag{3.3.24}$$

where r is a distance from the origin and R is a radius of the sphere occupied by force dipoles. In the same way as in the two-dimensional system, tracer particles were accumulated into the sphere and formed a steady distribution. Figure 3.3.3 shows numerical results on the accumulation of tracer particles inside the circular raft. The number density of the tracer particles n initially had uniform distribution ($n = 1$). Based on the Fokker-Planck equation in Eq. (3.2.21) with the Kramers-Moyal coefficients in Eqs. (3.3.21) and (3.3.22), the time evolution of the number density of the tracer particles n was calculated. The distribution of active proteins were given by Eq. (3.3.24). Finally, the distribution of tracer particles became steady in the same case as in the two-dimensional case, since the drift flow and diffusional flow was balanced.

3.4 Effect of orientational order of force dipoles

So far, we consider the active force dipoles without nematic order. In this section, we discuss the effect of the alignment of force dipoles. Of course, we can take into account the dynamics of the orientational order, but the model will become more complex. The aim of this section is to check whether the orientational order plays an important role. We use the model in Eq. (3.2.21) for a perfectly aligned force dipoles. For two dimensional systems, we consider the cases that the force dipoles are uniformly distributed inside a circular region. For three-dimensional systems, we consider two cases, (i) the force dipoles are uniformly distributed in the entire space and (ii) they are distributed inside a spherical region.

3.4.1 Two-dimensional system

For the two-dimensional case with perfectly orientated force dipoles, V_α and $D_{\alpha\alpha'}$ are simplified as

$$V_\alpha(\boldsymbol{r}) = \frac{1}{16\pi^2\eta^2}\int d\boldsymbol{r}'\frac{r'_\alpha}{r'^8}\left((r'_1)^2-(r'_2)^2\right)^2 S(\boldsymbol{r}+\boldsymbol{r}')c(\boldsymbol{r}+\boldsymbol{r}'), \tag{3.4.1}$$

$$D_{\alpha\alpha'}(\boldsymbol{r}) = D^T\delta_{\alpha\alpha'} + \frac{1}{32\pi^2\eta^2}\int d\boldsymbol{r}'\frac{r'_\alpha r'_{\alpha'}}{r'^8}\left((r'_1)^2-(r'_2)^2\right)^2 S(\boldsymbol{r}+\boldsymbol{r}')c(\boldsymbol{r}+\boldsymbol{r}'). \tag{3.4.2}$$

Here we assume that the force dipoles are aligned in r_1-direction. The detailed calculations are provided in Appendix B.2.3.

Using the above expressions for V_α and $D_{\alpha\alpha'}$, the drift velocity is obtained as

$$U_\alpha(\boldsymbol{r}) = \frac{\nabla(S(\boldsymbol{r})c(\boldsymbol{r}))}{32\pi\eta^2} + \mathcal{O}(\ell_c), \tag{3.4.3}$$

where $Q(\boldsymbol{r}) = S(\boldsymbol{r})c(\boldsymbol{r})$. The detailed calculation is also provided in Appendix B.3.3. Surprisingly, the orientational order does not appear in Eq. (3.4.3) and it is the same as the case when the orientation of the force dipoles is random at least with regard to the main term. To confirm the analytical results, we calculated the time evolution of the number density of tracer particles n based on the Fokker-Planck equation in Eq. (3.2.21) with the Kramers-Moyal coefficients in Eqs. (3.4.1) and (3.4.2). The distribution of active proteins is given by Eq. (3.4.2). The number density of the tracer particles n initially had uniform distribution ($n = 1$). Finally, the distribution of tracer particles become steady as shown in Fig. 3.4.1(a,b). It is noted that weak circulating flow of tracer particles remained as shown in Fig. 3.4.1(c,d). The profile of reflecting the symmetric property of the system.

3.4.2 Three-dimensional system

For the three-dimensional case with perfectly orientated force dipoles, V_α and $D_{\alpha\alpha'}$ are simplified as

$$V_\alpha(\boldsymbol{r}) = \frac{1}{8\pi^2\eta^2}\int d\boldsymbol{r}'\frac{r'_\alpha}{r'^6}P_2(\cos\theta')^2 S(\boldsymbol{r}+\boldsymbol{r}')c(\boldsymbol{r}+\boldsymbol{r}'), \tag{3.4.4}$$

$$D_{\alpha\alpha'}(\boldsymbol{r}) = D^T\delta_{\alpha\alpha'} + \frac{1}{16\pi^2\eta^2}\int d\boldsymbol{r}'\frac{r'_\alpha r'_{\alpha'}}{r'^6}P_2(\cos\theta')^2 S(\boldsymbol{r}+\boldsymbol{r}')c(\boldsymbol{r}+\boldsymbol{r}'), \tag{3.4.5}$$

where P_2 is Legendre polynomial of the second order. Here we use $r_3 = r\cos\theta$ and we assume that the force dipoles are aligned in r_3-direction. The detailed calculations are provided in Appendix B.2.4.

Then we obtain the general form of the drift velocity $\boldsymbol{U}$ as

$$U_\alpha(\boldsymbol{r}) = -\frac{1}{16\pi^2\eta^2}\int_\sigma ds_{\alpha'}\frac{r'_\alpha r'_{\alpha'}}{r'^6}P_2(\cos\theta')^2 S(\boldsymbol{r}+\boldsymbol{r}')c(\boldsymbol{r}+\boldsymbol{r}'). \tag{3.4.6}$$

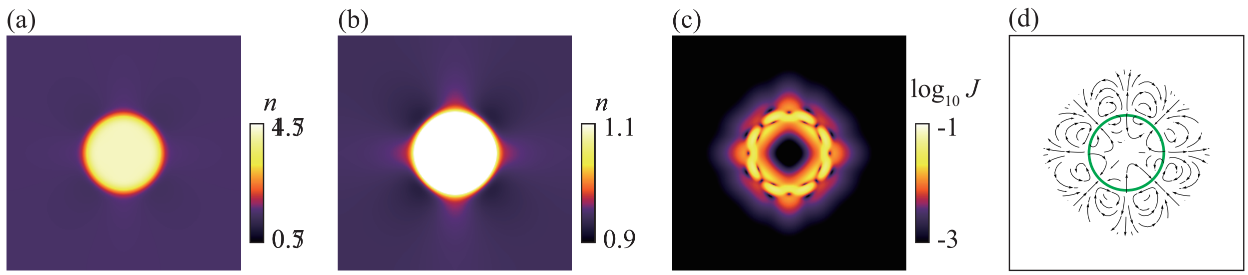

Figure 3.4.1: Numerical results on the distribution of tracer particles (a,b) and their fluxes (c,d) in the steady state of a two-dimensional system with orientationally ordered force dipoles that occupy a circle in the center. Panel (b) shows the distribution enhanced in the region of low number densities. The logarithm $\log_{10} \boldsymbol{j}(\boldsymbol{r})$ of the local magnitude of the fluxes and their streamlines are displayed in (c) and (d). The horizontal direction corresponds to the orientation line of force dipoles. The parameters were $R = 16\ell_c$, $\delta = 0.5\ell_c$, and $S = 1$. The spatial and time steps were $0.4\ell_c$ and 10^{-7}, respectively. Reproduced from Ref. [41].

The integration is taken over the physical boundary σ_{outside} and the small cut-off surface σ_{inside} around $\boldsymbol{r}$. The integration over the physical boundary σ_{outside} becomes zero if $S(\boldsymbol{r})c(\boldsymbol{r}) = 0$ at the boundary. Here we consider the situation that $S(\boldsymbol{r}+\boldsymbol{r}')c(\boldsymbol{r}+\boldsymbol{r}') \equiv Q(\boldsymbol{r}+\boldsymbol{r}')$ is given by $Q(\boldsymbol{r}+\boldsymbol{r}') = Q(\boldsymbol{r}) + r'_\beta \partial Q(\boldsymbol{r})/\partial r_\beta$. Then the integral over the small cut-off surface can be calculated as

$$\begin{aligned}
U_\alpha(\boldsymbol{r}) =& \frac{1}{64\pi^2\eta^2}\int_0^{2\pi} d\phi \int_0^{\pi} d\theta ({\ell_c}^2 \sin\theta)\hat{r'}_{\alpha'} \frac{\hat{r'}_\alpha \hat{r'}_{\alpha'}}{{\ell_c}^4}(1-3\hat{r'}^2_3)^2 \left(Q(\boldsymbol{r}) + \ell_c \hat{r'}_\beta \frac{\partial Q(\boldsymbol{r})}{\partial r_\beta}\right) \\
=& \frac{1}{64\pi^2\eta^2}\int_0^{2\pi} d\phi \int_0^{\pi} d\theta \sin\theta \frac{1}{{\ell_c}^2}\hat{r'}_\alpha (1-3\cos^2\theta)^2 \left(Q(\boldsymbol{r}) + \ell_c \hat{r'}_\beta \frac{\partial Q(\boldsymbol{r})}{\partial r_\beta}\right) \\
=& \frac{1}{28\pi\eta^2\ell_c}\left(\frac{1}{3}\frac{\partial Q(\boldsymbol{r})}{\partial r_1}\delta_{\alpha 1}\boldsymbol{e}_1 + \frac{1}{3}\frac{\partial Q(\boldsymbol{r})}{\partial r_2}\delta_{\alpha 2}\boldsymbol{e}_2 + \frac{11}{15}\frac{\partial Q(\boldsymbol{r})}{\partial r_3}\delta_{\alpha 3}\boldsymbol{e}_3\right),
\end{aligned} \tag{3.4.7}$$

where $\hat{\boldsymbol{r}}$ is a unit vector defined as $\hat{\boldsymbol{r}} = \boldsymbol{r}/|\boldsymbol{r}|$. The result for $\boldsymbol{U}$ is the different from the case when the orientation of the force dipoles is random. The average over r_1-, r_2-, and r_3-directions is given by considering the average of the numerical coefficient, $\frac{1}{28}\left(\frac{1}{3}+\frac{1}{3}+\frac{11}{15}\right) \times \frac{1}{3} = \frac{1}{60}$, which is the same as the case when the orientation of the active proteins is random.

Here we consider the case with constant gradient of $Q(\boldsymbol{r})$. Suppose that $Q(\boldsymbol{r}) = Q_0 + Q_1 \boldsymbol{a}\cdot\boldsymbol{r}$, where $\boldsymbol{a} = (a_1, a_2, a_3)$ is a constant unit vector, which denotes the direction of the gradient of Q. Then $\boldsymbol{V}$, D, and $\boldsymbol{U}$ are calculated as follows:

$$\boldsymbol{V}(\boldsymbol{r}) = \frac{Q_1}{32\pi^2\eta^2}\frac{1}{\ell_c}\begin{pmatrix} \frac{16\pi}{21}a_1 \\ \frac{16\pi}{21}a_2 \\ \frac{176\pi}{105}a_3 \end{pmatrix} = \frac{Q_1}{14\pi\eta^2}\frac{1}{\ell_c}\begin{pmatrix} \frac{1}{3}a_1 \\ \frac{1}{3}a_2 \\ \frac{11}{15}a_3 \end{pmatrix}, \tag{3.4.8}$$

and

$$D^A(\boldsymbol{r}) = \frac{Q(\boldsymbol{r})}{28\pi\eta^2}\frac{1}{\ell_c}\begin{pmatrix} \frac{1}{3} & 0 & 0 \\ 0 & \frac{1}{3} & 0 \\ 0 & 0 & \frac{11}{15} \end{pmatrix}. \tag{3.4.9}$$

It is noted that V_α and $(\partial D_{\alpha\alpha'})/(\partial r_{\alpha'})$ with constant gradient of Q still satisfy the equation $V_\alpha = 2(\partial D_{\alpha\alpha'})/(\partial r_{\alpha'})$, which is the same as the result in the case that the force dipoles are orientated randomly [39].

The drift velocity $\boldsymbol{U}$ is calculated as follows:

$$\boldsymbol{U} = \boldsymbol{V} - \frac{\partial D^A(\boldsymbol{r})}{\partial \boldsymbol{r}} = \frac{Q_1}{28\pi\eta^2}\frac{1}{\ell_c}\begin{pmatrix} \frac{1}{3}a_1 \\ \frac{1}{3}a_2 \\ \frac{11}{15}a_3 \end{pmatrix}. \tag{3.4.10}$$

The result is consistent with the general expression in Eq. (3.4.7). The detailed calculation is provided in Appendix B.3.4.

Nematic order parameter

To describe the nematic state, tensor and scalar order parameters are known in the field of the liquid crystals:

$$\begin{aligned} N =& s\left(\boldsymbol{nn} - \frac{1}{3}I\right) \\ =& s\left\{\begin{pmatrix} \sin^2\theta\cos^2\phi & \sin^2\theta\sin\phi\cos\phi & \sin\theta\cos\theta\cos\phi \\ \sin^2\theta\sin\phi\cos\phi & \sin^2\theta\sin^2\phi & \sin\theta\cos\theta\sin\phi \\ \sin\theta\cos\theta\cos\phi & \sin\theta\cos\theta\sin\phi & \cos^2\theta \end{pmatrix} - \frac{1}{3}\begin{pmatrix} 1 & 0 & 0 \\ 0 & 1 & 0 \\ 0 & 0 & 1 \end{pmatrix}\right\}, \end{aligned} \tag{3.4.11}$$

where N and s are the tensor and scalar order parameters, respectively. Here, s takes a value between 0 and 1, where $s = 0$ and $s = 1$ correspond to the completely disordered and ordered states, respectively. $\boldsymbol{n}$ is a unit vector, which represents the direction of the nematic phase.

Here we consider the situation that the orientation of active proteins is completely ordered in the direction of z-axis. Thus, we set $s = 1$ and $\theta = 0$. By using the tensor order parameter N, the flux $\boldsymbol{U}$ is represented as

$$\boldsymbol{U}(\boldsymbol{r}) = \frac{1}{60\pi\eta^2\ell_c}\left(I + \frac{6}{7}N\right)\nabla Q(\boldsymbol{r}). \tag{3.4.12}$$

The diffusion tensor D for $Q(\boldsymbol{r}) = Q_0 + Q_1\boldsymbol{a}\cdot\boldsymbol{r}$ (constant for $Q_1 = 0$ and linear profile with constant gradient for $Q_1 \neq 0$) is also represented by using N,

$$
\begin{aligned}
D^A(\boldsymbol{r}) =& \frac{Q(\boldsymbol{r})}{64\pi^2\eta^2}\frac{1}{\ell_c}\begin{pmatrix} \frac{16\pi}{21} & 0 & 0 \\ 0 & \frac{16\pi}{21} & 0 \\ 0 & 0 & \frac{176\pi}{105} \end{pmatrix} \\
=& \frac{Q(\boldsymbol{r})}{60\pi\eta^2\ell_c}\begin{pmatrix} 1 & 0 & 0 \\ 0 & 1 & 0 \\ 0 & 0 & 1 \end{pmatrix} + \frac{Q(\boldsymbol{r})}{70\pi\eta^2\ell_c}\begin{pmatrix} -\frac{1}{3} & 0 & 0 \\ 0 & -\frac{1}{3} & 0 \\ 0 & 0 & \frac{2}{3} \end{pmatrix} = \frac{Q(\boldsymbol{r})}{60\pi\eta^2\ell_c}\left(I + \frac{6}{7}N\right). \qquad (3.4.13)
\end{aligned}
$$

Steady state

Here we consider the steady state when the normal diffusion under thermal equilibrium is negligible. We set D^T to be 0. The diffusion tensor with local approximation is adopted. The Fokker-Planck equation is represented as

$$
\frac{\partial n(\boldsymbol{r},t)}{\partial t} = -\frac{\partial}{\partial r_\alpha}\left(U_\alpha(\boldsymbol{r})n(\boldsymbol{r},t)\right) + \frac{\partial}{\partial r_\alpha}\left(D_{\alpha\alpha'}(\boldsymbol{r})\frac{\partial n(\boldsymbol{r},t)}{\partial r_{\alpha'}}\right). \qquad (3.4.14)
$$

To obtain the steady state, the time derivative of n is set to be zero:

$$
\frac{\partial}{\partial r_\alpha}\left(U_\alpha(\boldsymbol{r})n(\boldsymbol{r})\right) = \frac{\partial}{\partial r_\alpha}\left(D_{\alpha\alpha'}(\boldsymbol{r})\frac{\partial n(\boldsymbol{r})}{\partial r_{\alpha'}}\right). \qquad (3.4.15)
$$

Then we integrate the both sides with regard to r_α, and obtain

$$
U_\alpha(\boldsymbol{r})n(\boldsymbol{r}) = D_{\alpha\alpha'}(\boldsymbol{r})\frac{\partial n(\boldsymbol{r})}{\partial r_{\alpha'}} + C_\alpha. \qquad (3.4.16)
$$

When $U_\alpha(\boldsymbol{r})$ and $D_{\alpha\alpha'}(\boldsymbol{r})$ are zero at $|\boldsymbol{r}| \to \infty$, C_α should be zero.

$$
U_\alpha(\boldsymbol{r}) = D_{\alpha\alpha'}(\boldsymbol{r})\frac{\partial \ln n(\boldsymbol{r})}{\partial r_{\alpha'}}. \qquad (3.4.17)
$$

By using $\boldsymbol{U}$ and D in Eqs. (3.4.12) and (3.4.13), we obtain

$$
\frac{1}{60\pi\eta^2\ell_c}\left(I_{\alpha\alpha'} + \frac{6}{7}N_{\alpha\alpha'}\right)\frac{\partial Q(\boldsymbol{r})}{\partial r_{\alpha'}} = \frac{Q(\boldsymbol{r})}{60\pi\eta^2\ell_c}\left(I_{\alpha\alpha'} + \frac{6}{7}N_{\alpha\alpha'}\right)\frac{\partial \ln n}{\partial r_{\alpha'}}, \qquad (3.4.18)
$$

$$
(3.4.19)
$$

and finally we have

$$
n(\boldsymbol{r}) = C''Q(\boldsymbol{r}). \qquad (3.4.20)
$$

It is noted that this result does not depend on the value of s.

Next we consider the steady state for $D^T \neq 0$. We cannot easily construct a general solution in the same way as in the case of $D^T = 0$, since the diffusional flow induced by thermal noise and active elements are not parallel. Here we consider the steady state of the distribution of tracer particles when the active proteins are distributed in a spherical region. We derive an approximated solution and show numerical results. We assume the active proteins inside the spherical region are aligned in the r_3-direction, and uniformly distributed, i.e.,

$$Q(r) = \begin{cases} Q_0, & (r < R), \\ 0, & (r > R), \end{cases} \tag{3.4.21}$$

where R is a radius of the spherical region. We also assume that the gradient of Q is $-Q_1\delta(r-R)\boldsymbol{e}_r$, where $\boldsymbol{e}_r$ is a unit vector directed in the radial direction.

The constant C in Eq. (3.4.16) should be considered to be $\varepsilon_{\alpha\beta\gamma}(\partial A_\gamma)/(\partial r_\beta)$, where $\varepsilon_{\alpha\beta\gamma}$ is Levi-Civita symbol (an asymmetric tensor) and $\boldsymbol{A}(\boldsymbol{r})$ is a vector that $\boldsymbol{A}(\boldsymbol{r}\to\boldsymbol{0}) = \boldsymbol{0}$ due to the boundary condition. Then we obtain

$$U_\alpha(\boldsymbol{r})n(\boldsymbol{r}) = D_{\alpha\alpha'}(\boldsymbol{r})\frac{\partial n(\boldsymbol{r})}{\partial r_{\alpha'}} + \varepsilon_{\alpha\beta\gamma}\frac{\partial A_\gamma}{\partial r_\beta}. \tag{3.4.22}$$

Here we transform to the radial coordinates (r,θ,ϕ). From the symmetrical consideration, $U(\boldsymbol{r})(\propto \nabla Q(r))$ and $n(\boldsymbol{r})$ should be independent of ϕ, and $\boldsymbol{A}$ should have a form as $\boldsymbol{A}(\boldsymbol{r}) = (0,0,A(r,\theta))$ in the polar coordinates. First, we consider the decomposition of U_α and $D_{\alpha\alpha'}(\partial n)/(\partial r_{\alpha'})$ with regard to $\boldsymbol{e}_r$ and $\boldsymbol{e}_\theta$. We obtain the decomposed U_α into r- and θ-directions from Eq. (3.4.12):

$$\begin{aligned} U_\alpha(\boldsymbol{r}) =& \frac{1}{60\pi\eta^2\ell_c}\left(I + \frac{6}{7}N\right)\nabla Q(\boldsymbol{r}) = \frac{Q_1\delta(r-R)}{60\pi\eta^2\ell_c}\left(I+\frac{6}{7}N\right)(-\boldsymbol{e}_r) \\ =& \frac{Q_1\delta(r-R)}{140\pi\eta^2\ell_c}\left\{\left(1+\frac{4}{7}P_2(\cos\theta)\right)\boldsymbol{e}_r - \frac{3}{7}\sin 2\theta\boldsymbol{e}_\theta\right\}. \end{aligned} \tag{3.4.23}$$

We also obtain the decomposed $D_{\alpha\alpha'}(\partial n)/(\partial r_{\alpha'})$ into r- and θ-directions from Eq. (3.4.13):

$$\begin{aligned} D_{\alpha\alpha'}\frac{\partial n}{\partial r_{\alpha'}} =& \left\{D^T I_{\alpha\alpha'} + \frac{Q(r)}{60\pi\eta^2\ell_c}\left(I_{\alpha\alpha'} + \frac{6}{7}N_{\alpha\alpha'}\right)\right\}\left(\boldsymbol{e}_r\frac{\partial n}{\partial r} + \boldsymbol{e}_\theta\frac{1}{r}\frac{\partial n}{\partial\theta}\right) \\ =& D^T\left(\frac{\partial n}{\partial r}\boldsymbol{e}_r + \frac{1}{r}\frac{\partial n}{\partial\theta}\boldsymbol{e}_\theta\right) \\ &+ \frac{Q(r)}{140\pi\eta^2\ell_c}\left\{\left(\left(1+\frac{4}{7}P_2(\cos\theta)\right)\frac{\partial n}{\partial r} - \frac{3}{7}\sin 2\theta\frac{1}{r}\frac{\partial n}{\partial\theta}\right)\boldsymbol{e}_r\right. \\ &\left.+\left(-\frac{3}{7}\sin 2\theta\frac{\partial n}{\partial r} + \left(\frac{9}{7} - \frac{4}{7}P_2(\cos\theta)\right)\frac{1}{r}\frac{\partial n}{\partial\theta}\right)\boldsymbol{e}_\theta\right\}. \end{aligned} \tag{3.4.24}$$

Thus, we obtain the following two equations:

$$\begin{aligned} &\frac{1}{60\pi\eta^2\ell_c}\frac{\partial Q}{\partial r}\left(1+\frac{4}{7}P_2(\cos\theta)\right)n - D^T\frac{\partial n}{\partial r} - \frac{Q}{60\pi\eta^2\ell_c}\left(\left(1+\frac{4}{7}P_2(\cos\theta)\right)\frac{\partial n}{\partial r} - \frac{3}{7}\sin 2\theta\frac{1}{r}\frac{\partial n}{\partial\theta}\right) \\ &= \frac{1}{r\sin\theta}\frac{\partial}{\partial\theta}(A\sin\theta), \end{aligned} \tag{3.4.25}$$

$$\begin{aligned} &-\frac{1}{60\pi\eta^2\ell_c}\frac{\partial Q}{\partial r}\frac{3}{7}\sin 2\theta\, n - D^T\frac{1}{r}\frac{\partial n}{\partial\theta} - \frac{Q}{60\pi\eta^2\ell_c}\left(-\frac{3}{7}\sin 2\theta\frac{\partial n}{\partial r} + \left(\frac{9}{7}-\frac{4}{7}P_2(\cos\theta)\right)\frac{1}{r}\frac{\partial n}{\partial\theta}\right) \\ &= -\frac{1}{r}\frac{\partial}{\partial r}(rA). \end{aligned} \tag{3.4.26}$$

Inside the circular region, Eqs. (3.4.25) and (3.4.26) lead to

$$-D^T\frac{\partial n}{\partial r}-\frac{Q}{60\pi\eta^2\ell_c}\left(\left(1+\frac{4}{7}P_2(\cos\theta)\right)\frac{\partial n}{\partial r}-\frac{3}{7}\sin 2\theta\frac{1}{r}\frac{\partial n}{\partial\theta}\right)=\frac{1}{r\sin\theta}\frac{\partial}{\partial\theta}(A\sin\theta), \tag{3.4.27}$$

$$-D^T\frac{1}{r}\frac{\partial n}{\partial\theta}-\frac{Q}{60\pi\eta^2\ell_c}\left(-\frac{3}{7}\sin 2\theta\frac{\partial n}{\partial r}+\left(\frac{9}{7}-\frac{4}{7}P_2(\cos\theta)\right)\frac{1}{r}\frac{\partial n}{\partial\theta}\right)=-\frac{1}{r}\frac{\partial}{\partial r}(rA). \tag{3.4.28}$$

Outside the raft, Eqs. (3.4.25) and (3.4.26) lead to

$$-D^T\frac{\partial n}{\partial r}=\frac{1}{r\sin\theta}\frac{\partial}{\partial\theta}(A\sin\theta), \tag{3.4.29}$$

$$-D^T\frac{1}{r}\frac{\partial n}{\partial\theta}=-\frac{1}{r}\frac{\partial}{\partial r}(rA). \tag{3.4.30}$$

Equations (3.4.29) and (3.4.30) are solved as

$$n(r,\theta)=\sum_{k=0}^{\infty}\left\{a_kr^k+\frac{b_k}{r^{k+1}}\right\}P_k(\cos\theta), \tag{3.4.31}$$

$$A(r,\theta)=\sum_{k=0}^{\infty}\left\{a_kkr^k+\frac{b_k(k+1)}{r^{k+1}}\right\}\frac{C_k^{-1/2}(\cos\theta)}{\sin\theta}. \tag{3.4.32}$$

Assuming that there are only 0 and 2 modes, then we have

$$n(r,\theta)=a+\frac{b}{r^3}P_2(\cos\theta), \tag{3.4.33}$$

$$A(r,\theta)=\frac{3b}{r^3}\frac{C_2^{-1/2}(\cos\theta)}{\sin\theta}, \tag{3.4.34}$$

where P_2 is the second-order Legendre polynomials and $C_2^{-1/2}$ is the second-order Gegenbauer polynomials (ultraspherical polynomials) of the degree of $-1/2$.

By integrating the both sides of Eqs. (3.4.29) and (3.4.30) with regard to $r\in[R-0,R+0]$, we obtain

$$\begin{aligned}-\frac{1}{60\pi\eta^2\ell_c}\left(1+\frac{4}{7}P_2(\cos\theta)\right)\frac{Q_0}{2}(n_{\text{out}}+n_{\text{in}})-D^T(n_{\text{out}}-n_{\text{in}})&\\ -\frac{1}{60\pi\eta^2\ell_c}\left(\left(1+\frac{4}{7}P_2(\cos\theta)\right)\frac{Q_0}{2}(n_{\text{out}}-n_{\text{in}})\right)&=0,\end{aligned} \tag{3.4.35}$$

$$\frac{1}{60\pi\eta^2\ell_c}\frac{3}{7}\sin 2\theta\frac{Q_0}{2}(n_{\text{out}}+n_{\text{in}})-\frac{1}{60\pi\eta^2\ell_c}\left(-\frac{3}{7}\sin 2\theta\frac{Q_0}{2}(n_{\text{out}}-n_{\text{in}})\right)=-(A_{\text{out}}-A_{\text{in}}), \tag{3.4.36}$$

where R is a radius of the spherical region. Here we used $\int\delta(x)\theta(x)dx=1/2$.

From Eq. (3.4.35), we obtain

$$D^Tn_{\text{in}}=\frac{1}{60\pi\eta^2\ell_c}\left(1+\frac{4}{7}P_2(\cos\theta)\right)Q_0n_{\text{out}}+D^Tn_{\text{out}}, \tag{3.4.37}$$

and thus we have

$$n_{\text{out}}=\frac{n_{\text{in}}}{\frac{1}{60\pi\eta^2\ell_cD^T}\left(1+\frac{4}{7}P_2(\cos\theta)\right)Q_0+1}. \tag{3.4.38}$$

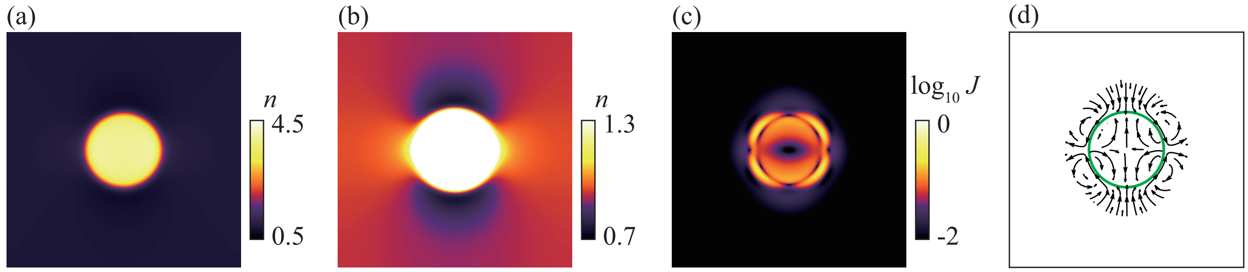

Figure 3.4.2: Numerical results on the distribution of tracer particles (a,b) and their fluxes (c,d) in the steady state of a three-dimensional system with orientationally ordered force dipoles that occupy a sphere in the center. Part (b) shows the distribution enhanced in the region of low number densities. The logarithm $\log_{10} \boldsymbol{j}(\boldsymbol{r})$ of the local magnitude of the fluxes and their streamlines are displayed in (c) and (d). The vertical direction corresponds to the orientation line of force dipoles. The parameters were $R = 16\ell_c$, $\delta = 0.5\ell_c$, and $S = 1$. The spatial and time steps were $0.4\ell_c(= 0.4)$ and 10^{-7}, respectively. Reproduced from Ref. [41].

We assumed that $D^T n_{\text{out}} \ll 1$ and $n_{\text{in}} = Q_0$, and then we have

$$n_{\text{out}} = 60\pi\eta^2\ell_c D^T \left(1 - \frac{4}{7}P_2(\cos\theta) + \frac{16}{49}P_2(\cos\theta)^2 - \cdots\right). \tag{3.4.39}$$

When we neglect the higher-orders of $4P_2(\cos\theta)/7$, then we have $a = 60\pi\eta^2\ell_c D^T$, $b = -240\pi\eta^2\ell_c D^T/7$ in Eqs. (3.4.33) and (3.4.34).

Since A has a value depending on r and θ, the steady flow of tracer particles exists. It is noted that the profile of tracer particles does not change in time, thus the flow should circulate. Here we show numerical results based on the Fokker-Planck equation (3.2.21) with the Kramers-Moyal coefficients in Eqs. (3.4.1) and (3.4.2). The distribution of the force dipoles is given in Eq. . The number density of the tracer particles n initially had uniform distribution ($n = 1$). We calculated the time evolution of the distribution of tracer particles, and obtained the steady state as shown in Fig. 3.4.2(a,b). We also obtained the steady flow of tracer particles as shown in Fig. 3.4.2(c,d). We can see the circulating flow, which clearly has the secondmode as expected by the theoretical calculation in Eq. (3.4.34).

3.5 Summary

In this chapter, we discussed the hydrodynamic collective effect of active elements modeled as force dipoles. Especially for a two-dimensional system, the finite size effect is critical since the diffusion coefficient diverges for an infinite system according to the proposed model. The real system, however, can be inhomogeneous or can have a typical size, thus it is worth investigating the localized effect of force dipoles. In the inhomogeneous system, directional flow takes place, resulting in the accumulation of tracer particles toward the force dipoles. We also investigated the effect of the alignment of active elements. We found that the accumulation of tracer particles occurs. For a three-dimensional system, circulating flow of tracer particles occurs even though the distribution of tracer particles is steady.

Chapter 4

Conclusion

So far we have studied the active system with continous energy injection and dissipation. As mentioned in Preface, seemingly-lower-entropy structures can emerge in dissipative systems, and our aim was to understand what kind of structure emerges in the actual systems – self-propelled motions through spontaneous symmetry breaking and collective effects of active elements.

In the first half, we investigate the motion of self-propelled particle emerging through spontaneous symmetry breaking. We consider three types of geometries; a one-dimensional finite system with inversion symmetry, a two-dimensional circular system with inversion and rotational symmetry, and a rotor system with rotational symmetry. We discussed motion of a camphor particle on water surface, based on the mathematical model. The model was reduced around the rest state, and the bifurcation structures were determined which indicate what kind motion occurs. As the future work, we would like to investigate the interaction between shape and motion. For example, using the camphor driven rotors, which discussed in Sec. 2.5, the interaction between them can be investigated.

In the latter half, we consider collective effects by active force dipoles, especially the localized and alignment effects. We considered the dynamics of fluid with active force dipoles, and derived that diffusion is enhanced by the recursive deformation of active proteins. When force dipoles are localized, not only the diffusion enhancement but also directional flow of tracer particles is induced by force dipoles. In this case, tracer particles are accumulated in the region with the force dipoles. As for the aligned force-dipole cluster, circulating flow of tracer particles ws found in a three-dimensional system, though the distribution of tracer particles is steady. In the model, it is assumed that force dipoles are dilute enough and that the flow induced force dipoles is described by the Oseen tensor. Thus it remains as future work to investigate whether diffusion enhancement can take place in a systems with denser active elements.

By proceeding our research on active systems further, we hope we will contribute generic understanding of nonequilibrium systems in future.

Acknowledgments

I acknowledge H. Kitahata, who is my advisor. I also thank to T. Sakurai, N. Yoshinaga, A. S. Mikhailov, J. Gorecki and the member of his laboratory, T. Ohta, N. J. Suematsu, Y. Sumino, S.-I. Ei, M. Nagayama, S. Nakata, K. Ikeda, and T. Miyaji, T. Banno, T. Toyota, B. Nanzai, Y. Abe, M. Shimokawa, S. Inagaki, H. Ebata, and F. Takabatake.

This work was supported by JSPS KAKENHI Grants No. JP17J05270, by the JSPS Core-to-Core Program "Non-equilibrium dynamics of soft matter and information", and by JSPS Bilateral Joint Research Program between Japan and the Polish Academy of Sciences. This work was also supported by Cooperative Research Program of "Network Joint Research Center for Materials and Devices" (No. 20165001 and 20175002), and the Sasakawa Scientific Research Grant from the Japan Science Society (No. 28-225).

Bibliography

[1] G. Nicolis and I. Prigogine, *Self-Organization in Nonequilibrium Systems: From Dissipative Structures to Order through Fluctuations* (Wiley, 1977).

[2] A. N. Zaikin and A. M. Zhabotinsky, *Nature* **225**, 535 (1970).

[3] R. Kapral and K. Showalter, *Chemical Waves and Patterns* (Springer, 1995)

[4] A. S. Mikhailov and G. Ertl, *Chemical Complexity: Self-Organization Processes in Molecular Systems* (Springer, 2017).

[5] S. Chandrasekhar, *Hydrodynamic and Hydromagnetic Stability* (Dover, 1981).

[6] P. Ball, *Flow – Nature's patterns: a tapestry in three parts* (Oxford Univ. Press, 2011).

[7] S. Ramaswamy, *Annu. Rev. Cond. Mat. Phys.* **1**, 323 (2010).

[8] M. C. Marchetti, J. F. Joanny, S. Ramaswamy, T. B. Liverpool, J. Prost, M. Rao, R. Aditi Simha, *Rev. Mod. Phys.* **85**, 1143 (2013).

[9] R. Cortini, M. Barbi, B. R. Car, C. Lavelle, A. Lesne, J. Mozziconacci, and J. Victor, *Rev. Mod. Phys.* **88**, 025002 (2016).

[10] S. Ramaswamy, *J. Stat. Mech.* **2017**, 054002 (2017).

[11] T. Ohta, *J. Phys. Soc. Jpn.* **86**, 072001 (2017).

[12] T. Ohta, M. Mimura, and R. Kobayashi, *Physica D* **34**, 115 (1989).

[13] K. Krischer and A. Mikhailov, *Phys. Rev. Lett.* **73**, 3165 (1994).

[14] C. P. Schenk, M. Or-Guil, M. Bode, and H.-G. Purwins, *Phys. Rev. Lett.* **78**, 3781 (1997).

[15] N. J. Cira, A. Benusiglio, and M. Prakash, *Nature* **519**, 446 (2015).

[16] T. Ishiwatari, M. Kawaguchi, and M. Mitsuishi, *J. Polym. Sci. A* **22**, 2699 (1984).

[17] R. Yoshida, T. Takahashi, T. Yamaguchi, and H. Ichijo, *J. Am. Chem. Soc.* **118**, 5134 (1996).

[18] J. R. Howse, R. A. L. Jones, A. J. Ryan, T. Gough, R. Vafabakhsh, and R. Golestanian, *Phys. Rev. Lett.* **99**, 048102 (2007).

[19] W. F. Paxton, A. Sen, and T. E. Mallouk, *Chem. Eur. J.* **11**, 6462 (2005).

[20] T. Toyota, N. Maru, M. M. Hanczyc, T. Ikegami, and T. Sugawara, *J. Am. Chem. Soc.* **131**, 5012 (2009).

[21] T. Banno, A. Asami, N. Ueno, H. Kitahata, Y. Koyano, K. Asakura, and T. Toyota, *Sci. Rep.* **6**, 31292 (2016).

[22] S. Nakata, M. Nagayama, H. Kitahata, N. J. Suematsu, and T. Hasegawa, *Phys. Chem. Chem. Phys.* **17**, 10326 (2015).

[23] K. Nagai, Y. Sumino, H. Kitahata, and K. Yoshikawa, *Phys. Rev. E* **71**, 065301 (2005).

[24] H. Tanimoto and M. Sano, *Phys. Rev. Lett.* **109**, 248110 (2012).

[25] T. Vicsek, A. Czirók, E. Ben-Jacob, I. Cohen, and O. Shochet, *Phys. Rev. Lett.* **75**, 1226 (1995).

[26] T. Vicsek and A. Zafeiris, *Phys. Rep.* **517**, 71 (2012).

[27] S. Yamanaka and T. Ohta, *Phys. Rev. E* **89**, 012918 (2014).

[28] S. Yamanaka and T. Ohta, *Phys. Rev. E* **90**, 042927 (2014).

[29] H. Wioland, F. G. Woodhouse, J. Dunkel, J. O. Kessler, and R. E. Goldstein, *Phys. Rev. Lett.* **110**, 268102 (2013).

[30] A. Mikhailov and V. Calenbuhr, *From Cells to Societies* (Springer-Verlag, 2002).

[31] F. Schweitzer, W. Ebeling, and B. Tilch, *Phys. Rev. Lett.* **80**, 5044 (1998).

[32] F. Schweitzer, *Brownian Agents and Active Particles* (Springer-Verlag, 2003).

[33] T. Ohta and T. Ohkuma, *Phys. Rev. Lett.* **102**, 154101 (2009).

[34] Y. Koyano, T. Sakurai, and H. Kitahata, *Phys. Rev. E* **94**, 042215 (2016).

[35] Y. Koyano, N. J. Suematsu, and H. Kitahata, in preparation.

[36] Y. Koyano, M. Gryciuk, P. Skrobanska, M. Malecki, Y. Sumino, H. Kitahata, and J. Gorecki, *Phys. Rev. E* **96**, 012609 (2017).

[37] Y. Koyano, N. Yoshinaga, and H, Kitahata, *J. Chem. Phys.* **143**, 014117 (2015).

[38] A. S. Mikhailov and R. Kapral, *Proc. Natl. Acad. Sci. USA* **112**, E3639 (2015).

[39] R. Kapral and A. S. Mikhailov, *Physica D* **318-319**, 100 (2016).

[40] Y. Koyano, H. Kitahata, and A. S. Mikhailov, *Phys. Rev. E* **94**, 022416 (2016).

[41] A. S. Mikhailov, Y. Koyano, and H. Kitahata, *J. Phys. Soc. Jpn.* **86**, 101013 (2017).

[42] C. Tomlinson, *Proc. R. Soc. Lond.* **11**, 575, (1860).

[43] W. Skey, *Trans. Proc. R. Soc. New Zealand* **11**, 473 (1878).

[44] L. Rayleigh, *Proc. R. Soc. Lond.* **34**, 364 (1890).

[45] S. Nakata, Y. Iguchi, S. Ose, M. Kuboyama, T. Ishii, and K. Yoshikawa, *Langmuir* **13**, 4454 (1997).

[46] S. Nakata, M. I. Kohira, and Y. Hayashima, *Chem. Phys. Lett.* **323**, 419 (2000).

[47] M. Nagayama, S. Nakata, Y. Doi, and Y. Hayashima, *Physica D* **194**, 151 (2004).

[48] Y. Hayashima, M. Nagayama, and S. Nakata, *J. Phys. Chem. B* **105**, 5353 (2001).

[49] K. Iida, N. J. Suematsu, Y. Miyahara, H. Kitahata, M. Nagayama, and S. Nakata, *Phys. Chem. Chem. Phys.* **12**, 1557 (2010).

[50] T. Bánsági, Jr., M. M. Wrobel, S. K. Scott, and A. F. Taylor, *J. Phys. Chem. B* **117**, 13572 (2013).

[51] Y. Satoh, Y. Sogabe, K. Kayahara, S. Tanaka, M. Nagayama, and S. Nakata, *Soft Matter* **13**, 3422 (2017).

[52] F. Takabatake, K. Yoshikawa, and M. Ichikawa, *J. Chem. Phys.* **141**, 051103 (2014).

[53] H. Moyses, J. Palacci, S. Sacanna, and D. G. Grier, *Soft Matter* **12**, 6323 (2016).

[54] F. Domingues Dos Santos and T. Ondarçuhu, *Phys. Rev. Lett.* **75**, 2972 (1995).

[55] N. Magome and K. Yoshikawa, *J. Phys. Chem.* **100**, 19102 (1996).

[56] Y. Sumino and K. Yoshikawa, *Chaos* **18**, 026106 (2008).

[57] H. Jin, A. Marmur, O. Ikkala, and R. H. A. Ras, *Chem. Sci.* **3**, 2526 (2012).

[58] S. Soh, K. J. M. Bishop, and B. A. Grzybowski, *J. Phys. Chem. B* **112**, 10848 (2008).

[59] N. J. Suematsu, S. Nakata, A. Awazu, and H. Nishimori, *Phys. Rev. E* **81**, 056210 (2010).

[60] S-I. Ei, K. Ikeda, M. Nagayama, and A. Tomoeda, *Math. Bohem.* **139**, 363 (2014).

[61] S. Nakata, H. Yamamoto, Y. Koyano, O. Yamanaka, Y. Sumino, N. J. Suematsu, H. Kitahata, P. Skrobanska, and J. Gorecki, *J. Phys. Chem. B* **120**, 9166 (2016).

[62] J. Gorecki, H. Kitahata, N. J. Suematsu, Y. Koyano, P. Skrobanska, M. Gryciuk, M. Malecki, T. Tanabe, H. Yamamotod, and S. Nakata, *Phys. Chem. Chem. Phys.* **19**, 18767 (2017).

[63] M. Mimura, T. Miyaji, and I. Ohnishi, *Hiroshima Math. J.* **37**, 343 (2007).

[64] X. Chen, S-I. Ei, and M. Mimura, *Netw. Heterog. Media* **4**, 1 (2009).

[65] T. Miyaji, *Physica D* **340**, 14 (2017).

[66] I. Lagzi, S. Soh, P. J. Wesson, K. P. Browne, and B. A. Grzybowski, *J. Am. Chem. Soc.* **132**, 1198 (2010)

[67] T. Ban, K. Tani, H. Nakata, and Y. Okano, *Soft Matter* **10**, 6316 (2014).

[68] A. G. Vecchiarelli, K. C. Neuman, and K. Mizuuchi, *Proc. Natl. Acad. Sci. USA* **111**, 4880 (2014).

[69] E. J. Banigan and J. F. Marko, *Phys. Rev. E* **93**, 012611 (2016).

[70] H. Kitahata and Yoshinaga, arXiv 1604.01108 (2016).

[71] L. D. Landau and E. M. Lifshitz, *Fluid Mechanics 2nd Edition* (Elsevier, 1987).

[72] T. Ohta, T. Ohkuma, and K. Shitara, *Phys. Rev. E* **80**, 056203 (2009).

[73] S. H. Strogatz, *Nonlinear Dynamics and Chaos* (Perseus Books, 1994).

[74] J. Guckenheimer and P. Holmes, *Nonlinear Oscillations, Dynamical Systems, and Bifurcations of Vector Fields* (Springer, 1983).

[75] N. J. Suematsu, T. Sasaki, S. Nakata, and H. Kitahata, *Langmuir* **30**, 8101 (2014).

[76] B. van der Pol, *Philos. Mag.* **3**, 65 (1927).

[77] J. W. S. Rayleigh, *The Theory of Sound* (Dover, 1945).

[78] W. L. Keith and R. H. Rand, *Int. J. Non-Linear Mech.* **20**, 325 (1985).

[79] K. Ikeda, T. Miyaji, N. Yoshinaga, and H. Kitahata, in preparation.

[80] F. Bowman, *Introduction to Bessel functions* (Dover, 1958).

[81] G. N. Watson, *A Treatise on the Theory of Bessel Functions* (Cambridge University Press, 1922).

[82] K. Iida, H. Kitahata, and M. Nagayama, *Physica D* **272**, 39 (2014).

[83] B. R. Parry, I. V. Surovtsev, M. T. Cabeen, C. S. Hern, E. R. Dufresne, and C. Jacobs-Wagner, *Cell* **156**, 183 (2014).

[84] M. Guo, A. J. Ehrlicher, M. H. Jensen, M. Renz, J. R. Moore, R. D. Goldman, J. Lippincott-Schwartz, F. C. Mackintosh, and D. A. Weitz, *Cell* **158**, 822 (2014).

[85] S. Sengupta, K. K. Dey, H. S. Muddana, T. Tabouillot, M. E. Ibele, P. J. Butler, and A. Sen, *J. Am. Chem. Soc.* **135**, 1406 (2013).

[86] Y. Togashi and A. S. Mikhailov, *Proc. Natl. Acad. Sci. USA* **104**, 8697 (2007).

[87] H. Diamant, *J. Phys. Soc. Jpn.* **78**, 041002 (2009).

[88] P. G. Saffman and M. Delbrück, *Proc. Natl. Acad. Sci. USA* **72**, 3111 (1975).

[89] H. Risken and T. Frank, *The Fokker-Planck Equation: Methods of Solution and Applications (2nd ed.)* (Springer, 1996),

[90] I. S. Gradshteyn and I. M. Ryzhik, *Table of Integrals, Series, and Products* (*Seventh Edition*) (Academic Press, 2007).

[91] M. Abramowitz and I. A. Stegu, *Handbook of Mathematical Functions: with Formulas, Graphs, and Mathematical Tables* (Dover, 1965).

Appendix A

Supplementary Information for Chapter 2

In this chapter, the supplementary information for Chapter 2 is provided.

A.1 Supplementary information for Section 2.2

A.1.1 Derivation of Eq. (2.2.20)

In this subsection, the driving force expanded with regard to the position, velocity, and acceleration of the camphor particle is derived. The gradient of concentration field expanded in wavenumber space is expressed as follows:

$$\frac{\partial c}{\partial x} = -\frac{1}{R}\sum_{k=1}^{\infty}\frac{k\pi}{R}c_k(X, \dot{X}, \ddot{X})\sin\left(\frac{k\pi}{R}x\right). \tag{A.1.1}$$

By calculating the expansion as in Eq. (2.2.17), we have

$$\begin{aligned}\frac{\partial c}{\partial x} = & -\frac{1}{R}\sum_{k=1}^{\infty}\frac{k\pi}{R}c_k\sin\left(\frac{k\pi}{R}x\right)\\ = & \underbrace{-\frac{1}{R}\sum_{k=1}^{\infty}\left(\frac{k\pi}{R}\frac{2}{A}\cos(\kappa X)\sin\left(\frac{k\pi}{R}x\right)\right)}_{\text{Term which is not related to the time derivative of } X}\\ & \underbrace{-\frac{1}{R}\sum_{k=1}^{\infty}\left(\frac{k\pi}{R}\frac{2\kappa}{A^2}\sin(\kappa X)\sin\left(\frac{k\pi}{R}x\right)\right)\dot{X}}_{\text{Term proportional to } \dot{X}} + \underbrace{\frac{1}{R}\sum_{k=1}^{\infty}\left(\frac{k\pi}{R}\frac{2\kappa}{A^3}\sin(\kappa X)\sin\left(\frac{k\pi}{R}x\right)\right)\ddot{X}}_{\text{Term proportional to } \ddot{X}}\\ & + \underbrace{\frac{1}{R}\sum_{k=1}^{\infty}\left(\frac{k\pi}{R}\frac{2\kappa^2}{A^3}\cos(\kappa X)\sin\left(\frac{k\pi}{R}x\right)\right)\dot{X}^2}_{\text{Term proportional to } \dot{X}^2} + \underbrace{\frac{1}{R}\sum_{k=1}^{\infty}\left(\frac{k\pi}{R}\frac{2\kappa^3}{A^4}\sin(\kappa X)\sin\left(\frac{k\pi}{R}x\right)\right)\dot{X}^3}_{\text{Term proportional to } \dot{X}^3},\end{aligned} \tag{A.1.2}$$

where we neglect the higher-order terms of X and the higher-order derivatives with regard to time. Here, we set $A = k^2\pi^2/R^2 + 1$ and $\kappa = k\pi/R$. The driving force is calculated by the definition in Eq. (2.2.12), and then expanded around $x = R/2$.

Here we show several relations for the calculation.

$$\sum_{k=1}^{\infty} \frac{k \sin kx}{k^2+\alpha^2} = \begin{cases} \dfrac{\pi}{2}\dfrac{\sinh \alpha(\pi - x)}{\sinh \alpha\pi}, & [0 < x < 2\pi], \\ -\dfrac{\pi}{2}\dfrac{\sinh \alpha(\pi + x)}{\sinh \alpha\pi}, & [-2\pi < x < 0]. \end{cases} \tag{A.1.3}$$

Equation (A.1.3) is referred from Ref. [90]. By differentiating Eq. (A.1.3) with regard to α and k, we obtain the following relations.

$$\sum_{k=1}^{\infty} \frac{k^2 \cos kx}{(k^2+\alpha^2)^2} = \begin{cases} \dfrac{\pi}{4\alpha}\dfrac{\cosh \alpha(\pi - x)}{\sinh \alpha\pi} \\ \quad + \dfrac{\pi}{4}\left\{\dfrac{(\pi - x)\sinh \alpha(\pi - x)}{\sinh \alpha\pi} - \dfrac{\pi \cosh \alpha(\pi - x)\cosh \alpha\pi}{(\sinh \alpha\pi)^2}\right\}, & [0 < x < 2\pi], \\ \dfrac{\pi}{4\alpha}\dfrac{\cosh \alpha(\pi + x)}{\sinh \alpha\pi} \\ \quad + \dfrac{\pi}{4}\left\{\dfrac{(\pi + x)\sinh \alpha(\pi + x)}{\sinh \alpha\pi} - \dfrac{\pi \cosh \alpha(\pi + x)\cosh \alpha\pi}{(\sinh \alpha\pi)^2}\right\}, & [-2\pi < x < 0]. \end{cases} \tag{A.1.4}$$

$$\sum_{k=1}^{\infty} \frac{k^2 \cos kx}{(k^2+\alpha^2)^3} = \begin{cases} \dfrac{\pi}{16\alpha^3}\dfrac{\cosh \alpha(\pi - x)}{\sinh \alpha\pi} \\ \quad - \dfrac{\pi}{16\alpha^2}\left\{\dfrac{(\pi - x)\sinh \alpha(\pi - x)}{\sinh \alpha\pi} - \dfrac{\pi \cosh \alpha(\pi - x)\cosh \alpha\pi}{(\sinh \alpha\pi)^2}\right\} \\ \quad - \dfrac{\pi}{16\alpha}\left\{\dfrac{(\pi - x)^2\cosh \alpha(\pi - x)}{\sinh \alpha\pi} - 2\dfrac{\pi(\pi - x)\sinh \alpha(\pi - x)\cosh \alpha\pi}{(\sinh \alpha\pi)^2}\right. \\ \qquad \left. - \dfrac{\pi^2\cosh \alpha(\pi - x)}{\sinh \alpha\pi} + 2\dfrac{\pi^2\cosh \alpha(\pi - x)(\cosh \alpha\pi)^2}{(\sinh \alpha\pi)^3}\right\}, & [0 < x < 2\pi], \\ \dfrac{\pi}{16\alpha^3}\dfrac{\cosh \alpha(\pi + x)}{\sinh \alpha\pi} \\ \quad - \dfrac{\pi}{16\alpha^2}\left\{\dfrac{(\pi + x)\sinh \alpha(\pi + x)}{\sinh \alpha\pi} - \dfrac{\pi \cosh \alpha(\pi + x)\cosh \alpha\pi}{(\sinh \alpha\pi)^2}\right\} \\ \quad - \dfrac{\pi}{16\alpha}\left\{\dfrac{(\pi + x)^2\cosh \alpha(\pi + x)}{\sinh \alpha\pi} - 2\dfrac{\pi(\pi + x)\sinh \alpha(\pi + x)\cosh \alpha\pi}{(\sinh \alpha\pi)^2}\right. \\ \qquad \left. - \dfrac{\pi^2\cosh \alpha(\pi + x)}{\sinh \alpha\pi} + 2\dfrac{\pi^2\cosh \alpha(\pi + x)(\cosh \alpha\pi)^2}{(\sinh \alpha\pi)^3}\right\}, & [-2\pi < x < 0]. \end{cases} \tag{A.1.5}$$

$$
\sum_{k=1}^{\infty} \frac{k^3 \sin kx}{(k^2+\alpha^2)^3} = \begin{cases} \dfrac{3\pi}{16\alpha}\left\{-\dfrac{(\pi-x)\cosh\alpha(\pi-x)}{\sinh\alpha\pi} + \dfrac{\pi\sinh\alpha(\pi-x)\cosh\alpha\pi}{(\sinh\alpha\pi)^2}\right\} \\ \quad + \dfrac{\pi}{16}\left\{-\dfrac{(\pi-x)^2\sinh\alpha(\pi-x)}{\sinh\alpha\pi} + 2\dfrac{\pi(\pi-x)\cosh\alpha(\pi-x)\cosh\alpha\pi}{(\sinh\alpha\pi)^2}\right. \\ \qquad \left. + \dfrac{\pi^2\sinh\alpha(\pi-x)}{\sinh\alpha\pi} - 2\dfrac{\pi^2\sinh\alpha(\pi-x)(\cosh\alpha\pi)^2}{(\sinh\alpha\pi)^3}\right\}, \ [0<x<2\pi], \\ \dfrac{3\pi}{16\alpha}\left\{\dfrac{(\pi+x)\cosh\alpha(\pi+x)}{\sinh\alpha\pi} - \dfrac{\pi\sinh\alpha(\pi+x)\cosh\alpha\pi}{(\sinh\alpha\pi)^2}\right\} \\ \quad + \dfrac{\pi}{16}\left\{\dfrac{(\pi+x)^2\sinh\alpha(\pi+x)}{\sinh\alpha\pi} - 2\dfrac{\pi(\pi+x)\cosh\alpha(\pi+x)\cosh\alpha\pi}{(\sinh\alpha\pi)^2}\right. \\ \qquad \left. - \dfrac{\pi^2\sinh\alpha(\pi+x)}{\sinh\alpha\pi} + 2\dfrac{\pi^2\sinh\alpha(\pi+x)(\cosh\alpha\pi)^2}{(\sinh\alpha\pi)^3}\right\}, \ [-2\pi<x<0]. \end{cases} \tag{A.1.6}
$$

$$
\sum_{k=1}^{\infty} \frac{k^4 \cos kx}{(k^2+\alpha^2)^4}
$$
$$
= \begin{cases} \dfrac{\pi}{32\alpha^3}\dfrac{\cosh\alpha(\pi-x)}{\sinh\alpha\pi} - \dfrac{\pi}{32\alpha^2}\left(\dfrac{(\pi-x)\sinh\alpha(\pi-x)}{\sinh\alpha\pi} - \dfrac{\pi\cosh\alpha(\pi-x)\cosh\alpha\pi}{(\sinh\alpha\pi)^2}\right) \\ \quad - \dfrac{\pi}{16\alpha}\left(\dfrac{(\pi-x)^2\cosh\alpha(\pi-x)}{\sinh\alpha\pi} - 2\dfrac{\pi(\pi-x)\sinh\alpha(\pi-x)\cosh\alpha\pi}{(\sinh\alpha\pi)^2}\right. \\ \qquad \left. - \dfrac{\pi^2\cosh\alpha(\pi-x)}{\sinh\alpha\pi} + 2\dfrac{\pi^2\cosh\alpha(\pi-x)(\cosh\alpha\pi)^2}{(\sinh\alpha\pi)^3}\right) \\ \quad - \dfrac{\pi}{96}\left(\dfrac{(\pi-x)^3\sinh\alpha(\pi-x)}{\sinh\alpha\pi} - 3\dfrac{\pi(\pi-x)^2\cosh\alpha(\pi-x)\cosh\alpha\pi}{(\sinh\alpha\pi)^2}\right. \\ \qquad - 3\dfrac{\pi^2(\pi-x)\sinh\alpha(\pi-x)}{\sinh\alpha\pi} + 6\dfrac{\pi^2(\pi-x)\sinh\alpha(\pi-x)(\cosh\alpha\pi)^2}{(\sinh\alpha\pi)^3} \\ \qquad \left. +5\dfrac{\pi^3\cosh\alpha(\pi-x)\cosh\alpha\pi}{(\sinh\alpha\pi)^2} - 6\dfrac{\pi^3\cosh\alpha(\pi-x)(\cosh\alpha\pi)^3}{(\sinh\alpha\pi)^4}\right), \\ \qquad [0<x<2\pi], \\ \dfrac{\pi}{32\alpha^3}\dfrac{\cosh\alpha(\pi+x)}{\sinh\alpha\pi} - \dfrac{\pi}{32\alpha^2}\left(\dfrac{(\pi+x)\sinh\alpha(\pi+x)}{\sinh\alpha\pi} - \dfrac{\pi\cosh\alpha(\pi+x)\cosh\alpha\pi}{(\sinh\alpha\pi)^2}\right) \\ \quad - \dfrac{\pi}{16\alpha}\left(\dfrac{(\pi+x)^2\cosh\alpha(\pi+x)}{\sinh\alpha\pi} - 2\dfrac{\pi(\pi+x)\sinh\alpha(\pi+x)\cosh\alpha\pi}{(\sinh\alpha\pi)^2}\right. \\ \qquad \left. - \dfrac{\pi^2\cosh\alpha(\pi+x)}{\sinh\alpha\pi} + 2\dfrac{\pi^2\cosh\alpha(\pi+x)(\cosh\alpha\pi)^2}{(\sinh\alpha\pi)^3}\right) \\ \quad - \dfrac{\pi}{96}\left(\dfrac{(\pi+x)^3\sinh\alpha(\pi+x)}{\sinh\alpha\pi} - 3\dfrac{\pi(\pi+x)^2\cosh\alpha(\pi+x)\cosh\alpha\pi}{(\sinh\alpha\pi)^2}\right. \\ \qquad - 3\dfrac{\pi^2(\pi+x)\sinh\alpha(\pi+x)}{\sinh\alpha\pi} + 6\dfrac{\pi^2(\pi+x)\sinh\alpha(\pi+x)(\cosh\alpha\pi)^2}{(\sinh\alpha\pi)^3} \\ \qquad \left. +5\dfrac{\pi^3\cosh\alpha(\pi+x)\cosh\alpha\pi}{(\sinh\alpha\pi)^2} - 6\dfrac{\pi^3\cosh\alpha(\pi+x)(\cosh\alpha\pi)^3}{(\sinh\alpha\pi)^4}\right), \\ \qquad [-2\pi<x<0]. \end{cases} \tag{A.1.7}
$$

By using the formulae, each term in Eq. (A.1.2) is calculated separately and then the driving force originating from the inhomogeneity of the surface tension is calculated.

Term which is not related to the time derivative of X

The term which is not related to the time derivative of X in Eq. (A.1.2) is expressed as follows:

$$\begin{aligned} &-\frac{1}{R}\sum_{k=1}^{\infty}\frac{k\pi}{R}\frac{2}{k^2\pi^2/R^2+1}\cos\left(\frac{k\pi}{R}x\right)\sin\left(\frac{k\pi}{R}x\right) \\ &\quad= -\frac{1}{\pi}\sum_{k=1}^{\infty}\frac{k}{k^2+R^2/\pi^2}\left(\sin\left(k\frac{\pi}{R}(x+X)\right)+\sin\left(k\frac{\pi}{R}(x-X)\right)\right). \end{aligned} \tag{A.1.8}$$

In the case of $\left[0<\frac{\pi}{R}(x+X)<2\pi\right]\cap\left[0<\frac{\pi}{R}(x-X)<\pi\right]$, we have

$$-\frac{1}{R}\sum_{k=1}^{\infty}\frac{k\pi}{R}\frac{2}{k^2\pi^2/R^2+1}\cos\left(\frac{k\pi}{R}x\right)\sin\left(\frac{k\pi}{R}x\right) = -\frac{\sinh(R-(x+X))+\sinh(R-(x-X))}{2\sinh R}, \tag{A.1.9}$$

where we apply Eq. (A.1.3). By substituting $x = X$, we have

$$-\frac{1}{R}\sum_{k=1}^{\infty}\frac{k\pi}{R}\frac{2}{k^2\pi^2/R^2+1}\cos\left(\frac{k\pi}{R}x\right)\sin\left(\frac{k\pi}{R}(X+0)\right) = -\frac{\sinh(R-2X)+\sinh R}{2\sinh R}. \tag{A.1.10}$$

In the case of $\left[0<\frac{\pi}{R}(x+X)<\pi\right]\cap\left[-2\pi<\frac{\pi}{R}(x-X)<0\right]$, we have

$$-\frac{1}{R}\sum_{k=1}^{\infty}\frac{k\pi}{R}\frac{2}{k^2\pi^2/R^2+1}\cos\left(\frac{k\pi}{R}x\right)\sin\left(\frac{k\pi}{R}x\right) = \frac{-\sinh(R-(x+X))+\sinh(R+(x-X))}{2\sinh R}, \tag{A.1.11}$$

where we apply Eq. (A.1.3). By substituting $x = X$, we have

$$-\frac{1}{R}\sum_{k=1}^{\infty}\frac{k\pi}{R}\frac{2}{k^2\pi^2/R^2+1}\cos\left(\frac{k\pi}{R}x\right)\sin\left(\frac{k\pi}{R}(X+0)\right) = \frac{-\sinh(R-2X)+\sinh R}{2\sinh R}. \tag{A.1.12}$$

The driving force originating from the component of concentration field which is not related to the time derivative of X is calculated as follows:

$$\begin{aligned} &-\left\{-\frac{1}{R}\sum_{k=1}^{\infty}\frac{k\pi}{R}\frac{2}{k^2\pi^2/R^2+1}\cos\left(\frac{k\pi}{R}x\right)\sin\left(\frac{k\pi}{R}x\right)\right\}\Bigg|_{x=X+0} \\ &\qquad -\left\{-\frac{1}{R}\sum_{k=1}^{\infty}\frac{k\pi}{R}\frac{2}{k^2\pi^2/R^2+1}\cos\left(\frac{k\pi}{R}x\right)\sin\left(\frac{k\pi}{R}x\right)\right\}\Bigg|_{x=X-0} \\ &= -\frac{-\sinh(R-2X)+\sinh R}{2\sinh R}-\left(-\frac{\sinh(R-2X)+\sinh R}{2\sinh R}\right) \\ &= \frac{\sinh(R-2X)}{\sinh R}. \end{aligned} \tag{A.1.13}$$

Term proportional to $\dot{X}$

The term proportional to $\dot{X}$ in Eq. (A.1.2) is expressed as follows:

$$\begin{aligned} &-\frac{1}{R}\sum_{k=1}^{\infty}\frac{k\pi}{R}\frac{2(k\pi/R)}{(k^2\pi^2/R^2+1)^2}\sin\left(\frac{k\pi}{R}x\right)\sin\left(\frac{k\pi}{R}x\right)\\ &\quad=-\frac{1}{R\,(\pi/R)^2}\sum_{k=1}^{\infty}\frac{k^2}{(k^2+R^2/\pi^2)^2}\left(\cos\left(k\frac{\pi}{R}\,(x-X)\right)-\cos\left(k\frac{\pi}{R}\,(x+X)\right)\right). \end{aligned} \tag{A.1.14}$$

In the case of $\left[0<\frac{\pi}{R}\,(x+X)<2\pi\right]\cap\left[0<\frac{\pi}{R}\,(x-X)<\pi\right]$, we have

$$\begin{aligned} &-\frac{1}{R}\sum_{k=1}^{\infty}\frac{k\pi}{R}\frac{2(k\pi/R)}{(k^2\pi^2/R^2+1)^2}\sin\left(\frac{k\pi}{R}x\right)\sin\left(\frac{k\pi}{R}x\right)\\ &\quad=-\frac{\cosh(R-(x-X))}{4\sinh R}\\ &\qquad-\frac{1}{4}\left\{\frac{(R-(x-X))\sinh(R-(x-X))}{\sinh R}-\frac{R\cosh(R-(x-X))\cosh R}{(\sinh R)^2}\right\}\\ &\qquad+\frac{\cosh(R-(x+X))}{4\sinh R}\\ &\qquad+\frac{1}{4}\left\{\frac{(R-(x+X))\sinh(R-(x+X))}{\sinh R}-\frac{R\cosh(R-(x+X))\cosh R}{(\sinh R)^2}\right\}, \end{aligned} \tag{A.1.15}$$

where we apply Eq. (A.1.4). By substituting $x=X$, we have

$$\begin{aligned} &-\frac{1}{R}\sum_{k=1}^{\infty}\frac{k\pi}{R}\frac{2(k\pi/R)}{(k^2\pi^2/R^2+1)^2}\sin\left(\frac{k\pi}{R}x\right)\sin\left(\frac{k\pi}{R}(X-0)\right)\\ &\quad=-\frac{\cosh R}{4\sinh R}-\frac{1}{4}\left\{R-\frac{R(\cosh R)^2}{(\sinh R)^2}\right\}\\ &\qquad+\frac{\cosh(R-2X)}{4\sinh R}+\frac{1}{4}\left\{\frac{(R-2X)\sinh(R-2X)}{\sinh R}-\frac{R\cosh(R-2X)\cosh R}{(\sinh R)^2}\right\}. \end{aligned} \tag{A.1.16}$$

In the case of $\left[0<\frac{\pi}{R}\,(x+X)<\pi\right]\cap\left[-2\pi<\frac{\pi}{R}\,(x-X)<0\right]$, we have

$$\begin{aligned} &-\frac{1}{R}\sum_{k=1}^{\infty}\frac{k\pi}{R}\frac{2(k\pi/R)}{(k^2\pi^2/R^2+1)^2}\sin\left(\frac{k\pi}{R}x\right)\sin\left(\frac{k\pi}{R}x\right)\\ &\quad=-\frac{\cosh(R+(x-X))}{4\sinh R}\\ &\qquad-\frac{1}{4}\left\{\frac{(R+(x-X))\sinh(R+(x-X))}{\sinh R}-\frac{R\cosh(R+(x-X))\cosh R}{(\sinh R)^2}\right\}\\ &\qquad+\frac{\cosh(R-(x+X))}{4\sinh R}\\ &\qquad+\frac{1}{4}\left\{\frac{(R-(x+X))\sinh(R-(x+X))}{\sinh R}-\frac{R\cosh(R-(x+X))\cosh R}{(\sinh R)^2}\right\}, \end{aligned} \tag{A.1.17}$$

where we apply Eq. (A.1.4). By substituting $x = X$, we have

$$
\begin{aligned}
&-\frac{1}{R}\sum_{k=1}^{\infty}\frac{k\pi}{R}\frac{2(k\pi/R)}{(k^2\pi^2/R^2+1)^2}\sin\left(\frac{k\pi}{R}x\right)\sin\left(\frac{k\pi}{R}X\right)\\
&\quad=-\frac{\cosh R}{4\sinh R}-\frac{1}{4}\left\{R-\frac{R(\cosh R)^2}{(\sinh R)^2}\right\}\\
&\qquad+\frac{\cosh(R-2X)}{4\sinh R}+\frac{1}{4}\left\{\frac{(R-2X)\sinh(R-2X)}{\sinh R}-\frac{R\cosh(R-2X)\cosh R}{(\sinh R)^2}\right\}.
\end{aligned}
\tag{A.1.18}
$$

The driving force proportional to $\dot{X}$ is calculated as follows:

$$
\begin{aligned}
&-\left\{-\frac{1}{R}\sum_{k=1}^{\infty}\frac{k\pi}{R}\frac{2(k\pi/R)}{(k^2\pi^2/R^2+1)^2}\sin\left(\frac{k\pi}{R}x\right)\sin\left(\frac{k\pi}{R}x\right)\right\}\Bigg|_{x=X+0}\\
&\qquad-\left\{-\frac{1}{R}\sum_{k=1}^{\infty}\frac{k\pi}{R}\frac{2(k\pi/R)}{(k^2\pi^2/R^2+1)^2}\sin\left(\frac{k\pi}{R}x\right)\sin\left(\frac{k\pi}{R}x\right)\right\}\Bigg|_{x=X-0}\\
&\quad=\frac{\cosh R}{2\sinh R}+\frac{1}{2}\left\{R-\frac{R(\cosh R)^2}{(\sinh R)^2}\right\}\\
&\qquad-\frac{\cosh(R-2X)}{2\sinh R}-\frac{1}{2}\left\{\frac{(R-2X)\sinh(R-2X)}{\sinh R}-\frac{R\cosh(R-2X)\cosh R}{(\sinh R)^2}\right\}\\
&\quad=\frac{\cosh R}{2\sinh R}-\frac{R}{2(\sinh R)^2}\\
&\qquad-\frac{\cosh(R-2X)}{2\sinh R}-\frac{1}{2}\left\{\frac{(R-2X)\sinh(R-2X)}{\sinh R}-\frac{R\cosh(R-2X)\cosh R}{(\sinh R)^2}\right\}.
\end{aligned}
\tag{A.1.19}
$$

Term proportional to $\ddot{X}$

The term proportional to $\ddot{X}$ in Eq. (A.1.2) is expressed as follows:

$$
\begin{aligned}
&-\frac{1}{R}\sum_{k=1}^{\infty}\frac{k\pi}{R}\left(-\frac{2(k\pi/R)}{(k^2\pi^2/R^2+1)^3}\right)\sin\left(\frac{k\pi}{R}x\right)\sin\left(\frac{k\pi}{R}x\right)\\
&\quad=\frac{1}{R\left(\pi/R\right)^4}\sum_{k=1}^{\infty}\frac{k^2}{\left(k^2+(R/\pi)^2\right)^3}\left(\cos\left(k\frac{\pi}{R}(x-X)\right)-\cos\left(k\frac{\pi}{R}(x+X)\right)\right).
\end{aligned}
\tag{A.1.20}
$$

In the case of $\left[0<\frac{\pi}{R}(x+X)<2\pi\right]\cap\left[0<\frac{\pi}{R}(x-X)<\pi\right]$, we have

$$
\begin{aligned}
&-\frac{1}{R}\sum_{k=1}^{\infty}\frac{k\pi}{R}\left(-\frac{2(k\pi/R)}{(k^2\pi^2/R^2+1)^3}\right)\sin\left(\frac{k\pi}{R}x\right)\sin\left(\frac{k\pi}{R}x\right)\\
&\quad=\frac{\cosh(R-(x-X))}{16\sinh R}\\
&\qquad-\frac{1}{16}\left\{\frac{(R-(x-X))\sinh(R-(x-X))}{\sinh R}-\frac{R\cosh(R-(x-X))\cosh R}{(\sinh R)^2}\right\}\\
&\qquad-\frac{1}{16}\left\{\frac{(R-(x-X))^2\cosh(R-(x-X))}{\sinh R}-2\frac{R(R-(x-X))\sinh(R-(x-X))\cosh R}{(\sinh R)^2}\right.
\end{aligned}
$$

$$
\begin{aligned}
&\qquad\qquad -\frac{R^2\cosh(R-(x-X))}{\sinh R}+2\frac{R^2\cosh(R-(x-X))(\cosh R)^2}{(\sinh R)^3}\Bigg\}\\
&-\frac{\cosh(R-(x+X))}{16\sinh R}\\
&+\frac{1}{16}\left\{\frac{(R-(x+X))\sinh(R-(x+X))}{\sinh R}-\frac{R\cosh(R-(x+X))\cosh R}{(\sinh R)^2}\right\}\\
&+\frac{1}{16}\Bigg\{\frac{(R-(x+X))^2\cosh(R-(x+X))}{\sinh R}-2\frac{R(R-(x+X))\sinh(R-(x+X))\cosh R}{(\sinh R)^2}\\
&\qquad\qquad -\frac{R^2\cosh(R-(x+X))}{\sinh R}+2\frac{R^2\cosh(R-(x+X))(\cosh R)^2}{(\sinh R)^3}\Bigg\},
\end{aligned}
\tag{A.1.21}
$$

where we apply Eq. (A.1.5). By substituting $x=X$, we have

$$
\begin{aligned}
&-\frac{1}{R}\sum_{k=1}^{\infty}\frac{k\pi}{R}\left(-\frac{2(k\pi/R)}{(k^2\pi^2/R^2+1)^3}\right)\sin\left(\frac{k\pi}{R}x\right)\sin\left(\frac{k\pi}{R}(X-0)\right)\\
&\quad=\frac{\cosh R}{16\sinh R}-\frac{1}{16}\left\{R-\frac{R(\cosh R)^2}{(\sinh R)^2}\right\}-\frac{1}{8}\left\{-\frac{R^2\cosh R}{\sinh R}+\frac{R^2(\cosh R)^3}{(\sinh R)^3}\right\}\\
&\qquad-\frac{\cosh(R-2X)}{16\sinh R}+\frac{1}{16}\left\{\frac{(R-2X)\sinh(R-2X)}{\sinh R}-\frac{R\cosh(R-2X)\cosh R}{(\sinh R)^2}\right\}\\
&\qquad+\frac{1}{16}\Bigg\{\frac{(R-2X)^2\cosh(R-2X)}{\sinh R}-2\frac{R(R-2X)\sinh(R-2X)\cosh R}{(\sinh R)^2}\\
&\qquad\qquad-\frac{R^2\cosh(R-2X)}{\sinh R}+2\frac{R^2\cosh(R-2X)(\cosh R)^2}{(\sinh R)^3}\Bigg\}.
\end{aligned}
\tag{A.1.22}
$$

In the case of $\left[0<\frac{\pi}{R}(x+X)<\pi\right]\cap\left[-2\pi<\frac{\pi}{R}(x-X)<0\right]$, we have

$$
\begin{aligned}
&-\frac{1}{R}\sum_{k=1}^{\infty}\frac{k\pi}{R}\left(-\frac{2(k\pi/R)}{(k^2\pi^2/R^2+1)^3}\right)\sin\left(\frac{k\pi}{R}x\right)\sin\left(\frac{k\pi}{R}x\right)\\
&\quad=\frac{\cosh(R+(x-X))}{16\sinh R}\\
&\qquad-\frac{1}{16}\left\{\frac{(R+(x-X))\sinh(R+(x-X))}{\sinh R}-\frac{R\cosh(R+(x-X))\cosh R}{(\sinh R)^2}\right\}\\
&\qquad-\frac{1}{16}\Bigg\{\frac{(R+(x-X))^2\cosh(R+(x-X))}{\sinh R}-2\frac{R(R+(x-X))\sinh(R+(x-X))\cosh R}{(\sinh R)^2}\\
&\qquad\qquad-\frac{R^2\cosh(R+(x-X))}{\sinh R}+2\frac{R^2\cosh(R+(x-X))(\cosh R)^2}{(\sinh R)^3}\Bigg\}\\
&\qquad-\frac{\cosh(R-(x+X))}{16\sinh R}\\
&\qquad+\frac{1}{16}\left\{\frac{(R-(x+X))\sinh(R-(x+X))}{\sinh R}-\frac{R\cosh(R-(x+X))\cosh R}{(\sinh R)^2}\right\}\\
&\qquad+\frac{1}{16}\Bigg\{\frac{(R-(x+X))^2\cosh(R-(x+X))}{\sinh R}-2\frac{R(R-(x+X))\sinh(R-(x+X))\cosh R}{(\sinh R)^2}\\
&\qquad\qquad-\frac{R^2\cosh(R-(x+X))}{\sinh R}+2\frac{R^2\cosh(R-(x+X))(\cosh R)^2}{(\sinh R)^3}\Bigg\},
\end{aligned}
\tag{A.1.23}
$$

where we apply Eq. (A.1.5). By substituting $x = X$, we have

$$\begin{aligned}
&-\frac{1}{R}\sum_{k=1}^{\infty}\frac{k\pi}{R}\left(-\frac{2(k\pi/R)}{(k^2\pi^2/R^2+1)^3}\right)\sin\left(\frac{k\pi}{R}x\right)\sin\left(\frac{k\pi}{R}x\right)\\
&\quad=\frac{\cosh R}{16\sinh R}-\frac{1}{16}\left\{R-\frac{R(\cosh R)^2}{(\sinh R)^2}\right\}-\frac{1}{8}\left\{-\frac{R^2\cosh R}{\sinh R}+\frac{R^2(\cosh R)^3}{(\sinh R)^3}\right\}\\
&\qquad-\frac{\cosh(R-2X)}{16\sinh R}+\frac{1}{16}\left\{\frac{(R-2X)\sinh(R-2X)}{\sinh R}-\frac{R\cosh(R-2X)\cosh R}{(\sinh R)^2}\right\}\\
&\qquad+\frac{1}{16}\left\{\frac{(R-2X)^2\cosh(R-2X)}{\sinh R}-2\frac{R(R-2X)\sinh(R-2X)\cosh R}{(\sinh R)^2}\right.\\
&\qquad\qquad\left.-\frac{R^2\cosh(R-2X)}{\sinh R}+2\frac{R^2\cosh(R-2X)(\cosh R)^2}{(\sinh R)^3}\right\}.
\end{aligned}\tag{A.1.24}$$

Therefore, the driving force proportional to $\ddot{X}$ is calculated as follows:

$$\begin{aligned}
&-\left.\left\{-\frac{1}{R}\sum_{k=1}^{\infty}\frac{k\pi}{R}\frac{2(k\pi/R)}{(k^2\pi^2/R^2+1)^2}\sin\left(\frac{k\pi}{R}x\right)\sin\left(\frac{k\pi}{R}x\right)\right\}\right|_{x=X+0}\\
&\qquad-\left.\left\{-\frac{1}{R}\sum_{k=1}^{\infty}\frac{k\pi}{R}\frac{2(k\pi/R)}{(k^2\pi^2/R^2+1)^2}\sin\left(\frac{k\pi}{R}x\right)\sin\left(\frac{k\pi}{R}x\right)\right\}\right|_{x=X-0}\\
&\quad=-\frac{\cosh R}{8\sinh R}-\frac{R}{8(\sinh R)^2}+\frac{R^2\cosh R}{4(\sinh R)^3}+\frac{\cosh(R-2X)}{8\sinh R}\\
&\qquad-\frac{1}{8}\left\{\frac{(R-2X)\sinh(R-2X)}{\sinh R}-\frac{R\cosh(R-2X)\cosh R}{(\sinh R)^2}\right\}\\
&\qquad-\frac{1}{8}\left\{\frac{(R-2X)^2\cosh(R-2X)}{\sinh R}-2\frac{R(R-2X)\sinh(R-2X)\cosh R}{(\sinh R)^2}\right.\\
&\qquad\qquad\left.-\frac{R^2\cosh(R-2X)}{\sinh R}+2\frac{R^2\cosh(R-2X)(\cosh R)^2}{(\sinh R)^3}\right\}.
\end{aligned}\tag{A.1.25}$$

Term proportional to $\dot{X}^2$

The term proportional to $\dot{X}^2$ in Eq. (A.1.2) is expressed as follows:

$$\begin{aligned}
&-\frac{1}{R}\sum_{k=1}^{\infty}\frac{k\pi}{R}\left(-\frac{2(k\pi/R)^2}{(k^2\pi^2/R^2+1)^3}\right)\cos\left(\frac{k\pi}{R}x\right)\sin\left(\frac{k\pi}{R}x\right)\\
&\quad=\frac{1}{R\left(\pi/R\right)^3}\sum_{k=1}^{\infty}\frac{k^3}{\left(k^2+\left(R/\pi\right)^2\right)^3}\left(\sin\left(k\frac{\pi}{R}\left(x+X\right)\right)+\sin\left(k\frac{\pi}{R}\left(x-X\right)\right)\right).
\end{aligned}\tag{A.1.26}$$

In the case of $\left[0<\frac{\pi}{R}\left(x+X\right)<2\pi\right]\cap\left[0<\frac{\pi}{R}\left(x-X\right)<\pi\right]$, we have

$$\begin{aligned}
&-\frac{1}{R}\sum_{k=1}^{\infty}\frac{k\pi}{R}\left(-\frac{2(k\pi/R)^2}{(k^2\pi^2/R^2+1)^3}\right)\cos\left(\frac{k\pi}{R}x\right)\sin\left(\frac{k\pi}{R}x\right)\\
&\quad=\frac{3}{16}\left\{-\frac{(R-(x+X))\cosh(R-(x+X))}{\sinh R}+\frac{R\sinh(R-(x+X))\cosh R}{(\sinh R)^2}\right\}
\end{aligned}$$

$$
\begin{aligned}
&+\frac{1}{16}\left\{-\frac{(R-(x+X))^2\sinh(R-(x+X))}{\sinh R}+2\frac{R(R-(x+X))\cosh(R-(x+X))\cosh R}{(\sinh R)^2}\right.\\
&\qquad\left.+\frac{R^2\sinh(R-(x+X))}{\sinh R}-2\frac{R^2\sinh(R-(x+X))(\cosh R)^2}{(\sinh R)^3}\right\}\\
&+\frac{3}{16}\left\{-\frac{(R-(x-X))\cosh(R-(x-X))}{\sinh R}+\frac{R\sinh(R-(x-X))\cosh R}{(\sinh R)^2}\right\}\\
&+\frac{1}{16}\left\{-\frac{(R-(x-X))^2\sinh(R-(x-X))}{\sinh R}+2\frac{R(R-(x-X))\cosh(R-(x-X))\cosh R}{(\sinh R)^2}\right.\\
&\qquad\left.+\frac{R^2\sinh(R-(x-X))}{\sinh R}-2\frac{R^2\sinh(R-(x-X))(\cosh R)^2}{(\sinh R)^3}\right\},
\end{aligned}
\tag{A.1.27}
$$

where we apply Eq. (A.1.6). By substituting $x=X$, we have

$$
\begin{aligned}
&-\frac{1}{R}\sum_{k=1}^{\infty}\frac{k\pi}{R}\left(-\frac{2(k\pi/R)^2}{(k^2\pi^2/R^2+1)^3}\right)\cos\left(\frac{k\pi}{R}x\right)\sin\left(\frac{k\pi}{R}(X-0)\right)\\
&\quad=\frac{3}{16}\left\{-\frac{(R-2X)\cosh(R-2X)}{\sinh R}+\frac{R\sinh(R-2X)\cosh R}{(\sinh R)^2}\right\}\\
&\qquad+\frac{1}{16}\left\{-\frac{(R-2X)^2\sinh(R-2X)}{\sinh R}+2\frac{R(R-2X)\cosh(R-2X)\cosh R}{(\sinh R)^2}\right.\\
&\qquad\qquad\left.+\frac{R^2\sinh(R-2X)}{\sinh R}-2\frac{R^2\sinh(R-2X)(\cosh R)^2}{(\sinh R)^3}\right\}.
\end{aligned}
\tag{A.1.28}
$$

In the case of $\left[0<\frac{\pi}{R}(x+X)<2\pi\right]\cap\left[-2\pi<\frac{\pi}{R}(x-X)<0\right]$, we have

$$
\begin{aligned}
&-\frac{1}{R}\sum_{k=1}^{\infty}\frac{k\pi}{R}\left(-\frac{2(k\pi/R)^2}{(k^2\pi^2/R^2+1)^3}\right)\cos\left(\frac{k\pi}{R}x\right)\sin\left(\frac{k\pi}{R}x\right)\\
&\quad=\frac{3}{16}\left\{-\frac{(R-(x+X))\cosh(R-(x+X))}{\sinh R}+\frac{R\sinh(R-(x+X))\cosh R}{(\sinh R)^2}\right\}\\
&\quad+\frac{1}{16}\left\{-\frac{(R-(x+X))^2\sinh(R-(x+X))}{\sinh R}+2\frac{R(R-(x+X))\cosh(R-(x+X))\cosh R}{(\sinh R)^2}\right.\\
&\qquad\left.+\frac{R^2\sinh(R-(x+X))}{\sinh R}-2\frac{R^2\sinh(R-(x+X))(\cosh R)^2}{(\sinh R)^3}\right\}\\
&\quad+\frac{3}{16}\left\{\frac{(R+(x-X))\cosh(R+(x-X))}{\sinh R}-\frac{R\sinh(R+(x-X))\cosh R}{(\sinh R)^2}\right\}\\
&\quad+\frac{1}{16}\left\{\frac{(R+(x-X))^2\sinh(R+(x-X))}{\sinh R}-2\frac{R(R+(x-X))\cosh(R+(x-X))\cosh R}{(\sinh R)^2}\right.\\
&\qquad\left.-\frac{R^2\sinh(R+(x-X))}{\sinh R}+2\frac{R^2\sinh(R+(x-X))(\cosh R)^2}{(\sinh R)^3}\right\},
\end{aligned}
\tag{A.1.29}
$$

where we apply Eq. (A.1.6). By substituting $x=X$, we have

$$
-\frac{1}{R}\sum_{k=1}^{\infty}\frac{k\pi}{R}\left(-\frac{2(k\pi/R)^2}{(k^2\pi^2/R^2+1)^3}\right)\cos\left(\frac{k\pi}{R}x\right)\sin\left(\frac{k\pi}{R}(X+0)\right)
$$

$$
\begin{aligned}
&= \frac{3}{16}\left\{-\frac{(R-2X)\cosh(R-2X)}{\sinh R} + \frac{R\sinh(R-2X)\cosh R}{(\sinh R)^2}\right\} \\
&\quad + \frac{1}{16}\left\{-\frac{(R-2X)^2\sinh(R-2X)}{\sinh R} + 2\frac{R(R-2X)\cosh(R-2X)\cosh R}{(\sinh R)^2}\right. \\
&\qquad\qquad \left. + \frac{R^2\sinh(R-2X)}{\sinh R} - 2\frac{R^2\sinh(R-2X)(\cosh R)^2}{(\sinh R)^3}\right\}.
\end{aligned} \tag{A.1.30}
$$

The driving force proportional to $\dot{X}^2$ is calculated as follows:

$$
\begin{aligned}
&- \left\{-\frac{1}{R}\sum_{k=1}^{\infty}\frac{k\pi}{R}\frac{2(k\pi/R)^2}{(k^2\pi^2/R^2+1)^3}\cos\left(\frac{k\pi}{R}x\right)\sin\left(\frac{k\pi}{R}x\right)\right\}\Bigg|_{x=X+0} \\
&\qquad - \left\{-\frac{1}{R}\sum_{k=1}^{\infty}\frac{k\pi}{R}\frac{2(k\pi/R)^2}{(k^2\pi^2/R^2+1)^3}\cos\left(\frac{k\pi}{R}x\right)\sin\left(\frac{k\pi}{R}x\right)\right\}\Bigg|_{x=X-0} \\
&= \frac{3}{8}\left\{\frac{(R-2X)\cosh(R-2X)}{\sinh R} - \frac{R\sinh(R-2X)\cosh R}{(\sinh R)^2}\right\} \\
&\quad + \frac{1}{8}\left\{\frac{(R-2X)^2\sinh(R-2X)}{\sinh R} - 2\frac{R(R-2X)\cosh(R-2X)\cosh R}{(\sinh R)^2}\right. \\
&\qquad\qquad \left. - \frac{R^2\sinh(R-2X)}{\sinh R} + 2\frac{R^2\sinh(R-2X)(\cosh R)^2}{(\sinh R)^3}\right\}.
\end{aligned} \tag{A.1.31}
$$

Term proportional to $\dot{X}^3$

The term proportional to $\dot{X}^3$ in Eq. (A.1.2) is expressed as follows:

$$
\begin{aligned}
&- \frac{1}{R}\sum_{k=1}^{\infty}\frac{k\pi}{R}\left(-\frac{2(k\pi/R)^3}{(k^2\pi^2/R^2+1)^4}\right)\sin\left(\frac{k\pi}{R}x\right)\sin\left(\frac{k\pi}{R}x\right) \\
&\quad = \frac{2}{R(\pi/R)^4}\sum_{k=1}^{\infty}\frac{k^4}{\left(k^2+(R/\pi)^2\right)^4}\frac{\cos\left(k\frac{\pi}{R}(x-X)\right)-\cos\left(k\frac{\pi}{R}(x+X)\right)}{2}.
\end{aligned} \tag{A.1.32}
$$

In the case of $\left[0 < \frac{\pi}{R}(x+X) < 2\pi\right] \cap \left[0 < \frac{\pi}{R}(x-X) < \pi\right]$, we have

$$
\begin{aligned}
&- \frac{1}{R}\sum_{k=1}^{\infty}\frac{k\pi}{R}\left(-\frac{2(k\pi/R)^3}{(k^2\pi^2/R^2+1)^4}\right)\sin\left(\frac{k\pi}{R}x\right)\sin\left(\frac{k\pi}{R}x\right) \\
&= \frac{1}{32}\frac{\cosh(R-(x-X))}{\sinh R} - \frac{1}{32}\left(\frac{(R-(x-X))\sinh(R-(x-X))}{\sinh R} - \frac{R\cosh(R-(x-X))\cosh R}{(\sinh R)^2}\right) \\
&\quad - \frac{1}{16}\left(\frac{(R-(x-X))^2\cosh(R-(x-X))}{\sinh R} - 2\frac{R(R-(x-X))\sinh(R-(x-X))\cosh R}{(\sinh R)^2}\right. \\
&\qquad\qquad \left. - \frac{R^2\cosh(R-(x-X))}{\sinh R} + 2\frac{R^2\cosh(R-(x-X))(\cosh R)^2}{(\sinh R)^3}\right) \\
&\quad - \frac{1}{96}\left(\frac{(R-(x-X))^3\sinh(R-(x-X))}{\sinh R} - 3\frac{R(R-(x-X))^2\cosh(R-(x-X))\cosh R}{(\sinh R)^2}\right. \\
&\qquad\qquad - 3\frac{R^2(R-(x-X))\sinh(R-(x-X))}{\sinh R} + 6\frac{R^2(R-(x-X))\sinh(R-(x-X))(\cosh R)^2}{(\sinh R)^3}
\end{aligned}
$$

$$
\begin{aligned}
&\qquad +5\frac{R^3\cosh(R-(x-X))\cosh R}{(\sinh R)^2}-6\frac{R^3\cosh(R-(x-X))(\cosh R)^3}{(\sinh R)^4}\Bigg)\\
&-\frac{1}{32}\frac{\cosh(R-(x+X))}{\sinh R}+\frac{1}{32}\left(\frac{(R-(x+X))\sinh(R-(x+X))}{\sinh R}-\frac{R\cosh(R-(x+X))\cosh R}{(\sinh R)^2}\right)\\
&+\frac{1}{16}\Bigg(\frac{(R-(x+X))^2\cosh(R-(x+X))}{\sinh R}-2\frac{R(R-(x+X))\sinh(R-(x+X))\cosh R}{(\sinh R)^2}\\
&\qquad -\frac{R^2\cosh(R-(x+X))}{\sinh R}+2\frac{R^2\cosh(R-(x+X))(\cosh R)^2}{(\sinh R)^3}\Bigg)\\
&+\frac{1}{96}\Bigg(\frac{(R-(x+X))^3\sinh(R-(x+X))}{\sinh R}-3\frac{R(R-(x+X))^2\cosh(R-(x+X))\cosh R}{(\sinh R)^2}\\
&\qquad -3\frac{R^2(R-(x+X))\sinh(R-(x+X))}{\sinh R}+6\frac{R^2(R-(x+X))\sinh(R-(x+X))(\cosh R)^2}{(\sinh R)^3}\\
&\qquad +5\frac{R^3\cosh(R-(x+X))\cosh R}{(\sinh R)^2}-6\frac{R^3\cosh(R-(x+X))(\cosh R)^3}{(\sinh R)^4}\Bigg),
\end{aligned}
\tag{A.1.33}
$$

where we apply Eq. (A.1.7). By substituting $x = X$, we have

$$
\begin{aligned}
&-\frac{1}{R}\sum_{k=1}^{\infty}\frac{k\pi}{R}\left(-\frac{2(k\pi/R)^3}{(k^2\pi^2/R^2+1)^4}\right)\sin\left(\frac{k\pi}{R}x\right)\sin\left(\frac{k\pi}{R}(X-0)\right)\\
&\quad =\frac{1}{32}\frac{\cosh R}{\sinh R}-\frac{1}{32}\left(R-\frac{R(\cosh R)^2}{(\sinh R)^2}\right)-\frac{1}{8}\left(-\frac{R^2\cosh R}{\sinh R}+\frac{R^2(\cosh R)^3}{(\sinh R)^3}\right)\\
&\quad -\frac{1}{96}\left(R^3-3\frac{R^3(\cosh R)^2}{(\sinh R)^2}-3R^3+6\frac{R^3(\cosh R)^2}{(\sinh R)^2}+5\frac{R^3(\cosh R)^2}{(\sinh R)^2}-6\frac{R^3(\cosh R)^4}{(\sinh R)^4}\right)\\
&\quad -\frac{1}{32}\frac{\cosh(R-2X)}{\sinh R}+\frac{1}{32}\left(\frac{(R-2X)\sinh(R-2X)}{\sinh R}-\frac{R\cosh(R-2X)\cosh R}{(\sinh R)^2}\right)\\
&\quad +\frac{1}{16}\Bigg(\frac{(R-2X)^2\cosh(R-2X)}{\sinh R}-2\frac{R(R-2X)\sinh(R-2X)\cosh R}{(\sinh R)^2}\\
&\qquad\quad -\frac{R^2\cosh(R-2X)}{\sinh R}+2\frac{R^2\cosh(R-2X)(\cosh R)^2}{(\sinh R)^3}\Bigg)\\
&\quad +\frac{1}{96}\Bigg(\frac{(R-2X)^3\sinh(R-2X)}{\sinh R}-3\frac{R(R-2X)^2\cosh(R-2X)\cosh R}{(\sinh R)^2}\\
&\qquad\quad -3\frac{R^2(R-2X)\sinh(R-2X)}{\sinh R}+6\frac{R^2(R-2X)\sinh(R-2X)(\cosh R)^2}{(\sinh R)^3}\\
&\qquad\quad +5\frac{R^3\cosh(R-2X)\cosh R}{(\sinh R)^2}-6\frac{R^3\cosh(R-2X)(\cosh R)^3}{(\sinh R)^4}\Bigg).
\end{aligned}
\tag{A.1.34}
$$

In the case of $\left[0<\frac{\pi}{R}(x+X)<2\pi\right]\cap\left[-2\pi<\frac{\pi}{R}(x-X)<0\right]$, we have

$$
\begin{aligned}
&-\frac{1}{R}\sum_{k=1}^{\infty}\frac{k\pi}{R}\left(-\frac{2(k\pi/R)^3}{(k^2\pi^2/R^2+1)^4}\right)\sin\left(\frac{k\pi}{R}x\right)\sin\left(\frac{k\pi}{R}x\right)\\
&=\frac{1}{32}\frac{\cosh(R+(x-X))}{\sinh R}-\frac{1}{32}\left(\frac{(R+(x-X))\sinh(R+(x-X))}{\sinh R}-\frac{R\cosh(R+(x-X))\cosh R}{(\sinh R)^2}\right)\\
&-\frac{1}{16}\Bigg(\frac{(R+(x-X))^2\cosh(R+(x-X))}{\sinh R}-2\frac{R(R+(x-X))\sinh(R+(x-X))\cosh R}{(\sinh R)^2}
\end{aligned}
$$

$$
\begin{aligned}
&\quad -\frac{R^2\cosh(R+(x-X))}{\sinh R}+2\frac{R^2\cosh(R+(x+X))(\cosh R)^2}{(\sinh R)^3}\Bigg)\\
&-\frac{1}{96}\Bigg(\frac{(R+(x-X))^3\sinh(R+(x-X))}{\sinh R}-3\frac{R(R+(x-X))^2\cosh(R+(x-X))\cosh R}{(\sinh R)^2}\\
&\quad -3\frac{R^2(R+(x-X))\sinh(R+(x-X))}{\sinh R}+6\frac{R^2(R+(x-X))\sinh(R+(x-X))(\cosh R)^2}{(\sinh R)^3}\\
&\quad +5\frac{R^3\cosh(R+(x-X))\cosh R}{(\sinh R)^2}-6\frac{R^3\cosh(R+(x-X))(\cosh R)^3}{(\sinh R)^4}\Bigg)\\
&-\frac{1}{32}\frac{\cosh(R-(x+X))}{\sinh R}+\frac{1}{32}\Bigg(\frac{(R-(x+X))\sinh(R-(x+X))}{\sinh R}-\frac{R\cosh(R-(x+X))\cosh R}{(\sinh R)^2}\Bigg)\\
&+\frac{1}{16}\Bigg(\frac{(R-(x+X))^2\cosh(R-(x+X))}{\sinh R}-2\frac{R(R-(x+X))\sinh(R-(x+X))\cosh R}{(\sinh R)^2}\\
&\quad -\frac{R^2\cosh(R-(x+X))}{\sinh R}+2\frac{R^2\cosh(R-(x+X))(\cosh R)^2}{(\sinh R)^3}\Bigg)\\
&+\frac{1}{96}\Bigg(\frac{(R-(x+X))^3\sinh(R-(x+X))}{\sinh R}-3\frac{R(R-(x+X))^2\cosh(R-(x+X))\cosh R}{(\sinh R)^2}\\
&\quad -3\frac{R^2(R-(x+X))\sinh(R-(x+X))}{\sinh R}+6\frac{R^2(R-(x+X))\sinh(R-(x+X))(\cosh R)^2}{(\sinh R)^3}\\
&\quad +5\frac{R^3\cosh(R-(x+X))\cosh R}{(\sinh R)^2}-6\frac{R^3\cosh(R-(x+X))(\cosh R)^3}{(\sinh R)^4}\Bigg),
\end{aligned}
\tag{A.1.35}
$$

where we apply Eq. (A.1.7). By substituting $x = X$, we have

$$
\begin{aligned}
&-\frac{1}{R}\sum_{k=1}^{\infty}\frac{k\pi}{R}\left(-\frac{2(k\pi/R)^3}{(k^2\pi^2/R^2+1)^4}\right)\sin\left(\frac{k\pi}{R}x\right)\sin\left(\frac{k\pi}{R}(X+0)\right)\\
&\quad=\frac{1}{32}\frac{\cosh R}{\sinh R}-\frac{1}{32}\left(R-\frac{R(\cosh R)^2}{(\sinh R)^2}\right)-\frac{1}{8}\left(-\frac{R^2\cosh R}{\sinh R}+\frac{R^2(\cosh R)^3}{(\sinh R)^3}\right)\\
&\qquad-\frac{1}{96}\left(R^3-3\frac{R^3(\cosh R)^2}{(\sinh R)^2}-3R^3+6\frac{R^3(\cosh R)^2}{(\sinh R)^2}+5\frac{R^3(\cosh R)^2}{(\sinh R)^2}-6\frac{R^3(\cosh R)^4}{(\sinh R)^4}\right)\\
&\qquad-\frac{1}{32}\frac{\cosh(R-2X)}{\sinh R}+\frac{1}{32}\left(\frac{(R-2X)\sinh(R-2X)}{\sinh R}-\frac{R\cosh(R-2X)\cosh R}{(\sinh R)^2}\right)\\
&\qquad+\frac{1}{16}\Bigg(\frac{(R-2X)^2\cosh(R-2X)}{\sinh R}-2\frac{R(R-2X)\sinh(R-2X)\cosh R}{(\sinh R)^2}\\
&\qquad\quad-\frac{R^2\cosh(R-2X)}{\sinh R}+2\frac{R^2\cosh(R-2X)(\cosh R)^2}{(\sinh R)^3}\Bigg)\\
&\qquad+\frac{1}{96}\Bigg(\frac{(R-2X)^3\sinh(R-2X)}{\sinh R}-3\frac{R(R-2X)^2\cosh(R-2X)\cosh R}{(\sinh R)^2}\\
&\qquad\quad-3\frac{R^2(R-2X)\sinh(R-2X)}{\sinh R}+6\frac{R^2(R-2X)\sinh(R-2X)(\cosh R)^2}{(\sinh R)^3}\\
&\qquad\quad+5\frac{R^3\cosh(R-2X)\cosh R}{(\sinh R)^2}-6\frac{R^3\cosh(R-2X)(\cosh R)^3}{(\sinh R)^4}\Bigg).
\end{aligned}
\tag{A.1.36}
$$

The driving force proportional to $\dot{X}^3$ is therefore calculated as follows:

$$
\begin{aligned}
&- \left\{ -\frac{1}{R} \sum_{k=1}^{\infty} \frac{k\pi}{R} \frac{2(k\pi/R)^3}{(k^2\pi^2/R^2+1)^4} \sin\left(\frac{k\pi}{R}x\right) \sin\left(\frac{k\pi}{R}x\right) \right\}\Bigg|_{x=X+0} \\
&\qquad - \left\{ -\frac{1}{R} \sum_{k=1}^{\infty} \frac{k\pi}{R} \frac{2(k\pi/R)^3}{(k^2\pi^2/R^2+1)^4} \sin\left(\frac{k\pi}{R}x\right) \sin\left(\frac{k\pi}{R}x\right) \right\}\Bigg|_{x=X-0} \\
&\quad = -\frac{\cosh R}{16\sinh R} - \frac{R}{16(\sinh R)^2} + \frac{R^2\cosh R}{4(\sinh R)^3} + \frac{R^3}{24(\sinh R)^2} - \frac{R^3(\cosh R)^2}{8(\sinh R)^4} \\
&\qquad + \frac{1}{16}\frac{\cosh(R-2X)}{\sinh R} - \frac{1}{16}\left(\frac{(R-2X)\sinh(R-2X)}{\sinh R} - \frac{R\cosh(R-2X)\cosh R}{(\sinh R)^2}\right) \\
&\qquad - \frac{1}{8}\Bigg(\frac{(R-2X)^2\cosh(R-2X)}{\sinh R} - 2\frac{R(R-2X)\sinh(R-2X)\cosh R}{(\sinh R)^2} \\
&\qquad\qquad -\frac{R^2\cosh(R-2X)}{\sinh R} + 2\frac{R^2\cosh(R-2X)(\cosh R)^2}{(\sinh R)^3}\Bigg) \\
&\qquad - \frac{1}{48}\Bigg(\frac{(R-2X)^3\sinh(R-2X)}{\sinh R} - 3\frac{R(R-2X)^2\cosh(R-2X)\cosh R}{(\sinh R)^2} \\
&\qquad\qquad - 3\frac{R^2(R-2X)\sinh(R-2X)}{\sinh R} + 6\frac{R^2(R-2X)\sinh(R-2X)(\cosh R)^2}{(\sinh R)^3} \\
&\qquad\qquad +5\frac{R^3\cosh(R-2X)\cosh R}{(\sinh R)^2} - 6\frac{R^3\cosh(R-2X)(\cosh R)^3}{(\sinh R)^4}\Bigg).
\end{aligned}
\tag{A.1.37}
$$

Taylor expansion of the driving force

The driving force F is obtained as

$$
\begin{aligned}
F = &-\left(\frac{\partial c}{\partial x}\bigg|_{x=X+0} + \frac{\partial c}{\partial x}\bigg|_{x=X-0}\right) \\
=&\frac{\sinh(R-2X)}{\sinh R} \\
&+\Bigg(\frac{\cosh R}{2\sinh R} - \frac{R}{2(\sinh R)^2} - \frac{\cosh(R-2X)}{2\sinh R} \\
&\qquad -\frac{1}{2}\left\{\frac{(R-2X)\sinh(R-2X)}{\sinh R} - \frac{R\cosh(R-2X)\cosh R}{(\sinh R)^2}\right\}\Bigg)\frac{dX}{dt} \\
&+\Bigg(-\frac{\cosh R}{8\sinh R} - \frac{R}{8(\sinh R)^2} + \frac{R^2\cosh R}{4(\sinh R)^3} + \frac{\cosh(R-2X)}{8\sinh R} \\
&\qquad - \frac{1}{8}\left\{\frac{(R-2X)\sinh(R-2X)}{\sinh R} - \frac{R\cosh(R-2X)\cosh R}{(\sinh R)^2}\right\} \\
&\qquad - \frac{1}{8}\Bigg\{\frac{(R-2X)^2\cosh(R-2X)}{\sinh R} - 2\frac{R(R-2X)\sinh(R-2X)\cosh R}{(\sinh R)^2} \\
&\qquad\qquad -\frac{R^2\cosh(R-2X)}{\sinh R} + 2\frac{R^2\cosh(R-2X)(\cosh R)^2}{(\sinh R)^3}\Bigg\}\Bigg)\frac{d^2X}{dt^2} \\
&+\Bigg(\frac{3}{8}\left\{\frac{(R-2X)\cosh(R-2X)}{\sinh R} - \frac{R\sinh(R-2X)\cosh R}{(\sinh R)^2}\right\}
\end{aligned}
$$

$$
\begin{aligned}
&+\frac{1}{8}\left\{\frac{(R-2X)^2\sinh(R-2X)}{\sinh R}-2\frac{R(R-2X)\cosh(R-2X)\cosh R}{(\sinh R)^2}\right.\\
&\qquad\left.\left.-\frac{R^2\sinh(R-2X)}{\sinh R}+2\frac{R^2\sinh(R-2X)(\cosh R)^2}{(\sinh R)^3}\right\}\right)\left(\frac{dX}{dt}\right)^2\\
&+\left(-\frac{\cosh R}{16\sinh R}-\frac{R}{16(\sinh R)^2}+\frac{R^2\cosh R}{4(\sinh R)^3}+\frac{R^3}{24(\sinh R)^2}-\frac{R^3(\cosh R)^2}{8(\sinh R)^4}\right.\\
&\qquad+\frac{1}{16}\frac{\cosh(R-2X)}{\sinh R}-\frac{1}{16}\left(\frac{(R-2X)\sinh(R-2X)}{\sinh R}-\frac{R\cosh(R-2X)\cosh R}{(\sinh R)^2}\right)\\
&\qquad-\frac{1}{8}\left(\frac{(R-2X)^2\cosh(R-2X)}{\sinh R}-2\frac{R(R-2X)\sinh(R-2X)\cosh R}{(\sinh R)^2}\right.\\
&\qquad\qquad\left.-\frac{R^2\cosh(R-2X)}{\sinh R}+2\frac{R^2\cosh(R-2X)(\cosh R)^2}{(\sinh R)^3}\right)\\
&\qquad-\frac{1}{48}\left(\frac{(R-2X)^3\sinh(R-2X)}{\sinh R}-3\frac{R(R-2X)^2\cosh(R-2X)\cosh R}{(\sinh R)^2}\right.\\
&\qquad\qquad-3\frac{R^2(R-2X)\sinh(R-2X)}{\sinh R}+6\frac{R^2(R-2X)\sinh(R-2X)(\cosh R)^2}{(\sinh R)^3}\\
&\qquad\qquad\left.\left.+5\frac{R^3\cosh(R-2X)\cosh R}{(\sinh R)^2}-6\frac{R^3\cosh(R-2X)(\cosh R)^3}{(\sinh R)^4}\right)\right)\left(\frac{dX}{dt}\right)^3.
\end{aligned}
\tag{A.1.38}
$$

To analyze the stability of the rest state, F is expanded around the fixed point $X=R/2$. We set $X=R/2+\delta X$ ($\delta X \ll R$) and obtain the force related to δX as

$$
\begin{aligned}
F=&-\frac{6\delta X+4(\delta X)^3}{3\sinh R}\\
&+\left(\frac{\cosh R}{2\sinh R}-\frac{R}{2(\sinh R)^2}-\frac{1+2(\delta X)^2}{2\sinh R}-\frac{1}{2}\left\{\frac{4(\delta X)^2}{\sinh R}-\frac{R(1+2(\delta X)^2)\cosh R}{(\sinh R)^2}\right\}\right)\dot{\delta X}\\
&+\left(\frac{R^2\cosh R}{4(\sinh R)^3}+\frac{1+2(\delta X)^2}{8\sinh R}-\frac{\cosh R}{8\sinh R}-\frac{R}{8(\sinh R)^2}-\frac{1}{8}\left\{\frac{4(\delta X)^2}{\sinh R}-\frac{R(1+2(\delta X)^2)\cosh R}{(\sinh R)^2}\right\}\right.\\
&\quad\left.-\frac{1}{8}\left\{\frac{4(\delta X)^2}{\sinh R}-\frac{8R(\delta X)^2\cosh R}{(\sinh R)^2}-\frac{R^2(1+2(\delta X)^2)}{\sinh R}+2\frac{R^2(1+2(\delta X)^2)(\cosh R)^2}{(\sinh R)^3}\right\}\right)\ddot{\delta X}\\
&+\left(\frac{3}{8}\left\{-\frac{2\delta X+8(\delta X)^3}{\sinh R}+\frac{R(6\delta X+4(\delta X)^3)\cosh R}{3(\sinh R)^2}\right\}\right.\\
&\quad+\frac{1}{8}\left\{-\frac{8(\delta X)^3}{\sinh R}+\frac{R(4\delta X+8(\delta X)^3)\cosh R}{(\sinh R)^2}\right.\\
&\qquad\left.\left.+\frac{R^2(6\delta X+4(\delta X)^3)}{3\sinh R}-\frac{R^2(12\delta X+8(\delta X)^3)(\cosh R)^2}{3(\sinh R)^3}\right\}\right)\left(\dot{\delta X}\right)^2\\
&+\left(-\frac{\cosh R}{16\sinh R}-\frac{R}{16(\sinh R)^2}+\frac{R^2\cosh R}{4(\sinh R)^3}+\frac{R^3}{24(\sinh R)^2}-\frac{R^3(\cosh R)^2}{8(\sinh R)^4}+\frac{1}{16}\frac{1+2(\delta X)^2}{\sinh R}\right.\\
&\quad-\frac{1}{16}\left(\frac{4(\delta X)^2}{\sinh R}-\frac{R(1+2(\delta X)^2)\cosh R}{(\sinh R)^2}\right)\\
&\quad-\frac{1}{8}\left(\frac{4(\delta X)^2}{\sinh R}-\frac{8R\,(\delta X)^2\cosh R}{(\sinh R)^2}-\frac{R^2(1+2(\delta X)^2)}{\sinh R}+\frac{R^2(2+4(\delta X)^2)(\cosh R)^2}{(\sinh R)^3}\right)
\end{aligned}
$$

$$- \frac{1}{48}\left(-\frac{12R(\delta X)^2\cosh R}{(\sinh R)^2} - \frac{12R^2(\delta X)^2}{\sinh R} + \frac{24R^2(\delta X)^2(\cosh R)^2}{(\sinh R)^3} \right.$$
$$\left. +5\frac{R^3(1+2(\delta X)^2)\cosh R}{(\sinh R)^2} - 6\frac{R^3(1+2(\delta X)^2)(\cosh R)^3}{(\sinh R)^4}\right)\Bigg)\left(\delta\dot{X}\right)^3. \quad \text{(A.1.39)}$$

By neglecting the higher-order terms of δX, $\delta\dot{X}$, and $\delta\ddot{X}$, we have

$$\begin{aligned}
F(\delta X, \delta\dot{X}, \delta\ddot{X}) =& -\frac{2}{\sinh R}\delta X - \frac{4}{3\sinh R}(\delta X)^3 + \frac{(\cosh R - 1)(\sinh R + R)}{2(\sinh R)^2}\delta\dot{X} \\
&+ \frac{1}{(\sinh R)^2}\left(-3\sinh R + R\cosh R\right)(\delta X)^2\delta\dot{X} \\
&- \frac{1}{8(\sinh R)^3}(\sinh R(\sinh R - R) + R^2(\cosh R - 1))(\cosh R - 1)\delta\ddot{X} \\
&- \frac{1}{4(\sinh R)^3}\left\{\sinh R(3\sinh R - 5R\cosh R) + R^2(2 + (\sinh R)^2)\right\}\delta X\left(\delta\dot{X}\right)^2 \\
&- \frac{1}{48(\sinh R)^4}\left((2 - \cosh R)R^3 + 6R^2\sinh R\right. \\
&\qquad \left. +3(\cosh R + 1)(\sinh R - R)\right)(\cosh R - 1)^2\left(\delta\dot{X}\right)^3,
\end{aligned} \quad \text{(A.1.40)}$$

which is Eq. (2.2.20).

A.1.2 Dependence of the coefficients in Eq. (2.2.20) on the water channel length R

The coefficients of δX, $\delta\dot{X}$, and $\delta\ddot{X}$ and their cross terms in the driving force in Eq. (2.2.20) depends on R. Here we show the dependence of A, B, C, E, G, H, and I on the water channel length R in Fig. A.1.1.

A.1.3 Derivation of Eq. (2.2.22)

The dimensionless form of the equation for concentration field is given by

$$\frac{\partial c(x,t)}{\partial t} = \frac{\partial^2 c(x,t)}{\partial x^2} - c(x,t) + f(x,t), \quad \text{(A.1.41)}$$

Here, $f(x,t)$ is the source term. The Green's function $g(x,t)$, which is the concentration field with $f(x,t) = \delta(x)\delta(t)$, is considered. By introducing the Green's function and the source term in wavenumber space,

$$g(x,t) = \frac{1}{(2\pi)^2}\int_{-\infty}^{\infty}\int_{-\infty}^{\infty}\tilde{\tilde{g}}(k,\omega)e^{ikx+i\omega t}dkd\omega, \quad \text{(A.1.42)}$$
$$f(x,t) = \frac{1}{(2\pi)^2}\int_{-\infty}^{\infty}\int_{-\infty}^{\infty}e^{ikx+i\omega t}dkd\omega, \quad \text{(A.1.43)}$$

and substituting them into Eq. (A.1.41), we have the equation for the Green's function in wavenumber space, $\tilde{\tilde{g}}$, as follows:

$$\left(i\omega - (ik)^2 + 1\right)\tilde{\tilde{g}}(k,\omega) = 1. \quad \text{(A.1.44)}$$

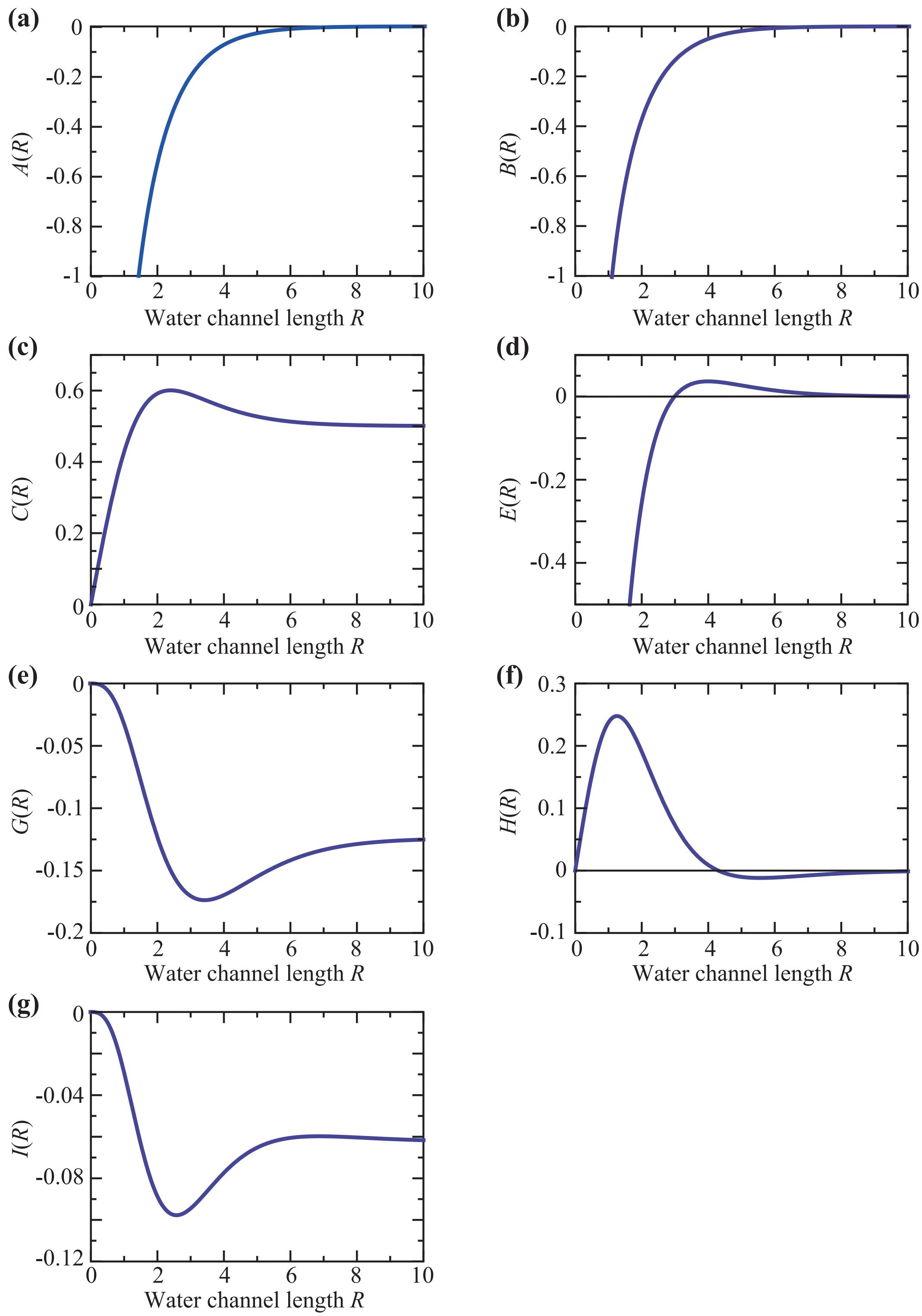

Figure A.1.1: Plots of the coefficients $A(R)$, $B(R)$, $C(R)$, $E(R)$, $G(R)$, $H(R)$, and $I(R)$ against the water channel length R.

Thus we have

$$\tilde{\tilde{g}}(k,\omega) = \frac{1}{i\omega + k^2 + 1}. \tag{A.1.45}$$

Then $\tilde{\tilde{g}}(k,\omega)$ is transformed with regard to ω as follows.

$$\begin{aligned}\frac{1}{2\pi}\int_{-\infty}^{\infty}\tilde{\tilde{g}}(k,\omega)e^{i\omega t}d\omega =& \frac{1}{2\pi i}\int_{-\infty}^{\infty}\frac{1}{\omega - i(k^2+1)}e^{i\omega t}d\omega \\ =& e^{-(k^2+1)t}\Theta(t) \\ \equiv& \tilde{g}(k,t),\end{aligned} \tag{A.1.46}$$

where $\Theta(t)$ is the Heaviside's step function. It is noted that the function $\tilde{g}(k,t)$ satisfies the following equations:

$$g(x,t) = \frac{1}{2\pi}\int_{-\infty}^{\infty}\tilde{g}(k,t)e^{ikx}dk, \tag{A.1.47}$$

$$\left(\frac{\partial}{\partial t} + k^2 + 1\right)\tilde{g}(k,t) = \delta(t). \tag{A.1.48}$$

Here we define $c(x,t)$ as the concentration field when the source term in Eq. (A.1.41) is $f = \delta(x - X(t))$. The concentration field and source term in wavenumber space are expressed as

$$\tilde{c}(k,t) \equiv \int_{-\infty}^{\infty} c(x,t)e^{-ikx}dx, \tag{A.1.49}$$

$$\int_{-\infty}^{\infty}\delta(x - X(t))e^{-ikx} = e^{-ikX(t)}dx. \tag{A.1.50}$$

Using the Green's function $\tilde{g}(k,t)$, $\tilde{c}(k,t)$ is expressed as in the following integral.

$$\tilde{c}(k,t) = \int_{-\infty}^{\infty} e^{-ikX(t')}\tilde{g}(k,t-t')dt'. \tag{A.1.51}$$

Using partial integration, the integral form in Eq. (A.1.51) is expanded as follows:

$$\begin{aligned}\tilde{c}(k,t) =& \frac{e^{-ikX(t)}}{k^2+1} + \frac{ik\dot{X}(t)e^{-ikX(t)}}{(k^2+1)^2} - \frac{(ik\ddot{X}(t) + k^2(\dot{X}(t))^2)e^{-ikX(t)}}{(k^2+1)^3} \\ &- \frac{ik^3(\dot{X}(t'))^3e^{-ikX(t')}}{(k^2+1)^4} + (\text{higher order terms}).\end{aligned} \tag{A.1.52}$$

Since the concentration field in real space is expressed as

$$c(x,t) = \frac{1}{2\pi}\int_{-\infty}^{\infty}\tilde{c}(k,t)e^{ikx}dk, \tag{A.1.53}$$

the gradient of the concentration field is obtained by integrating the following form:

$$\begin{aligned}\frac{\partial}{\partial x}c(x,t) =& \frac{i}{2\pi}\int_{-\infty}^{\infty}k\tilde{c}(k,t)e^{ikx}dk \\ =& \frac{i}{2\pi}\int_{-\infty}^{\infty}\left\{\frac{k}{k^2+1} + \frac{ik^2\dot{X}(t)}{(k^2+1)^2} - \frac{ik^2\ddot{X}(t) + k^3(\dot{X}(t))^2}{(k^2+1)^3} - \frac{ik^4(\dot{X}(t))^3}{(k^2+1)^4}\right\}e^{ik(x-X(t))}dk.\end{aligned} \tag{A.1.54}$$

Then each term is calculated. The first term, which corresponds the gradient of the steady state, is integrated as follows:

$$\begin{aligned}\frac{i}{2\pi}\int_{-\infty}^{\infty}\frac{k}{k^2+1}e^{ik(x-X(t))}dk =&\frac{i}{2\pi}\int_{-\infty}^{\infty}\frac{1}{2}\left\{\frac{1}{k+i}+\frac{1}{k-i}\right\}e^{ik(x-X(t))}dk\\ =&\frac{1}{2}\begin{cases}-e^{-(x-X(t))}, & x-X(t)>0,\\ e^{(x-X(t))}, & x-X(t)<0.\end{cases}\end{aligned}\tag{A.1.55}$$

From the definition of the driving force, the driving force originating from the concentration field of the steady state is given by

$$-\left(\left.\frac{\partial c}{\partial x}\right|_{X(t)+0}+\left.\frac{\partial c}{\partial x}\right|_{X(t)-0}\right)=0.\tag{A.1.56}$$

The second term is integrated as follows:

$$\begin{aligned}&-\frac{1}{2\pi}\int_{-\infty}^{\infty}\frac{k^2}{(k^2+1)^2}\dot{X}(t)e^{ik(x-X(t))}dk\\ &\quad=-\frac{1}{2\pi}\int_{-\infty}^{\infty}\left\{\frac{1}{4i}\left(\frac{1}{k-i}-\frac{1}{k+i}\right)+\frac{1}{4}\left(\frac{1}{(k-i)^2}+\frac{1}{(k+i)^2}\right)\right\}\dot{X}(t)e^{ik(x-X(t))}dk\\ &\quad=\frac{1}{4}\begin{cases}-\dot{X}(t)e^{-(x-X(t))}+\dot{X}(t)(x-X(t))e^{-(x-X(t))}, & x-X(t)>0,\\ -\dot{X}(t)e^{x-X(t)}-\dot{X}(t)(x-X(t))e^{(x-X(t))}, & x-X(t)<0\end{cases}\\ &\quad=-\frac{1}{4}\dot{X}(t)e^{-|x-X(t)|}+\dot{X}(t)|x-X(t)|e^{-|x-X(t)|}.\end{aligned}\tag{A.1.57}$$

From the definition of the driving force, the driving force originating from the second term is given by

$$-\left(\left.\frac{\partial c}{\partial x}\right|_{X(t)+0}+\left.\frac{\partial c}{\partial x}\right|_{X(t)-0}\right)=\frac{1}{2}\dot{X}(t).\tag{A.1.58}$$

The third term is integrated as follows:

$$\begin{aligned}&\frac{1}{2\pi}\int_{-\infty}^{\infty}\frac{k^2}{(k^2+1)^3}\ddot{X}(t)e^{ik(x-X(t))}dk\\ &\quad=\frac{1}{2\pi}\int_{-\infty}^{\infty}\left\{\frac{1}{16i}\left(\frac{1}{k-i}-\frac{1}{k+i}\right)\right.\\ &\qquad\left.-\frac{1}{16}\left(\frac{1}{(k-i)^2}+\frac{1}{(k+i)^2}\right)+\frac{1}{8i}\left(\frac{1}{(k-i)^3}-\frac{1}{(k+i)^3}\right)\right\}\ddot{X}(t)e^{ik(x-X(t))}dk\\ &\quad=\frac{1}{8}\begin{cases}\frac{1}{2}\ddot{X}(t)e^{-(x-X(t))}+\frac{1}{2}\ddot{X}(t)(x-X(t))e^{-(x-X(t))}-\frac{1}{2}\ddot{X}(t)(x-X(t))^2e^{-(x-X(t))},\\ \hfill x-X(t)>0,\\ \frac{1}{2}\ddot{X}(t)e^{(x-X(t))}-\frac{1}{2}\ddot{X}(t)(x-X(t))e^{(x-X(t))}-\frac{1}{2}\ddot{X}(t)(x-X(t))^2e^{(x-X(t))},\\ \hfill x-X(t)<0\end{cases}\\ &\quad=\frac{1}{16}\ddot{X}(t)e^{-|x-X(t)|}+\frac{1}{16}\ddot{X}(t)|x-X(t)|e^{-|x-X(t)|}-\frac{1}{16}\ddot{X}(t)(x-X(t))^2e^{-|x-X(t)|}.\end{aligned}\tag{A.1.59}$$

From the definition of the driving force, the driving force originating from the third term is given by

$$-\left(\frac{\partial c}{\partial x}\bigg|_{X(t)+0}+\frac{\partial c}{\partial x}\bigg|_{X(t)-0}\right)=-\frac{1}{8}\ddot{X}(t). \tag{A.1.60}$$

The fourth term is integrated as follows:

$$\begin{aligned}
&-\frac{i}{2\pi}\int_{-\infty}^{\infty}\frac{k^3}{(k^2+1)^3}(\dot{X}(t))^2e^{ik(x-X(t))}dk\\
&\quad=-\frac{i}{2\pi}\int_{-\infty}^{\infty}\left\{\frac{3}{16i}\left(\frac{1}{(k-i)^2}-\frac{1}{(k+i)^2}\right)+\frac{1}{8}\left(\frac{1}{(k-i)^3}+\frac{1}{(k+i)^3}\right)\right\}(\dot{X}(t))^2e^{ik(x-X(t))}dk\\
&\quad=\frac{1}{16}\begin{cases}3(\dot{X}(t))^2(x-X(t))e^{-(x-X(t))}-(\dot{X}(t))^2(x-X(t))^2e^{-(x-X(t))}, & x-X(t)>0,\\ 3(\dot{X}(t))^2(x-X(t))e^{(x-X(t))}+(\dot{X}(t))^2(x-X(t))^2e^{(x-X(t))}, & x-X(t)<0.\end{cases}
\end{aligned} \tag{A.1.61}$$

From the definition of the driving force, the driving force originating from the fourth term is given by

$$-\left(\frac{\partial c}{\partial x}\bigg|_{X(t)+0}+\frac{\partial c}{\partial x}\bigg|_{X(t)-0}\right)=0. \tag{A.1.62}$$

The fifth term is integrated as follows:

$$\begin{aligned}
&\frac{1}{2\pi}\int_{-\infty}^{\infty}\frac{k^3}{(k^2+1)^3}(\dot{X}(t))^3e^{ik(x-X(t))}dk\\
&\quad=\frac{1}{2\pi}\int_{-\infty}^{\infty}\left\{\frac{1}{32i}\left(\frac{1}{k-i}-\frac{1}{k+i}\right)-\frac{1}{32}\left(\frac{1}{(k-i)^2}+\frac{1}{(k+i)^2}\right)\right.\\
&\qquad\left.+\frac{1}{8i}\left(\frac{1}{(k-i)^3}-\frac{1}{(k+i)^3}\right)-\frac{1}{16}\left(\frac{1}{(k-i)^4}+\frac{1}{(k+i)^4}\right)\right\}(\dot{X}(t))^3e^{ik(x-X(t))}dk\\
&\quad=\frac{1}{8}\begin{cases}\frac{1}{4}(\dot{X}(t))^3e^{-(x-X(t))}+\frac{1}{4}(\dot{X}(t))^3(x-X(t))e^{-(x-X(t))}\\ -\frac{1}{2}(\dot{X}(t))^3(x-X(t))^2e^{-(x-X(t))}-\frac{1}{12}(\dot{X}(t))^3(x-X(t))^3e^{-(x-X(t))}, & x-X(t)>0\\ \frac{1}{4}(\dot{X}(t))^3e^{-(x-X(t))}-\frac{1}{4}(\dot{X}(t))^3(x-X(t))e^{-(x-X(t))}\\ -\frac{1}{2}(\dot{X}(t))^3(x-X(t))^2e^{-(x-X(t))}+\frac{1}{12}(\dot{X}(t))^3(x-X(t))^3e^{-(x-X(t))}, & x-X(t)<0\end{cases}\\
&\quad=\frac{1}{32}(\dot{X}(t))^3e^{-(x-X(t))}+\frac{1}{32}(\dot{X}(t))^3|x-X(t)|e^{-(x-X(t))}\\
&\qquad-\frac{1}{16}(\dot{X}(t))^3(x-X(t))^2e^{-(x-X(t))}-\frac{1}{96}(\dot{X}(t))^3|x-X(t)|^3e^{-(x-X(t))}.
\end{aligned} \tag{A.1.63}$$

From the definition of the driving force, the driving force originating from the fifth term is given by

$$-\left(\frac{\partial c}{\partial x}\bigg|_{X(t)+0}+\frac{\partial c}{\partial x}\bigg|_{X(t)-0}\right)=-\frac{1}{16}(\dot{X}(t))^3. \tag{A.1.64}$$

From Eqs. (A.1.56), (A.1.58), (A.1.60), (A.1.62), and (A.1.64), the driving force F is given by

$$F=-\left(\frac{\partial c}{\partial x}\bigg|_{X(t)+0}+\frac{\partial c}{\partial x}\bigg|_{X(t)-0}\right)=\frac{1}{2}\dot{X}(t)-\frac{1}{8}\ddot{X}(t)-\frac{1}{16}(\dot{X}(t))^3, \tag{A.1.65}$$

which is the same as Eq. (2.2.22).

A.2 Supplementary information for Section 2.3

A.2.1 Details in numerical calculation

To make phase diagrams shown in Fig. 2.3.7, we calculated the time evolution with four initial conditions for each parameter set and unified the results. We used several initial conditions since several types of motion are stable (typically two types of motion can be bistable) . The initial conditions are summarized in Table A.1, and the phase diagram obtained by calculating each initial condition is shown in Fig. A.2.1.

Table A.1: Initial conditions for x_1, x_2, v_1, and v_2. The variables R_o, R_r, and K in the table are set to be $R_\mathrm{o} = \sqrt{|2\mu/(8A+\epsilon)|}$, $R_\mathrm{r} = \sqrt{|2\mu/(4B+\epsilon)|}$, and $K = \sqrt{(n+j)/(k+\epsilon)}$, respectively. Here we set $A = (3k+n+j)/8$, $B = (k+n)/4$, $\mu = b/2$, $\delta = 0.01$, and $\epsilon = 0.005$. Reproduced from Ref. [37].

	x_1	x_2	v_1	v_2
(i)	$R_\mathrm{r}+\delta$	δ	0	R_r
(ii)	R_o	0	δ	2δ
(iii)	$50R_\mathrm{o}/b$	$50R_\mathrm{o}/b+\delta$	$50KR_\mathrm{o}$	$50KR_\mathrm{o}+\delta$
(iv)	δ	0	$50R_\mathrm{o}$	$50R_\mathrm{o}+\delta$

A.3 Supplementary information for Section 2.4

A.3.1 Hankel transform and discrete Hankel transform

In this subsection, Hankel transform and "discrete Hankel transform" are introduced.

Hankel transform

Here we consider a function $f(r)$ whose domain is $r \in (0, \infty)$. The Hankel transform of $f(r)$ is given by

$$f(r) = \int_0^\infty kF(k)\mathcal{J}_n(kr)dk, \tag{A.3.1}$$

where the $F(k)$ is a function in wavenumber space, which is given by

$$F(k) = \int_0^\infty rf(r)\mathcal{J}_n(kr)dr. \tag{A.3.2}$$

The function $\mathcal{J}_n(r)$ is the first-kind Bessel function of n-th order.

Prepration for the calculation of the norm of Bessel function

The Bessel differential equation is given as

$$\left(\frac{d^2}{dr^2} + \frac{1}{r}\frac{d}{dr} + \left(1 - \frac{\nu^2}{r^2}\right)\right)\mathcal{J}_\nu(r) = 0. \tag{A.3.3}$$

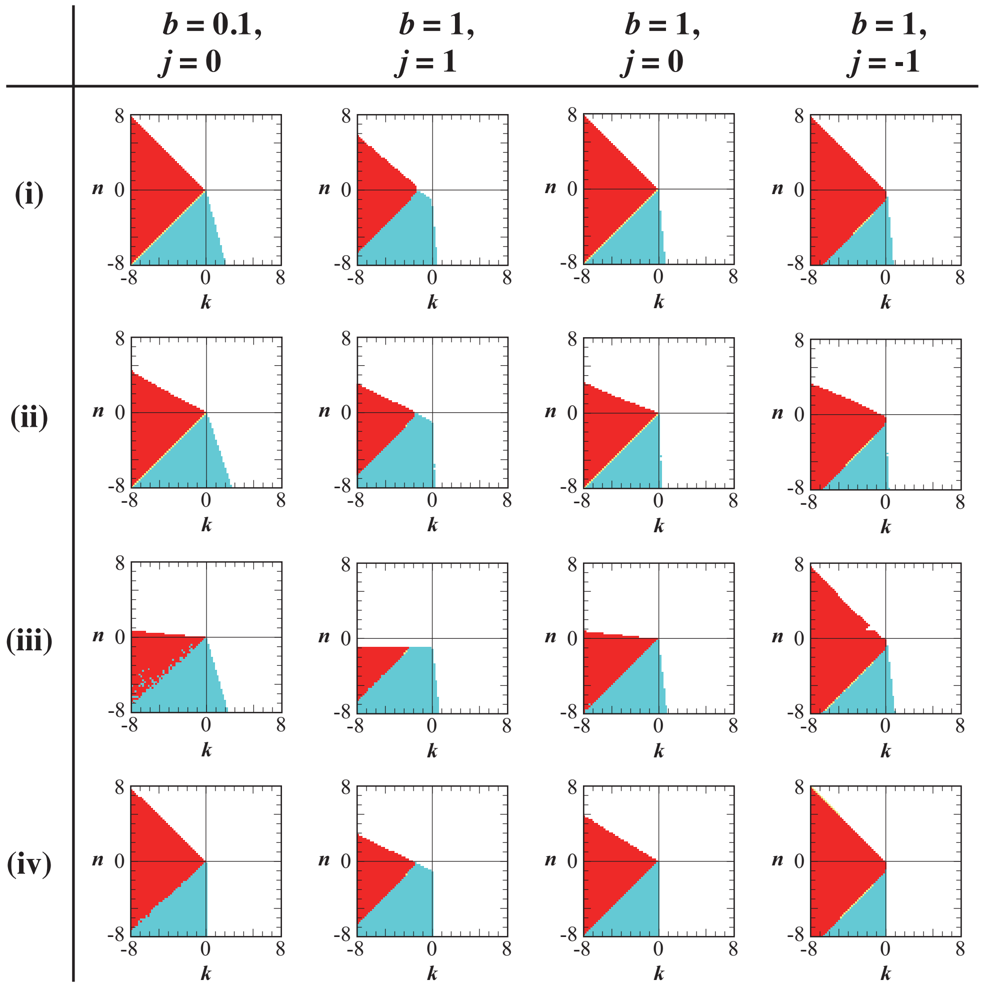

Figure A.2.1: Phase diagrams obtained by the numerical calculation with different initial conditions. The Roman numerals (i)-(iv) in the figure correspond to the initial conditions (i)-(iv) in Table A.2.1. The parameters are set to be $c = h = p = 0$. The red, blue white, and yellow regions are corresponding to the parameter regions where rotation, oscillation, divergence, and undeterminable motion was observed. Here we clarified trajectories sufficiently distant from the origin with time as divergence. Reproduced from Ref. [37].

By replacing r with λr, we have

$$\left(\frac{d^2}{dr^2}+\frac{1}{r}\frac{d}{dr}+\left(\lambda^2-\frac{\nu^2}{r^2}\right)\right)\mathcal{J}_\nu(\lambda r)=0. \tag{A.3.4}$$

Equation (A.3.4) is transformed in the following form:

$$\frac{d}{dr}\left(r\frac{d\mathcal{J}_\nu(\lambda r)}{dr}\right)-\frac{\nu^2}{r}\mathcal{J}_\nu(\lambda r)+\lambda^2 r\mathcal{J}_\nu(\lambda r)=0. \tag{A.3.5}$$

Here we consider the difference between the following equations:

$$\begin{cases}\mathcal{J}_\nu(\lambda_n r)\left[\dfrac{d}{dr}\left(r\dfrac{d\mathcal{J}_\nu(\lambda_m r)}{dr}\right)-\dfrac{\nu^2}{r}\mathcal{J}_\nu(\lambda_m r)+{\lambda_m}^2 r\mathcal{J}_\nu(\lambda_m r)\right]=0, & \text{(A.3.6a)}\\ \mathcal{J}_\nu(\lambda_m r)\left[\dfrac{d}{dr}\left(r\dfrac{d\mathcal{J}_\nu(\lambda_n r)}{dr}\right)-\dfrac{\nu^2}{r}\mathcal{J}_\nu(\lambda_n r)+{\lambda_n}^2 r\mathcal{J}_\nu(\lambda_n r)\right]=0, & \text{(A.3.6b)}\end{cases}$$

where these equations are obtained by multiplying $\mathcal{J}_\nu(\lambda_n r)$ and $\mathcal{J}_\nu(\lambda_m r)$ with (A.3.5) for $\lambda=\lambda_m$ and $\lambda=\lambda_n$, respectively. We have

$$\mathcal{J}_\nu(\lambda_n r)\frac{d}{dr}\left(r\frac{d\mathcal{J}_\nu(\lambda_m r)}{dr}\right)-\mathcal{J}_\nu(\lambda_m r)\frac{d}{dr}\left(r\frac{d\mathcal{J}_\nu(\lambda_n r)}{dr}\right)+({\lambda_m}^2-{\lambda_n}^2)r\mathcal{J}_\nu(\lambda_m r)\mathcal{J}_\nu(\lambda_n r)=0. \tag{A.3.7}$$

Using Eq. (A.3.7), we have

$$\begin{aligned}&-({\lambda_m}^2-{\lambda_n}^2)\int r\mathcal{J}_\nu(\lambda_m r)\mathcal{J}_\nu(\lambda_n r)dr\\ &=\int\left\{\mathcal{J}_\nu(\lambda_n r)\frac{d}{dr}\left(r\frac{d\mathcal{J}_\nu(\lambda_m r)}{dr}\right)-\mathcal{J}_\nu(\lambda_m r)\frac{d}{dr}\left(r\frac{d\mathcal{J}_\nu(\lambda_n r)}{dr}\right)\right\}dr\\ &=\left[\mathcal{J}_\nu(\lambda_n r)\left(r\frac{d\mathcal{J}_\nu(\lambda_m r)}{dr}\right)-\mathcal{J}_\nu(\lambda_m r)\left(r\frac{d\mathcal{J}_\nu(\lambda_n r)}{dr}\right)\right].\end{aligned} \tag{A.3.8}$$

Bases satisfying the Dirichlet condition

From Eq. (A.3.8), we have

$$\begin{aligned}&-({\lambda_m}^2-{\lambda_n}^2)\int_0^R r\mathcal{J}_\nu(\lambda_m r)\mathcal{J}_\nu(\lambda_n r)dr\\ &=\left[\mathcal{J}_\nu(\lambda_n r)\left(r\frac{d\mathcal{J}_\nu(\lambda_m r)}{dr}\right)-\mathcal{J}_\nu(\lambda_m r)\left(r\frac{d\mathcal{J}_\nu(\lambda_n r)}{dr}\right)\right]_0^R,\end{aligned} \tag{A.3.9}$$

Here we set $\lambda_n\equiv\xi_n/R$. Since $\mathcal{J}_\nu(\lambda_m r)=0$ holds considering the Dirichlet condition, we have

$$({\lambda_m}^2-{\lambda_n}^2)\int_0^R r\mathcal{J}_\nu(\lambda_m r)\mathcal{J}_\nu(\lambda_n r)dr=0, \tag{A.3.10}$$

where $\{\xi_n\}$ is the set of points which satisfy $\mathcal{J}_\nu(\xi_n)=0$ and $\xi_n>\xi_m$ for $n>m$. For $m\neq n$, we have

$$\int_0^R r\mathcal{J}_\nu(\lambda_m r)\mathcal{J}_\nu(\lambda_n r)dr=0, \tag{A.3.11}$$

and thus $\mathcal{J}_\nu(\lambda_m r)$ and $\mathcal{J}_\nu(\lambda_n r)$ whose domains are $[0, R]$ are orthogonal to each other for $m \neq n$.

To obtain the norm of $\mathcal{J}_\nu(\lambda_n r)$, we calculate the following integration:

$$\begin{aligned}
&\int_0^R r\mathcal{J}_\nu(\lambda_n r)\mathcal{J}_\nu(\lambda_n r)dr \\
&= \lim_{\lambda\to\lambda_n} \int_0^R r\mathcal{J}_\nu(\lambda r)\mathcal{J}_\nu(\lambda_n r)dr \\
&= -\lim_{\lambda\to\lambda_n} \frac{1}{\lambda^2 - {\lambda_n}^2} \left[\mathcal{J}_\nu(\lambda_n r)\left(r\frac{d\mathcal{J}_\nu(\lambda r)}{dr}\right) - \mathcal{J}_\nu(\lambda r)\left(r\frac{d\mathcal{J}_\nu(\lambda_n r)}{dr}\right)\right]_0^R \\
&= -\lim_{\lambda\to\lambda_n} \frac{R\left(\lambda\mathcal{J}_\nu(\lambda_n R)\mathcal{J}'_\nu(\lambda R) - \lambda_n\mathcal{J}_\nu(\lambda R)\mathcal{J}'_\nu(\lambda_n R)\right)}{\lambda^2 - {\lambda_n}^2}.
\end{aligned} \tag{A.3.12}$$

By applying L'Hôpital's rule, we have

$$\begin{aligned}
&\int_0^R r\mathcal{J}_\nu(\lambda_n r)\mathcal{J}_\nu(\lambda_n r)dr \\
&= -\lim_{\lambda\to\lambda_n} \frac{R\left(\mathcal{J}_\nu(\lambda_n R)\mathcal{J}'_\nu(\lambda R) + \lambda R\mathcal{J}_\nu(\lambda_n R)\mathcal{J}''_\nu(\lambda R) - \lambda_n R\mathcal{J}'_\nu(\lambda R)\mathcal{J}'_\nu(\lambda_n R)\right)}{2\lambda} \\
&= \lim_{\lambda\to\lambda_n} \frac{R^2}{2}\left(\frac{\lambda_n}{\lambda}\mathcal{J}'_\nu(\lambda R)\mathcal{J}'_\nu(\lambda_n R) - \left(\frac{1}{\lambda R}\mathcal{J}'_\nu(\lambda R) + \mathcal{J}''_\nu(\lambda R)\right)\mathcal{J}_\nu(\lambda_n R)\right) \\
&= \frac{R^2}{2}\left(\mathcal{J}'_\nu(\lambda_n R)\mathcal{J}'_\nu(\lambda_n R) - \left(\frac{1}{\lambda_n R}\mathcal{J}'_\nu(\lambda_n R) + \mathcal{J}''_\nu(\lambda_n R)\right)\mathcal{J}_\nu(\lambda_n R)\right).
\end{aligned} \tag{A.3.13}$$

Since $\mathcal{J}_\nu(\lambda_n R) = 0$ holds considering the Dirichlet condition, we have

$$\int_0^R r\mathcal{J}_\nu(\lambda_n r)\mathcal{J}_\nu(\lambda_n r)dr = \frac{R^2}{2}\left(\mathcal{J}'_\nu(\lambda_n R)\right)^2 = \frac{R^2}{2}\left(\mathcal{J}'_\nu(\xi_n)\right)^2 \equiv \frac{1}{b_{\nu n}}. \tag{A.3.14}$$

Thus the functions $\left\{\sqrt{b_{\nu n}}\mathcal{J}_\nu(\lambda_n r)\right\}$ are the bases of the function space for $[0, R]$. The function $f(r)$ which satisfy the Dirichlet condition at $r = R$ is given by

$$f(r) = \sum_{n\in\mathbb{N}} b_{\nu n} f_n \lambda_n \mathcal{J}_\nu(\lambda_n r), \tag{A.3.15}$$

where

$$f_n \equiv \int_0^R f(r)\mathcal{J}_\nu(\lambda_n r) r dr. \tag{A.3.16}$$

The typical examples of the bases which satisfy the Dirichlet condition are plotted in Fig. A.3.1(a).

Bases satisfying the Neumann condition

From Eq. (A.3.8), we have

$$\begin{aligned}
&-\left({\lambda_m}^2 - {\lambda_n}^2\right)\int_0^R r\mathcal{J}_\nu(\lambda_m r)\mathcal{J}_\nu(\lambda_n r)dr \\
&\qquad = \left[\mathcal{J}_\nu(\lambda_n r)\left(r\frac{d\mathcal{J}_\nu(\lambda_m r)}{dr}\right) - \mathcal{J}_\nu(\lambda_m r)\left(r\frac{d\mathcal{J}_\nu(\lambda_n r)}{dr}\right)\right]_0^R.
\end{aligned} \tag{A.3.17}$$

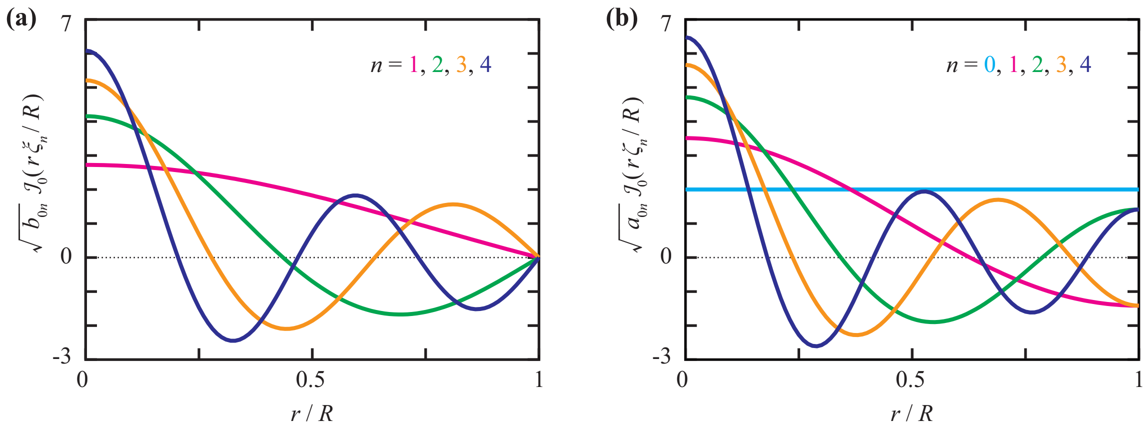

Figure A.3.1: Typical examples of the bases which satisfy (a) Dirichlet and (b) Neumann conditions.

Here we set $\lambda_n \equiv \zeta_n/R$. Since $(\partial\mathcal{J}_\nu(\lambda_m r))/(\partial r) = 0$ holds considering the Neumann condition, we have

$$(\lambda_m{}^2 - \lambda_n{}^2)\int_0^R r\mathcal{J}_\nu(\lambda_m r)\mathcal{J}_\nu(\lambda_n r)dr = 0, \tag{A.3.18}$$

where $\{\zeta_n\}$ is the set of points which satisfy $\mathcal{J}'_\nu(\zeta_n) = 0$ and $\zeta_n > \zeta_m$ for $n > m$. Here $\mathcal{J}'_\nu(r)$ means $(\partial\mathcal{J}_\nu(r))/(\partial r)$. For $m \neq n$, we have

$$\int_0^R r\mathcal{J}_\nu(\lambda_m r)\mathcal{J}_\nu(\lambda_n r)dr = 0, \tag{A.3.19}$$

and thus $\mathcal{J}_\nu(\lambda_m r)$ and $\mathcal{J}_\nu(\lambda_n r)$ whose domains are $[0, R]$ are orthogonal to each other for $m \neq n$.

To obtain the norm of $\mathcal{J}_\nu(\lambda_n r)$, we calculate the following integration:

$$\int_0^R r\mathcal{J}_\nu(\lambda_n r)\mathcal{J}_\nu(\lambda_n r)dr. \tag{A.3.20}$$

From Eq. (A.3.13) and $\mathcal{J}'_\nu(\lambda_n R) = 0$ from the Neumann condition, we have

$$\int_0^R r\mathcal{J}_\nu(\lambda_n r)\mathcal{J}_\nu(\lambda_n r)dr = -\frac{R^2}{2}\mathcal{J}''_\nu(\lambda_n R)\mathcal{J}_\nu(\lambda_n R) = -\frac{R^2}{2}\mathcal{J}''_\nu(\zeta_n)\mathcal{J}_\nu(\zeta_n) \equiv \frac{1}{a_{\nu n}}. \tag{A.3.21}$$

Thus the functions $\{\sqrt{a_{\nu n}}\mathcal{J}_\nu(\lambda_n r)\}$ are the bases of the function space for $[0, R]$. The function $f(r)$ which satisfy the Neumann condition at $r = R$ is given by

$$f(r) = \sum_{n\in\mathbb{N}} a_{\nu n} f_n \lambda_n \mathcal{J}_\nu(\lambda_n r), \tag{A.3.22}$$

where

$$f_n \equiv \int_0^R f(r)\mathcal{J}_\nu(\lambda_n r)rdr. \tag{A.3.23}$$

The typical examples of the bases which satisfy the Neumann condition are plotted in Fig. A.3.1(b).

A.3.2 Calculation of the driving force in the two-dimensional infinite system

The concentration field and source term are decomposed by Hankel and Fourier transform in r- and θ-directions, respectively.

$$c(r,\theta;\rho,\phi) = \frac{1}{2\pi}\sum_{m=-\infty}^{\infty}\int_0^{\infty} c_m(k)\mathcal{J}_{|m|}(kr)e^{im\theta}kdk, \tag{A.3.24}$$

$$f(r,\theta;\rho,\phi) =\frac{1}{2\pi}\sum_{m=-\infty}^{\infty}\int_0^{\infty} \mathcal{J}_{|m|}(k\rho(t))\mathcal{J}_{|m|}(kr)e^{im(\theta-\phi(t))}kdk. \tag{A.3.25}$$

By substituting Eqs. (A.3.24) and (A.3.25) into Eq. (2.4.18), we have

$$\frac{\partial c_m(k)}{\partial t} = -(k^2+1)c_m(k) + \mathcal{J}_{|m|}(k\rho(t))e^{-im\phi(t)}. \tag{A.3.26}$$

First, we derive the Green's function $g_m(k,t)$, which satisfies the following equation:

$$\frac{\partial g_m(k)}{\partial t} = -(k^2+1)g_m(k) + \delta(t). \tag{A.3.27}$$

The solution of Eq. (A.3.27) is obtained as

$$g_m(k) = \left\{\begin{array}{l} e^{-(k^2+1)t} \\ 0 \end{array}\right. = e^{-(k^2+1)t}\Theta(t), \tag{A.3.28}$$

where $\Theta(t)$ is the Heaviside's step function. By using the Green's function $g_m(k,t)$, the concentration field $c_m(k,t)$ is expressed as

$$\begin{aligned} c_m(k,t) =& \int_{-\infty}^{\infty} \mathcal{J}_{|m|}(k\rho(t'))e^{-im\phi(t')}g_m(k,t-t')dt' \\ =& \int_{-\infty}^{t} \mathcal{J}_{|m|}(k\rho(t'))e^{-im\phi(t')}e^{-(k^2+1)(t-t')}dt' \\ =& e^{-(k^2+1)t}\int_{-\infty}^{t} \mathcal{J}_{|m|}(k\rho(t'))e^{-im\phi(t')}e^{(k^2+1)t'}dt' \equiv e^{-(k^2+1)t}I. \end{aligned} \tag{A.3.29}$$

The integral I is expanded using partial integration.

$$\begin{aligned} I =& \frac{1}{A}\mathcal{J}_{|m|}(k\rho(t))e^{-im\phi(t)} + \frac{1}{A^2}\left\{-k\dot{\rho}(t)\mathcal{J}'_{|m|}(k\rho(t)) + im\dot{\phi}(t)\mathcal{J}_{|m|}(k\rho(t))\right\}e^{-im\phi(t)} \\ &+ \frac{1}{A^3}\Big\{k\ddot{\rho}(t)\mathcal{J}'_{|m|}(k\rho(t)) + k^2(\dot{\rho}(t))^2\mathcal{J}''_{|m|}(k\rho(t)) \\ &\qquad -2ikm\dot{\rho}(t)\dot{\phi}(t)\mathcal{J}'_{|m|}(k\rho(t)) - im\ddot{\phi}(t)\mathcal{J}_{|m|}(k\rho(t)) - m^2(\dot{\phi}(t))^2\mathcal{J}_{|m|}(k_{mn}\rho(t))\Big\}e^{-im\phi(t)} \\ &+ \frac{1}{A^4}\Big\{-k^3(\dot{\rho}(t))^3\mathcal{J}'''_{|m|}(k\rho(t)) + 3ik^2m(\dot{\rho}(t))^2\dot{\phi}(t)\mathcal{J}''_{|m|}(k\rho(t)) \\ &\qquad + 3km^2\dot{\rho}(t)(\dot{\phi}(t))^2\mathcal{J}'_{|m|}(k\rho(t)) - im^3(\dot{\phi}(t))^3\mathcal{J}_{|m|}(k\rho(t)) \\ &\qquad + k\dddot{\rho}(t)\mathcal{J}'_{|m|}(k\rho(t)) + 3k^2\dot{\rho}\ddot{\rho}\mathcal{J}''_{|m|}(k\rho(t)) - 3ikm\ddot{\rho}\dot{\phi}\mathcal{J}'_{|m|}(k\rho(t)) \\ &\qquad -3ikm\dot{\rho}\ddot{\phi}\mathcal{J}'_{|m|}(k\rho(t)) - im\dddot{\rho}\mathcal{J}'_{|m|}(k\rho(t)) - 3m^2\dot{\phi}\ddot{\phi}\mathcal{J}'_{|m|}(k\rho(t))\Big\}e^{-im\phi(t)} \\ &+ \cdots . \end{aligned} \tag{A.3.30}$$

Here we denote k^2+1 as A. Thus we have

$$
\begin{aligned}
&c(r,\theta;\rho,\phi)\\
&\quad= \frac{1}{2\pi}\sum_{m=-\infty}^{\infty}\int_0^\infty \frac{1}{A}\mathcal{J}_{|m|}(k\rho(t))\mathcal{J}_{|m|}(kr)e^{im(\theta-\phi(t))}kdk\\
&\qquad+\frac{1}{2\pi}\sum_{m=-\infty}^{\infty}\int_0^\infty \frac{1}{A^2}\left\{-k\dot{\rho}(t)\mathcal{J}'_{|m|}(k\rho(t))+im\dot{\phi}(t)\mathcal{J}_{|m|}(k\rho(t))\right\}\mathcal{J}_{|m|}(kr)e^{im(\theta-\phi(t))}kdk\\
&\qquad+\frac{1}{2\pi}\sum_{m=-\infty}^{\infty}\int_0^\infty \frac{1}{A^3}\Big\{k\ddot{\rho}(t)\mathcal{J}'_{|m|}(k\rho(t))+k^2(\dot{\rho}(t))^2\mathcal{J}''_{|m|}(k\rho(t))-2ikm\dot{\rho}(t)\dot{\phi}(t)\mathcal{J}'_{|m|}(k\rho(t))\\
&\qquad\qquad\qquad-im\ddot{\phi}(t)\mathcal{J}_{|m|}(k\rho(t))-m^2(\dot{\phi}(t))^2\mathcal{J}_{|m|}(k\rho(t))\Big\}\mathcal{J}_{|m|}(kr)e^{im(\theta-\phi(t))}kdk\\
&\qquad+\frac{1}{2\pi}\sum_{m=-\infty}^{\infty}\int_0^\infty \frac{1}{A^4}\Big\{-k^3(\dot{\rho}(t))^3\mathcal{J}'''_{|m|}(k\rho(t))+3ik^2m(\dot{\rho}(t))^2\dot{\phi}(t)\mathcal{J}''_{|m|}(k\rho(t))\\
&\qquad\quad+3km^2\dot{\rho}(t)(\dot{\phi}(t))^2\mathcal{J}'_{|m|}(k\rho(t))-im^3(\dot{\phi}(t))^3\mathcal{J}_{|m|}(k\rho(t))\\
&\qquad\quad-k\dddot{\rho}(t)\mathcal{J}'_{|m|}(k\rho(t))-3k^2\dot{\rho}\ddot{\rho}\mathcal{J}''_{|m|}(k\rho(t))+3ikm\ddot{\rho}\dot{\phi}\mathcal{J}'_{|m|}(k\rho(t))\\
&\qquad\quad+3ikm\dot{\rho}\ddot{\phi}\mathcal{J}'_{|m|}(k\rho(t))+im\dddot{\rho}\mathcal{J}'_{|m|}(k\rho(t))+3m^2\dot{\phi}\ddot{\phi}\mathcal{J}'_{|m|}(k\rho(t))\Big\}\mathcal{J}_{|m|}(kr)e^{im(\theta-\phi(t))}kdk.
\end{aligned}
\tag{A.3.31}
$$

The first term in Eq. (A.3.31) should correspond to the steady state:

$$
\frac{1}{2\pi}\mathcal{K}_0\left(\sqrt{r^2+\rho^2-2r\rho\cos(\theta-\phi)}\right)=\frac{1}{2\pi}\sum_{m=-\infty}^{\infty}\int_0^\infty\frac{1}{k^2+1}\mathcal{J}_m(k\rho(t))\mathcal{J}_m(kr)e^{im(\theta-\phi(t))}kdk.
\tag{A.3.32}
$$

By changing the spatial scale as $r=\lambda\tilde{r}$, $\rho=\lambda\tilde{\rho}$, and $k=\tilde{k}/\lambda$, we have

$$
\frac{1}{2\pi}\mathcal{K}_0\left(\lambda\sqrt{\tilde{r}^2+\tilde{\rho}^2-2\tilde{r}\tilde{\rho}\cos(\theta-\phi)}\right)=\frac{1}{2\pi}\sum_{m=-\infty}^{\infty}\int_0^\infty\frac{1}{\tilde{k}^2+\lambda^2}\mathcal{J}_m(\tilde{k}\tilde{\rho}(t))\mathcal{J}_m(\tilde{k}\tilde{r})e^{im(\theta-\phi(t))}\tilde{k}d\tilde{k}.
\tag{A.3.33}
$$

By differentiating the both sides of Eq. (A.3.33) with regard to λ, we have

$$
\begin{aligned}
&\frac{1}{4\pi\lambda}\sqrt{\tilde{r}^2+\tilde{\rho}^2-2\tilde{r}\tilde{\rho}\cos(\theta-\phi)}\mathcal{K}_1\left(\lambda\sqrt{\tilde{r}^2+\tilde{\rho}^2-2\tilde{r}\tilde{\rho}\cos(\theta-\phi)}\right)\\
&\qquad=\frac{1}{2\pi}\sum_{m=-\infty}^{\infty}\int_0^\infty\frac{1}{(\tilde{k}^2+\lambda^2)^2}\mathcal{J}_m(\tilde{k}\tilde{\rho}(t))\mathcal{J}_m(\tilde{k}\tilde{r})e^{im(\theta-\phi(t))}\tilde{k}d\tilde{k}.
\end{aligned}
\tag{A.3.34}
$$

By setting $\lambda=1$, we have

$$
\begin{aligned}
&\frac{1}{4\pi}\sqrt{r^2+\rho^2-2r\rho\cos(\theta-\phi)}\mathcal{K}_1\left(\sqrt{r^2+\rho^2-2r\rho\cos(\theta-\phi)}\right)\\
&\qquad=\frac{1}{2\pi}\sum_{m=-\infty}^{\infty}\int_0^\infty\frac{1}{(k^2+1)^2}\mathcal{J}_m(k\rho(t))\mathcal{J}_m(kr)e^{im(\theta-\phi(t))}kdk.
\end{aligned}
\tag{A.3.35}
$$

Term proportional to $\dot{\rho}$

By differentiating the both sides of Eq. (A.3.35) with regard to ρ,

$$\begin{aligned}
&\frac{1}{4\pi}\frac{\rho - r\cos(\theta-\phi)}{\sqrt{r^2+\rho^2-2r\rho\cos(\theta-\phi)}}\mathcal{K}_1\left(\sqrt{r^2+\rho^2-2r\rho\cos(\theta-\phi)}\right)\\
&+\frac{1}{4\pi}(\rho - r\cos(\theta-\phi))\mathcal{K}_1{}'\left(\sqrt{r^2+\rho^2-2r\rho\cos(\theta-\phi)}\right)\\
&\qquad=\frac{1}{2\pi}\sum_{m=-\infty}^{\infty}\int_0^{\infty}\frac{k}{(k^2+1)^2}\mathcal{J}_m{}'(k\rho(t))\mathcal{J}_m(kr)e^{im(\theta-\phi(t))}kdk.
\end{aligned}\tag{A.3.36}$$

Using the relation $z\mathcal{K}_\nu{}'(z)+\nu\mathcal{K}_\nu(z) = -z\mathcal{K}_{\nu-1}(z)$ on page 79 in Ref. [81], we have

$$\begin{aligned}
&-\frac{1}{4\pi}\left(\rho - r\cos(\theta-\phi)\right)\mathcal{K}_0\left(\sqrt{r^2+\rho^2-2r\rho\cos(\theta-\phi)}\right)\\
&\qquad=\frac{1}{2\pi}\sum_{m=-\infty}^{\infty}\int_0^{\infty}\frac{k}{(k^2+1)^2}\mathcal{J}_m{}'(k\rho(t))\mathcal{J}_m(kr)e^{im(\theta-\phi(t))}kdk.
\end{aligned}\tag{A.3.37}$$

The term proportional to $\dot{\rho}$ is calculated using Eq. (A.3.37). We multiply the both sides of Eq. (A.3.37) by $-\cos t$ and $-\sin t$ and integrate them on the small circle with the radius of ϵ around $\boldsymbol{r}=\boldsymbol{\rho}$ for $\boldsymbol{e}_\rho$ and $\boldsymbol{e}_\phi$ directions, respectively. Here we set $\epsilon = \sqrt{r^2+\rho^2-2r\rho\cos(\theta-\phi)}$ and $\rho - r\cos(\theta-\phi) = \epsilon\cos t$.

$$\frac{-k}{\pi\epsilon^2}\frac{\dot{\rho}\boldsymbol{e}_\rho}{4\pi}\int_0^{2\pi}\left(\epsilon\mathcal{K}_0(\epsilon)\cos t\right)(-\cos t)\epsilon dt = \frac{k}{4\pi}\mathcal{K}_0(\epsilon)\dot{\rho}\boldsymbol{e}_\rho = \frac{k}{4\pi}\left(-\gamma_{\text{Euler}}+\log\frac{2}{\epsilon}\right)\dot{\rho}\boldsymbol{e}_\rho, \tag{A.3.38}$$

$$\frac{-k}{\pi\epsilon^2}\frac{\dot{\rho}\boldsymbol{e}_\phi}{4\pi}\int_0^{2\pi}\left(\epsilon\mathcal{K}_0(\epsilon)\cos t\right)(-\sin t)\epsilon dt = 0, \tag{A.3.39}$$

where γ_{Euler} is the Euler's constant ($\gamma_{\text{Euler}} \simeq 0.577$).

Term proportional to $\dot{\phi}$

By differentiating the both sides of Eq. (A.3.35) with regard to θ,

$$\begin{aligned}
&\frac{1}{4\pi}\frac{r\rho\sin(\theta-\phi)}{\sqrt{r^2+\rho^2-2r\rho\cos(\theta-\phi)}}\mathcal{K}_1\left(\sqrt{r^2+\rho^2-2r\rho\cos(\theta-\phi)}\right)\\
&+\frac{1}{4\pi}r\rho\sin(\theta-\phi)\mathcal{K}_1{}'\left(\sqrt{r^2+\rho^2-2r\rho\cos(\theta-\phi)}\right)\\
&\qquad=\frac{1}{2\pi}\sum_{m=-\infty}^{\infty}\int_0^{\infty}\frac{im}{(k^2+1)^2}\mathcal{J}_m(k\rho(t))\mathcal{J}_m(kr)e^{im(\theta-\phi(t))}kdk.
\end{aligned}\tag{A.3.40}$$

Using the relation $z\mathcal{K}_\nu{}'(z)+\nu\mathcal{K}_\nu(z) = -z\mathcal{K}_{\nu-1}(z)$, we have

$$\begin{aligned}
&\frac{1}{4\pi}r\rho\sin(\theta-\phi)\mathcal{K}_0\left(\sqrt{r^2+\rho^2-2r\rho\cos(\theta-\phi)}\right)\\
&\qquad=\frac{1}{2\pi}\sum_{m=-\infty}^{\infty}\int_0^{\infty}\frac{-im}{(k^2+1)^2}\mathcal{J}_m(k\rho(t))\mathcal{J}_m(kr)e^{im(\theta-\phi(t))}kdk.
\end{aligned}\tag{A.3.41}$$

The term proportional to $\dot{\phi}$ is calculated using Eq. (A.3.41). We multiply the both sides of Eq. (A.3.41) by $\cos t$ and $\sin t$ and integrate them on the small circle with the radius of ϵ around $\boldsymbol{r} = \boldsymbol{\rho}$ for $\boldsymbol{e}_\rho$ and $\boldsymbol{e}_\phi$ directions, respectively. Here we set $\epsilon = \sqrt{r^2 + \rho^2 - 2r\rho\cos(\theta - \phi)}$ and $\rho - r\cos(\theta - \phi) = \epsilon \cos t$.

$$\frac{-k}{\pi\epsilon^2}\frac{\dot{\phi}\boldsymbol{e}_\rho}{4\pi}\int_0^{2\pi} \epsilon\rho\mathcal{K}_0(\epsilon)\sin t(-\cos t)\epsilon dt = 0, \tag{A.3.42}$$

$$\frac{-k}{\pi\epsilon^2}\frac{\dot{\phi}\boldsymbol{e}_\phi}{4\pi}\int_0^{2\pi} \epsilon\rho\mathcal{K}_0(\epsilon)\sin t(-\sin t)\epsilon dt = \frac{k}{4\pi}\epsilon\mathcal{K}_0(\epsilon)\rho\dot{\theta}\boldsymbol{e}_\phi = \frac{k}{4\pi}\left(-\gamma_{\text{Euler}} + \log\frac{2}{\epsilon}\right)\rho\dot{\phi}\boldsymbol{e}_\phi. \tag{A.3.43}$$

Term proportional to $\ddot{\rho}$

By differentiating the both sides of Eq. (A.3.34) with regard to λ,

$$\begin{aligned}
&-\frac{1}{4\pi\lambda^2}\sqrt{\tilde{r}^2 + \tilde{\rho}^2 - 2\tilde{r}\tilde{\rho}\cos(\theta - \phi)}\mathcal{K}_1\left(\lambda\sqrt{\tilde{r}^2 + \tilde{\rho}^2 - 2\tilde{r}\tilde{\rho}\cos(\theta - \phi)}\right) \\
&+\frac{1}{4\pi\lambda}\left(\tilde{r}^2 + \tilde{\rho}^2 - 2\tilde{r}\tilde{\rho}\cos(\theta - \phi)\right)\mathcal{K}_1{}'\left(\lambda\sqrt{\tilde{r}^2 + \tilde{\rho}^2 - 2\tilde{r}\tilde{\rho}\cos(\theta - \phi)}\right) \\
&\quad = \frac{1}{2\pi}\sum_{m=-\infty}^{\infty}\int_0^\infty \frac{-4\lambda}{(\tilde{k}^2 + \lambda^2)^3}\mathcal{J}_m(\tilde{k}\tilde{\rho}(t))\mathcal{J}_m(\tilde{k}\tilde{r})e^{im(\theta - \phi(t))}\tilde{k}d\tilde{k}.
\end{aligned} \tag{A.3.44}$$

By dividing the both sides by -4λ, we have

$$\begin{aligned}
&\frac{1}{16\pi\lambda^3}\sqrt{\tilde{r}^2 + \tilde{\rho}^2 - 2\tilde{r}\tilde{\rho}\cos(\theta - \phi)}\mathcal{K}_1\left(\lambda\sqrt{\tilde{r}^2 + \tilde{\rho}^2 - 2\tilde{r}\tilde{\rho}\cos(\theta - \phi)}\right) \\
&-\frac{1}{16\pi\lambda^2}\left(\tilde{r}^2 + \tilde{\rho}^2 - 2\tilde{r}\tilde{\rho}\cos(\theta - \phi)\right)\mathcal{K}_1{}'\left(\lambda\sqrt{\tilde{r}^2 + \tilde{\rho}^2 - 2\tilde{r}\tilde{\rho}\cos(\theta - \phi)}\right) \\
&\quad = \frac{1}{2\pi}\sum_{m=-\infty}^{\infty}\int_0^\infty \frac{1}{(\tilde{k}^2 + \lambda^2)^3}\mathcal{J}_m(\tilde{k}\tilde{\rho}(t))\mathcal{J}_m(\tilde{k}\tilde{r})e^{im(\theta - \phi(t))}\tilde{k}d\tilde{k}.
\end{aligned} \tag{A.3.45}$$

Using the relation $z\mathcal{K}_\nu{}'(z) + \nu\mathcal{K}_\nu(z) = -z\mathcal{K}_{\nu-1}(z)$, we have

$$\begin{aligned}
&\frac{1}{16\pi\lambda^2}\left(\tilde{r}^2 + \tilde{\rho}^2 - 2\tilde{r}\tilde{\rho}\cos(\theta - \phi)\right)\mathcal{K}_2\left(\lambda\sqrt{\tilde{r}^2 + \tilde{\rho}^2 - 2\tilde{r}\tilde{\rho}\cos(\theta - \phi)}\right) \\
&\quad = \frac{1}{2\pi}\sum_{m=-\infty}^{\infty}\int_0^\infty \frac{1}{(\tilde{k}^2 + \tilde{\lambda}^2)^3}\mathcal{J}_m(\tilde{k}\tilde{\rho}(t))\mathcal{J}_m(\tilde{k}\tilde{r})e^{im(\theta - \phi(t))}\tilde{k}d\tilde{k}.
\end{aligned} \tag{A.3.46}$$

By setting $\lambda = 1$, we have

$$\begin{aligned}
&\frac{1}{16\pi}\left(r^2 + \rho^2 - 2r\rho\cos(\theta - \phi)\right)\mathcal{K}_2\left(\sqrt{r^2 + \rho^2 - 2r\rho\cos(\theta - \phi)}\right) \\
&\quad = \frac{1}{2\pi}\sum_{m=-\infty}^{\infty}\int_0^\infty \frac{1}{(k^2 + 1)^3}\mathcal{J}_m(k\rho(t))\mathcal{J}_m(kr)e^{im(\theta - \phi(t))}kdk.
\end{aligned} \tag{A.3.47}$$

By differentiating Eq. (A.3.47) with regard to ρ, we have

$$\begin{aligned}
&\frac{1}{16\pi}2\left(\rho - r\cos(\theta - \phi)\right)\mathcal{K}_2\left(\sqrt{r^2 + \rho^2 - 2r\rho\cos(\theta - \phi)}\right) \\
&+\frac{1}{16\pi}(\rho - r\cos(\theta - \phi))\sqrt{r^2 + \rho^2 - 2r\rho\cos(\theta - \phi)}\mathcal{K}_2{}'\left(\sqrt{r^2 + \rho^2 - 2r\rho\cos(\theta - \phi)}\right) \\
&\quad = \frac{1}{2\pi}\sum_{m=-\infty}^{\infty}\int_0^\infty \frac{k}{(k^2 + 1)^3}\mathcal{J}_m{}'(k\rho(t))\mathcal{J}_m(kr)e^{im(\theta - \phi(t))}kdk.
\end{aligned} \tag{A.3.48}$$

Using the relation $z\mathcal{K}_\nu{}'(z) + \nu\mathcal{K}_\nu(z) = -z\mathcal{K}_{\nu-1}(z)$, we have

$$\begin{aligned}
&-\frac{1}{16\pi}(\rho - r\cos(\theta-\phi))\sqrt{r^2+\rho^2-2r\rho\cos(\theta-\phi)}\mathcal{K}_1\left(\sqrt{r^2+\rho^2-2r\rho\cos(\theta-\phi)}\right)\\
&\quad = \frac{1}{2\pi}\sum_{m=-\infty}^{\infty}\int_0^\infty \frac{k}{(k^2+1)^3}\mathcal{J}_m{}'(k\rho(t))\mathcal{J}_m(kr)e^{im(\theta-\phi(t))}kdk.
\end{aligned} \tag{A.3.49}$$

The term proportional to $\ddot{\rho}$ is calculated using Eq. (A.3.49). We multiply the both sides of Eq. (A.3.49) by $-\cos t$ and $\sin t$ and integrate them on the small circle with the radius of ϵ around $\boldsymbol{r} = \boldsymbol{\rho}$ for $\boldsymbol{e}_\rho$ and $\boldsymbol{e}_\phi$ directions, respectively. Here we set $\epsilon = \sqrt{r^2+\rho^2-2r\rho\cos(\theta-\phi)}$ and $\rho - r\cos(\theta-\phi) = \epsilon\cos t$.

$$\frac{-k}{\pi\epsilon^2}\frac{\ddot{\rho}\boldsymbol{e}_\rho}{16\pi}\int_0^{2\pi}\left(-\epsilon^2\mathcal{K}_1(\epsilon)\cos t\right)(-\cos t)\epsilon dt = -k\frac{\ddot{\rho}\boldsymbol{e}_\rho}{16\pi}\epsilon\mathcal{K}_1(\epsilon) = -k\frac{\ddot{\rho}\boldsymbol{e}_\rho}{16\pi}, \tag{A.3.50}$$

$$\frac{-k}{\pi\epsilon^2}\frac{\ddot{\rho}\boldsymbol{e}_\rho}{16\pi}\int_0^{2\pi}\left(-\epsilon^2\mathcal{K}_1(\epsilon)\cos t\right)(-\sin t)\epsilon dt = 0. \tag{A.3.51}$$

Term proportional to $\dot{\rho}^2$

By differentiating the both sides of Eq. (A.3.49) with regard to ρ, we have

$$\begin{aligned}
&-\frac{1}{16\pi}\sqrt{r^2+\rho^2-2r\rho\cos(\theta-\phi)}\mathcal{K}_1\left(\sqrt{r^2+\rho^2-2r\rho\cos(\theta-\phi)}\right)\\
&-\frac{1}{16\pi}\frac{(\rho-r\cos(\theta-\phi))^2}{\sqrt{r^2+\rho^2-2r\rho\cos(\theta-\phi)}}\mathcal{K}_1\left(\sqrt{r^2+\rho^2-2r\rho\cos(\theta-\phi)}\right)\\
&-\frac{1}{16\pi}(\rho-r\cos(\theta-\phi))^2\mathcal{K}_1{}'\left(\sqrt{r^2+\rho^2-2r\rho\cos(\theta-\phi)}\right)\\
&\quad = \frac{1}{2\pi}\sum_{m=-\infty}^{\infty}\int_0^\infty \frac{k^2}{(k^2+1)^3}\mathcal{J}_m{}''(k\rho(t))\mathcal{J}_m(kr)e^{im(\theta-\phi(t))}kdk.
\end{aligned} \tag{A.3.52}$$

Using the relation $z\mathcal{K}_\nu{}'(z) + \nu\mathcal{K}_\nu(z) = -z\mathcal{K}_{\nu-1}(z)$, we have

$$\begin{aligned}
&-\frac{1}{16\pi}\sqrt{r^2+\rho^2-2r\rho\cos(\theta-\phi)}\mathcal{K}_1\left(\sqrt{r^2+\rho^2-2r\rho\cos(\theta-\phi)}\right)\\
&+\frac{1}{16\pi}(\rho-r\cos(\theta-\phi))^2\mathcal{K}_0\left(\sqrt{r^2+\rho^2-2r\rho\cos(\theta-\phi)}\right)\\
&\quad = \frac{1}{2\pi}\sum_{m=-\infty}^{\infty}\int_0^\infty \frac{k^2}{(k^2+1)^3}\mathcal{J}_m{}''(k\rho(t))\mathcal{J}_m(kr)e^{im(\theta-\phi(t))}kdk.
\end{aligned} \tag{A.3.53}$$

The term proportional to $\dot{\rho}^2$ is calculated using Eq. (A.3.53). We multiply $\cos t$ and $-\sin t$ to the both sides of Eq. (A.3.53) and integrate them on the small circle with the radius of ϵ around $\boldsymbol{r} = \boldsymbol{\rho}$ for $\boldsymbol{e}_\rho$ and $\boldsymbol{e}_\phi$ directions, respectively. Here we set $\epsilon = \sqrt{r^2+\rho^2-2r\rho\cos(\theta-\phi)}$ and $\rho - r\cos(\theta-\phi) = \epsilon\cos t$.

$$\frac{-k}{\pi\epsilon^2}\frac{\dot{\rho}^2\boldsymbol{e}_\rho}{16\pi}\int_0^{2\pi}\left(-\epsilon\mathcal{K}_1(\epsilon)+\epsilon^2\mathcal{K}_0(\epsilon)\cos^2 t\right)(-\cos t)\epsilon dt = 0, \tag{A.3.54}$$

$$\frac{-k}{\pi\epsilon^2}\frac{\dot{\rho}^2\boldsymbol{e}_\phi}{16\pi}\int_0^{2\pi}\left(-\epsilon\mathcal{K}_1(\epsilon)+\epsilon^2\mathcal{K}_0(\epsilon)\cos^2 t\right)(-\sin t)\epsilon dt = 0. \tag{A.3.55}$$

The result that the driving force proportional to $\dot{r}^2$ is zero is consistent with the translational symmetry of the system.

Term proportional to $\dot{\rho}\dot{\phi}$

By differentiating the both sides of Eq. (A.3.49) with regard to θ, we have

$$\begin{aligned}
&-\frac{1}{16\pi}r\sin(\theta-\phi)\sqrt{r^2+\rho^2-2r\rho\cos(\theta-\phi)}\mathcal{K}_1\left(\sqrt{r^2+\rho^2-2r\rho\cos(\theta-\phi)}\right)\\
&-\frac{1}{16\pi}\frac{(\rho-r\cos(\theta-\phi))r\rho\sin(\theta-\phi)}{\sqrt{r^2+\rho^2-2r\rho\cos(\theta-\phi)}}\mathcal{K}_1\left(\sqrt{r^2+\rho^2-2r\rho\cos(\theta-\phi)}\right)\\
&-\frac{1}{16\pi}(\rho-r\cos(\theta-\phi))r\rho\sin(\theta-\phi)\mathcal{K}_1{}'\left(\sqrt{r^2+\rho^2-2r\rho\cos(\theta-\phi)}\right)\\
&\qquad=\frac{1}{2\pi}\sum_{m=-\infty}^{\infty}\int_0^{\infty}\frac{ikm}{(k^2+1)^3}\mathcal{J}_m{}'(k\rho(t))\mathcal{J}_m(kr)e^{im(\theta-\phi(t))}kdk.
\end{aligned}\tag{A.3.56}$$

Using the relation $z\mathcal{K}_\nu{}'(z)+\nu\mathcal{K}_\nu(z)=-z\mathcal{K}_{\nu-1}(z)$, we have

$$\begin{aligned}
&-\frac{1}{16\pi}r\sin(\theta-\phi)\sqrt{r^2+\rho^2-2r\rho\cos(\theta-\phi)}\mathcal{K}_1\left(\sqrt{r^2+\rho^2-2r\rho\cos(\theta-\phi)}\right)\\
&+\frac{1}{16\pi}(\rho-r\cos(\theta-\phi))r\rho\sin(\theta-\phi)\mathcal{K}_0\left(\sqrt{r^2+\rho^2-2r\rho\cos(\theta-\phi)}\right)\\
&\qquad=\frac{1}{2\pi}\sum_{m=-\infty}^{\infty}\int_0^{\infty}\frac{ikm}{(k^2+1)^3}\mathcal{J}_m{}'(k\rho(t))\mathcal{J}_m(kr)e^{im(\theta-\phi(t))}kdk.
\end{aligned}\tag{A.3.57}$$

The term proportional to $\dot{\rho}\dot{\phi}$ is calculated using Eq. (A.3.57). We multiply the both sides of Eq. (A.3.57) by $\cos t$ and $-\sin t$ and integrate them on the small circle with the radius of ϵ around $\boldsymbol{r}=\boldsymbol{\rho}$ for $\boldsymbol{e}_\rho$ and $\boldsymbol{e}_\phi$ directions, respectively. Here we set $\epsilon=\sqrt{r^2+\rho^2-2r\rho\cos(\theta-\phi)}$ and $\rho-r\cos(\theta-\phi)=\epsilon\cos t$.

$$(-2)\frac{-k}{\pi\epsilon^2}\frac{\dot{\rho}\dot{\phi}\boldsymbol{e}_\rho}{16\pi}\int_0^{2\pi}\left(\epsilon^2\sin t\mathcal{K}_1(\epsilon)-\epsilon^2\rho^2\sin t\cos t\mathcal{K}_0(\epsilon)\right)(-\cos t)\epsilon dt=0,\tag{A.3.58}$$

$$(-2)\frac{-k}{\pi\epsilon^2}\frac{\dot{\rho}\dot{\phi}\boldsymbol{e}_\phi}{16\pi}\int_0^{2\pi}\left(\epsilon^2\sin t\mathcal{K}_1(\epsilon)-\epsilon^2\rho^2\sin t\cos t\mathcal{K}_0(\epsilon)\right)(-\sin t)\epsilon dt=-k\frac{\dot{\rho}\dot{\phi}\boldsymbol{e}_\phi}{8\pi}\epsilon\mathcal{K}_1(\epsilon)=-\frac{\dot{\rho}\dot{\phi}\boldsymbol{e}_\phi}{8\pi}.\tag{A.3.59}$$

Term proportional to $\ddot{\phi}$

By differentiating the both sides of Eq. (A.3.47) with regard to θ, we have

$$\begin{aligned}
&\frac{1}{8\pi}r\rho\sin(\theta-\phi)\mathcal{K}_2\left(\sqrt{r^2+\rho^2-2r\rho\cos(\theta-\phi)}\right)\\
&+\frac{1}{16\pi}r\rho\sin(\theta-\phi)\sqrt{r^2+\rho^2-2r\rho\cos(\theta-\phi)}\mathcal{K}_2{}'\left(\sqrt{r^2+\rho^2-2r\rho\cos(\theta-\phi)}\right)\\
&\qquad=\frac{1}{2\pi}\sum_{m=-\infty}^{\infty}\int_0^{\infty}\frac{im}{(k^2+1)^3}\mathcal{J}_m(k\rho(t))\mathcal{J}_m(kr)e^{im(\theta-\phi(t))}kdk.
\end{aligned}\tag{A.3.60}$$

Using the relation $z\mathcal{K}_\nu{}'(z)+\nu\mathcal{K}_\nu(z)=-z\mathcal{K}_{\nu-1}(z)$, we have

$$\begin{aligned}
&-\frac{1}{16\pi}r\rho\sin(\theta-\phi)\sqrt{r^2+\rho^2-2r\rho\cos(\theta-\phi)}\mathcal{K}_1\left(\sqrt{r^2+\rho^2-2r\rho\cos(\theta-\phi)}\right)\\
&\qquad=\frac{1}{2\pi}\sum_{m=-\infty}^{\infty}\int_0^{\infty}\frac{im}{(k^2+1)^3}\mathcal{J}_m(k\rho(t))\mathcal{J}_m(kr)e^{im(\theta-\phi(t))}kdk.
\end{aligned}\tag{A.3.61}$$

The term proportional to $\ddot{\phi}$ is calculated using Eq. (A.3.61). We multiply the both sides of Eq. (A.3.61) by $-\cos t$ and $\sin t$ and integrate them on the small circle with the radius of ϵ around $\boldsymbol{r} = \boldsymbol{\rho}$ for $\boldsymbol{e}_\rho$ and $\boldsymbol{e}_\phi$ directions, respectively. Here we set $\epsilon = \sqrt{r^2+\rho^2-2r\rho\cos(\theta-\phi)}$ and $\rho - r\cos(\theta-\phi) = \epsilon\cos t$.

$$\frac{-k}{\pi\epsilon^2}\frac{\ddot{\phi}\boldsymbol{e}_\rho}{16\pi}\int_0^{2\pi}\left(-\epsilon^2\rho\mathcal{K}_1(\epsilon)\sin t\right)(-\cos t)\epsilon dt = 0, \tag{A.3.62}$$

$$\frac{-k}{\pi\epsilon^2}\frac{\ddot{\phi}\boldsymbol{e}_\phi}{16\pi}\int_0^{2\pi}\left(-\epsilon^2\rho\mathcal{K}_1(\epsilon)\sin t\right)(-\sin t)\epsilon dt = -k\frac{\rho\ddot{\phi}\boldsymbol{e}_\phi}{16\pi}\epsilon\mathcal{K}_1(\epsilon) = -k\frac{\rho\ddot{\phi}\boldsymbol{e}_\phi}{16\pi}. \tag{A.3.63}$$

Term proportional to $\dot{\phi}^2$

By differentiating the both sides of Eq. (A.3.61) with regard to θ, we have

$$\begin{aligned}
&\frac{1}{16\pi}r\rho\cos(\theta-\phi)\sqrt{r^2+\rho^2-2r\rho\cos(\theta-\phi)}\mathcal{K}_1\left(\sqrt{r^2+\rho^2-2r\rho\cos(\theta-\phi)}\right)\\
&+\frac{1}{16\pi}\frac{(r\rho\sin(\theta-\phi))^2}{\sqrt{r^2+\rho^2-2r\rho\cos(\theta-\phi)}}\mathcal{K}_1\left(\sqrt{r^2+\rho^2-2r\rho\cos(\theta-\phi)}\right)\\
&+\frac{1}{16\pi}(r\rho\sin(\theta-\phi))^2\mathcal{K}_1{}'\left(\sqrt{r^2+\rho^2-2r\rho\cos(\theta-\phi)}\right)\\
&\quad=\frac{1}{2\pi}\sum_{m=-\infty}^{\infty}\int_0^\infty\frac{m^2}{(k^2+1)^3}\mathcal{J}_m(k\rho(t))\mathcal{J}_m(kr)e^{im(\theta-\phi(t))}kdk.
\end{aligned} \tag{A.3.64}$$

Using the relation $z\mathcal{K}_\nu{}'(z)+\nu\mathcal{K}_\nu(z) = -z\mathcal{K}_{\nu-1}(z)$, we have

$$\begin{aligned}
&\frac{1}{16\pi}r\rho\cos(\theta-\phi)\sqrt{r^2+\rho^2-2r\rho\cos(\theta-\phi)}\mathcal{K}_1\left(\sqrt{r^2+\rho^2-2r\rho\cos(\theta-\phi)}\right)\\
&-\frac{1}{16\pi}(r\rho\sin(\theta-\phi))^2\mathcal{K}_0\left(\sqrt{r^2+\rho^2-2r\rho\cos(\theta-\phi)}\right)\\
&\quad=\frac{1}{2\pi}\sum_{m=-\infty}^{\infty}\int_0^\infty\frac{m^2}{(k^2+1)^3}\mathcal{J}_m(k\rho(t))\mathcal{J}_m(kr)e^{im(\theta-\phi(t))}kdk.
\end{aligned} \tag{A.3.65}$$

The term proportional to $\dot{\phi}^2$ is calculated using Eq. (A.3.65). We multiply the both sides of Eq. (A.3.65) by $-\cos t$ and $\sin t$ and integrate them on the small circle with the radius of ϵ around $\boldsymbol{r} = \boldsymbol{\rho}$ for $\boldsymbol{e}_\rho$ and $\boldsymbol{e}_\phi$ directions, respectively. Here we set $\epsilon = \sqrt{r^2+\rho^2-2r\rho\cos(\theta-\phi)}$ and $\rho - r\cos(\theta-\phi) = \epsilon\cos t$.

$$\frac{-k}{\pi\epsilon^2}\frac{\dot{\phi}^2\boldsymbol{e}_\rho}{16\pi}\int_0^{2\pi}\left(-\epsilon\rho(\rho-\epsilon\cos t)\mathcal{K}_1(\epsilon)+\epsilon^2\rho^2\sin^2 t\mathcal{K}_0(\epsilon)\right)(-\cos t)\epsilon dt = k\frac{\rho\dot{\phi}^2\boldsymbol{e}_\rho}{16\pi}\epsilon\mathcal{K}_1(\epsilon) = k\frac{\rho\dot{\phi}^2\boldsymbol{e}_\rho}{16\pi}, \tag{A.3.66}$$

$$\frac{-k}{\pi\epsilon^2}\frac{\dot{\phi}^2\boldsymbol{e}_\phi}{16\pi}\int_0^{2\pi}\left(-\epsilon\rho(\rho-\epsilon\cos t)\mathcal{K}_1(\epsilon)+\epsilon^2\rho^2\sin^2 t\mathcal{K}_0(\epsilon)\right)(-\sin t)\epsilon dt = 0. \tag{A.3.67}$$

Term proportional to $\dot{\rho}^3$

By differentiating the both sides of Eq. (A.3.46) with regard to λ, we have

$$\begin{aligned}
&-\frac{2}{16\pi\lambda^3}\left(\tilde{r}^2+\tilde{\rho}^2-2\tilde{r}\tilde{\rho}\cos(\theta-\phi)\right)\mathcal{K}_2\left(\lambda\sqrt{\tilde{r}^2+\tilde{\rho}^2-2\tilde{r}\tilde{\rho}\cos(\theta-\phi)}\right)\\
&+\frac{1}{16\pi\lambda^2}\left(\tilde{r}^2+\tilde{\rho}^2-2\tilde{r}\tilde{\rho}\cos(\theta-\phi)\right)^{\frac{3}{2}}\mathcal{K}_2{}'\left(\lambda\sqrt{\tilde{r}^2+\tilde{\rho}^2-2\tilde{r}\tilde{\rho}\cos(\theta-\phi)}\right)\\
&\quad=\frac{1}{2\pi}\sum_{m=-\infty}^{\infty}\int_0^{\infty}\frac{-6\lambda}{(\tilde{k}^2+\tilde{\lambda}^2)^4}\mathcal{J}_m(\tilde{k}\tilde{\rho}(t))\mathcal{J}_m(\tilde{k}\tilde{r})e^{im(\theta-\phi(t))}\tilde{k}d\tilde{k}. \qquad \text{(A.3.68)}
\end{aligned}$$

$$\begin{aligned}
&\frac{2}{96\pi\lambda^4}\left(\tilde{r}^2+\tilde{\rho}^2-2\tilde{r}\tilde{\rho}\cos(\theta-\phi)\right)\mathcal{K}_2\left(\lambda\sqrt{\tilde{r}^2+\tilde{\rho}^2-2\tilde{r}\tilde{\rho}\cos(\theta-\phi)}\right)\\
&-\frac{1}{96\pi\lambda^3}\left(\tilde{r}^2+\tilde{\rho}^2-2\tilde{r}\tilde{\rho}\cos(\theta-\phi)\right)^{\frac{3}{2}}\mathcal{K}_2{}'\left(\lambda\sqrt{\tilde{r}^2+\tilde{\rho}^2-2\tilde{r}\tilde{\rho}\cos(\theta-\phi)}\right)\\
&\quad=\frac{1}{2\pi}\sum_{m=-\infty}^{\infty}\int_0^{\infty}\frac{1}{(\tilde{k}^2+\tilde{\lambda}^2)^4}\mathcal{J}_m(\tilde{k}\tilde{\rho}(t))\mathcal{J}_m(\tilde{k}\tilde{r})e^{im(\theta-\phi(t))}\tilde{k}d\tilde{k}. \qquad \text{(A.3.69)}
\end{aligned}$$

Using the relation $z\mathcal{K}_\nu{}'(z)+\nu\mathcal{K}_\nu(z)=-z\mathcal{K}_{\nu-1}(z)$, we have

$$\begin{aligned}
&\frac{1}{96\pi\lambda^3}\left(\tilde{r}^2+\tilde{\rho}^2-2\tilde{r}\tilde{\rho}\cos(\theta-\phi)\right)^{\frac{3}{2}}\mathcal{K}_3\left(\lambda\sqrt{\tilde{r}^2+\tilde{\rho}^2-2\tilde{r}\tilde{\rho}\cos(\theta-\phi)}\right)\\
&\quad=\frac{1}{2\pi}\sum_{m=-\infty}^{\infty}\int_0^{\infty}\frac{1}{(\tilde{k}^2+\tilde{\lambda}^2)^4}\mathcal{J}_m(\tilde{k}\tilde{\rho}(t))\mathcal{J}_m(\tilde{k}\tilde{r})e^{im(\theta-\phi(t))}\tilde{k}d\tilde{k}. \qquad \text{(A.3.70)}
\end{aligned}$$

By setting $\lambda=1$, we have

$$\begin{aligned}
&\frac{1}{96\pi}\left(r^2+\rho^2-2r\rho\cos(\theta-\phi)\right)^{\frac{3}{2}}\mathcal{K}_3\left(\sqrt{r^2+\rho^2-2r\rho\cos(\theta-\phi)}\right)\\
&\quad=\frac{1}{2\pi}\sum_{m=-\infty}^{\infty}\int_0^{\infty}\frac{1}{(k^2+1)^4}\mathcal{J}_m(k\rho(t))\mathcal{J}_m(kr)e^{im(\theta-\phi(t))}kdk. \qquad \text{(A.3.71)}
\end{aligned}$$

By differentiating the both sides of Eq. (A.3.71) with regard to ρ, we have

$$\begin{aligned}
&\frac{3}{96\pi}(\rho-r\cos(\theta-\phi))\sqrt{r^2+\rho^2-2r\rho\cos(\theta-\phi)}\mathcal{K}_3\left(\sqrt{r^2+\rho^2-2r\rho\cos(\theta-\phi)}\right)\\
&+\frac{1}{96\pi}(\rho-r\cos(\theta-\phi))\left(r^2+\rho^2-2r\rho\cos(\theta-\phi)\right)\mathcal{K}_3{}'\left(\sqrt{r^2+\rho^2-2r\rho\cos(\theta-\phi)}\right)\\
&\quad=\frac{1}{2\pi}\sum_{m=-\infty}^{\infty}\int_0^{\infty}\frac{k}{(k^2+1)^4}\mathcal{J}_m{}'(k\rho(t))\mathcal{J}_m(kr)e^{im(\theta-\phi(t))}kdk. \qquad \text{(A.3.72)}
\end{aligned}$$

Using the relation $z\mathcal{K}_\nu{}'(z)+\nu\mathcal{K}_\nu(z)=-z\mathcal{K}_{\nu-1}(z)$, we have

$$\begin{aligned}
&-\frac{1}{96\pi}(\rho-r\cos(\theta-\phi))\left(r^2+\rho^2-2r\rho\cos(\theta-\phi)\right)\mathcal{K}_2\left(\sqrt{r^2+\rho^2-2r\rho\cos(\theta-\phi)}\right)\\
&\quad=\frac{1}{2\pi}\sum_{m=-\infty}^{\infty}\int_0^{\infty}\frac{k}{(k^2+1)^4}\mathcal{J}_m{}'(k\rho(t))\mathcal{J}_m(kr)e^{im(\theta-\phi(t))}kdk. \qquad \text{(A.3.73)}
\end{aligned}$$

By differentiating the both sides of Eq. (A.3.73) with regard to ρ, we have

$$\begin{aligned}
&-\frac{1}{96\pi}\left(r^2+\rho^2-2r\rho\cos(\theta-\phi)\right)\mathcal{K}_2\left(\sqrt{r^2+\rho^2-2r\rho\cos(\theta-\phi)}\right)\\
&-\frac{2}{96\pi}(\rho-r\cos(\theta-\phi))^2\mathcal{K}_2\left(\sqrt{r^2+\rho^2-2r\rho\cos(\theta-\phi)}\right)\\
&-\frac{1}{96\pi}(\rho-r\cos(\theta-\phi))^2\sqrt{r^2+\rho^2-2r\rho\cos(\theta-\phi)}\mathcal{K}_2{}'\left(\sqrt{r^2+\rho^2-2r\rho\cos(\theta-\phi)}\right)\\
&\quad=\frac{1}{2\pi}\sum_{m=-\infty}^{\infty}\int_0^{\infty}\frac{k^2}{(k^2+1)^4}\mathcal{J}_m{}''(k\rho(t))\mathcal{J}_m(kr)e^{im(\theta-\phi(t))}kdk.
\end{aligned} \tag{A.3.74}$$

Using the relation $z\mathcal{K}_\nu{}'(z)+\nu\mathcal{K}_\nu(z)=-z\mathcal{K}_{\nu-1}(z)$, we have

$$\begin{aligned}
&-\frac{1}{96\pi}\left(r^2+\rho^2-2r\rho\cos(\theta-\phi)\right)\mathcal{K}_2\left(\sqrt{r^2+\rho^2-2r\rho\cos(\theta-\phi)}\right)\\
&+\frac{1}{96\pi}(\rho-r\cos(\theta-\phi))^2\sqrt{r^2+\rho^2-2r\rho\cos(\theta-\phi)}\mathcal{K}_1\left(\sqrt{r^2+\rho^2-2r\rho\cos(\theta-\phi)}\right)\\
&\quad=\frac{1}{2\pi}\sum_{m=-\infty}^{\infty}\int_0^{\infty}\frac{k^2}{(k^2+1)^4}\mathcal{J}_m{}''(k\rho(t))\mathcal{J}_m(kr)e^{im(\theta-\phi(t))}kdk.
\end{aligned} \tag{A.3.75}$$

By differentiating the both sides of Eq. (A.3.75) with regard to ρ, we have

$$\begin{aligned}
&-\frac{2}{96\pi}(\rho-r\cos(\theta-\phi))\mathcal{K}_2\left(\sqrt{r^2+\rho^2-2r\rho\cos(\theta-\phi)}\right)\\
&-\frac{1}{96\pi}(\rho-r\cos(\theta-\phi))\sqrt{r^2+\rho^2-2r\rho\cos(\theta-\phi)}\mathcal{K}_2{}'\left(\sqrt{r^2+\rho^2-2r\rho\cos(\theta-\phi)}\right)\\
&+\frac{2}{96\pi}(\rho-r\cos(\theta-\phi))\sqrt{r^2+\rho^2-2r\rho\cos(\theta-\phi)}\mathcal{K}_1\left(\sqrt{r^2+\rho^2-2r\rho\cos(\theta-\phi)}\right)\\
&+\frac{1}{96\pi}\frac{(\rho-r\cos(\theta-\phi))^3}{\sqrt{r^2+\rho^2-2r\rho\cos(\theta-\phi)}}\mathcal{K}_1\left(\sqrt{r^2+\rho^2-2r\rho\cos(\theta-\phi)}\right)\\
&+\frac{1}{96\pi}(\rho-r\cos(\theta-\phi))^3\mathcal{K}_1{}'\left(\sqrt{r^2+\rho^2-2r\rho\cos(\theta-\phi)}\right)\\
&\quad=\frac{1}{2\pi}\sum_{m=-\infty}^{\infty}\int_0^{\infty}\frac{k^3}{(k^2+1)^4}\mathcal{J}_m{}'''(k\rho(t))\mathcal{J}_m(kr)e^{im(\theta-\phi(t))}kdk.
\end{aligned} \tag{A.3.76}$$

Using the relation $z\mathcal{K}_\nu{}'(z)+\nu\mathcal{K}_\nu(z)=-z\mathcal{K}_{\nu-1}(z)$, we have

$$\begin{aligned}
&\frac{3}{96\pi}(\rho-r\cos(\theta-\phi))\sqrt{r^2+\rho^2-2r\rho\cos(\theta-\phi)}\mathcal{K}_1\left(\sqrt{r^2+\rho^2-2r\rho\cos(\theta-\phi)}\right)\\
&-\frac{1}{96\pi}(\rho-r\cos(\theta-\phi))^3\mathcal{K}_0\left(\sqrt{r^2+\rho^2-2r\rho\cos(\theta-\phi)}\right)\\
&\quad=\frac{1}{2\pi}\sum_{m=-\infty}^{\infty}\int_0^{\infty}\frac{k^3}{(k^2+1)^4}\mathcal{J}_m{}'''(k\rho(t))\mathcal{J}_m(kr)e^{im(\theta-\phi(t))}kdk.
\end{aligned} \tag{A.3.77}$$

The term proportional to $\dot{\rho}^3$ is calculated using Eq. (A.3.77). We multiply the both sides of Eq. (A.3.77) by $\cos t$ and $-\sin t$ and integrate them on the small circle with the radius of ϵ around $\boldsymbol{r}=\boldsymbol{\rho}$ for $\boldsymbol{e}_\rho$ and $\boldsymbol{e}_\phi$ directions, respectively. Here we set $\epsilon=\sqrt{r^2+\rho^2-2r\rho\cos(\theta-\phi)}$ and

$\rho - r\cos(\theta-\phi) = \epsilon\cos t$.

$$\frac{-k}{\pi\epsilon^2}\frac{\dot{\rho}^3\boldsymbol{e}_\rho}{96\pi}\int_0^{2\pi}\left(-3\epsilon^2\mathcal{K}_1(\epsilon)\cos t + \epsilon^3\mathcal{K}_0(\epsilon)\cos^3 t\right)(-\cos t)\epsilon dt$$
$$= k\frac{\dot{\rho}^3\boldsymbol{e}_\rho}{96\pi}\left(-3\epsilon\mathcal{K}_1(\epsilon) + \frac{3}{4}\epsilon^3\mathcal{K}_0(\epsilon)\right) = -k\frac{\dot{\rho}^3\boldsymbol{e}_\rho}{32\pi}, \tag{A.3.78}$$

$$\frac{-k}{\pi\epsilon^2}\frac{\dot{\rho}^3\boldsymbol{e}_\phi}{96\pi}\int_0^{2\pi}\left(3\epsilon^2\mathcal{K}_1(\epsilon)\cos t + \epsilon^3\mathcal{K}_0(\epsilon)\cos^3 t\right)(-\sin t)\epsilon dt = 0. \tag{A.3.79}$$

Term proportional to $\dot{\rho}^2\dot{\phi}$

By differentiating the both sides of Eq. (A.3.75) with regard to θ, we have

$$\begin{aligned}
&-\frac{2}{96\pi}r\rho\sin(\theta-\phi)\mathcal{K}_2\left(\sqrt{r^2+\rho^2-2r\rho\cos(\theta-\phi)}\right)\\
&-\frac{1}{96\pi}r\rho\sin(\theta-\phi)\sqrt{r^2+\rho^2-2r\rho\cos(\theta-\phi)}\mathcal{K}_2{}'\left(\sqrt{r^2+\rho^2-2r\rho\cos(\theta-\phi)}\right)\\
&+\frac{2}{96\pi}r\sin(\theta-\phi)(\rho-r\cos(\theta-\phi))\sqrt{r^2+\rho^2-2r\rho\cos(\theta-\phi)}\mathcal{K}_1\left(\sqrt{r^2+\rho^2-2r\rho\cos(\theta-\phi)}\right)\\
&+\frac{1}{96\pi}\frac{r\rho\sin(\theta-\phi)(\rho-r\cos(\theta-\phi))^2}{\sqrt{r^2+\rho^2-2r\rho\cos(\theta-\phi)}}\mathcal{K}_1\left(\sqrt{r^2+\rho^2-2r\rho\cos(\theta-\phi)}\right)\\
&+\frac{1}{96\pi}r\rho\sin(\theta-\phi)(\rho-r\cos(\theta-\phi))^2\mathcal{K}_1{}'\left(\sqrt{r^2+\rho^2-2r\rho\cos(\theta-\phi)}\right)\\
&\qquad=\frac{1}{2\pi}\sum_{m=-\infty}^{\infty}\int_0^\infty\frac{ik^2m}{(k^2+1)^4}\mathcal{J}_m{}''(k\rho(t))\mathcal{J}_m(kr)e^{im(\theta-\phi(t))}kdk.
\end{aligned} \tag{A.3.80}$$

Using the relation $z\mathcal{K}_\nu{}'(z) + \nu\mathcal{K}_\nu(z) = -z\mathcal{K}_{\nu-1}(z)$, we have

$$\begin{aligned}
&\frac{1}{96\pi}r\rho\sin(\theta-\phi)\sqrt{r^2+\rho^2-2r\rho\cos(\theta-\phi)}\mathcal{K}_1\left(\sqrt{r^2+\rho^2-2r\rho\cos(\theta-\phi)}\right)\\
&+\frac{2}{96\pi}r\sin(\theta-\phi)(\rho-r\cos(\theta-\phi))\sqrt{r^2+\rho^2-2r\rho\cos(\theta-\phi)}\mathcal{K}_1\left(\sqrt{r^2+\rho^2-2r\rho\cos(\theta-\phi)}\right)\\
&-\frac{1}{96\pi}r\rho\sin(\theta-\phi)(\rho-r\cos(\theta-\phi))^2\mathcal{K}_0\left(\sqrt{r^2+\rho^2-2r\rho\cos(\theta-\phi)}\right)\\
&\qquad=\frac{1}{2\pi}\sum_{m=-\infty}^{\infty}\int_0^\infty\frac{ik^2m}{(k^2+1)^4}\mathcal{J}_m{}''(k\rho(t))\mathcal{J}_m(kr)e^{im(\theta-\phi(t))}kdk.
\end{aligned} \tag{A.3.81}$$

The term proportional to $\dot{\rho}^2\dot{\phi}$ is calculated using Eq. (A.3.81). We multiply the both sides of Eq. (A.3.81) by $-3\cos t$ and $-3\sin t$ and integrate them on the small circle with the radius of ϵ around $\boldsymbol{r} = \boldsymbol{\rho}$ for $\boldsymbol{e}_\rho$ and $\boldsymbol{e}_\phi$ directions, respectively. Here we set $\epsilon = \sqrt{r^2+\rho^2-2r\rho\cos(\theta-\phi)}$ and $\rho - r\cos(\theta-\phi) = \epsilon\cos t$.

$$3\frac{-k}{\pi\epsilon^2}\frac{\dot{\rho}^2\dot{\phi}\boldsymbol{e}_\rho}{96\pi}\int_0^{2\pi}\left(-\epsilon^2\rho\mathcal{K}_1(\epsilon)\sin t - 2\epsilon^3\mathcal{K}_1(\epsilon)\sin t\cos t + \epsilon^3\rho\mathcal{K}_0(\epsilon)\sin t\cos^2 t\right)(-\cos t)\epsilon dt = 0, \tag{A.3.82}$$

$$
\begin{aligned}
&3\frac{-k}{\pi\epsilon^2}\frac{\dot{\rho}^2\dot{\phi}\boldsymbol{e}_\phi}{96\pi}\int_0^{2\pi}\left(-\epsilon^2\rho\mathcal{K}_1(\epsilon)\sin t-2\epsilon^3\mathcal{K}_1(\epsilon)\sin t\cos t+\epsilon^3\rho\mathcal{K}_0(\epsilon)\sin t\cos^2 t\right)(-\sin t)\epsilon dt\\
&\qquad=\frac{k}{\pi\epsilon^2}\frac{\dot{\rho}^2\dot{\phi}\boldsymbol{e}_\phi}{32\pi}\left(-\epsilon\rho\mathcal{K}_1(\epsilon)+\frac{\epsilon^2}{4}\rho\mathcal{K}_0(\epsilon)\right)=-\frac{k}{\pi\epsilon^2}\frac{\dot{\rho}^2\rho\dot{\phi}\boldsymbol{e}_\phi}{32\pi}.
\end{aligned}
\tag{A.3.83}
$$

Term proportional to $\dot{\rho}\dot{\phi}^2$

By differentiating the both sides of Eq. (A.3.73) with regard to θ, we have

$$
\begin{aligned}
&-\frac{1}{96\pi}r\sin(\theta-\phi)\left(r^2+\rho^2-2r\rho\cos(\theta-\phi)\right)\mathcal{K}_2\left(\sqrt{r^2+\rho^2-2r\rho\cos(\theta-\phi)}\right)\\
&-\frac{2}{96\pi}r\rho\sin(\theta-\phi)(\rho-r\cos(\theta-\phi))\mathcal{K}_2\left(\sqrt{r^2+\rho^2-2r\rho\cos(\theta-\phi)}\right)\\
&-\frac{1}{96\pi}r\rho\sin(\theta-\phi)(\rho-r\cos(\theta-\phi))\sqrt{r^2+\rho^2-2r\rho\cos(\theta-\phi)}\mathcal{K}_2{}'\left(\sqrt{r^2+\rho^2-2r\rho\cos(\theta-\phi)}\right)\\
&\qquad=\frac{1}{2\pi}\sum_{m=-\infty}^{\infty}\int_0^\infty\frac{ikm}{(k^2+1)^4}\mathcal{J}_m{}'(k\rho(t))\mathcal{J}_m(kr)e^{im(\theta-\phi(t))}kdk.
\end{aligned}
\tag{A.3.84}
$$

Using the relation $z\mathcal{K}_\nu{}'(z)+\nu\mathcal{K}_\nu(z)=-z\mathcal{K}_{\nu-1}(z)$, we have

$$
\begin{aligned}
&-\frac{1}{96\pi}r\sin(\theta-\phi)\left(r^2+\rho^2-2r\rho\cos(\theta-\phi)\right)\mathcal{K}_2\left(\sqrt{r^2+\rho^2-2r\rho\cos(\theta-\phi)}\right)\\
&+\frac{1}{96\pi}r\rho\sin(\theta-\phi)(\rho-r\cos(\theta-\phi))\sqrt{r^2+\rho^2-2r\rho\cos(\theta-\phi)}\mathcal{K}_1\left(\sqrt{r^2+\rho^2-2r\rho\cos(\theta-\phi)}\right)\\
&\qquad=\frac{1}{2\pi}\sum_{m=-\infty}^{\infty}\int_0^\infty\frac{ikm}{(k^2+1)^4}\mathcal{J}_m{}'(k\rho(t))\mathcal{J}_m(kr)e^{im(\theta-\phi(t))}kdk.
\end{aligned}
\tag{A.3.85}
$$

By differentiating the both sides of Eq. (A.3.85) with regard to θ, we have

$$
\begin{aligned}
&-\frac{1}{96\pi}r\cos(\theta-\phi)\left(r^2+\rho^2-2r\rho\cos(\theta-\phi)\right)\mathcal{K}_2\left(\sqrt{r^2+\rho^2-2r\rho\cos(\theta-\phi)}\right)\\
&-\frac{2}{96\pi}r^2\rho\sin^2(\theta-\phi)\mathcal{K}_2\left(\sqrt{r^2+\rho^2-2r\rho\cos(\theta-\phi)}\right)\\
&-\frac{1}{96\pi}r^2\rho\sin^2(\theta-\phi)\sqrt{r^2+\rho^2-2r\rho\cos(\theta-\phi)}\mathcal{K}_2{}'\left(\sqrt{r^2+\rho^2-2r\rho\cos(\theta-\phi)}\right)\\
&+\frac{1}{96\pi}r\rho\cos(\theta-\phi)(\rho-r\cos(\theta-\phi))\sqrt{r^2+\rho^2-2r\rho\cos(\theta-\phi)}\mathcal{K}_1\left(\sqrt{r^2+\rho^2-2r\rho\cos(\theta-\phi)}\right)\\
&+\frac{1}{96\pi}r^2\rho\sin^2(\theta-\phi)\sqrt{r^2+\rho^2-2r\rho\cos(\theta-\phi)}\mathcal{K}_1\left(\sqrt{r^2+\rho^2-2r\rho\cos(\theta-\phi)}\right)\\
&+\frac{1}{96\pi}\frac{r^2\rho^2\sin^2(\theta-\phi)(\rho-r\cos(\theta-\phi))}{\sqrt{r^2+\rho^2-2r\rho\cos(\theta-\phi)}}\mathcal{K}_1\left(\sqrt{r^2+\rho^2-2r\rho\cos(\theta-\phi)}\right)\\
&+\frac{1}{96\pi}r^2\rho^2\sin^2(\theta-\phi)(\rho-r\cos(\theta-\phi))\mathcal{K}_1{}'\left(\sqrt{r^2+\rho^2-2r\rho\cos(\theta-\phi)}\right)\\
&\qquad=\frac{1}{2\pi}\sum_{m=-\infty}^{\infty}\int_0^\infty\frac{-km^2}{(k^2+1)^4}\mathcal{J}_m{}'(k\rho(t))\mathcal{J}_m(kr)e^{im(\theta-\phi(t))}kdk.
\end{aligned}
\tag{A.3.86}
$$

Using the relation $z\mathcal{K}_\nu{}'(z) + \nu\mathcal{K}_\nu(z) = -z\mathcal{K}_{\nu-1}(z)$, we have

$$\begin{aligned}
&-\frac{1}{96\pi} r\cos(\theta-\phi)\left(r^2+\rho^2-2r\rho\cos(\theta-\phi)\right)\mathcal{K}_2\left(\sqrt{r^2+\rho^2-2r\rho\cos(\theta-\phi)}\right) \\
&+\frac{2}{96\pi} r^2\rho\sin^2(\theta-\phi)\sqrt{r^2+\rho^2-2r\rho\cos(\theta-\phi)}\mathcal{K}_1\left(\sqrt{r^2+\rho^2-2r\rho\cos(\theta-\phi)}\right) \\
&+\frac{1}{96\pi} r\rho\cos(\theta-\phi)(\rho-r\cos(\theta-\phi))\sqrt{r^2+\rho^2-2r\rho\cos(\theta-\phi)}\mathcal{K}_1\left(\sqrt{r^2+\rho^2-2r\rho\cos(\theta-\phi)}\right) \\
&+\frac{1}{96\pi} r^2\rho^2\sin^2(\theta-\phi)(\rho-r\cos(\theta-\phi))\mathcal{K}_0\left(\sqrt{r^2+\rho^2-2r\rho\cos(\theta-\phi)}\right) \\
&\quad=\frac{1}{2\pi}\sum_{m=-\infty}^{\infty}\int_0^\infty \frac{-km^2}{(k^2+1)^4}\mathcal{J}_m{}'(k\rho(t))\mathcal{J}_m(kr)e^{im(\theta-\phi(t))}kdk. \qquad \text{(A.3.87)}
\end{aligned}$$

The term proportional to $\dot\rho\dot\phi^2$ is calculated using Eq. (A.3.87). We multiply the both sides of Eq. (A.3.87) by $3\cos t$ and $3\sin t$ and integrate them on the small circle with the radius of ϵ around $\boldsymbol{r}=\boldsymbol{\rho}$ for $\boldsymbol{e}_\rho$ and $\boldsymbol{e}_\phi$ directions, respectively. Here we set $\epsilon = \sqrt{r^2+\rho^2-2r\rho\cos(\theta-\phi)}$ and $\rho - r\cos(\theta-\phi) = \epsilon\cos t$.

$$\begin{aligned}
&3\frac{-k}{\pi\epsilon^2}\frac{\dot\rho\dot\phi^2\boldsymbol{e}_\rho}{96\pi}\int_0^{2\pi}\left(-(\rho-\epsilon\cos t)\epsilon^2\mathcal{K}_2(\epsilon)+2\epsilon^3\rho\mathcal{K}_1(\epsilon)\sin^2 t+\epsilon^2\mathcal{K}_1(\epsilon)\rho(\rho-\epsilon\cos t)\cos t\right. \\
&\qquad\qquad\left.-\epsilon^3\rho^3\mathcal{K}_0(\epsilon)\sin^2 t\cos t\right)(-\cos t)\epsilon dt \\
&\quad= k\frac{\dot\rho\dot\phi^2\boldsymbol{e}_\rho}{32\pi}\left(-\epsilon^2\mathcal{K}_2(\epsilon)-\epsilon\rho^2\mathcal{K}_1(\epsilon)+\frac{\epsilon^2\rho^3}{4}\mathcal{K}_0(\epsilon)\right) = k\frac{\dot\rho\dot\phi^2\boldsymbol{e}_\rho}{32\pi}(-2+\rho^2), \qquad \text{(A.3.88)}
\end{aligned}$$

$$\begin{aligned}
&3\frac{-k}{\pi\epsilon^2}\frac{\dot\rho\dot\phi^2\boldsymbol{e}_\phi}{96\pi}\int_0^{2\pi}\left(-(\rho-\epsilon\cos t)\epsilon^2\mathcal{K}_2(\epsilon)+2\epsilon^3\rho\mathcal{K}_1(\epsilon)\sin^2 t+\epsilon^2\mathcal{K}_1(\epsilon)\rho(\rho-\epsilon\cos t)\cos t\right. \\
&\qquad\qquad\left.-\epsilon^3\rho^3\sin^2 t\cos t\mathcal{K}_0(\epsilon)\right)(-\sin t)\epsilon dt \\
&\quad= 0. \qquad \text{(A.3.89)}
\end{aligned}$$

Term proportional to $\dot\phi^3$

By differentiating the both sides of Eq. (A.3.71) with regard to θ, we have

$$\begin{aligned}
&\frac{3}{96\pi} r\rho\sin(\theta-\phi)\sqrt{r^2+\rho^2-2r\rho\cos(\theta-\phi)}\mathcal{K}_3\left(\sqrt{r^2+\rho^2-2r\rho\cos(\theta-\phi)}\right) \\
&+\frac{1}{96\pi} r\rho\sin(\theta-\phi)\left(r^2+\rho^2-2r\rho\cos(\theta-\phi)\right)\mathcal{K}_3{}'\left(\sqrt{r^2+\rho^2-2r\rho\cos(\theta-\phi)}\right) \\
&\quad=\frac{1}{2\pi}\sum_{m=-\infty}^{\infty}\int_0^\infty \frac{im}{(k^2+1)^4}\mathcal{J}_m(k\rho(t))\mathcal{J}_m(kr)e^{im(\theta-\phi(t))}kdk. \qquad \text{(A.3.90)}
\end{aligned}$$

From the formula $z\mathcal{K}_\nu{}'(z) + \nu\mathcal{K}_\nu(z) = -z\mathcal{K}_{\nu-1}$, we have

$$\begin{aligned}
&-\frac{1}{96\pi} r\rho\sin(\theta-\phi)\left(r^2+\rho^2-2r\rho\cos(\theta-\phi)\right)\mathcal{K}_2\left(\sqrt{r^2+\rho^2-2r\rho\cos(\theta-\phi)}\right) \\
&\quad=\frac{1}{2\pi}\sum_{m=-\infty}^{\infty}\int_0^\infty \frac{im}{(k^2+1)^4}\mathcal{J}_m(k\rho(t))\mathcal{J}_m(kr)e^{im(\theta-\phi(t))}kdk. \qquad \text{(A.3.91)}
\end{aligned}$$

By differentiating the both sides of Eq. (A.3.91) with regard to θ, we have

$$\begin{aligned}
&-\frac{1}{96\pi} r\rho\cos(\theta-\phi)\left(r^2+\rho^2-2r\rho\cos(\theta-\phi)\right)\mathcal{K}_2\left(\sqrt{r^2+\rho^2-2r\rho\cos(\theta-\phi)}\right)\\
&-\frac{2}{96\pi} r^2\rho^2\sin^2(\theta-\phi)\mathcal{K}_2\left(\sqrt{r^2+\rho^2-2r\rho\cos(\theta-\phi)}\right)\\
&-\frac{1}{96\pi} r^2\rho^2\sin^2(\theta-\phi)\sqrt{r^2+\rho^2-2r\rho\cos(\theta-\phi)}\mathcal{K}_2{}'\left(\sqrt{r^2+\rho^2-2r\rho\cos(\theta-\phi)}\right)\\
&\quad=\frac{1}{2\pi}\sum_{m=-\infty}^{\infty}\int_0^{\infty}\frac{-m^2}{(k^2+1)^4}\mathcal{J}_m(k\rho(t))\mathcal{J}_m(kr)e^{im(\theta-\phi(t))}kdk. \qquad \text{(A.3.92)}
\end{aligned}$$

Using the relation $z\mathcal{K}_\nu{}'(z)+\nu\mathcal{K}_\nu(z)=-z\mathcal{K}_{\nu-1}$, we have

$$\begin{aligned}
&-\frac{1}{96\pi} r\rho\cos(\theta-\phi)\left(r^2+\rho^2-2r\rho\cos(\theta-\phi)\right)\mathcal{K}_2\left(\sqrt{r^2+\rho^2-2r\rho\cos(\theta-\phi)}\right)\\
&+\frac{1}{96\pi} r^2\rho^2\sin^2(\theta-\phi)\sqrt{r^2+\rho^2-2r\rho\cos(\theta-\phi)}\mathcal{K}_1\left(\sqrt{r^2+\rho^2-2r\rho\cos(\theta-\phi)}\right)\\
&\quad=\frac{1}{2\pi}\sum_{m=-\infty}^{\infty}\int_0^{\infty}\frac{-m^2}{(k^2+1)^4}\mathcal{J}_m(k\rho(t))\mathcal{J}_m(kr)e^{im(\theta-\phi(t))}kdk. \qquad \text{(A.3.93)}
\end{aligned}$$

By differentiating the both sides of Eq. (A.3.93) with regard to θ, we have

$$\begin{aligned}
&\frac{1}{96\pi} r\rho\sin(\theta-\phi)\left(r^2+\rho^2-2r\rho\cos(\theta-\phi)\right)\mathcal{K}_2\left(\sqrt{r^2+\rho^2-2r\rho\cos(\theta-\phi)}\right)\\
&-\frac{2}{96\pi} r^2\rho^2\sin(\theta-\phi)\cos(\theta-\phi)\mathcal{K}_2\left(\sqrt{r^2+\rho^2-2r\rho\cos(\theta-\phi)}\right)\\
&-\frac{1}{96\pi} r^2\rho^2\sin(\theta-\phi)\cos(\theta-\phi)\sqrt{r^2+\rho^2-2r\rho\cos(\theta-\phi)}\mathcal{K}_2{}'\left(\sqrt{r^2+\rho^2-2r\rho\cos(\theta-\phi)}\right)\\
&+\frac{2}{96\pi} r^2\rho^2\sin(\theta-\phi)\cos(\theta-\phi)\sqrt{r^2+\rho^2-2r\rho\cos(\theta-\phi)}\mathcal{K}_1\left(\sqrt{r^2+\rho^2-2r\rho\cos(\theta-\phi)}\right)\\
&+\frac{1}{96\pi}\frac{r^3\rho^3\sin^3(\theta-\phi)}{\sqrt{r^2+\rho^2-2r\rho\cos(\theta-\phi)}}\mathcal{K}_1\left(\sqrt{r^2+\rho^2-2r\rho\cos(\theta-\phi)}\right)\\
&+\frac{1}{96\pi} r^3\rho^3\sin^3(\theta-\phi)\mathcal{K}_1{}'\left(\sqrt{r^2+\rho^2-2r\rho\cos(\theta-\phi)}\right)\\
&\quad=\frac{1}{2\pi}\sum_{m=-\infty}^{\infty}\int_0^{\infty}\frac{-im^3}{(k^2+1)^4}\mathcal{J}_m(k\rho(t))\mathcal{J}_m(kr)e^{-im(\theta-\phi(t))}kdk. \qquad \text{(A.3.94)}
\end{aligned}$$

Using the relation $z\mathcal{K}_\nu{}'(z)+\nu\mathcal{K}_\nu(z)=-z\mathcal{K}_{\nu-1}(z)$, we have

$$\begin{aligned}
&\frac{1}{96\pi} r\rho\sin(\theta-\phi)\left(r^2+\rho^2-2r\rho\cos(\theta-\phi)\right)\mathcal{K}_2\left(\sqrt{r^2+\rho^2-2r\rho\cos(\theta-\phi)}\right)\\
&+\frac{3}{96\pi} r^2\rho^2\sin(\theta-\phi)\cos(\theta-\phi)\sqrt{r^2+\rho^2-2r\rho\cos(\theta-\phi)}\mathcal{K}_1\left(\sqrt{r^2+\rho^2-2r\rho\cos(\theta-\phi)}\right)\\
&-\frac{1}{96\pi} r^3\rho^3\sin^3(\theta-\phi)\mathcal{K}_0\left(\sqrt{r^2+\rho^2-2r\rho\cos(\theta-\phi)}\right)\\
&\quad=\frac{1}{2\pi}\sum_{m=-\infty}^{\infty}\int_0^{\infty}\frac{-im^3}{(k^2+1)^4}\mathcal{J}_m(k\rho(t))\mathcal{J}_m(kr)e^{-im(\theta-\phi(t))}kdk. \qquad \text{(A.3.95)}
\end{aligned}$$

The term proportional to $\dot{\phi}^3$ is calculated using Eq. (A.3.95). We multiply to the both sides of Eq. (A.3.95) by $\cos t$ and $-\sin t$ and integrate them on the small circle with the radius of ϵ around $\boldsymbol{r} = \boldsymbol{\rho}$ for $\boldsymbol{e}_\rho$ and $\boldsymbol{e}_\phi$ directions, respectively. Here we set $\epsilon = \sqrt{r^2+\rho^2-2r\rho\cos(\theta-\phi)}$ and $\rho - r\cos(\theta-\phi) = \epsilon\cos t$.

$$\frac{k}{\pi\epsilon^2}\frac{\dot{\phi}^3\boldsymbol{e}_\rho}{96\pi}\int_0^{2\pi}\left(-\epsilon^3\rho\mathcal{K}_2(\epsilon)\sin t - 3\epsilon^2\rho^2\sin t(\rho-\cos t)\mathcal{K}_1(\epsilon)+\epsilon^3\rho^3\mathcal{K}_0(\epsilon)\sin^3 t\right)(-\cos t)\epsilon dt = 0, \tag{A.3.96}$$

$$\begin{aligned}\frac{k}{\pi\epsilon^2}\frac{\dot{\phi}^3\boldsymbol{e}_\phi}{96\pi}&\int_0^{2\pi}\left(-\epsilon^3\rho\mathcal{K}_2(\epsilon)\sin t - 3\epsilon^2\rho^2\sin t(\rho-\cos t)\mathcal{K}_1(\epsilon)+\epsilon^3\rho^3\mathcal{K}_0(\epsilon)\sin^3 t\right)(-\sin t)\epsilon dt\\ &= k\frac{\dot{\phi}^3\boldsymbol{e}_\phi}{96\pi}\left(\epsilon^2\rho\mathcal{K}_2(\epsilon)+3\epsilon\rho^3\mathcal{K}_1(\epsilon)-\frac{\epsilon^2}{4}\rho^3\mathcal{K}_0(\epsilon)\right) = k\frac{\dot{\phi}^3\boldsymbol{e}_\phi}{96\pi}(2\rho+3\rho^3).\end{aligned} \tag{A.3.97}$$

Results

The driving force is obtained as follows:

$$\begin{aligned}\boldsymbol{F} =&\frac{k}{4\pi}\left(-\gamma_{\text{Euler}}+\log\frac{2}{\epsilon}\right)\left(\dot{\rho}\boldsymbol{e}_\rho+\rho\dot{\phi}\boldsymbol{e}_\phi\right)-\frac{k}{16\pi}\left\{\left(\ddot{\rho}-\rho\dot{\phi}^2\right)\boldsymbol{e}_\rho+\left(\rho\ddot{\phi}+2\dot{\rho}\dot{\phi}\right)\boldsymbol{e}_\phi\right\}\\ &-\frac{k}{32\pi}\left\{\dot{\rho}\left(\dot{\rho}^2+\rho^2\dot{\phi}^2\right)\boldsymbol{e}_\rho+\rho\dot{\phi}\left(\dot{\rho}^2+\rho^2\dot{\phi}^2\right)\boldsymbol{e}_\phi\right\}+\frac{k}{48\pi}\left\{-3\dot{\rho}\dot{\phi}^2\boldsymbol{e}_\rho+\rho\dot{\phi}^3\boldsymbol{e}_\phi\right\}.\end{aligned} \tag{A.3.98}$$

When the positional vector is represented as $\boldsymbol{\rho} = \rho\boldsymbol{e}_\rho$, then the velocity $\dot{\boldsymbol{\rho}}$, acceleration $\ddot{\boldsymbol{\rho}}$, and jerk (time derivative of acceleration) $\dddot{\boldsymbol{\rho}}$ are expressed as

$$\dot{\boldsymbol{\rho}} =\dot{\rho}\boldsymbol{e}_\rho+\rho\dot{\phi}\boldsymbol{e}_\phi, \tag{A.3.99}$$
$$\ddot{\boldsymbol{\rho}} =\left(\ddot{\rho}-\rho\dot{\phi}^2\right)\boldsymbol{e}_\rho+\left(\rho\ddot{\phi}+2\dot{\rho}\dot{\phi}\right)\boldsymbol{e}_\phi, \tag{A.3.100}$$
$$\dddot{\boldsymbol{\rho}} =\left(\dddot{\rho}-3\dot{\rho}\dot{\phi}^2-3\rho\dot{\phi}\ddot{\phi}\right)\boldsymbol{e}_\rho+\left(\rho\dddot{\phi}+3\ddot{\rho}\dot{\phi}+3\dot{\rho}\ddot{\phi}-\rho\dot{\phi}^3\right)\boldsymbol{e}_\phi. \tag{A.3.101}$$

Thus the driving force is expressed as

$$\begin{aligned}\boldsymbol{F} =&\frac{k}{4\pi}\left(-\gamma_{\text{Euler}}+\log\frac{2}{\epsilon}\right)\left(\dot{\rho}\boldsymbol{e}_\rho+\rho\dot{\phi}\boldsymbol{e}_\phi\right)-\frac{k}{16\pi}\left\{\left(\ddot{\rho}-\rho\dot{\phi}^2\right)\boldsymbol{e}_\rho+\left(\rho\ddot{\phi}+2\dot{\rho}\dot{\phi}\right)\boldsymbol{e}_\phi\right\}\\ &-\frac{k}{32\pi}\left\{\dot{\rho}\left(\dot{\rho}^2+\rho^2\dot{\phi}^2\right)\boldsymbol{e}_\rho+\rho\dot{\phi}\left(\dot{\rho}^2+\rho^2\dot{\phi}^2\right)\boldsymbol{e}_\phi\right\},\end{aligned} \tag{A.3.102}$$

where we neglected the terms related to the jerk. In vector form, we have

$$\boldsymbol{F} = \frac{k}{4\pi}\left(-\gamma_{\text{Euler}}+\log\frac{2}{\epsilon}\right)\dot{\boldsymbol{\rho}}-\frac{k}{16\pi}\ddot{\boldsymbol{\rho}}-\frac{k}{32\pi}\left|\dot{\boldsymbol{\rho}}\right|^2\dot{\boldsymbol{\rho}}. \tag{A.3.103}$$

The righthand side of the expanded concentration field in Eq. (A.3.31) is also obtained as follows:

$$
\begin{aligned}
&c(\boldsymbol{r};\boldsymbol{\rho}) \qquad\qquad\qquad\qquad\qquad\qquad\qquad\qquad\qquad\qquad\qquad\qquad\qquad\qquad\qquad (\text{A.3.104})\\
&= \frac{1}{2\pi}\mathcal{K}_0\left(|\boldsymbol{r}-\boldsymbol{\rho}|\right) - \frac{1}{4\pi}\mathcal{K}_0\left(|\boldsymbol{r}-\boldsymbol{\rho}|\right)(\boldsymbol{r}-\boldsymbol{\rho})\cdot\dot{\boldsymbol{\rho}} + \frac{1}{16\pi}|\boldsymbol{r}-\boldsymbol{\rho}|\mathcal{K}_1\left(|\boldsymbol{r}-\boldsymbol{\rho}|\right)(\boldsymbol{r}-\boldsymbol{\rho})\cdot\ddot{\boldsymbol{\rho}}\\
&\quad + \frac{1}{16\pi}|\dot{\boldsymbol{\rho}}|^2\mathcal{K}_0\left(|\boldsymbol{r}-\boldsymbol{\rho}|\right) + \frac{1}{16\pi}\mathcal{K}_0\left(|\boldsymbol{r}-\boldsymbol{\rho}|\right)\left((\boldsymbol{r}-\boldsymbol{\rho})\cdot\dot{\boldsymbol{\rho}}\right)^2 + \frac{1}{32\pi}|\dot{\boldsymbol{\rho}}|^2|\boldsymbol{r}-\boldsymbol{\rho}|\mathcal{K}_1\left(|\boldsymbol{r}-\boldsymbol{\rho}|\right)(\boldsymbol{r}-\boldsymbol{\rho})\cdot\dot{\boldsymbol{\rho}}\\
&\quad - \frac{1}{96\pi}\mathcal{K}_0\left(|\boldsymbol{r}-\boldsymbol{\rho}|\right)\left((\boldsymbol{r}-\boldsymbol{\rho})\cdot\dot{\boldsymbol{\rho}}\right)^3 + \frac{1}{32\pi}|\boldsymbol{r}-\boldsymbol{\rho}|^2\mathcal{K}_2\left(|\boldsymbol{r}-\boldsymbol{\rho}|\right)\dot{\boldsymbol{\rho}}\cdot\ddot{\boldsymbol{\rho}}\\
&\quad - \frac{1}{32\pi}|\boldsymbol{r}-\boldsymbol{\rho}|\mathcal{K}_1\left(|\boldsymbol{r}-\boldsymbol{\rho}|\right)\left((\boldsymbol{r}-\boldsymbol{\rho})\cdot\dot{\boldsymbol{\rho}}\right)\left((\boldsymbol{r}-\boldsymbol{\rho})\cdot\ddot{\boldsymbol{\rho}}\right) - \frac{1}{96\pi}|\boldsymbol{r}-\boldsymbol{\rho}|^2\mathcal{K}_2\left(|\boldsymbol{r}-\boldsymbol{\rho}|\right)(\boldsymbol{r}-\boldsymbol{\rho})\cdot\dddot{\boldsymbol{\rho}} \qquad (\text{A.3.105})\\
&= c_{00}\left(|\boldsymbol{r}-\boldsymbol{\rho}|\right) + c_{10}\left(|\boldsymbol{r}-\boldsymbol{\rho}|\right)(\boldsymbol{r}-\boldsymbol{\rho})\cdot\dot{\boldsymbol{\rho}} + c_{20}\left(|\boldsymbol{r}-\boldsymbol{\rho}|\right)(\boldsymbol{r}-\boldsymbol{\rho})\cdot\ddot{\boldsymbol{\rho}} + c_{21}\left(|\boldsymbol{r}-\boldsymbol{\rho}|\right)|\dot{\boldsymbol{\rho}}|^2\\
&\quad + c_{22}\left(|\boldsymbol{r}-\boldsymbol{\rho}|\right)\left[(\boldsymbol{r}-\boldsymbol{\rho})\cdot\dot{\boldsymbol{\rho}}\right]^2 + c_{30}\left(|\boldsymbol{r}-\boldsymbol{\rho}|\right)(\boldsymbol{r}-\boldsymbol{\rho})\cdot\dddot{\boldsymbol{\rho}} + c_{31}\left(|\boldsymbol{r}-\boldsymbol{\rho}|\right)|\dot{\boldsymbol{\rho}}|^2(\boldsymbol{r}-\boldsymbol{\rho})\cdot\dot{\boldsymbol{\rho}}\\
&\quad + c_{32}\left(|\boldsymbol{r}-\boldsymbol{\rho}|\right)\left[(\boldsymbol{r}-\boldsymbol{\rho})\cdot\dot{\boldsymbol{\rho}}\right]^3 + c_{33}\left(|\boldsymbol{r}-\boldsymbol{\rho}|\right)\dot{\boldsymbol{\rho}}\cdot\ddot{\boldsymbol{\rho}} + c_{34}\left(|\boldsymbol{r}-\boldsymbol{\rho}|\right)\left[(\boldsymbol{r}-\boldsymbol{\rho})\cdot\dot{\boldsymbol{\rho}}\right]\left[(\boldsymbol{r}-\boldsymbol{\rho})\cdot\ddot{\boldsymbol{\rho}}\right]. \qquad (\text{A.3.106})
\end{aligned}
$$

Here we used Eqs. (A.3.32), (A.3.37), (A.3.41), (A.3.49), (A.3.53), (A.3.57), (A.3.61), (A.3.65), (A.3.77), (A.3.81), (A.3.87), and (A.3.95), and defined the following functions:

$$
\begin{aligned}
c_{00}\left(|\boldsymbol{r}-\boldsymbol{\rho}|\right) &= \frac{1}{2\pi}\mathcal{K}_0\left(|\boldsymbol{r}-\boldsymbol{\rho}|\right), & c_{10}\left(|\boldsymbol{r}-\boldsymbol{\rho}|\right) &= -\frac{1}{4\pi}\mathcal{K}_0\left(|\boldsymbol{r}-\boldsymbol{\rho}|\right),\\
c_{20}\left(|\boldsymbol{r}-\boldsymbol{\rho}|\right) &= \frac{1}{16\pi}|\boldsymbol{r}-\boldsymbol{\rho}|\mathcal{K}_1\left(|\boldsymbol{r}-\boldsymbol{\rho}|\right), & c_{21}\left(|\boldsymbol{r}-\boldsymbol{\rho}|\right) &= -\frac{1}{16\pi}|\boldsymbol{r}-\boldsymbol{\rho}|\mathcal{K}_1\left(|\boldsymbol{r}-\boldsymbol{\rho}|\right),\\
c_{22}\left(|\boldsymbol{r}-\boldsymbol{\rho}|\right) &= \frac{1}{16\pi}\mathcal{K}_0\left(|\boldsymbol{r}-\boldsymbol{\rho}|\right), & c_{30}\left(|\boldsymbol{r}-\boldsymbol{\rho}|\right) &= -\frac{1}{96\pi}|\boldsymbol{r}-\boldsymbol{\rho}|^2\mathcal{K}_2\left(|\boldsymbol{r}-\boldsymbol{\rho}|\right),\\
c_{31}\left(|\boldsymbol{r}-\boldsymbol{\rho}|\right) &= \frac{1}{32\pi}|\boldsymbol{r}-\boldsymbol{\rho}|\mathcal{K}_1\left(|\boldsymbol{r}-\boldsymbol{\rho}|\right), & c_{32}\left(|\boldsymbol{r}-\boldsymbol{\rho}|\right) &= -\frac{1}{96\pi}\mathcal{K}_0\left(|\boldsymbol{r}-\boldsymbol{\rho}|\right),\\
c_{33}\left(|\boldsymbol{r}-\boldsymbol{\rho}|\right) &= \frac{1}{32\pi}|\boldsymbol{r}-\boldsymbol{\rho}|^2\mathcal{K}_2\left(|\boldsymbol{r}-\boldsymbol{\rho}|\right), & c_{34}\left(|\boldsymbol{r}-\boldsymbol{\rho}|\right) &= -\frac{1}{32\pi}|\boldsymbol{r}-\boldsymbol{\rho}|\mathcal{K}_1\left(|\boldsymbol{r}-\boldsymbol{\rho}|\right). \qquad (\text{A.3.107})
\end{aligned}
$$

The terms in Eq. (A.3.107) for the camphor particle located at $\boldsymbol{\rho} = (\rho, \phi) = (0.1, 0)$ in the water chamber with a radius of $R = 1$ are plotted in Fig. A.3.2.

A.3.3 Derivation of Eq. (2.4.58)

Equation (2.4.57) is

$$
\begin{aligned}
c_{mn}(t) &= \int_{-\infty}^{t} \mathcal{J}_{|m|}(k_{mn}\rho(t'))e^{-im\phi(t')}e^{-({k_{mn}}^2+1)(t-t')}dt'\\
&= e^{-({k_{mn}}^2+1)t}\int_{-\infty}^{t} \mathcal{J}_{|m|}(k_{mn}\rho(t'))e^{-im\phi(t')}e^{({k_{mn}}^2+1)t'}dt'\\
&= e^{-({k_{mn}}^2+1)t}I, \qquad (\text{A.3.108})
\end{aligned}
$$

where I is defined as

$$
I = \int_{-\infty}^{t} \mathcal{J}_{|m|}(k_{mn}\rho(t'))e^{-im\phi(t')}e^{({k_{mn}}^2+1)t'}dt'. \qquad (\text{A.3.109})
$$

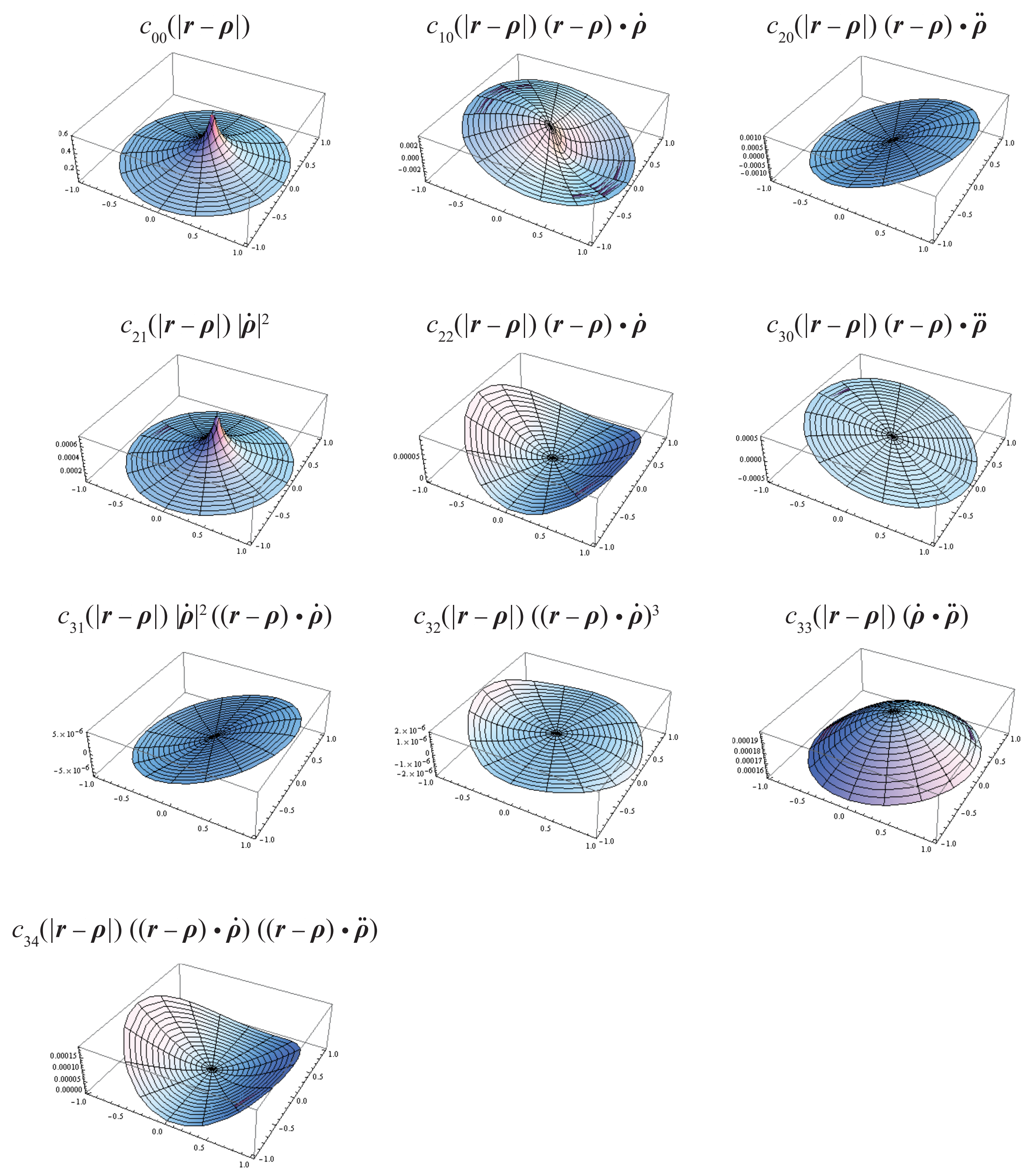

Figure A.3.2: Concentration fields expanded with regarded to the position, velocity, acceleration, and jerk shown in Eq. (A.3.106). The radius of the water chamber R is $R = 1$. Here we set $\boldsymbol{\rho} = (\rho, \phi) = (0.1, 0)$, $\dot{\boldsymbol{\rho}} = (\dot{\rho}, \dot{\phi}) = (0.1, 0)$, $\ddot{\boldsymbol{\rho}} = (\ddot{\rho}, \ddot{\phi}) = (0.1, 0)$, and $\dddot{\boldsymbol{\rho}} = (\dddot{\rho}, \dddot{\phi}) = (0.1, 0)$.

By expanding I using the partial integration, we have

$$
\begin{aligned}
&\int_{-\infty}^{t} \mathcal{J}_{|m|}(k\rho(t'))e^{-im\phi(t')}e^{At'}dt' \\
&= \frac{1}{A}\mathcal{J}_{|m|}(k\rho(t))e^{-im\phi(t)}e^{At} - \frac{1}{A^2}\left\{k\dot{\rho}(t)\mathcal{J}'_{|m|}(k\rho(t)) - im\dot{\phi}(t)\mathcal{J}_{|m|}(k\rho(t))\right\}e^{-im\phi(t)}e^{At} \\
&\quad + \frac{1}{A^3}\left\{k\ddot{\rho}(t)\mathcal{J}'_{|m|}(k\rho(t)) + k^2(\dot{\rho}(t))^2\mathcal{J}''_{|m|}(k\rho(t))\right. \\
&\qquad \left. -2ikm\dot{\rho}(t)\dot{\phi}(t)\mathcal{J}'_{|m|}(k\rho(t)) - im\ddot{\phi}(t)\mathcal{J}_{|m|}(k\rho(t)) - m^2(\dot{\phi}(t))^2\mathcal{J}_{|m|}(k\rho(t))\right\}e^{-im\phi(t)}e^{At} \\
&\quad - \frac{1}{A^4}\left\{k\dddot{\rho}(t)\mathcal{J}'_{|m|}(k\rho(t)) + k^2\dot{\rho}(t)\ddot{\rho}(t)\mathcal{J}''_{|m|}(k\rho(t)) - 3ikm\ddot{\rho}(t)\dot{\phi}(t)\mathcal{J}'_{|m|}(k\rho(t)) + k^3(\dot{\rho}(t))^3\mathcal{J}'''_{|m|}(k\rho(t))\right. \\
&\qquad - 3ik^2m(\dot{\rho}(t))^2\dot{\phi}(t)\mathcal{J}''_{|m|}(k\rho(t)) - 3ikm\dot{\rho}(t)\ddot{\phi}(t)\mathcal{J}'_{|m|}(k\rho(t)) - 3km^2\dot{\rho}(t)(\dot{\phi}(t))^2\mathcal{J}'_{|m|}(k\rho(t)) \\
&\qquad \left. -im\dddot{\phi}(t)\mathcal{J}_{|m|}(k\rho(t)) - 3m^2\dot{\phi}(t)\ddot{\phi}(t)\mathcal{J}_{|m|}(k\rho(t)) + im^3(\dot{\phi}(t))^3\mathcal{J}_{|m|}(k\rho(t))\right\}e^{-im\phi(t)}e^{At} \\
&\quad + \cdots, \qquad \text{(A.3.110)}
\end{aligned}
$$

where we denote $k_{mn} = k$ and ${k_{mn}}^2 + 1 = A$. By truncating the higher-order terms of ρ and high-order time derivatives, we have Eq. (2.4.58).

A.3.4 Derivation of Eq. (2.4.60)

The first term in the righthand side in Eq. (2.4.59) should correspond to the steady state with a fixed camphor particle located at (ρ, ϕ). The steady state is independently obtained as shown in Eq. (2.4.47). Thus we have

$$
\begin{aligned}
&\frac{1}{2\pi}\sum_{m=-\infty}^{\infty}\sum_{n=0}^{\infty} a_{mn}\frac{1}{{k_{mn}}^2+1}\mathcal{J}_{|m|}(k_{mn}\rho)\mathcal{J}_{|m|}(k_{mn}r)e^{im(\theta-\phi)} \\
&\qquad = \frac{1}{2\pi}\mathcal{K}_0\left(\sqrt{r^2+\rho^2-2r\rho\cos(\theta-\phi)}\right) - \frac{1}{2\pi}\sum_{m=-\infty}^{\infty}\frac{{\mathcal{K}_m}'(R)}{{\mathcal{I}_m}'(R)}\mathcal{I}_m(\rho)\mathcal{I}_m(r)e^{im(\theta-\phi)} \\
&\qquad = (\text{main term}) - \frac{1}{2\pi}\sum_{m=-\infty}^{\infty}\frac{{\mathcal{K}_m}'(R)}{{\mathcal{I}_m}'(R)}\mathcal{I}_m(\rho)\mathcal{I}_m(r)e^{im(\theta-\phi)} \\
&\qquad = (\text{main term}) - \frac{1}{2\pi}\frac{{\mathcal{K}_0}'(R)}{{\mathcal{I}_0}'(R)}\mathcal{I}_m(\rho)\mathcal{I}_m(r) - \frac{1}{\pi}\sum_{m=1}^{\infty}\frac{{\mathcal{K}_m}'(R)}{{\mathcal{I}_m}'(R)}\mathcal{I}_m(\rho)\mathcal{I}_m(r)\cos m(\theta-\phi) \\
&\qquad = (\text{main term}) + \sum_{m=0}^{\infty} h_m^{00}(R)g_m^{00}(r,\rho)\cos m(\theta-\phi) \\
&\qquad = (\text{main term}) + a^{01}(R,r) + a^{02}(R,r)\rho^2 + a^{03}(R,r)\rho\cos(\theta-\phi) + a^{04}(R,r)\rho^3\cos(\theta-\phi) \\
&\quad + a^{05}(R,r)\rho^2\cos 2(\theta-\phi) + a^{06}(R,r)\rho^3\cos 3(\theta-\phi) + \mathcal{O}(\rho^4). \qquad \text{(A.3.111)}
\end{aligned}
$$

By changing the length scale, i.e., $\rho \to \lambda\rho$, $r \to \lambda r$, $R \to \lambda R$, $k_{mn} \to k_{mn}/\lambda$, $a_{mn} \to a_{mn}/\lambda^2$, we have

$$\begin{aligned}
&\frac{1}{2\pi}\sum_{m=-\infty}^{\infty}\sum_{n=0}^{\infty} a_{mn}\frac{1}{{k_{mn}}^2+\lambda^2}\mathcal{J}_{|m|}(k_{mn}\rho)\mathcal{J}_{|m|}(k_{mn}r)e^{im(\theta-\phi)} \\
&\quad= (\text{main term}) - \frac{1}{2\pi}\frac{\mathcal{K}_0{}'(\lambda R)}{\mathcal{I}_0{}'(\lambda R)}\mathcal{I}_m(\lambda\rho)\mathcal{I}_m(\lambda r) - \frac{1}{\pi}\sum_{m=1}^{\infty}\frac{\mathcal{K}_m{}'(\lambda R)}{\mathcal{I}_m{}'(\lambda R)}\mathcal{I}_m(\lambda\rho)\mathcal{I}_m(\lambda r)\cos m(\theta-\phi) \\
&\quad= (\text{main term}) + \sum_{m=0}^{\infty}\bar{h}_m^{00}(\lambda, R)\bar{g}_m^{00}(\lambda, r, \rho)\cos m(\theta-\phi). \qquad \text{(A.3.112)}
\end{aligned}$$

Here we do not consider the main term, since the effect by the main term corresponds to the concentration field without boundaries and is already calculated as shown in Eq. (A.3.105). By differentiating the both sides with regard to λ and then dividing the both sides by 2λ, we have

$$\begin{aligned}
&\frac{1}{2\pi}\sum_{m=-\infty}^{\infty}\sum_{n=0}^{\infty} a_{mn}\frac{-1}{({k_{mn}}^2+\lambda^2)^2}\mathcal{J}_{|m|}(k_{mn}\rho)\mathcal{J}_{|m|}(k_{mn}r)e^{im(\theta-\phi)} \\
&\quad= \sum_{m=0}^{\infty}\left(\bar{h}_m^{10}(\lambda, R)\bar{g}_m^{00}(\lambda, r, \rho) + \bar{h}_m^{11}(\lambda, R)\bar{g}_m^{10}(\lambda, r, \rho)\right)\cos m(\theta-\phi). \qquad \text{(A.3.113)}
\end{aligned}$$

By setting λ to be 1, we have

$$\begin{aligned}
&\frac{1}{2\pi}\sum_{m=-\infty}^{\infty}\sum_{n=0}^{\infty} a_{mn}\frac{-1}{({k_{mn}}^2+1)^2}\mathcal{J}_{|m|}(k_{mn}\rho)\mathcal{J}_{|m|}(k_{mn}r)e^{im(\theta-\phi)} \\
&\quad= \sum_{m=0}^{\infty}\left(h_m^{10}(R)g_m^{00}(r, \rho) + h_m^{11}(R)g_m^{10}(r, \rho)\right)\cos m(\theta-\phi). \qquad \text{(A.3.114)}
\end{aligned}$$

By differentiating the both sides of Eq. (A.3.114) with regard to ρ, we have

$$\begin{aligned}
&\frac{1}{2\pi}\sum_{m=-\infty}^{\infty}\sum_{n=0}^{\infty} a_{mn}\frac{-k_{mn}}{({k_{mn}}^2+1)^2}\mathcal{J}'_{|m|}(k_{mn}\rho)\mathcal{J}_{|m|}(k_{mn}r)e^{im(\theta-\phi)} \\
&\quad= \sum_{m=0}^{\infty}\left(h_m^{10}(R)g_m^{01}(r, \rho) + h_m^{11}(R)g_m^{11}(r, \rho)\right)\cos m(\theta-\phi) \\
&\quad= a^{11}(R, r)\rho + a^{12}(R, r)\cos(\theta-\phi) + 3a^{13}(R, r)\rho^2\cos(\theta-\phi) + a^{14}(R, r)\rho\cos 2(\theta-\phi) \\
&\qquad + a^{15}(R, r)\rho^2\cos 3(\theta-\phi) + \mathcal{O}(\rho^3). \qquad \text{(A.3.115)}
\end{aligned}$$

Similarly, by differentiating the both sides of Eq. (A.3.114) with regard to ϕ, we have

$$\begin{aligned}
&\frac{1}{2\pi}\sum_{m=-\infty}^{\infty}\sum_{n=0}^{\infty} a_{mn}\frac{im}{({k_{mn}}^2+1)^2}\mathcal{J}_{|m|}(k_{mn}\rho)\mathcal{J}_{|m|}(k_{mn}r)e^{im(\theta-\phi)} \\
&\quad= \sum_{m=1}^{\infty} m\left(h_m^{10}(R)g_m^{00}(r, \rho) + h_m^{11}(R)g_m^{10}(r, \rho)\right)\sin m(\theta-\phi) \\
&\quad= a^{12}(R, r)\rho\sin(\theta-\phi) + a^{13}(R, r)\rho^3\sin(\theta-\phi) + a^{14}(R, r)\rho^2\sin 2(\theta-\phi) \\
&\qquad + a^{15}(R, r)\rho^3\sin 3(\theta-\phi) + \mathcal{O}(\rho^4). \qquad \text{(A.3.116)}
\end{aligned}$$

By differentiating the both sides of Eq. (A.3.113) with regard to λ and then dividing the both sides by 4λ, we have

$$\begin{aligned}&\frac{1}{2\pi}\sum_{m=-\infty}^{\infty}\sum_{n=0}^{\infty}a_{mn}\frac{1}{({k_{mn}}^2+\lambda^2)^3}\mathcal{J}_{|m|}(k_{mn}\rho)\mathcal{J}_{|m|}(k_{mn}r)e^{im(\theta-\phi)}\\&=\sum_{m=0}^{\infty}\left(\bar{h}_m^{20}(\lambda,R)\bar{g}_m^{00}(\lambda,r,\rho)+\bar{h}_m^{21}(\lambda,R)\bar{g}_m^{10}(\lambda,r,\rho)+\bar{h}_m^{22}(\lambda,R)\bar{g}_m^{20}(\lambda,r,\rho)\right)\cos m(\theta-\phi).\end{aligned} \tag{A.3.117}$$

By setting λ to be 1, we have

$$\begin{aligned}&\frac{1}{2\pi}\sum_{m=-\infty}^{\infty}\sum_{n=0}^{\infty}a_{mn}\frac{1}{({k_{mn}}^2+1)^3}\mathcal{J}_{|m|}(k_{mn}\rho)\mathcal{J}_{|m|}(k_{mn}r)e^{im(\theta-\phi)}\\&=\sum_{m=0}^{\infty}\left(h_m^{20}(R)g_m^{00}(r,\rho)+h_m^{21}(R)g_m^{10}(r,\rho)+h_m^{22}(R)g_m^{20}(r,\rho)\right)\cos m(\theta-\phi).\end{aligned} \tag{A.3.118}$$

By differentiating the both sides of Eq. (A.3.118) with regard to ρ, we have

$$\frac{1}{2\pi}\sum_{m=-\infty}^{\infty}\sum_{n=0}^{\infty}a_{mn}\frac{k_{mn}}{({k_{mn}}^2+1)^3}\mathcal{J}'_{|m|}(k_{mn}\rho)\mathcal{J}_{|m|}(k_{mn}r)e^{im(\theta-\phi)}$$

$$=\sum_{m=0}^{\infty}\left(h_m^{20}(R)g_m^{01}(r,\rho)+h_m^{21}(R)g_m^{11}(r,\rho)+h_m^{22}(R)g_m^{21}(r,\rho)\right)\cos m(\theta-\phi) \tag{A.3.119}$$

$$\begin{aligned}&=a^{21}(R,r)\rho+a^{22}(R,r)\cos(\theta-\phi)+3a^{23}(R,r)\rho^2\cos(\theta-\phi)+a^{24}(R,r)\rho\cos 2(\theta-\phi)\\&\quad+a^{25}(R,r)\rho^2\cos 3(\theta-\phi)+\mathcal{O}(\rho^3).\end{aligned} \tag{A.3.120}$$

By differentiating the both sides of Eq. (A.3.119) with regard to ρ, we have

$$\frac{1}{2\pi}\sum_{m=-\infty}^{\infty}\sum_{n=0}^{\infty}a_{mn}\frac{{k_{mn}}^2}{({k_{mn}}^2+1)^3}\mathcal{J}''_{|m|}(k_{mn}\rho)\mathcal{J}_{|m|}(k_{mn}r)e^{im(\theta-\phi)}$$

$$=\sum_{m=0}^{\infty}\left(h_m^{20}(R)g_m^{02}(r,\rho)+h_m^{21}(R)g_m^{12}(r,\rho)+h_m^{22}(R)g_m^{22}(r,\rho)\right)\cos m(\theta-\phi) \tag{A.3.121}$$

$$=a^{21}(R,r)+6a^{23}(R,r)\rho\cos(\theta-\phi)+a^{24}(R,r)\cos 2(\theta-\phi)+2a^{25}(R,r)\rho\cos 3(\theta-\phi)+\mathcal{O}(\rho^2). \tag{A.3.122}$$

By differentiating the both sides of Eq. (A.3.119) with regard to ϕ, we have

$$\frac{1}{2\pi}\sum_{m=-\infty}^{\infty}\sum_{n=0}^{\infty}a_{mn}\frac{-imk_{mn}}{({k_{mn}}^2+1)^3}\mathcal{J}'_{|m|}(k_{mn}\rho)\mathcal{J}_{|m|}(k_{mn}r)e^{im(\theta-\phi)}$$

$$=\sum_{m=1}^{\infty}m\left(h_m^{20}(R)g_m^{01}(r,\rho)+h_m^{21}(R)g_m^{11}(r,\rho)+h_m^{22}(R)g_m^{21}(r,\rho)\right)\sin m(\theta-\phi) \tag{A.3.123}$$

$$\begin{aligned}&=\frac{1}{2}\left[2a^{22}(R,r)\sin(\theta-\phi)+6a^{23}(R,r)\rho^2\sin(\theta-\phi)+4a^{24}(R,r)\rho\sin 2(\theta-\phi)\right.\\&\quad\left.+6a^{25}(R,r)\rho^2\sin 3(\theta-\phi)\right]+\mathcal{O}(\rho^3).\end{aligned} \tag{A.3.124}$$

By differentiating the both sides of Eq. (A.3.118) with regard to ϕ, we have

$$\begin{aligned}
&\frac{1}{2\pi}\sum_{m=-\infty}^{\infty}\sum_{n=0}^{\infty}a_{mn}\frac{-im}{({k_{mn}}^2+1)^3}\mathcal{J}_{|m|}(k_{mn}\rho)\mathcal{J}_{|m|}(k_{mn}r)e^{im(\theta-\phi)}\\
&\quad=\sum_{m=1}^{\infty}m\left(h_m^{20}(R)g_m^{00}(r,\rho)+h_m^{21}(R)g_m^{10}(r,\rho)+h_m^{22}(R)g_m^{20}(r,\rho)\right)\sin m(\theta-\phi) \qquad \text{(A.3.125)}\\
&\quad=a^{22}(R,r)\rho\sin(\theta-\phi)+a^{23}(R,r)\rho^3\sin(\theta-\phi)+a^{24}(R,r)\rho^2\sin 2(\theta-\phi)\\
&\qquad+a^{25}(R,r)\rho^3\sin 3(\theta-\phi)+\mathcal{O}(\rho^4). \qquad \text{(A.3.126)}
\end{aligned}$$

By differentiating the both sides of Eq. (A.3.125) with regard to ϕ, we have

$$\begin{aligned}
&\frac{1}{2\pi}\sum_{m=-\infty}^{\infty}\sum_{n=0}^{\infty}a_{mn}\frac{-m^2}{({k_{mn}}^2+1)^3}\mathcal{J}_{|m|}(k_{mn}\rho)\mathcal{J}_{|m|}(k_{mn}r)e^{im(\theta-\phi)}\\
&\quad=-\sum_{m=1}^{\infty}m^2\left(h_m^{20}(R)g_m^{00}(r,\rho)+h_m^{21}(R)g_m^{10}(r,\rho)+h_m^{22}(R)g_m^{20}(r,\rho)\right)\cos m(\theta-\phi) \qquad \text{(A.3.127)}\\
&\quad=-a^{22}(R,r)\rho\cos(\theta-\phi)-a^{23}(R,r)\rho^3\cos(\theta-\phi)-2a^{24}(R,r)\rho^2\cos 2(\theta-\phi)\\
&\qquad-3a^{25}(R,r)\rho^3\cos 3(\theta-\phi)+\mathcal{O}(\rho^4). \qquad \text{(A.3.128)}
\end{aligned}$$

By differentiating the both sides of Eq. (A.3.117) with regard to λ and then dividing the both sides by 6λ, we have

$$\begin{aligned}
&\frac{1}{2\pi}\sum_{m=-\infty}^{\infty}\sum_{n=0}^{\infty}a_{mn}\frac{-1}{({k_{mn}}^2+\lambda^2)^4}\mathcal{J}_{|m|}(k_{mn}\rho)\mathcal{J}_{|m|}(k_{mn}r)e^{im(\theta-\phi)}\\
&\quad=\sum_{m=0}^{\infty}\left(\bar{h}_m^{30}(\lambda,R)\bar{g}_m^{00}(\lambda,r,\rho)+\bar{h}_m^{31}(\lambda,R)\bar{g}_m^{10}(\lambda,r,\rho)+\bar{h}_m^{32}(\lambda,R)\bar{g}_m^{20}(\lambda,r,\rho)\right.\\
&\qquad\left.+\bar{h}_m^{33}(\lambda,R)\bar{g}_m^{30}(\lambda,r,\rho)\right)\cos m(\theta-\phi). \qquad \text{(A.3.129)}
\end{aligned}$$

By setting λ to be 1, we have

$$\begin{aligned}
&\frac{1}{2\pi}\sum_{m=-\infty}^{\infty}\sum_{n=0}^{\infty}a_{mn}\frac{-1}{({k_{mn}}^2+1)^4}\mathcal{J}_{|m|}(k_{mn}\rho)\mathcal{J}_{|m|}(k_{mn}r)e^{im(\theta-\phi)}\\
&\quad=\sum_{m=0}^{\infty}\left(h_m^{30}(R)g_m^{00}(r,\rho)+h_m^{31}(R)g_m^{10}(r,\rho)+h_m^{32}(R)g_m^{20}(r,\rho)+h_m^{33}(R)g_m^{30}(r,\rho)\right)\cos m(\theta-\phi).\\
&\qquad \text{(A.3.130)}
\end{aligned}$$

By differentiating the both sides of Eq. (A.3.130) with regard to ρ, we have

$$\begin{aligned}
&\frac{1}{2\pi}\sum_{m=-\infty}^{\infty}\sum_{n=0}^{\infty}a_{mn}\frac{-k_{mn}}{({k_{mn}}^2+1)^4}\mathcal{J}'_{|m|}(k_{mn}\rho)\mathcal{J}_{|m|}(k_{mn}r)e^{im(\theta-\phi)}\\
&\quad=\sum_{m=0}^{\infty}\left(h_m^{30}(R)g_m^{01}(r,\rho)+h_m^{31}(R)g_m^{11}(r,\rho)+h_m^{32}(R)g_m^{21}(r,\rho)+h_m^{33}(R)g_m^{31}(r,\rho)\right)\cos m(\theta-\phi)\\
&\qquad \text{(A.3.131)}\\
&\quad=a^{31}(R,r)\rho+a^{32}(R,r)\rho\cos(\theta-\phi)+3a^{33}(R,r)\rho^2\cos(\theta-\phi)+a^{34}(R,r)\rho\cos 2(\theta-\phi)\\
&\qquad+a^{35}(R,r)\rho^2\cos 3(\theta-\phi)+\mathcal{O}(\rho^3). \qquad \text{(A.3.132)}
\end{aligned}$$

By differentiating the both sides of Eq. (A.3.131) with regard to ρ, we have

$$\frac{1}{2\pi}\sum_{m=-\infty}^{\infty}\sum_{n=0}^{\infty}a_{mn}\frac{-{k_{mn}}^2}{({k_{mn}}^2+1)^4}\mathcal{J}''_{|m|}(k_{mn}\rho)\mathcal{J}_{|m|}(k_{mn}r)e^{im(\theta-\phi)}$$
$$=\sum_{m=0}^{\infty}\left(h_m^{30}(R)g_m^{02}(r,\rho)+h_m^{31}(R)g_m^{12}(r,\rho)+h_m^{32}(R)g_m^{22}(r,\rho)+h_m^{33}(R)g_m^{32}(r,\rho)\right)\cos m(\theta-\phi) \tag{A.3.133}$$
$$=a^{31}(R,r)+6a^{33}(R,r)\rho\cos(\theta-\phi)+a^{34}(R,r)\cos 2(\theta-\phi)+2a^{35}(R,r)\rho\cos 3(\theta-\phi)+\mathcal{O}(\rho^2). \tag{A.3.134}$$

By differentiating the both sides of Eq. (A.3.133) with regard to ρ, we have

$$\frac{1}{2\pi}\sum_{m=-\infty}^{\infty}\sum_{n=0}^{\infty}a_{mn}\frac{-{k_{mn}}^3}{({k_{mn}}^2+1)^4}\mathcal{J}'''_{|m|}(k_{mn}\rho)\mathcal{J}_{|m|}(k_{mn}r)e^{im(\theta-\phi)}$$
$$=\sum_{m=0}^{\infty}\left(h_m^{30}(R)g_m^{03}(r,\rho)+h_m^{31}(R)g_m^{13}(r,\rho)+h_m^{32}(R)g_m^{23}(r,\rho)+h_m^{33}(R)g_m^{33}(r,\rho)\right)\cos m(\theta-\phi) \tag{A.3.135}$$
$$=6a^{33}(R,r)\cos(\theta-\phi)+2a^{35}(R,r)\cos 3(\theta-\phi)+\mathcal{O}(\rho). \tag{A.3.136}$$

By differentiating the both sides of Eq. (A.3.131) with regard to ϕ, we have

$$\frac{1}{2\pi}\sum_{m=-\infty}^{\infty}\sum_{n=0}^{\infty}a_{mn}\frac{-imk_{mn}}{({k_{mn}}^2+1)^4}\mathcal{J}'_{|m|}(k_{mn}\rho)\mathcal{J}_{|m|}(k_{mn}r)e^{im(\theta-\phi)}$$
$$=\sum_{m=1}^{\infty}m\left(h_m^{30}(R)g_m^{01}(r,\rho)+h_m^{31}(R)g_m^{11}(r,\rho)+h_m^{32}(R)g_m^{21}(r,\rho)+h_m^{33}(R)g_m^{31}(r,\rho)\right)\sin m(\theta-\phi) \tag{A.3.137}$$
$$=a^{32}(R,r)\sin(\theta-\phi)+3a^{33}(R,r)\rho^2\sin(\theta-\phi)+2a^{34}(R,r)\rho\sin 2(\theta-\phi)$$
$$+3a^{35}(R,r)\rho^2\sin 3(\theta-\phi)+\mathcal{O}(\rho^3). \tag{A.3.138}$$

By differentiating the both sides of Eq. (A.3.137) with regard to ϕ, we have

$$\frac{1}{2\pi}\sum_{m=-\infty}^{\infty}\sum_{n=0}^{\infty}a_{mn}\frac{-m^2k_{mn}}{({k_{mn}}^2+1)^4}\mathcal{J}'_{|m|}(k_{mn}\rho)\mathcal{J}_{|m|}(k_{mn}r)e^{im(\theta-\phi)}$$
$$=-\sum_{m=1}^{\infty}m^2\left(h_m^{30}(R)g_m^{01}(r,\rho)+h_m^{31}(R)g_m^{11}(r,\rho)+h_m^{32}(R)g_m^{21}(r,\rho)+h_m^{33}(R)g_m^{31}(r,\rho)\right)\cos m(\theta-\phi) \tag{A.3.139}$$
$$=-a^{32}(R,r)\cos(\theta-\phi)-3a^{33}(R,r)\rho^2\cos(\theta-\phi)-4a^{34}(R,r)\rho\cos 2(\theta-\phi)$$
$$-9a^{35}(R,r)\rho^2\cos 3(\theta-\phi)+\mathcal{O}(\rho^3). \tag{A.3.140}$$

By differentiating the both sides of Eq. (A.3.133) with regard to ϕ, we have

$$\frac{1}{2\pi}\sum_{m=-\infty}^{\infty}\sum_{n=0}^{\infty}a_{mn}\frac{-imk_{mn}{}^2}{(k_{mn}{}^2+1)^4}\mathcal{J}''_{|m|}(k_{mn}\rho)\mathcal{J}_{|m|}(k_{mn}r)e^{im(\theta-\phi)}$$

$$=\sum_{m=1}^{\infty}m\left(h_m^{30}(R)g_m^{02}(r,\rho)+h_m^{31}(R)g_m^{12}(r,\rho)+h_m^{32}(R)g_m^{22}(r,\rho)+h_m^{33}(R)g_m^{32}(r,\rho)\right)\sin m(\theta-\phi) \tag{A.3.141}$$

$$=6a^{33}(R,r)\rho\sin(\theta-\phi)+2a^{34}(R,r)\sin 2(\theta-\phi)+6a^{35}(R,r)\rho\sin 3(\theta-\phi)+\mathcal{O}(\rho^2). \tag{A.3.142}$$

By differentiating the both sides of Eq. (A.3.130) with regard to ϕ, we have

$$\frac{1}{2\pi}\sum_{m=-\infty}^{\infty}\sum_{n=0}^{\infty}a_{mn}\frac{-im}{(k_{mn}{}^2+1)^4}\mathcal{J}_{|m|}(k_{mn}\rho)\mathcal{J}_{|m|}(k_{mn}r)e^{im(\theta-\phi)}$$

$$=\sum_{m=1}^{\infty}m\left(h_m^{30}(R)g_m^{00}(r,\rho)+h_m^{31}(R)g_m^{10}(r,\rho)+h_m^{32}(R)g_m^{20}(r,\rho)+h_m^{33}(R)g_m^{30}(r,\rho)\right)\sin m(\theta-\phi) \tag{A.3.143}$$

$$=a^{32}(R,r)\rho\sin(\theta-\phi)+a^{33}(R,r)\rho^3\sin(\theta-\phi)+a^{34}(R,r)\rho^2\sin 2(\theta-\phi)$$
$$+a^{35}(R,r)\rho^3\sin 3(\theta-\phi)+\mathcal{O}(\rho^4). \tag{A.3.144}$$

By differentiating the both sides of Eq. (A.3.143) with regard to ϕ, we have

$$\frac{1}{2\pi}\sum_{m=-\infty}^{\infty}\sum_{n=0}^{\infty}a_{mn}\frac{-m^2}{(k_{mn}{}^2+1)^4}\mathcal{J}_{|m|}(k_{mn}\rho)\mathcal{J}_{|m|}(k_{mn}r)e^{im(\theta-\phi)}$$

$$=-\sum_{m=1}^{\infty}m^2\left(h_m^{30}(R)g_m^{00}(r,\rho)+h_m^{31}(R)g_m^{10}(r,\rho)+h_m^{32}(R)g_m^{20}(r,\rho)+h_m^{33}(R)g_m^{30}(r,\rho)\right)\cos m(\theta-\phi) \tag{A.3.145}$$

$$=-a^{32}(R,r)\rho\cos(\theta-\phi)-a^{33}(R,r)\rho^3\cos(\theta-\phi)-2a^{34}(R,r)\rho^2\cos 2(\theta-\phi)$$
$$-3a^{35}(R,r)\rho^3\cos 3(\theta-\phi)+\mathcal{O}(\rho^4). \tag{A.3.146}$$

By differentiating the both sides of Eq. (A.3.145) with regard to ϕ, we have

$$\frac{1}{2\pi}\sum_{m=-\infty}^{\infty}\sum_{n=0}^{\infty}a_{mn}\frac{im^3}{(k_{mn}{}^2+1)^4}\mathcal{J}_{|m|}(k_{mn}\rho)\mathcal{J}_{|m|}(k_{mn}r)e^{im(\theta-\phi)}$$

$$=-\sum_{m=1}^{\infty}m^3\left(h_m^{30}(R)g_m^{00}(r,\rho)+h_m^{31}(R)g_m^{10}(r,\rho)+h_m^{32}(R)g_m^{20}(r,\rho)+h_m^{33}(R)g_m^{30}(r,\rho)\right)\sin m(\theta-\phi) \tag{A.3.147}$$

$$=-a^{32}(R,r)\rho\sin(\theta-\phi)-a^{33}(R,r)\rho^2\sin(\theta-\phi)-4a^{34}(R,r)\rho\sin 2(\theta-\phi)$$
$$-9a^{35}(R,r)\rho^3\sin 3(\theta-\phi)+\mathcal{O}(\rho^4). \tag{A.3.148}$$

Here we define $h_m^{ij}(R)=\bar{h}_m^{ij}(1,R)$ and the explicit forms of $\bar{h}_m^{ij}(\lambda,R)$ are as follows:

$$\bar{h}_m^{00}(\lambda,R)=-\frac{\sigma_m}{\pi}\frac{\mathcal{K}'_m(\lambda R)}{\mathcal{I}'_m(\lambda R)}, \tag{A.3.149}$$

$$\bar{h}_m^{10}(\lambda,R) = \frac{1}{2\lambda}\frac{d}{d\lambda}\bar{h}_m^{00}(\lambda,R) = -\frac{\sigma_m}{2\pi}\left(\frac{1}{\lambda^2}+\frac{m^2}{\lambda^4R^2}\right)\frac{1}{(\mathcal{I}_m'(\lambda R))^2}, \tag{A.3.150}$$

$$\bar{h}_m^{11}(\lambda,R) = \frac{1}{2\lambda}\bar{h}_m^{00}(\lambda,R) = -\frac{\sigma_m}{2\pi\lambda}\frac{\mathcal{K}_m'(\lambda R)}{\mathcal{I}_m'(\lambda R)}, \tag{A.3.151}$$

$$\begin{aligned}\bar{h}_m^{20}(\lambda,R) =& \frac{1}{4\lambda}\frac{d}{d\lambda}\left(\frac{1}{2\lambda}\frac{d}{d\lambda}\bar{h}_m^{00}(\lambda,R)\right)\\ =&\frac{\sigma_m}{4\pi}\left(\left(\frac{1}{\lambda^4}+\frac{2m^2}{\lambda^6R^2}\right)\frac{1}{(\mathcal{I}_m'(\lambda R))^2}+\left(\frac{1}{\lambda^3}+\frac{m^2}{\lambda^5R^2}\right)\frac{R\mathcal{I}_m''(\lambda R)}{(\mathcal{I}_m'(\lambda R))^3}\right),\end{aligned} \tag{A.3.152}$$

$$\begin{aligned}\bar{h}_m^{21}(\lambda,R) =& \frac{1}{4\lambda}\left(\frac{1}{2\lambda}\frac{d}{d\lambda}\bar{h}_0^{00}(\lambda,R)\right)+\frac{1}{4\lambda}\frac{d}{d\lambda}\left(\frac{1}{2\lambda}\bar{h}_0^{00}(\lambda,R)\right)\\ =&\frac{\sigma_m}{8\pi}\left(-2\left(\frac{1}{\lambda^3}+\frac{m^2}{\lambda^5R^2}\right)\frac{1}{(\mathcal{I}_m'(\lambda R))^2}+\frac{\mathcal{K}_m'(\lambda R)}{\lambda^3\mathcal{I}_m'(\lambda R)}\right),\end{aligned} \tag{A.3.153}$$

$$\bar{h}_m^{22}(\lambda,R) = \frac{1}{4\lambda}h_m^{11}(\lambda,R) = -\frac{\sigma_m}{8\pi\lambda^2}\frac{\mathcal{K}_m'(\lambda R)}{\mathcal{I}_m'(\lambda R)}, \tag{A.3.154}$$

$$\begin{aligned}\bar{h}_m^{30}(\lambda,R) =& \frac{1}{6\lambda}\frac{d}{d\lambda}\left(\frac{1}{4\lambda}\frac{d}{d\lambda}\left(\frac{1}{2\lambda}\frac{d}{d\lambda}\bar{h}_m^{00}(\lambda,R)\right)\right)\\ =&-\frac{\sigma_m}{24\pi}\left(4\left(\frac{1}{\lambda^6}+\frac{3m^2}{\lambda^8R^2}\right)\frac{1}{(\mathcal{I}_m'(\lambda R))^2}+\left(\frac{5}{\lambda^5}+\frac{9m^2}{\lambda^7R^2}\right)\frac{R\mathcal{I}_m''(\lambda R)}{(\mathcal{I}_m'(\lambda R))^3}\right.\\ &\left.-\left(\frac{1}{\lambda^4}+\frac{m^2}{\lambda^6R^2}\right)\frac{R^2\mathcal{I}_m'''(\lambda R)}{(\mathcal{I}_m'(\lambda R))^3}+3\left(\frac{1}{\lambda^4}+\frac{m^2}{\lambda^6R^2}\right)\frac{R^2(\mathcal{I}_m''(\lambda R))^2}{(\mathcal{I}_m'(\lambda R))^4}\right),\end{aligned} \tag{A.3.155}$$

$$\begin{aligned}\bar{h}_m^{31}(\lambda,R) =& \frac{1}{6\lambda}\left(\frac{1}{4\lambda}\frac{d}{d\lambda}\left(\frac{1}{2\lambda}\frac{d}{d\lambda}\bar{h}_m^{00}(\lambda,R)\right)\right)+\frac{1}{6\lambda}\frac{d}{d\lambda}\left(\frac{1}{4\lambda}\left(\frac{1}{2\lambda}\frac{d}{d\lambda}\bar{h}_m^{00}(\lambda,R)\right)\right)\\ &+\frac{1}{6\lambda}\frac{d}{d\lambda}\left(\frac{1}{4\lambda}\frac{d}{d\lambda}\left(\frac{1}{2\lambda}\bar{h}_m^{00}(\lambda,R)\right)\right)\\ =&\frac{\sigma_m}{16\pi}\left(\left(\frac{3}{\lambda^5}+\frac{5m^2}{\lambda^7R^2}\right)\frac{1}{(\mathcal{I}_m'(\lambda R))^2}+2\left(\frac{1}{\lambda^4}+\frac{m^2}{\lambda^6R^2}\right)\frac{R\mathcal{I}_m''(\lambda R)}{(\mathcal{I}_m'(\lambda R))^3}-\frac{\mathcal{K}_m'(\lambda R)}{\lambda^5\mathcal{I}_m'(\lambda R)}\right),\end{aligned} \tag{A.3.156}$$

$$\begin{aligned}&\bar{h}_m^{32}(\lambda,R)\\ &=\frac{1}{6\lambda}\left(\frac{1}{4\lambda}\left(\frac{1}{2\lambda}\frac{d}{d\lambda}\bar{h}_m^{00}(\lambda,R)\right)\right)+\frac{1}{6\lambda}\left(\frac{1}{4\lambda}\frac{d}{d\lambda}\left(\frac{1}{2\lambda}\bar{h}_m^{00}(\lambda,R)\right)\right)+\frac{1}{6\lambda}\frac{d}{d\lambda}\left(\frac{1}{4\lambda}\left(\frac{1}{2\lambda}\bar{h}_m^{00}(\lambda,R)\right)\right)\\ &=\frac{\sigma_m}{16\pi}\left(\frac{\mathcal{K}_m'(\lambda R)}{\lambda^4\mathcal{I}_m'(\lambda R)}-\left(\frac{1}{\lambda^4}+\frac{m^2}{\lambda^6R^2}\right)\frac{1}{(\mathcal{I}_m'(\lambda R))^2}\right),\end{aligned} \tag{A.3.157}$$

$$\bar{h}_m^{33}(\lambda,R) = \frac{1}{6\lambda}\bar{h}_m^{22}(\lambda,R) = -\frac{\sigma_m}{48\pi\lambda^3}\frac{\mathcal{K}_m'(\lambda R)}{\mathcal{I}_m'(\lambda R)}, \tag{A.3.158}$$

where σ_m is equal to 1 for $m \neq 0$ and $1/2$ for $m = 0$. We also define $g_m^{i0}(r,\rho) = \bar{g}_m^{i0}(1,r,\rho)$ and the explicit forms of $\bar{g}_m^{i0}(\lambda,r,\rho)$ are as follows:

$$\bar{g}_m^{00}(\lambda,r,\rho) = \mathcal{I}_m(\lambda r)\mathcal{I}_m(\lambda\rho), \tag{A.3.159}$$

$$\bar{g}_m^{10}(\lambda,r,\rho) = \frac{d}{d\lambda}\bar{g}_m^{00}(\lambda,r,\rho) = r\mathcal{I}_m'(\lambda r)\mathcal{I}_m(\lambda\rho) + \rho\mathcal{I}_m(\lambda r)\mathcal{I}_m'(\lambda\rho), \tag{A.3.160}$$

$$\bar{g}_m^{20}(\lambda,r,\rho) = \frac{d^2}{d\lambda^2}\bar{g}_m^{00}(\lambda,r,\rho) = r^2\mathcal{I}_m''(\lambda r)\mathcal{I}_m(\lambda\rho) + 2r\rho\mathcal{I}_m'(\lambda r)\mathcal{I}_m'(\lambda\rho) + \rho^2\mathcal{I}_m(\lambda r)\mathcal{I}_m''(\lambda\rho), \tag{A.3.161}$$

$$\begin{aligned}\bar{g}_m^{30}(\lambda,r,\rho) =& \frac{d^3}{d\lambda^3}\bar{g}_m^{00}(\lambda,r,\rho)\\ =& r^3\mathcal{I}_m'''(\lambda r)\mathcal{I}_m(\lambda\rho) + 3r^2\rho\mathcal{I}_m''(\lambda r)\mathcal{I}_m'(\lambda\rho) + 3r\rho^2\mathcal{I}_m'(\lambda r)\mathcal{I}_m''(\lambda\rho) + \rho^3\mathcal{I}_m(\lambda r)\mathcal{I}_m'''(\lambda\rho).\end{aligned} \tag{A.3.162}$$

The functions $g_m^{ij}(r,\rho)$ $(j \neq 0)$ are defined by the derivatives of $g_m^{i0}(r,\rho)$ with regard to r and/or ρ as follows:

$$g_m^{01}(r,\rho) = \frac{d}{d\rho}\left(g_m^{00}(r,\rho)\right) = \mathcal{I}_m(r)\mathcal{I}_m'(\rho), \tag{A.3.163}$$

$$g_m^{02}(r,\rho) = \frac{d^2}{d\rho^2}\left(g_m^{00}(r,\rho)\right) = \mathcal{I}_m(r)\mathcal{I}_m''(\rho), \tag{A.3.164}$$

$$g_m^{03}(r,\rho) = \frac{d^3}{d\rho^3}\left(g_m^{00}(r,\rho)\right) = \mathcal{I}_m(r)\mathcal{I}_m'''(\rho), \tag{A.3.165}$$

$$g_m^{11}(r,\rho) = \frac{d}{d\rho}g_m^{10}(r,\rho) = r\mathcal{I}_m'(r)\mathcal{I}_m'(\rho) + \mathcal{I}_m(r)\mathcal{I}_m'(\rho) + \rho\mathcal{I}_m(r)\mathcal{I}_m''(\rho), \tag{A.3.166}$$

$$g_m^{12}(r,\rho) = \frac{d^2}{d\rho^2}g_m^{10}(r,\rho) = r\mathcal{I}_m'(r)\mathcal{I}_m''(\rho) + 2\mathcal{I}_m(r)\mathcal{I}_m''(\rho) + \rho\mathcal{I}_m(r)\mathcal{I}_m'''(\rho), \tag{A.3.167}$$

$$g_m^{13}(r,\rho) = \frac{d^3}{d\rho^3}g_m^{10}(r,\rho) = r\mathcal{I}_m'(r)\mathcal{I}_m'''(\rho) + 3\mathcal{I}_m(r)\mathcal{I}_m'''(\rho) + \rho\mathcal{I}_m(r)\mathcal{I}_m^{(4)}(\rho), \tag{A.3.168}$$

$$\begin{aligned}g_m^{21}(r,\rho) =& \frac{d}{d\rho}g_m^{20}(r,\rho)\\ =& r^2\mathcal{I}_m''(r)\mathcal{I}_m'(\rho) + 2r\mathcal{I}_m'(r)\mathcal{I}_m'(\rho) + 2r\rho\mathcal{I}_m'(r)\mathcal{I}_m''(\rho) + 2\rho\mathcal{I}_m(r)\mathcal{I}_m''(\rho) + \rho^2\mathcal{I}_m(r)\mathcal{I}_m'''(\rho),\end{aligned} \tag{A.3.169}$$

$$\begin{aligned}g_m^{22}(r,\rho) =& \frac{d^2}{d\rho^2}g_m^{20}(r,\rho)\\ =& r^2\mathcal{I}_m''(r)\mathcal{I}_m''(\rho) + 4r\mathcal{I}_m'(r)\mathcal{I}_m''(\rho) + 2r\rho\mathcal{I}_m'(r)\mathcal{I}_m'''(\rho) + 2\mathcal{I}_m(r)\mathcal{I}_m''(\rho)\\ &+ 4\rho\mathcal{I}_m(r)\mathcal{I}_m'''(\rho) + \rho^2\mathcal{I}_m(r)\mathcal{I}_m^{(4)}(\rho),\end{aligned} \tag{A.3.170}$$

$$\begin{aligned}g_m^{23}(r,\rho) =& \frac{d^3}{d\rho^3}g_m^{20}(r,\rho)\\ =& r^2\mathcal{I}_m''(r)\mathcal{I}_m'''(\rho) + 6r\mathcal{I}_m'(r)\mathcal{I}_m'''(\rho) + 2r\rho\mathcal{I}_m'(r)\mathcal{I}_m^{(4)}(\rho) + 6\mathcal{I}_m(r)\mathcal{I}_m'''(\rho)\\ &+ 6\rho\mathcal{I}_m(r)\mathcal{I}_m^{(4)}(\rho) + \rho^2\mathcal{I}_m(r)\mathcal{I}_m^{(5)}(\rho),\end{aligned} \tag{A.3.171}$$

$$\begin{aligned}
g_m^{31}(r,\rho) =& \frac{d}{d\rho} g_m^{30}(r,\rho) \\
=& r^3 \mathcal{I}_m'''(r)\mathcal{I}_m'(\rho) + 3r^2\mathcal{I}_m''(r)\mathcal{I}_m'(\rho) + 3r^2\rho\mathcal{I}_m''(r)\mathcal{I}_m''(\rho) + 6r\rho\mathcal{I}_m'(r)\mathcal{I}_m''(\rho) + 3r\rho^2\mathcal{I}_m'(r)\mathcal{I}_m'''(\rho) \\
&+ 3\rho^2\mathcal{I}_m(r)\mathcal{I}_m'''(\rho) + \rho^3\mathcal{I}_m(r)\mathcal{I}_m^{(4)}(\rho), \qquad \text{(A.3.172)}\\
g_m^{32}(r,\rho) =& \frac{d^2}{d\rho^2} g_m^{30}(r,\rho) \\
=& r^3 \mathcal{I}_m'''(r)\mathcal{I}_m''(\rho) + 6r^2\mathcal{I}_m''(r)\mathcal{I}_m''(\rho) + 3r^2\rho\mathcal{I}_m''(r)\mathcal{I}_m'''(\rho) + 6r\mathcal{I}_m'(r)\mathcal{I}_m''(\rho) + 12r\rho\mathcal{I}_m'(r)\mathcal{I}_m'''(\rho) \\
&+ 3r\rho^2\mathcal{I}_m'(r)\mathcal{I}_m^{(4)}(\rho) + 6\rho\mathcal{I}_m(r)\mathcal{I}_m'''(\rho) + 6\rho^2\mathcal{I}_m(r)\mathcal{I}_m^{(4)}(\rho) + \rho^3\mathcal{I}_m(r)\mathcal{I}_m^{(5)}(\rho), \qquad \text{(A.3.173)}\\
g_m^{33}(r,\rho) =& \frac{d^3}{d\rho^3} g_m^{30}(r,\rho) \\
=& r^3 \mathcal{I}_m'''(r)\mathcal{I}_m'''(\rho) + 9r^2\mathcal{I}_m''(r)\mathcal{I}_m'''(\rho) + 3r^2\rho\mathcal{I}_m''(r)\mathcal{I}_m^{(4)}(\rho) + 18r\mathcal{I}_m'(r)\mathcal{I}_m'''(\rho) \\
&+ 18r\rho\mathcal{I}_m'(r)\mathcal{I}_m^{(4)}(\rho) + 3r\rho^2\mathcal{I}_m'(r)\mathcal{I}_m^{(5)}(\rho) + 6\mathcal{I}_m(r)\mathcal{I}_m'''(\rho) + 18\rho\mathcal{I}_m(r)\mathcal{I}_m^{(4)}(\rho) \\
&+ 9\rho^2\mathcal{I}_m(r)\mathcal{I}_m^{(5)}(\rho) + \rho^3\mathcal{I}_m(r)\mathcal{I}_m^{(6)}(\rho), \qquad \text{(A.3.174)}
\end{aligned}$$

By expanding the explicit form of g_m^{ij} with respect to ρ, the functions $a^{kl}(R,r)$ are determined as follows:

$$\begin{aligned}
a^{01}(R,r) &= h_0^{00}(R)\mathcal{I}_0(r), & a^{02}(R,r) &= \frac{1}{4}h_0^{00}(R)\mathcal{I}_0(r),\\
a^{03}(R,r) &= \frac{1}{2}h_1^{00}(R)\mathcal{I}_1(r), & a^{04}(R,r) &= \frac{1}{16}h_1^{00}(R)\mathcal{I}_1(r),\\
a^{05}(R,r) &= \frac{1}{8}h_2^{00}(R)\mathcal{I}_2(r), & a^{06}(R,r) &= \frac{1}{48}h_3^{00}(R)\mathcal{I}_3(r), \qquad \text{(A.3.175)}
\end{aligned}$$

$$\begin{aligned}
a^{11}(R,r) =& \frac{1}{2}((h_0^{10}(R) + 2h_0^{11}(R))\mathcal{I}_0(r) + h_0^{11}(R)r\mathcal{I}_0'(r)), \qquad \text{(A.3.176)}\\
a^{12}(R,r) =& \frac{1}{2}((h_1^{10}(R) + h_1^{11}(R))\mathcal{I}_1(r) + h_1^{11}(R)r\mathcal{I}_1'(r)), \qquad \text{(A.3.177)}\\
a^{13}(R,r) =& \frac{3}{16}((h_1^{10}(R) + 3h_1^{11}(R))\mathcal{I}_1(r) + h_1^{11}(R)r\mathcal{I}_1'(r)), \qquad \text{(A.3.178)}\\
a^{14}(R,r) =& \frac{1}{4}((h_2^{10}(R) + 2h_2^{11}(R))\mathcal{I}_2(r) + h_2^{11}(R)r\mathcal{I}_2'(r)), \qquad \text{(A.3.179)}\\
a^{15}(R,r) =& \frac{1}{16}((h_3^{10}(R) + 3h_3^{11}(R))\mathcal{I}_3(r) + h_3^{11}(R)r\mathcal{I}_3'(r)), \qquad \text{(A.3.180)}
\end{aligned}$$

$$\begin{aligned}
a^{21}(R,r) =& \frac{1}{2}((h_0^{20}(R) + 2h_0^{21}(R) + 2h_0^{22}(R))\mathcal{I}_0(r) + (h_0^{21}(R) + 4h_0^{22}(R))r\mathcal{I}_0'(r) + h_0^{22}(R)r^2\mathcal{I}_0''(r)), \\
& \qquad \text{(A.3.181)}\\
a^{22}(R,r) =& \frac{1}{2}((h_1^{20}(R) + h_1^{21}(R))\mathcal{I}_1(r) + (h_1^{21}(R) + 2h_1^{22}(R))r\mathcal{I}_1'(r) + h_1^{22}(R)r^2\mathcal{I}_1''(r)), \qquad \text{(A.3.182)}\\
a^{23}(R,r) =& \frac{1}{16}((h_1^{20}(R) + 3h_1^{21}(R) + 6h_1^{22}(R))\mathcal{I}_1(r) + (h_1^{21}(R) + 6h_1^{22}(R))r\mathcal{I}_1'(r) + h_1^{22}(R)r^2\mathcal{I}_1''(r)), \\
& \qquad \text{(A.3.183)}\\
a^{24}(R,r) =& \frac{1}{4}((h_2^{20}(R) + 2h_2^{21}(R) + 2h_2^{22}(R))\mathcal{I}_2(r) + (h_2^{21}(R) + 4h_2^{22}(R))r\mathcal{I}_2'(r) + h_2^{22}(R)r^2\mathcal{I}_2''(r)), \\
& \qquad \text{(A.3.184)}
\end{aligned}$$

$$a^{25}(R,r) = \frac{1}{16}((h_3^{20}(R) + 3h_3^{21}(R) + 6h_3^{22}(R))\mathcal{I}_1(r) + (h_3^{21}(R) + 6h_3^{22}(R))r\mathcal{I}_1'(r) + h_3^{22}(R)r^2\mathcal{I}_3''(r)). \tag{A.3.185}$$

$$a^{31}(R,r) = \frac{1}{2}((h_0^{30}(R) + 2h_0^{31}(R) + 2h_0^{32}(R))\mathcal{I}_0(r) + (h_0^{31}(R) + 4h_0^{32}(R) + 6h_0^{36}(R))r\mathcal{I}_0'(r) + (h_0^{32}(R) + 6h_0^{32}(R))r^2\mathcal{I}_0''(r) + h_0^{31}(R))r^3\mathcal{I}_0'''(r)), \tag{A.3.186}$$

$$a^{32}(R,r) = \frac{1}{2}((h_1^{30}(R) + h_1^{31}(R))\mathcal{I}_1(r) + (h_1^{31}(R) + 2h_0^{32}(R))r\mathcal{I}_1'(r) + (h_0^{32}(R) + 3h_0^{32}(R))r^2\mathcal{I}_1''(r) + h_0^{33}(R))r^3\mathcal{I}_1'''(r)), \tag{A.3.187}$$

$$a^{33}(R,r) = \frac{1}{16}((h_1^{30}(R) + 3h_1^{31}(R) + 6h_1^{32}(R) + 6h_1^{33}(R))\mathcal{I}_1(r) + (h_1^{31}(R) + 6h_1^{32}(R) + 18h_1^{36}(R))r\mathcal{I}_1'(r) + (h_1^{32}(R) + 9h_1^{33}(R))r^2\mathcal{I}_1''(r) + h_1^{33}(R))r^3\mathcal{I}_1'''(r)), \tag{A.3.188}$$

$$a^{34}(R,r) = \frac{1}{4}((h_2^{30}(R) + 2h_2^{31}(R) + 2h_2^{32}(R))\mathcal{I}_2(r) + (h_2^{31}(R) + 4h_2^{32}(R) + 6h_2^{36}(R))r\mathcal{I}_2'(r) + (h_2^{32}(R) + 6h_2^{32}(R))r^2\mathcal{I}_2''(r) + h_2^{31}(R))r^3\mathcal{I}_2'''(r)), \tag{A.3.189}$$

$$a^{35}(R,r) = \frac{1}{16}((h_3^{30}(R) + 3h_3^{31}(R) + 6h_3^{32}(R) + 6h_3^{33}(R))\mathcal{I}_3(r) + (h_3^{31}(R) + 6h_3^{32}(R) + 18h_3^{36}(R))r\mathcal{I}_3'(r) + (h_3^{32}(R) + 9h_3^{33}(R))r^2\mathcal{I}_3''(r) + h_3^{33}(R))r^3\mathcal{I}_3'''(r)), \tag{A.3.190}$$

From the symmetric property of the system, the concentration field expanded with regard to $\boldsymbol{\rho}$ should have the following form:

$$\begin{aligned}
&c(\boldsymbol{r};\boldsymbol{\rho}) \\
&= c_0^{00}(R,r) + c_0^{10}(R,r)(\boldsymbol{r}\cdot\boldsymbol{\rho}) + c_0^{20}(R,r)(\boldsymbol{r}\cdot\boldsymbol{\rho})^2 + c_1^{20}(R,r)|\boldsymbol{\rho}|^2 + c_0^{11}(R,r)\,(\boldsymbol{r}\cdot\dot{\boldsymbol{\rho}}) \\
&\quad + c_0^{30}(R,r)(\boldsymbol{r}\cdot\boldsymbol{\rho})^3 + c_1^{30}(R,r)|\boldsymbol{\rho}|^2(\boldsymbol{r}\cdot\boldsymbol{\rho}) \\
&\quad + c_0^{21}(R,r)\,(\boldsymbol{\rho}\cdot\dot{\boldsymbol{\rho}}) + c_1^{21}(R,r)\,(\boldsymbol{r}\cdot\boldsymbol{\rho})\,(\boldsymbol{r}\cdot\dot{\boldsymbol{\rho}}) + c_0^{12}(R,r)\,(\boldsymbol{r}\cdot\ddot{\boldsymbol{\rho}}) \\
&\quad + c_0^{31}(R,r)|\boldsymbol{\rho}|^2\,(\boldsymbol{r}\cdot\dot{\boldsymbol{\rho}}) + c_1^{31}(R,r)\,(\boldsymbol{r}\cdot\boldsymbol{\rho})\,(\boldsymbol{\rho}\cdot\dot{\boldsymbol{\rho}}) + c_2^{31}(R,r)\,(\boldsymbol{r}\cdot\boldsymbol{\rho})^2\,(\boldsymbol{r}\cdot\dot{\boldsymbol{\rho}}) \\
&\quad + c_0^{22}(R,r)\,(\boldsymbol{\rho}\cdot\ddot{\boldsymbol{\rho}}) + c_1^{22}(R,r)\,|\dot{\boldsymbol{\rho}}|^2 + c_2^{22}(R,r)\,(\boldsymbol{r}\cdot\boldsymbol{\rho})\,(\boldsymbol{r}\cdot\ddot{\boldsymbol{\rho}}) + c_3^{22}(R,r)\,(\boldsymbol{r}\cdot\dot{\boldsymbol{\rho}})^2 + c_0^{13}(R,r)\,(\boldsymbol{r}\cdot\dddot{\boldsymbol{\rho}}) \\
&\quad + c_0^{32}(R,r)\,|\dot{\boldsymbol{\rho}}|^2\,(\boldsymbol{r}\cdot\boldsymbol{\rho}) + c_1^{32}(R,r)\,(\boldsymbol{r}\cdot\dot{\boldsymbol{\rho}})\,(\boldsymbol{\rho}\cdot\dot{\boldsymbol{\rho}}) + c_2^{32}(R,r)\,(\boldsymbol{r}\cdot\boldsymbol{\rho})\,(\boldsymbol{r}\cdot\dot{\boldsymbol{\rho}})^2 + c_3^{32}(R,r)\,(\boldsymbol{r}\cdot\boldsymbol{\rho})\,(\boldsymbol{\rho}\cdot\ddot{\boldsymbol{\rho}}) \\
&\quad + c_4^{32}(R,r)\,|\boldsymbol{\rho}|^2\,(\boldsymbol{r}\cdot\ddot{\boldsymbol{\rho}}) + c_5^{32}(R,r)\,(\boldsymbol{r}\cdot\boldsymbol{\rho})^2\,(\boldsymbol{r}\cdot\ddot{\boldsymbol{\rho}}) \\
&\quad + c_0^{23}(R,r)\,(\boldsymbol{\rho}\cdot\dddot{\boldsymbol{\rho}}) + c_1^{23}(R,r)\,(\dot{\boldsymbol{\rho}}\cdot\ddot{\boldsymbol{\rho}}) + c_2^{23}(R,r)\,(\boldsymbol{r}\cdot\dot{\boldsymbol{\rho}})\,(\boldsymbol{r}\cdot\ddot{\boldsymbol{\rho}}) + c_3^{23}(R,r)\,(\boldsymbol{r}\cdot\boldsymbol{\rho})\,(\boldsymbol{r}\cdot\dddot{\boldsymbol{\rho}}) \\
&\quad + c_0^{33}(R,r)\,|\boldsymbol{\rho}|^2\,(\boldsymbol{r}\cdot\dddot{\boldsymbol{\rho}}) + c_1^{33}(R,r)\,|\dot{\boldsymbol{\rho}}|^2\,(\boldsymbol{r}\cdot\dot{\boldsymbol{\rho}}) + c_2^{33}(R,r)\,(\boldsymbol{r}\cdot\boldsymbol{\rho})\,(\boldsymbol{\rho}\cdot\dddot{\boldsymbol{\rho}}) + c_3^{33}(R,r)\,(\boldsymbol{r}\cdot\dot{\boldsymbol{\rho}})^3 \\
&\quad + c_4^{33}(R,r)\,(\boldsymbol{r}\cdot\boldsymbol{\rho})\,(\dot{\boldsymbol{\rho}}\cdot\ddot{\boldsymbol{\rho}}) + c_5^{33}(R,r)\,(\boldsymbol{r}\cdot\boldsymbol{\rho})^2\,(\boldsymbol{r}\cdot\dddot{\boldsymbol{\rho}}) + c_6^{33}(R,r)\,(\boldsymbol{r}\cdot\dot{\boldsymbol{\rho}})\,(\boldsymbol{\rho}\cdot\ddot{\boldsymbol{\rho}}) \\
&\quad + c_7^{33}(R,r)\,(\boldsymbol{r}\cdot\ddot{\boldsymbol{\rho}})\,(\boldsymbol{\rho}\cdot\dot{\boldsymbol{\rho}}) + c_8^{33}(R,r)\,(\boldsymbol{r}\cdot\boldsymbol{\rho})\,(\boldsymbol{r}\cdot\dot{\boldsymbol{\rho}})\,(\boldsymbol{r}\cdot\ddot{\boldsymbol{\rho}})\,.
\end{aligned} \tag{A.3.191}$$

Comparing Eq. (A.3.191) with Eq. (A.3.111), we have

$$\begin{aligned}
c_0^{00}(R,r) &= a^{01}(R,r), & c_0^{10}(R,r) &= \frac{1}{r}a^{03}(R,r), \\
c_0^{20}(R,r) &= \frac{2}{r^2}a^{05}(R,r), & c_1^{20}(R,r) &= a^{02}(R,r) - a^{05}(R,r), \\
c_0^{30}(R,r) &= \frac{4}{r^3}a^{06}(R,r), & c_1^{30}(R,r) &= \frac{1}{r}(a^{04}(R,r) - 3a^{06}(R,r)).
\end{aligned} \tag{A.3.192}$$

Comparing Eq. (A.3.191) with Eqs. (A.3.115) and (A.3.116), we have

$$\begin{aligned}
c_0^{11}(R,r) &= \frac{1}{r}a^{12}(R,r), & c_0^{21}(R,r) &= a^{11}(R,r) - a^{14}(R,r),\\
c_1^{21}(R,r) &= \frac{2}{r^2}a^{14}(R,r), & c_0^{31}(R,r) &= \frac{1}{r}(a^{13}(R,r) - a^{15}(R,r)),\\
c_1^{31}(R,r) &= \frac{2}{r}(a^{13}(R,r) - a^{15}(R,r)), & c_2^{31}(R,r) &= \frac{4}{r^3}a^{15}(R,r).
\end{aligned} \tag{A.3.193}$$

Comparing Eq. (A.3.191) with Eqs. (A.3.120), (A.3.122), (A.3.124), (A.3.126), and (A.3.128), we have

$$\begin{aligned}
c_0^{12}(R,r) &= \frac{1}{r}a^{22}(R,r), & c_0^{22}(R,r) &= a^{21}(R,r) - a^{24}(R,r),\\
c_1^{22}(R,r) &= a^{21}(R,r) - a^{24}(R,r), & c_2^{22}(R,r) &= \frac{2}{r^2}a^{24}(R,r),\\
c_3^{22}(R,r) &= \frac{2}{r^2}a^{24}(R,r), & c_0^{32}(R,r) &= \frac{2}{r}(a^{23}(R,r) - a^{25}(R,r)),\\
c_1^{32}(R,r) &= \frac{4}{r}(a^{23}(R,r) - a^{25}(R,r)), & c_2^{32}(R,r) &= \frac{8}{r^3}a^{25}(R,r),\\
c_3^{32}(R,r) &= \frac{2}{r}(a^{23}(R,r) - a^{25}(R,r)), & c_4^{32}(R,r) &= \frac{1}{r}(a^{23}(R,r) - a^{25}(R,r)),\\
c_5^{32}(R,r) &= \frac{4}{r^3}a^{25}(R,r).
\end{aligned} \tag{A.3.194}$$

Comparing Eq. (A.3.191) with Eqs. (A.3.132), (A.3.134), (A.3.136), (A.3.138), (A.3.140), (A.3.142), (A.3.144), (A.3.146), and (A.3.148), we have

$$\begin{aligned}
c_0^{13}(R,r) &= \frac{1}{r}a^{32}(R,r), & c_0^{23}(R,r) &= a^{31}(R,r) - a^{34}(R,r),\\
c_1^{23}(R,r) &= 3(a^{31}(R,r) - a^{34}(R,r)), & c_2^{23}(R,r) &= \frac{6}{r^2}a^{34}(R,r),\\
c_3^{23}(R,r) &= \frac{2}{r^2}a^{34}(R,r), & c_0^{33}(R,r) &= \frac{1}{r}(a^{33}(R,r) - a^{35}(R,r)),\\
c_1^{33}(R,r) &= \frac{6}{r}(a^{33}(R,r) - a^{35}(R,r)), & c_2^{33}(R,r) &= \frac{2}{r}(a^{33}(R,r) - a^{35}(R,r)),\\
c_3^{33}(R,r) &= \frac{8}{r^3}a^{35}(R,r), & c_4^{33}(R,r) &= \frac{6}{r}(a^{33}(R,r) - a^{35}(R,r)),\\
c_5^{33}(R,r) &= \frac{4}{r^3}a^{35}(R,r), & c_6^{33}(R,r) &= \frac{6}{r}(a^{33}(R,r) - a^{35}(R,r)),\\
c_7^{33}(R,r) &= \frac{6}{r}(a^{33}(R,r) - a^{35}(R,r)), & c_8^{33}(R,r) &= \frac{24}{r^3}a^{35}(R,r).
\end{aligned} \tag{A.3.195}$$

The terms in Eq. (A.3.191) for the camphor particle located at $\boldsymbol{\rho} = (\rho, \phi) = (0.1, 0)$ in the water chamber with a radius of $R = 1$ are plotted in Figs. A.3.3, A.3.4, A.3.5, A.3.6, A.3.7, A.3.8, and A.3.9.

Then we calculate the reduced driving force as follows:

$$
\begin{aligned}
&\nabla_{\boldsymbol{r}} c(\boldsymbol{r};\boldsymbol{\rho}) \\
&= \frac{1}{r} c'^{00}_{0}(R,r)\boldsymbol{r} + \frac{1}{r} c'^{10}_{0}(R,r)(\boldsymbol{r}\cdot\boldsymbol{\rho})\boldsymbol{r} + c^{10}_{0}(R,r)\boldsymbol{\rho} \\
&\quad + \frac{1}{r} c'^{20}_{0}(R,r)(\boldsymbol{r}\cdot\boldsymbol{\rho})^2\boldsymbol{r} + 2c^{20}_{0}(R,r)(\boldsymbol{r}\cdot\boldsymbol{\rho})\boldsymbol{\rho} + \frac{1}{r} c'^{20}_{1}(R,r)|\boldsymbol{\rho}|^2\boldsymbol{r} + \frac{1}{r} c'^{11}_{0}(R,r)\left(\boldsymbol{r}\cdot\dot{\boldsymbol{\rho}}\right)\boldsymbol{r} + c^{11}_{0}(R,r)\dot{\boldsymbol{\rho}} \\
&\quad + \frac{1}{r} c'^{30}_{0}(R,r)(\boldsymbol{r}\cdot\boldsymbol{\rho})^3\boldsymbol{r} + 3c^{30}_{0}(R,r)(\boldsymbol{r}\cdot\boldsymbol{\rho})^2\boldsymbol{\rho} + \frac{1}{r} c'^{30}_{1}(R,r)|\boldsymbol{\rho}|^2(\boldsymbol{r}\cdot\boldsymbol{\rho})\boldsymbol{r} + c^{30}_{1}(R,r)|\boldsymbol{\rho}|^2\boldsymbol{\rho} \\
&\quad + \frac{1}{r} c'^{21}_{0}(R,r)\left(\boldsymbol{\rho}\cdot\dot{\boldsymbol{\rho}}\right)\boldsymbol{r} + \frac{1}{r} c'^{21}_{1}(R,r)\left(\boldsymbol{r}\cdot\boldsymbol{\rho}\right)\left(\boldsymbol{r}\cdot\dot{\boldsymbol{\rho}}\right)\boldsymbol{r} + c^{21}_{1}(R,r)\left(\boldsymbol{r}\cdot\dot{\boldsymbol{\rho}}\right)\boldsymbol{\rho} + c^{21}_{1}(R,r)\left(\boldsymbol{r}\cdot\boldsymbol{\rho}\right)\dot{\boldsymbol{\rho}} \\
&\quad + \frac{1}{r} c'^{12}_{0}(R,r)\left(\boldsymbol{r}\cdot\ddot{\boldsymbol{\rho}}\right)\boldsymbol{r} + c^{12}_{0}(R,r)\ddot{\boldsymbol{\rho}} \\
&\quad + \frac{1}{r} c'^{31}_{0}(R,r)|\boldsymbol{\rho}|^2\left(\boldsymbol{r}\cdot\dot{\boldsymbol{\rho}}\right)\boldsymbol{r} + c^{31}_{0}(R,r)|\boldsymbol{\rho}|^2\dot{\boldsymbol{\rho}} + \frac{1}{r} c'^{31}_{1}(R,r)\left(\boldsymbol{r}\cdot\boldsymbol{\rho}\right)\left(\boldsymbol{\rho}\cdot\dot{\boldsymbol{\rho}}\right)\boldsymbol{r} + c^{31}_{1}(R,r)\left(\boldsymbol{\rho}\cdot\dot{\boldsymbol{\rho}}\right)\boldsymbol{\rho} \\
&\quad + \frac{1}{r} c'^{31}_{2}(R,r)\left(\boldsymbol{r}\cdot\boldsymbol{\rho}\right)^2\left(\boldsymbol{r}\cdot\dot{\boldsymbol{\rho}}\right)\boldsymbol{r} + 2c^{31}_{2}(R,r)\left(\boldsymbol{r}\cdot\boldsymbol{\rho}\right)\left(\boldsymbol{r}\cdot\dot{\boldsymbol{\rho}}\right)\boldsymbol{\rho} + c^{31}_{2}(R,r)\left(\boldsymbol{r}\cdot\boldsymbol{\rho}\right)^2\dot{\boldsymbol{\rho}} \\
&\quad + \frac{1}{r} c'^{22}_{0}(R,r)\left(\boldsymbol{\rho}\cdot\ddot{\boldsymbol{\rho}}\right)\boldsymbol{r} + \frac{1}{r} c'^{22}_{1}(R,r)\left|\dot{\boldsymbol{\rho}}\right|^2\boldsymbol{r} + \frac{1}{r} c'^{22}_{2}(R,r)\left(\boldsymbol{r}\cdot\boldsymbol{\rho}\right)\left(\boldsymbol{r}\cdot\ddot{\boldsymbol{\rho}}\right)\boldsymbol{r} + c^{22}_{2}(R,r)\left(\boldsymbol{r}\cdot\ddot{\boldsymbol{\rho}}\right)\boldsymbol{\rho} \\
&\quad + c^{22}_{2}(R,r)\left(\boldsymbol{r}\cdot\boldsymbol{\rho}\right)\ddot{\boldsymbol{\rho}} + \frac{1}{r} c'^{22}_{3}(R,r)\left(\boldsymbol{r}\cdot\dot{\boldsymbol{\rho}}\right)^2\boldsymbol{r} + 2c^{22}_{3}(R,r)\left(\boldsymbol{r}\cdot\dot{\boldsymbol{\rho}}\right)\dot{\boldsymbol{\rho}} + \frac{1}{r} c'^{13}_{0}(R,r)\left(\boldsymbol{r}\cdot\dddot{\boldsymbol{\rho}}\right)\boldsymbol{r} + c^{13}_{0}(R,r)\dddot{\boldsymbol{\rho}} \\
&\quad + \frac{1}{r} c'^{32}_{0}(R,r)\left|\dot{\boldsymbol{\rho}}\right|^2\left(\boldsymbol{r}\cdot\boldsymbol{\rho}\right)\boldsymbol{r} + c^{32}_{0}(R,r)\left|\dot{\boldsymbol{\rho}}\right|^2\boldsymbol{\rho} + \frac{1}{r} c'^{32}_{1}(R,r)\left(\boldsymbol{r}\cdot\dot{\boldsymbol{\rho}}\right)\left(\boldsymbol{\rho}\cdot\dot{\boldsymbol{\rho}}\right)\boldsymbol{r} + c^{32}_{1}(R,r)\left(\boldsymbol{\rho}\cdot\dot{\boldsymbol{\rho}}\right)\dot{\boldsymbol{\rho}} \\
&\quad + \frac{1}{r} c'^{32}_{2}(R,r)\left(\boldsymbol{r}\cdot\boldsymbol{\rho}\right)\left(\boldsymbol{r}\cdot\dot{\boldsymbol{\rho}}\right)^2\boldsymbol{r} + c^{32}_{2}(R,r)\left(\boldsymbol{r}\cdot\dot{\boldsymbol{\rho}}\right)^2\boldsymbol{\rho} + 2c^{32}_{2}(R,r)\left(\boldsymbol{r}\cdot\boldsymbol{\rho}\right)\left(\boldsymbol{r}\cdot\dot{\boldsymbol{\rho}}\right)\dot{\boldsymbol{\rho}} \\
&\quad + \frac{1}{r} c'^{32}_{3}(R,r)\left(\boldsymbol{r}\cdot\boldsymbol{\rho}\right)\left(\boldsymbol{\rho}\cdot\ddot{\boldsymbol{\rho}}\right)\boldsymbol{r} + c^{32}_{3}(R,r)\left(\boldsymbol{\rho}\cdot\ddot{\boldsymbol{\rho}}\right)\boldsymbol{\rho} + \frac{1}{r} c'^{32}_{4}(R,r)\left|\boldsymbol{\rho}\right|^2\left(\boldsymbol{r}\cdot\ddot{\boldsymbol{\rho}}\right)\boldsymbol{r} + c^{32}_{4}(R,r)\left|\boldsymbol{\rho}\right|^2\ddot{\boldsymbol{\rho}}\boldsymbol{r} \\
&\quad + \frac{1}{r} c'^{32}_{5}(R,r)\left(\boldsymbol{r}\cdot\boldsymbol{\rho}\right)^2\left(\boldsymbol{r}\cdot\ddot{\boldsymbol{\rho}}\right) + 2c^{32}_{5}(R,r)\left(\boldsymbol{r}\cdot\boldsymbol{\rho}\right)\left(\boldsymbol{r}\cdot\ddot{\boldsymbol{\rho}}\right)\boldsymbol{\rho} + c^{32}_{5}(R,r)\left(\boldsymbol{r}\cdot\boldsymbol{\rho}\right)^2\ddot{\boldsymbol{\rho}} \\
&\quad + \frac{1}{r} c'^{23}_{0}(R,r)\left(\boldsymbol{\rho}\cdot\dddot{\boldsymbol{\rho}}\right)\boldsymbol{r} + \frac{1}{r} c'^{23}_{1}(R,r)\left(\dot{\boldsymbol{\rho}}\cdot\ddot{\boldsymbol{\rho}}\right)\boldsymbol{r} + \frac{1}{r} c'^{23}_{2}(R,r)\left(\boldsymbol{r}\cdot\dot{\boldsymbol{\rho}}\right)\left(\boldsymbol{r}\cdot\ddot{\boldsymbol{\rho}}\right)\boldsymbol{r} + c^{23}_{2}(R,r)\left(\boldsymbol{r}\cdot\ddot{\boldsymbol{\rho}}\right)\dot{\boldsymbol{\rho}} \\
&\quad + c^{23}_{2}(R,r)\left(\boldsymbol{r}\cdot\dot{\boldsymbol{\rho}}\right)\ddot{\boldsymbol{\rho}} + \frac{1}{r} c'^{23}_{3}(R,r)\left(\boldsymbol{r}\cdot\boldsymbol{\rho}\right)\left(\boldsymbol{r}\cdot\dddot{\boldsymbol{\rho}}\right)\boldsymbol{r} + c^{23}_{3}(R,r)\left(\boldsymbol{r}\cdot\dddot{\boldsymbol{\rho}}\right)\boldsymbol{\rho} + c^{23}_{3}(R,r)\left(\boldsymbol{r}\cdot\boldsymbol{\rho}\right)\dddot{\boldsymbol{\rho}} \\
&\quad + \frac{1}{r} c'^{33}_{0}(R,r)\left|\boldsymbol{\rho}\right|^2\left(\boldsymbol{r}\cdot\dddot{\boldsymbol{\rho}}\right)\boldsymbol{r} + c^{33}_{0}(R,r)\left|\boldsymbol{\rho}\right|^2\dddot{\boldsymbol{\rho}} + \frac{1}{r} c'^{33}_{1}(R,r)\left|\dot{\boldsymbol{\rho}}\right|^2\left(\boldsymbol{r}\cdot\dot{\boldsymbol{\rho}}\right)\boldsymbol{r} + c^{33}_{1}(R,r)\left|\dot{\boldsymbol{\rho}}\right|^2\dot{\boldsymbol{\rho}} \\
&\quad + \frac{1}{r} c'^{33}_{2}(R,r)\left(\boldsymbol{r}\cdot\boldsymbol{\rho}\right)\left(\boldsymbol{\rho}\cdot\dddot{\boldsymbol{\rho}}\right)\boldsymbol{r} + c^{33}_{2}(R,r)\left(\boldsymbol{\rho}\cdot\dddot{\boldsymbol{\rho}}\right)\boldsymbol{\rho} + \frac{1}{r} c'^{33}_{3}(R,r)\left(\boldsymbol{r}\cdot\dot{\boldsymbol{\rho}}\right)^3\boldsymbol{r} + 3c^{33}_{3}(R,r)\left(\boldsymbol{r}\cdot\dot{\boldsymbol{\rho}}\right)^2\dot{\boldsymbol{\rho}} \\
&\quad + \frac{1}{r} c'^{33}_{4}(R,r)\left(\boldsymbol{r}\cdot\boldsymbol{\rho}\right)\left(\dot{\boldsymbol{\rho}}\cdot\ddot{\boldsymbol{\rho}}\right)\boldsymbol{r} + c^{33}_{4}(R,r)\left(\dot{\boldsymbol{\rho}}\cdot\ddot{\boldsymbol{\rho}}\right)\boldsymbol{\rho} + \frac{1}{r} c'^{33}_{5}(R,r)\left(\boldsymbol{r}\cdot\boldsymbol{\rho}\right)^2\left(\boldsymbol{r}\cdot\dddot{\boldsymbol{\rho}}\right)\boldsymbol{r} \\
&\quad + 2c^{33}_{5}(R,r)\left(\boldsymbol{r}\cdot\boldsymbol{\rho}\right)\left(\boldsymbol{r}\cdot\dddot{\boldsymbol{\rho}}\right)\boldsymbol{\rho} + c^{33}_{5}(R,r)\left(\boldsymbol{r}\cdot\boldsymbol{\rho}\right)^2\dddot{\boldsymbol{\rho}} + \frac{1}{r} c'^{33}_{6}(R,r)\left(\boldsymbol{r}\cdot\dot{\boldsymbol{\rho}}\right)\left(\boldsymbol{\rho}\cdot\ddot{\boldsymbol{\rho}}\right)\boldsymbol{r} + c^{33}_{6}(R,r)\left(\boldsymbol{\rho}\cdot\ddot{\boldsymbol{\rho}}\right)\dot{\boldsymbol{\rho}} \\
&\quad + \frac{1}{r} c'^{33}_{7}(R,r)\left(\boldsymbol{r}\cdot\ddot{\boldsymbol{\rho}}\right)\left(\boldsymbol{\rho}\cdot\dot{\boldsymbol{\rho}}\right)\boldsymbol{r} + c^{33}_{7}(R,r)\left(\boldsymbol{\rho}\cdot\dot{\boldsymbol{\rho}}\right)\ddot{\boldsymbol{\rho}} + \frac{1}{r} c'^{33}_{8}(R,r)\left(\boldsymbol{r}\cdot\boldsymbol{\rho}\right)\left(\boldsymbol{r}\cdot\dot{\boldsymbol{\rho}}\right)\left(\boldsymbol{r}\cdot\ddot{\boldsymbol{\rho}}\right)\boldsymbol{r} \\
&\quad + c^{33}_{8}(R,r)\left(\boldsymbol{r}\cdot\dot{\boldsymbol{\rho}}\right)\left(\boldsymbol{r}\cdot\ddot{\boldsymbol{\rho}}\right)\boldsymbol{\rho} + c^{33}_{8}(R,r)\left(\boldsymbol{r}\cdot\boldsymbol{\rho}\right)\left(\boldsymbol{r}\cdot\ddot{\boldsymbol{\rho}}\right)\dot{\boldsymbol{\rho}} + c^{33}_{8}(R,r)\left(\boldsymbol{r}\cdot\boldsymbol{\rho}\right)\left(\boldsymbol{r}\cdot\dot{\boldsymbol{\rho}}\right)\ddot{\boldsymbol{\rho}},
\end{aligned}
\tag{A.3.196}
$$

where prime ($'$) represents the differentiation with regard to r. By substituting $\boldsymbol{\rho}$ with $\boldsymbol{r}$, we have

$$
\begin{aligned}
&\nabla_{\boldsymbol{\rho}} c(\boldsymbol{\rho};\boldsymbol{\rho}) \\
&= \Big[\frac{1}{\rho}c'^{00}_{0}(R,\rho) + c'^{10}_{0}(R,\rho)\rho + c^{10}_{0}(R,\rho) + c'^{20}_{0}(R,\rho)\rho^3 + 2c^{20}_{0}(R,\rho)\rho^2 + c'^{20}_{1}(R,\rho)\rho + c'^{30}_{0}(R,\rho)\rho^5 \\
&\qquad +3c^{30}_{0}(R,\rho)\rho^4 + c'^{30}_{1}(R,\rho)\rho^3 + c^{30}_{1}(R,\rho)\rho^2\Big]\,\boldsymbol{\rho} \\
&\quad + \Big[\frac{1}{\rho}c'^{11}_{0}(R,\rho) + \frac{1}{\rho}c'^{21}_{0}(R,\rho) + c'^{21}_{1}(R,\rho)\rho + c^{21}_{1}(R,\rho) + c'^{31}_{0}(R,\rho)\rho + c'^{31}_{1}(R,\rho)\rho \\
&\qquad +c^{31}_{1}(R,\rho) + c'^{31}_{2}(R,\rho)\rho^3 + 2c^{31}_{2}(R,\rho)\rho^2\Big]\,(\boldsymbol{\rho}\cdot\dot{\boldsymbol{\rho}})\,\boldsymbol{\rho} \\
&\quad + \left[c^{11}_{0}(R,\rho) + c^{21}_{1}(R,\rho)\rho^2 + c^{31}_{0}(R,\rho)\rho^2 + c^{31}_{2}(R,\rho)\rho^4\right]\dot{\boldsymbol{\rho}} \\
&\quad + \Big[\frac{1}{\rho}c'^{12}_{0}(R,\rho) + \frac{1}{\rho}c'^{22}_{0}(R,\rho) + c'^{22}_{2}(R,\rho)\rho + c^{22}_{2}(R,\rho) + c'^{32}_{3}(R,\rho)\rho + c^{32}_{3}(R,\rho) + c'^{32}_{4}(R,\rho)\rho \\
&\qquad +c'^{32}_{5}(R,\rho)\rho^3 + 2c^{32}_{5}(R,\rho)\rho^2\Big]\,(\boldsymbol{\rho}\cdot\ddot{\boldsymbol{\rho}})\,\boldsymbol{\rho} \\
&\quad + \left[c^{12}_{0}(R,\rho) + c^{22}_{2}(R,\rho)\rho^2 + c^{32}_{4}(R,\rho)\rho^2 + c^{32}_{5}(R,\rho)\rho^4\right]\ddot{\boldsymbol{\rho}} \\
&\quad + \left[\frac{1}{\rho}c'^{22}_{1}(R,\rho) + c'^{32}_{0}(R,\rho)\rho + c^{32}_{0}(R,\rho)\right]|\dot{\boldsymbol{\rho}}|^2\,\boldsymbol{\rho} \\
&\quad + \left[\frac{1}{\rho}c'^{22}_{3}(R,\rho) + \frac{1}{\rho}c'^{32}_{1}(R,\rho) + c'^{32}_{2}(R,\rho)\rho + c^{32}_{2}(R,\rho)\right](\boldsymbol{\rho}\cdot\dot{\boldsymbol{\rho}})^2\,\boldsymbol{\rho} \\
&\quad + \left[2c^{22}_{3}(R,\rho) + c^{32}_{1}(R,\rho) + 2c^{32}_{2}(R,\rho)\rho^2\right](\boldsymbol{\rho}\cdot\dot{\boldsymbol{\rho}})\,\dot{\boldsymbol{\rho}} \\
&\quad + \Big[\frac{1}{\rho}c'^{13}_{0}(R,\rho) + \frac{1}{\rho}c'^{23}_{0}(R,\rho) + c'^{23}_{3}(R,\rho)\rho + c^{23}_{3}(R,\rho) + c'^{33}_{0}(R,\rho)\rho + c'^{33}_{2}(R,\rho)\rho \\
&\qquad +c^{33}_{2}(R,\rho) + c'^{33}_{5}(R,\rho)\rho^3 + 2c^{33}_{5}(R,\rho)\rho^2\Big]\,(\boldsymbol{\rho}\cdot\dddot{\boldsymbol{\rho}})\,\boldsymbol{\rho} \\
&\quad + \left[c^{13}_{0}(R,\rho) + c^{23}_{3}(R,\rho)\rho^2 + c^{33}_{0}(R,\rho)\rho^2 + c^{33}_{5}(R,\rho)\rho^4\right]\dddot{\boldsymbol{\rho}} \\
&\quad + \left[\frac{1}{\rho}c'^{23}_{1}(R,\rho) + c'^{33}_{4}(R,\rho)\rho + c^{33}_{4}(R,\rho)\right](\dot{\boldsymbol{\rho}}\cdot\ddot{\boldsymbol{\rho}})\,\boldsymbol{\rho} \\
&\quad + \left[\frac{1}{\rho}c'^{23}_{2}(R,\rho) + \frac{1}{\rho}c'^{33}_{6}(R,\rho) + \frac{1}{\rho}c'^{33}_{7}(R,\rho) + c'^{33}_{8}(R,\rho)\rho + c^{33}_{8}(R,\rho)\right](\boldsymbol{\rho}\cdot\dot{\boldsymbol{\rho}})\,(\boldsymbol{\rho}\cdot\ddot{\boldsymbol{\rho}})\,\boldsymbol{\rho} \\
&\quad + \left[c^{23}_{2}(R,\rho) + c^{33}_{6}(R,\rho) + c^{33}_{8}(R,\rho)\rho^2\right](\boldsymbol{\rho}\cdot\ddot{\boldsymbol{\rho}})\,\dot{\boldsymbol{\rho}} + \left[c^{23}_{2}(R,\rho) + c^{33}_{7}(R,\rho) + c^{33}_{8}(R,\rho)\rho^2\right](\boldsymbol{\rho}\cdot\dot{\boldsymbol{\rho}})\,\ddot{\boldsymbol{\rho}} \\
&\quad + \frac{1}{\rho}c'^{33}_{1}(R,\rho)\,|\dot{\boldsymbol{\rho}}|^2\,(\boldsymbol{\rho}\cdot\dot{\boldsymbol{\rho}})\,\boldsymbol{\rho} + c^{33}_{1}(R,\rho)\,|\dot{\boldsymbol{\rho}}|^2\,\dot{\boldsymbol{\rho}} + \frac{1}{\rho}c'^{33}_{3}(R,\rho)\,(\boldsymbol{\rho}\cdot\dot{\boldsymbol{\rho}})^3\,\boldsymbol{\rho} + 3c^{33}_{3}(R,\rho)\,(\boldsymbol{\rho}\cdot\dot{\boldsymbol{\rho}})^2\,\dot{\boldsymbol{\rho}}
\end{aligned}
\tag{A.3.197}
$$

$$
\begin{aligned}
&= \beta_1(R,\rho)\boldsymbol{\rho} + \beta_2(R,\rho)\,(\boldsymbol{\rho}\cdot\dot{\boldsymbol{\rho}})\,\boldsymbol{\rho} + \beta_3(R,\rho)\dot{\boldsymbol{\rho}} + \beta_4(R,\rho)\,(\boldsymbol{\rho}\cdot\ddot{\boldsymbol{\rho}})\,\boldsymbol{\rho} + \beta_5(R,\rho)\ddot{\boldsymbol{\rho}} + \beta_6(R,\rho)\,|\dot{\boldsymbol{\rho}}|^2\,\boldsymbol{\rho} \\
&\quad + \beta_7(R,\rho)\,(\boldsymbol{\rho}\cdot\dot{\boldsymbol{\rho}})^2\,\boldsymbol{\rho} + \beta_8(R,\rho)\,(\boldsymbol{\rho}\cdot\dot{\boldsymbol{\rho}})\,\dot{\boldsymbol{\rho}} + \beta_9(R,\rho)\,(\boldsymbol{\rho}\cdot\dddot{\boldsymbol{\rho}})\,\boldsymbol{\rho} + \beta_{10}(R,\rho)\dddot{\boldsymbol{\rho}} + \beta_{11}(R,\rho)\,(\dot{\boldsymbol{\rho}}\cdot\ddot{\boldsymbol{\rho}})\,\boldsymbol{\rho} \\
&\quad + \beta_{12}(R,\rho)\,(\boldsymbol{\rho}\cdot\dot{\boldsymbol{\rho}})\,(\boldsymbol{\rho}\cdot\ddot{\boldsymbol{\rho}})\,\boldsymbol{\rho} + \beta_{13}(R,\rho)\,(\boldsymbol{\rho}\cdot\ddot{\boldsymbol{\rho}})\,\dot{\boldsymbol{\rho}} + \beta_{14}(R,\rho)\,(\boldsymbol{\rho}\cdot\dot{\boldsymbol{\rho}})\,\ddot{\boldsymbol{\rho}} + \beta_{15}(R,\rho)\,|\dot{\boldsymbol{\rho}}|^2\,(\boldsymbol{\rho}\cdot\dot{\boldsymbol{\rho}})\,\boldsymbol{\rho} \\
&\quad + \beta_{16}(R,\rho)\,|\dot{\boldsymbol{\rho}}|^2\,\dot{\boldsymbol{\rho}} + \beta_{17}(R,\rho)\,(\boldsymbol{\rho}\cdot\dot{\boldsymbol{\rho}})^3\,\boldsymbol{\rho} + \beta_{18}(R,\rho)\,(\boldsymbol{\rho}\cdot\dot{\boldsymbol{\rho}})^2\,\dot{\boldsymbol{\rho}}.
\end{aligned}
\tag{A.3.198}
$$

By expanding the functions $\beta_i(R,\rho)$ with regard to ρ, we have

$$\begin{aligned}\boldsymbol{F}(\boldsymbol{\rho},\dot{\boldsymbol{\rho}},\ddot{\boldsymbol{\rho}}) =& -\left.\nabla c(\boldsymbol{r};\boldsymbol{\rho})\right|_{\boldsymbol{r}=\boldsymbol{\rho}} \\ =& a(R)\boldsymbol{\rho} + b(R)\dot{\boldsymbol{\rho}} + c(R)|\boldsymbol{\rho}|^2\boldsymbol{\rho} + g(R)\ddot{\boldsymbol{\rho}} + h(R)|\dot{\boldsymbol{\rho}}|^2\boldsymbol{\rho} + j(R)(\boldsymbol{\rho}\cdot\dot{\boldsymbol{\rho}})\boldsymbol{\rho} \\ &+ k(R)|\dot{\boldsymbol{\rho}}|^2\dot{\boldsymbol{\rho}} + h(R)|\boldsymbol{\rho}|^2\dot{\boldsymbol{\rho}} + p(R)(\boldsymbol{\rho}\cdot\dot{\boldsymbol{\rho}})\dot{\boldsymbol{\rho}},\end{aligned} \tag{A.3.199}$$

where the functions $a(R)$ and $c(R)$ are the zeroth and second order coefficients of Taylor expansion of $\beta_1(R,\rho)$ with regard to ρ, $j(R)$ is the zeroth order coefficient of Taylor expansion of $\beta_2(R,\rho)$ with regard to ρ, $b(R)$ is the summation of $(-\gamma_{\text{Euler}}+\log(2/\epsilon))/(4\pi)$ and the zeroth order coefficient of Taylor expansion of $\beta_3(R,\rho)$ with regard to ρ, $n(R)$ is the second order coefficient of Taylor expansion of $\beta_3(R,\rho)$ with regard to ρ, $g(R)$ is the summation of $-1/(16\pi)$ and the zeroth order coefficient of Taylor expansion of $\beta_5(R,\rho)$ with regard to ρ, $h(R)$ is the zeroth order coefficient of Taylor expansion of $\beta_6(R,\rho)$ with regard to ρ, $p(R)$ is the zeroth order coefficient of Taylor expansion of $\beta_8(R,\rho)$ with regard to ρ, and $k(R)$ is the summation of $-1/(32\pi)$ and the zeroth order coefficient of Taylor expansion of $\beta_{16}(R,\rho)$ with regard to ρ.

The dependence of the coefficients on R is shown in Fig. A.3.10. When R goes to infinity, the coefficients $a(R)$, $c(R)$, $h(R)$, $j(R)$, $n(R)$, and $p(R)$ go to zero and $b(R)$, $g(R)$, and $k(R)$ go to $(-\gamma_{\text{Euler}}+\log(2/\epsilon))/(4\pi)$, $-1/(16\pi)$, and $-1/(32\pi)$, respectively, and thus these calculations are consistent with the results for infinite case shown in Eq. (A.3.103).

A.3.5 Dependence of the coefficients in Eq. (2.4.61) on the water channel length R

The coefficients of the terms in the driving force in Eq. (2.4.61) depends on R. Here we show the dependence of $a(R)$, $b(R)$, $c(R)$, $g(R)$, $h(R)$, $j(R)$, $k(R)$, $n(R)$, and $p(R)$ on the water channel length R in Fig. A.3.10.

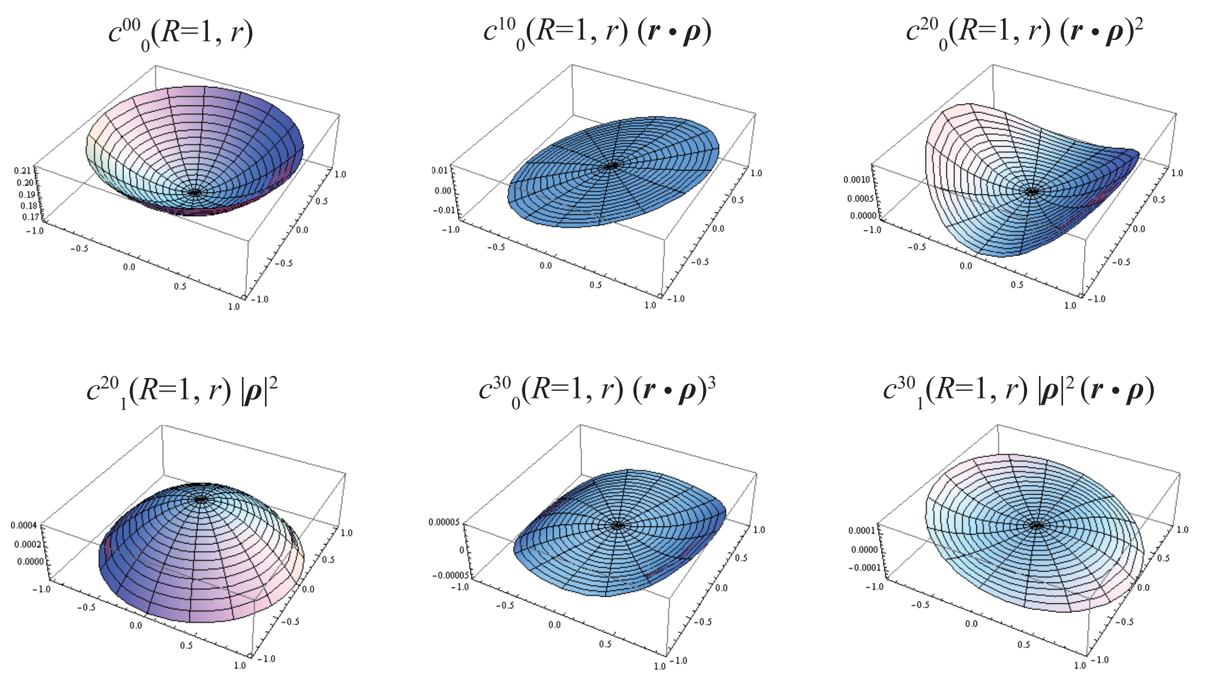

Figure A.3.3: Concentration fields related to the steady state for the stopping camphor particle at $\boldsymbol{r} = \boldsymbol{\rho}$. The explicit expressions for the components of the concentration field are in Eq. (A.3.192). The radius of the water chamber R is $R = 1$. Here we set $\boldsymbol{\rho} = (\rho, \phi) = (0.1, 0)$.

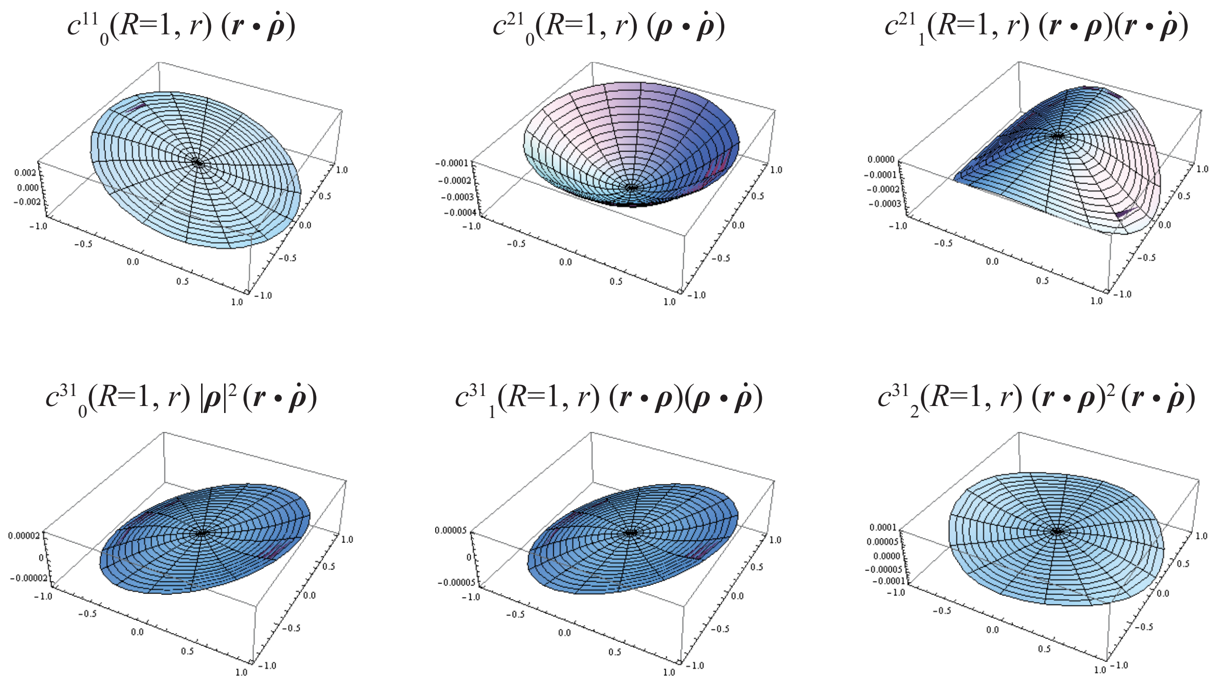

Figure A.3.4: Concentration fields related to the first order of the velocity. The explicit expressions for the components of the concentration field are in Eq. (A.3.193). The radius of the water chamber R is $R = 1$. Here we set $\boldsymbol{\rho} = (\rho, \phi) = (0.1, 0)$ and $\dot{\boldsymbol{\rho}} = (\dot{\rho}, \dot{\phi}) = (0.1, 0)$.

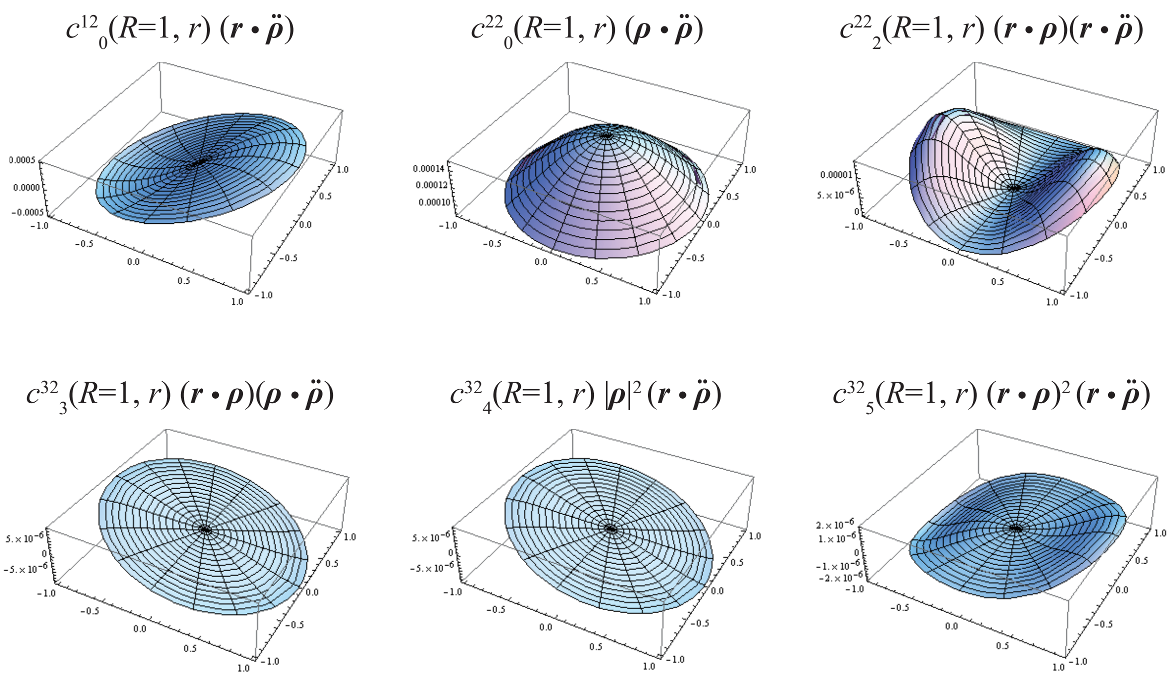

Figure A.3.5: Concentration fields related to the first order of the acceleration. The explicit expressions for the components of the concentration field are in Eq. (A.3.194). The radius of the water chamber R is $R = 1$. Here we set $\boldsymbol{\rho} = (\rho, \phi) = (0.1, 0)$ and $\ddot{\boldsymbol{\rho}} = (\ddot{\rho}, \ddot{\phi}) = (0.1, 0)$.

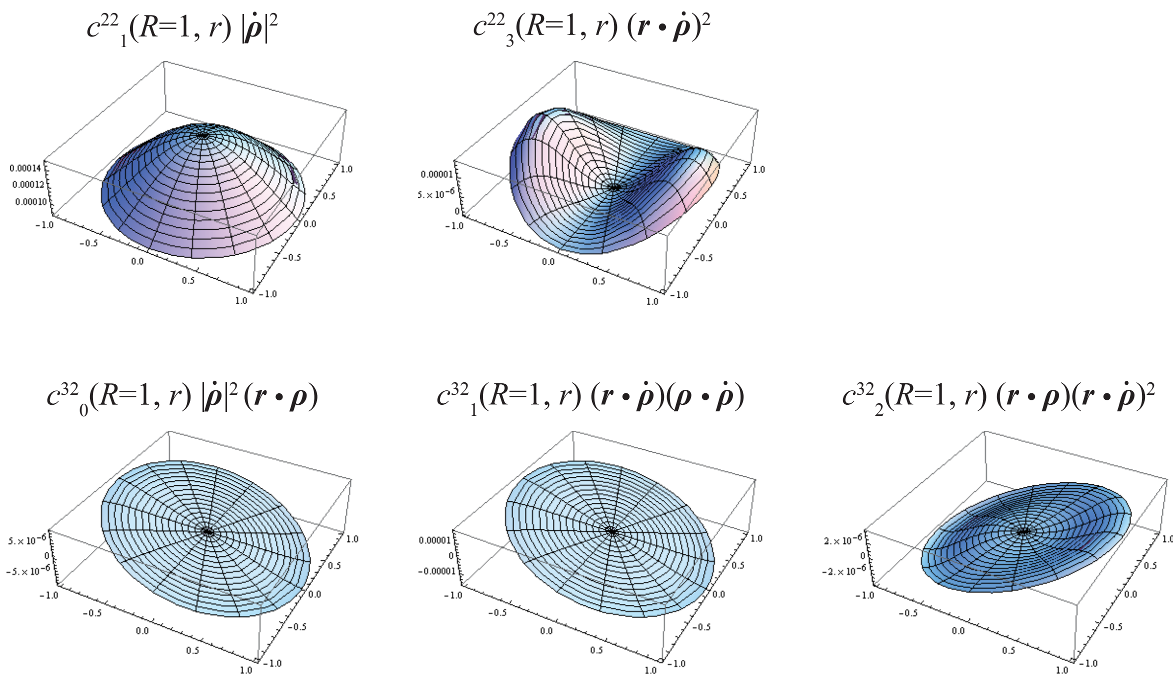

Figure A.3.6: Concentration fields related to the second order of the velocity. The explicit expressions for the components of the concentration field are in Eq. (A.3.194). The radius of the water chamber R is $R = 1$. Here we set $\boldsymbol{\rho} = (\rho, \phi) = (0.1, 0)$ and $\dot{\boldsymbol{\rho}} = (\dot{\rho}, \dot{\phi}) = (0.1, 0)$.

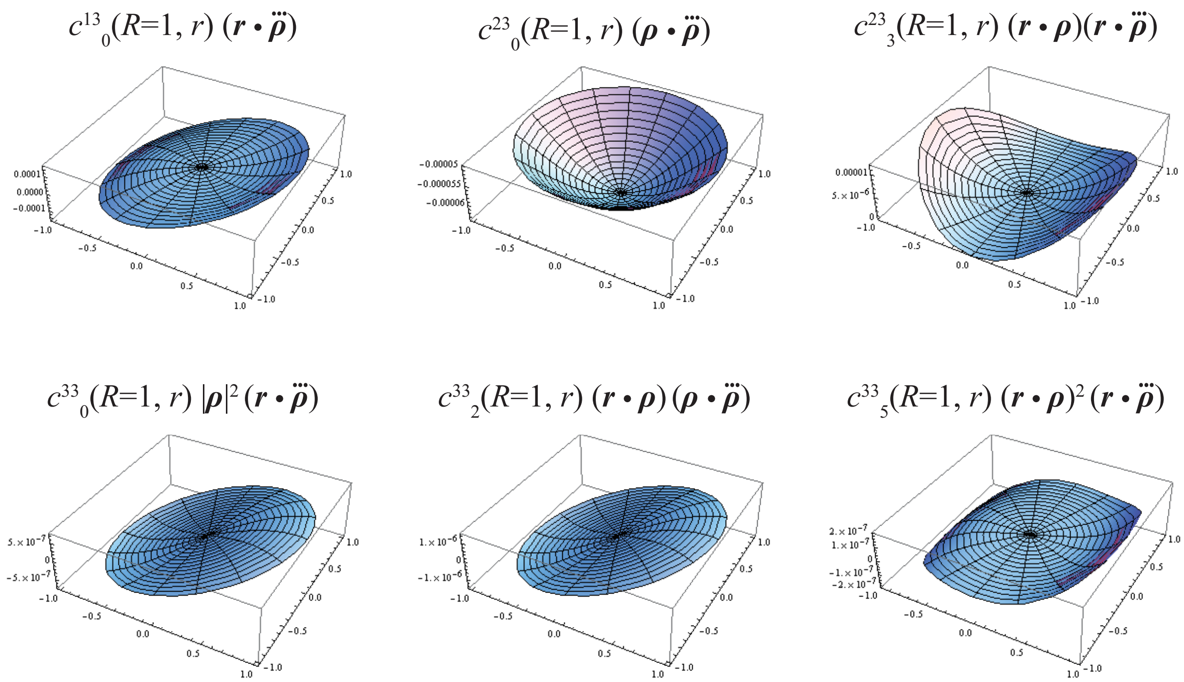

Figure A.3.7: Concentration fields related to the first order of the jerk (time derivative of acceleration). The explicit expressions for the components of the concentration field are in Eq. (A.3.195). The radius of the water chamber R is $R = 1$. Here we set $\boldsymbol{\rho} = (\rho, \phi) = (0.1, 0)$ and $\ddot{\boldsymbol{\rho}} = (\ddot{\rho}, \ddot{\phi}) = (0.1, 0)$.

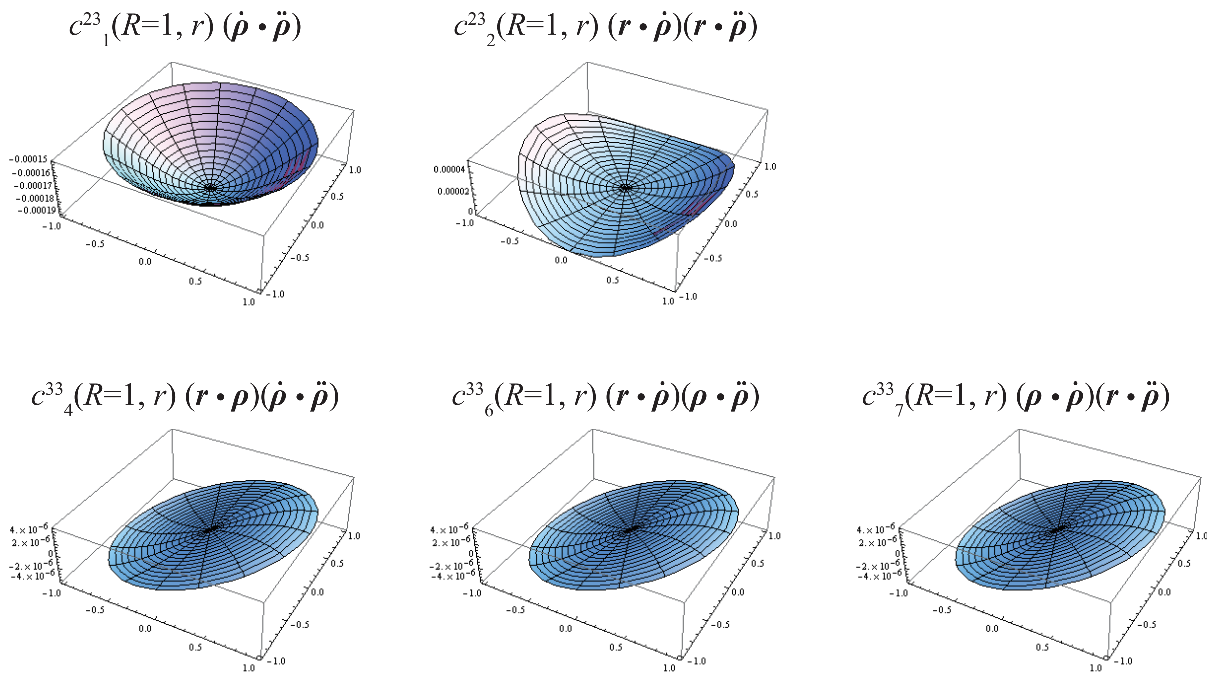

Figure A.3.8: Concentration fields related to the cross term of first order of the velocity and acceleration. The explicit expressions for the components of the concentration field are in Eq. (A.3.195). The radius of the water chamber R is $R = 1$. Here we set $\boldsymbol{\rho} = (\rho, \phi) = (0.1, 0)$ and $\dot{\boldsymbol{\rho}} = (\dot{\rho}, \dot{\phi}) = (0.1, 0)$.

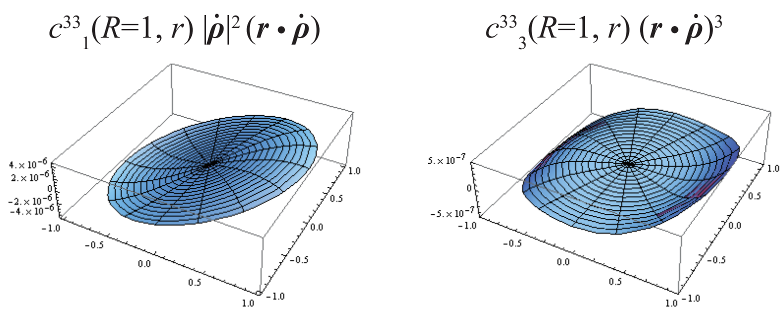

Figure A.3.9: Concentration fields related to the third order of the velocity. The explicit expressions for the components of the concentration field are in Eq. (A.3.195). The radius of the water chamber R is $R = 1$. Here we set $\boldsymbol{\rho} = (\rho, \phi) = (0.1, 0)$ and $\dot{\boldsymbol{\rho}} = (\dot{\rho}, \dot{\phi}) = (0.1, 0)$.

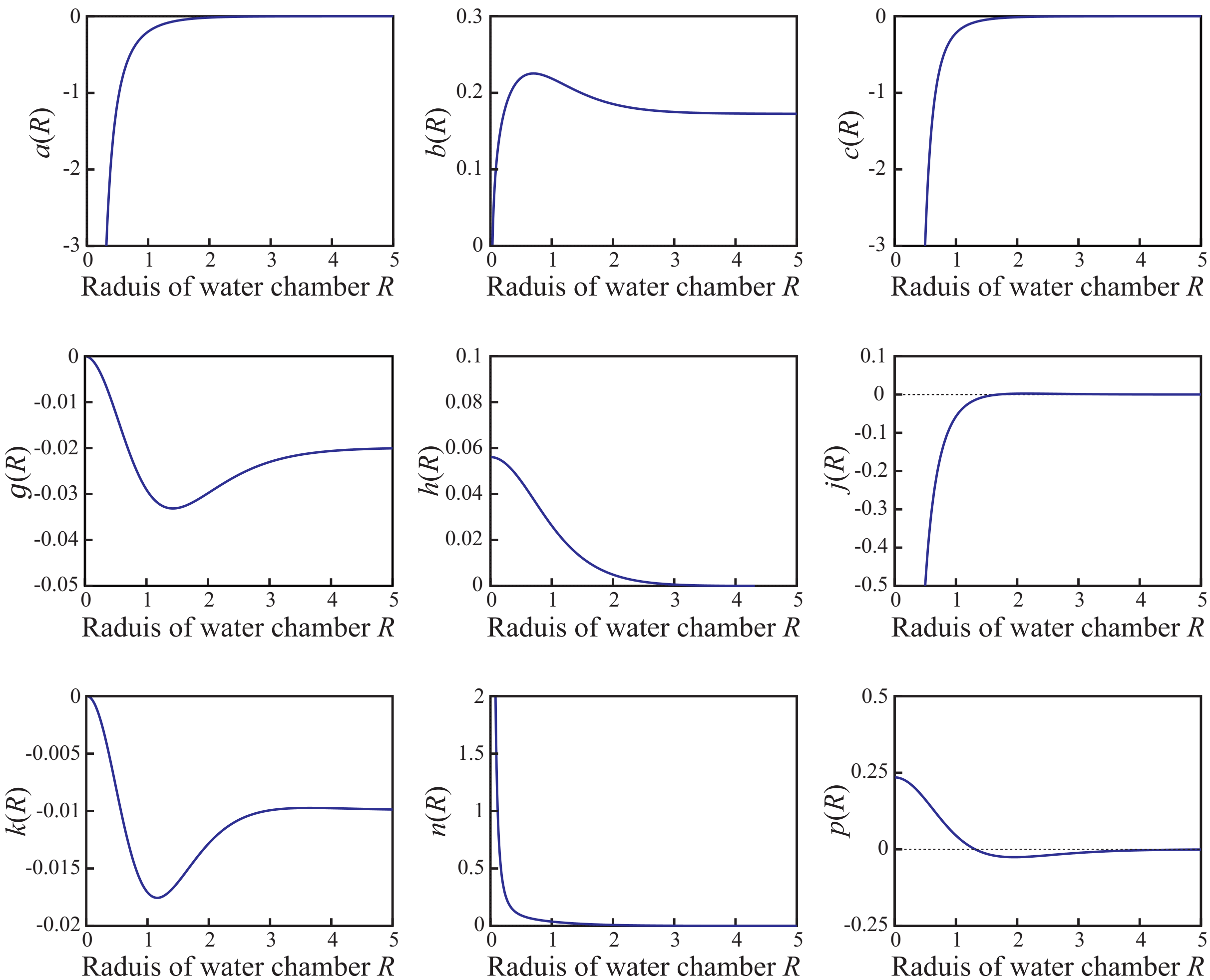

Figure A.3.10: Plots of the coefficients $a(R)$, $b(R)$, $c(R)$, $g(R)$, $h(R)$, $j(R)$, $k(R)$, $n(R)$, and $p(R)$ against the radius of water chamber R, which are shown in Eqs. (2.4.62), (2.4.63), (2.4.64), (2.4.65), (2.4.66), (2.4.67), (2.4.68), (2.4.69), and (2.4.70).

Appendix B

Supplementary Information for Chapter 3

In this chapter, the supplementary information for Chapter 3 is provided.

B.1 Derivation of Oseen tensors in a two- and three-dimensional fluid

In this section, we derive the Oseen tensors in a two- and three-dimensional systems. The Oseen tensors are the Green's function of the Stokesian equation with point force at the origin:

$$\nabla p - \eta \nabla^2 \boldsymbol{v} = \boldsymbol{F}\delta(\boldsymbol{r}), \tag{B.1.1}$$

where p is pressure, η is kinetic viscosity, $\boldsymbol{v}$ is flow field, $\boldsymbol{F}$ is a constant vector corresponding to the external point force, and $\delta(\boldsymbol{r})$ is the Dirac's delta function. We also assume incompressibility of fluid:

$$\nabla \cdot \boldsymbol{v} = 0. \tag{B.1.2}$$

We consider the Fourier transform of $p(\boldsymbol{r})$, $\boldsymbol{v}(\boldsymbol{r})$, and $\delta(\boldsymbol{r})$.

$$p(\boldsymbol{r}) = \frac{1}{(2\pi)^d} \int \tilde{p}(\boldsymbol{k}) e^{i\boldsymbol{k}\cdot\boldsymbol{r}} d\boldsymbol{k}, \tag{B.1.3}$$

$$\boldsymbol{v}(\boldsymbol{r}) = \frac{1}{(2\pi)^d} \int \tilde{\boldsymbol{v}}(\boldsymbol{k}) e^{i\boldsymbol{k}\cdot\boldsymbol{r}} d\boldsymbol{k}, \tag{B.1.4}$$

$$\delta(\boldsymbol{r}) = \frac{1}{(2\pi)^d} \int e^{i\boldsymbol{k}\cdot\boldsymbol{r}} d\boldsymbol{k}, \tag{B.1.5}$$

where $d = 2, 3$ denotes the spatial dimension. Then Eqs. (B.1.1) and (B.1.2) in wavenumber space are

$$i\boldsymbol{k}\tilde{p}(\boldsymbol{k}) + \eta k^2 \tilde{\boldsymbol{v}}(\boldsymbol{k}) = \boldsymbol{F}, \tag{B.1.6}$$

$$\tag{B.1.7}$$

$$i\boldsymbol{k} \cdot \tilde{\boldsymbol{v}}(\boldsymbol{k}) = 0. \tag{B.1.8}$$

By operating the scalar product with $\boldsymbol{k}$ to Eq. (B.1.6), the second term of the lefthand side becomes 0 from Eq. (B.1.8). Then we have

$$\tilde{p}(\boldsymbol{k}) = -i\frac{1}{k^2}\boldsymbol{k}\cdot\boldsymbol{F}. \tag{B.1.9}$$

By substituting Eq. (B.1.9) to Eq. (B.1.6), we have

$$\tilde{\boldsymbol{v}}(\boldsymbol{k}) = \frac{1}{\eta k^2}\left(\mathbb{1} - \frac{\boldsymbol{k}\boldsymbol{k}}{k^2}\right)\cdot\boldsymbol{F}, \tag{B.1.10}$$

where $\mathbb{1}$ is the unit tensor.

Here we derive the Oseen tensor in the two-dimensional system [87]. In the calculation below, we assume $\boldsymbol{r} = r\boldsymbol{e}_x$.

$$\begin{aligned}
G =& \frac{1}{(2\pi)^2}\int \frac{1}{\eta k^2}\left(\mathbb{1} - \frac{\boldsymbol{k}\boldsymbol{k}}{k^2}\right)e^{i\boldsymbol{k}\cdot\boldsymbol{r}}d\boldsymbol{k}\\
=& \frac{1}{(2\pi)^2\eta}\int_0^{2\pi}\int_0^{\infty}\frac{1}{k}\left(\mathbb{1} - \frac{\boldsymbol{k}\boldsymbol{k}}{k^2}\right)e^{ikr\cos\theta}dkd\theta\\
=& \frac{\mathbb{1}}{2\pi\eta}\int_0^{\infty}\frac{1}{k}\mathcal{J}_0(kr)dk - \frac{1}{4\pi^2\eta}\int_0^{2\pi}\int_0^{\infty}\frac{1}{k}\begin{pmatrix}\cos^2\theta & \sin\theta\cos\theta\\ \sin\theta\cos\theta & \sin^2\theta\end{pmatrix}e^{ikr\cos\theta}dkd\theta\\
=& \frac{\mathbb{1}}{2\pi\eta}\int_0^{\infty}\frac{1}{k}\mathcal{J}_0(kr)dk - \frac{1}{2\pi\eta}\int_0^{\infty}\frac{1}{k}\begin{pmatrix}\frac{\mathcal{J}_1(kr)}{kr} - \mathcal{J}_2(kr) & 0\\ 0 & \frac{\mathcal{J}_1(kr)}{kr}\end{pmatrix}dk\\
=& \frac{1}{2\pi\eta}\int_0^{\infty}\frac{1}{k}\left[\frac{1}{2}\left(\mathcal{J}_0(kr) - \mathcal{J}_2(kr)\right)\mathbb{1} + \begin{pmatrix}\mathcal{J}_2(kr) & 0\\ 0 & 0\end{pmatrix}\right]dk\\
=& \frac{1}{4\pi\eta}\left[\left(-\gamma_{\mathrm{Euler}} + \ln\frac{2}{\epsilon'} + 1\right)\mathbb{1} + \begin{pmatrix}1 & 0\\ 0 & 0\end{pmatrix}\right]\\
=& \frac{1}{4\pi\eta}\left[\left(-\gamma_{\mathrm{Euler}} + \ln\frac{2}{\epsilon}\right)\mathbb{1} + \boldsymbol{e}_x\boldsymbol{e}_x\right],
\end{aligned} \tag{B.1.11}$$

where γ_{Euler} is the Euler's constant ($\gamma_{\mathrm{Euler}} \simeq 0.577$). Here we used the following integrals (from Eq. (5) on page 19 in Ref. [81]):

$$\int_0^{2\pi} e^{ix\cos\theta}d\theta = 2\pi\mathcal{J}_0(x), \tag{B.1.12}$$

$$\int_0^{2\pi}\cos^2\theta e^{ix\cos\theta}d\theta = \frac{2\pi\mathcal{J}_1(x)}{x} - 2\pi\mathcal{J}_2(x), \tag{B.1.13}$$

$$\int_0^{2\pi}\sin\theta\cos\theta e^{ix\cos\theta}d\theta = 0, \tag{B.1.14}$$

$$\int_0^{2\pi}\sin^2\theta e^{ix\cos\theta}d\theta = \int_0^{2\pi}(1-\cos^2\theta)e^{ix\cos\theta}d\theta = 2\pi\mathcal{J}_0(x) - \left(\frac{2\pi\mathcal{J}_1(x)}{x} - 2\pi J_2(x)\right) = \frac{2\pi\mathcal{J}_1(x)}{x}, \tag{B.1.15}$$

where $\mathcal{J}_0(x) + \mathcal{J}_2(x) = -\mathcal{J}_1(x)/2$. We also use the following definite integrals:

$$\int_\epsilon^{\infty}\frac{\mathcal{J}_0(x)}{x}d\theta = -\gamma_{\mathrm{Euler}} + \ln\frac{2}{\epsilon}, \tag{B.1.16}$$

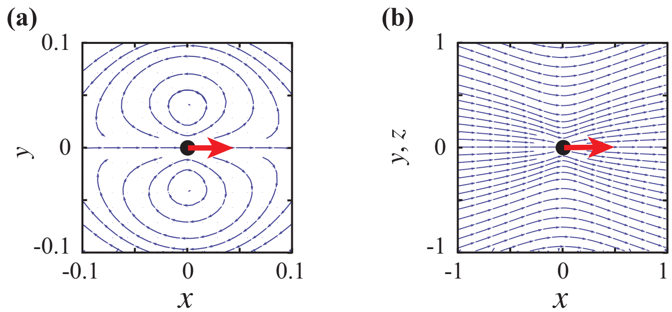

Figure B.1.1: Streamlines of flow field induced by a point force. The flow fields $G_{\alpha\beta}F_\beta$ in (a) a two-dimensional and (b) a three-dimensional systems are shown. Here we set $\boldsymbol{F} = \boldsymbol{e}_x$.

$$\int_0^\infty \frac{\mathcal{J}_2(x)}{x} d\theta = \frac{1}{2}. \tag{B.1.17}$$

By considering the symmetry, the Oseen tensor for arbitrary $\boldsymbol{r}$ is expressed as

$$G_{\alpha\beta} = \frac{1}{4\pi\eta}\left(-(1+\ln(\kappa r))\mathbb{1} + \frac{r_\alpha r_\beta}{r^2}\right), \tag{B.1.18}$$

where κ is a positive constant. The streamlines of flow field $G_{\alpha\beta}F_\beta$ induced by a point force in the two-dimensional system are expressed in Fig. B.1.1(a).

Next, we derive the Oseen tensor in a three-dimensional system. In the calculation below, we assume $\boldsymbol{r} = r\boldsymbol{e}_z$.

$$
\begin{aligned}
G =& \frac{1}{(2\pi)^3} \int \frac{1}{\eta k^2} \left(\mathbb{1} - \frac{\boldsymbol{k}\boldsymbol{k}}{k^2} \right) e^{i\boldsymbol{k}\cdot\boldsymbol{r}} d\boldsymbol{k} \\
=& \frac{1}{(2\pi)^3 \eta} \int_0^{2\pi} \int_{-1}^{1} \int_0^{\infty} \left(\mathbb{1} - \frac{\boldsymbol{k}\boldsymbol{k}}{k^2} \right) e^{ikr\cos\theta} dk d(\cos\theta) d\phi \\
=& \frac{\mathbb{1}}{4\pi^2\eta} \int_0^{\infty} \frac{2\sin(kr)}{kr} dk d(\cos\theta) \\
& - \frac{\mathbb{1}}{8\pi^3\eta} \int_0^{2\pi} \int_{-1}^{1} \int_0^{\infty} \begin{pmatrix} \sin^2\theta\cos^2\phi & \sin^2\theta\sin\phi\cos\phi & \sin\theta\cos\theta\cos\phi \\ \sin^2\theta\sin\phi\cos\phi & \sin^2\theta\sin^2\phi & \sin\theta\cos\theta\sin\phi \\ \sin\theta\cos\theta\cos\phi & \sin\theta\cos\theta\sin\phi & \cos^2\theta \end{pmatrix} e^{ikr\cos\theta} dk d(\cos\theta) d\phi \\
=& \frac{\mathbb{1}}{4\pi\eta r} - \frac{1}{8\pi^2\eta} \int_{-1}^{1} \int_0^{\infty} \begin{pmatrix} \sin^2\theta & 0 & 0 \\ 0 & \sin^2\theta & 0 \\ 0 & 0 & 2\cos^2\theta \end{pmatrix} e^{ikr\cos\theta} dk d(\cos\theta) \\
=& \frac{\mathbb{1}}{4\pi\eta r} - \frac{1}{8\pi^2\eta} \int_0^{\infty} \begin{pmatrix} -\frac{4\cos(kr)}{k^2r^2} + \frac{4\sin(kr)}{k^3r^3} & 0 & 0 \\ 0 & -\frac{4\cos(kr)}{k^2r^2} + \frac{4\sin(kr)}{k^3r^3} & 0 \\ 0 & 0 & \frac{4\sin(kr)}{kr} + \frac{8\cos(kr)}{k^2r^2} - \frac{8\sin(kr)}{k^3r^3} \end{pmatrix} dk \\
=& \frac{\mathbb{1}}{4\pi\eta r} - \frac{1}{8\pi\eta r} \begin{pmatrix} 1 & 0 & 0 \\ 0 & 1 & 0 \\ 0 & 0 & 0 \end{pmatrix} \\
=& \frac{\mathbb{1}}{8\pi\eta r} - \frac{1}{8\pi\eta r} \begin{pmatrix} 0 & 0 & 0 \\ 0 & 0 & 0 \\ 0 & 0 & 1 \end{pmatrix} \\
=& \frac{\mathbb{1}}{8\pi\eta r} + \frac{\boldsymbol{e}_z\boldsymbol{e}_z}{8\pi\eta r}.
\end{aligned} \tag{B.1.19}
$$

In the above calculation, we use the following integral

$$
\begin{aligned}
\int_{-1}^{1} x^2 e^{ikrx} dx =& \left[e^{ikrx} \left(\frac{x^2}{ikr} - \frac{2x}{(ikr)^2} + \frac{2}{(ikr)^3} \right) \right]_{-1}^{1} \\
=& e^{ikr} \left(\frac{1}{ikr} + \frac{2}{k^2r^2} - \frac{2}{ik^3r^3} \right) - e^{-ikr} \left(\frac{1}{ikr} - \frac{2}{k^2r^2} + \frac{2}{ik^3r^3} \right) \\
=& \frac{2\sin(kr)}{kr} - \frac{4\cos(kr)}{k^2r^2} + \frac{4\sin(kr)}{k^3r^3}.
\end{aligned} \tag{B.1.20}
$$

We also use the following integrals (from Eq. (4.3.142) on page 78 in Ref. [91]):

$$
\int_0^{\infty} \frac{\sin x}{x} dx = \frac{\pi}{2}, \tag{B.1.21}
$$

$$
\int_0^{\infty} \left(-\frac{\cos x}{x^2} + \frac{\sin x}{x^3} \right) dx = \frac{\pi}{4}. \tag{B.1.22}
$$

By considering the symmetry, the Oseen tensor for arbitrary $\boldsymbol{r}$ is expressed as

$$
G_{\alpha\beta} = \frac{1}{8\pi\eta} \left(\frac{1}{r}\delta_{\alpha\beta} + \frac{r_\alpha r_\beta}{r^3} \right). \tag{B.1.23}
$$

The streamlines of flow field $G_{\alpha\beta}F_\beta$ induced by a point force in a three-dimensional system are expressed in Fig. B.1.1(b).

B.2 Derivation of the simple forms of the Kramers-Moyal coefficients of the first and second orders

In this section, we simplify the Kramers-Moyal coefficients of the first and second orders in Eqs. (3.2.22) and (3.2.23).

B.2.1 Derivation of Eqs. (3.3.3) and (3.3.4)

According to the definition of the Kramers-Moyal coefficients of the first and second orders in Eqs. (3.2.22) and (3.2.23) and the Oseen tensor in Eq. (B.1.18), we have

$$\begin{aligned}V(\boldsymbol{R}) =&\frac{1}{8}\int\left[2\left(\frac{\partial G_{\alpha 1}}{\partial r_1}\frac{\partial G_{\alpha' 1}}{\partial r_1}+\frac{\partial G_{\alpha 2}}{\partial r_2}\frac{\partial G_{\alpha' 2}}{\partial r_2}\right)+\left(\frac{\partial G_{\alpha 1}}{\partial r_2}+\frac{\partial G_{\alpha' 2}}{\partial r_1}\right)\left(\frac{\partial G_{\alpha' 1}}{\partial r_2}+\frac{\partial G_{\alpha' 2}}{\partial r_1}\right)\right.\\ &\left.+\left(\frac{\partial G_{\alpha 1}}{\partial r_1}+\frac{\partial G_{\alpha 2}}{\partial r_2}\right)\left(\frac{\partial G_{\alpha' 1}}{\partial r_1}+\frac{\partial G_{\alpha' 2}}{\partial r_2}\right)\right]S(\boldsymbol{R}+\boldsymbol{r})c(\boldsymbol{R}+\boldsymbol{r})d\boldsymbol{r}. \qquad \text{(B.2.1)}\end{aligned}$$

Here, we used

$$\begin{aligned}\Lambda_{\beta\beta'\gamma\gamma'} =&\frac{1}{2\pi}\int_0^{2\pi} e_\beta e_{\beta'} e_\gamma e_{\gamma'} d\theta\\ =&\frac{1}{8}\left(\delta_{\beta\beta'}\delta_{\gamma\gamma'}+\delta_{\beta\gamma}\delta_{\beta'\gamma'}+\delta_{\beta\gamma'}\delta_{\beta'\gamma}\right)\\ =&\begin{cases}\frac{3}{8} & (\beta,\beta',\gamma,\gamma')=(1,1,1,1),(2,2,2,2),\\ \frac{1}{8} & (\beta,\beta',\gamma,\gamma')=(1,1,2,2),(1,2,1,2),(1,2,2,1),(2,1,1,2),(2,1,2,1),(2,2,1,1),\\ 0 & \text{otherwise},\end{cases}\end{aligned} \qquad \text{(B.2.2)}$$

where e_1 and e_2 are first and second components of a unit vector $\boldsymbol{e}=(\cos\theta,\sin\theta)$, respectively.

The first term in the integral can be calculated as

$$\begin{aligned}&\frac{\partial^2 G_{\alpha 1}}{\partial r_1 \partial r_\delta}\frac{\partial G_{\delta 1}}{\partial r_1}+\frac{\partial^2 G_{\alpha 2}}{\partial r_2 \partial r_\delta}\frac{\partial G_{\delta 2}}{\partial r_2}\\ &=\frac{1}{(4\pi\eta)^2}\left[\left(\frac{\delta_{\alpha\delta}}{r^2}-\frac{2}{r^4}(2r_\alpha r_1\delta_{1\delta}+r_\alpha r_\delta+{r_1}^2\delta_{\alpha\delta})+\frac{8{r_1}^2 r_\alpha r_\delta}{r^6}\right)\left(\frac{r_\delta}{r^2}-\frac{2r_\delta {r_1}^2}{r^4}\right)\right.\\ &\qquad\left.+\left(\frac{\delta_{\alpha\delta}}{r^2}-\frac{2}{r^4}(2r_\alpha r_2\delta_{2\delta}+r_\alpha r_\delta+{r_2}^2\delta_{\alpha\delta})+\frac{8{r_2}^2 r_\alpha r_\delta}{r^6}\right)\left(\frac{r_\delta}{r^2}-\frac{2r_\delta {r_2}^2}{r^4}\right)\right]\\ &=\frac{1}{(4\pi\eta)^2}\left(-\frac{2r_\alpha}{r^4}+\frac{8{r_1}^2{r_2}^2 r_\alpha}{r^8}\right). \qquad \text{(B.2.3)}\end{aligned}$$

The second term in the integral can be calculated as

$$
\begin{aligned}
&\left(\frac{\partial^2 G_{\alpha 1}}{\partial r_2 \partial r_\delta}+\frac{\partial^2 G_{\alpha 2}}{\partial r_1 \partial r_\delta}\right)\left(\frac{\partial G_{\delta 1}}{\partial r_2}+\frac{\partial G_{\delta 2}}{\partial r_1}\right) \\
&\quad=\frac{4}{(4\pi\eta)^2}\left(-\frac{1}{r^4}(r_\alpha r_1\delta_{2\delta}+r_\alpha r_2\delta_{1\delta}+r_1 r_2\delta_{\alpha\delta})+\frac{4r_1r_2r_\alpha r_\delta}{r^6}\right)\left(-\frac{4r_1r_2r_\delta}{r^4}\right) \\
&\quad=\frac{1}{(4\pi\eta)^2}\left(-\frac{16r_1r_2}{r^4}\right)\left(-\frac{1}{r^4}(r_\alpha r_1 r_2+r_\alpha r_2 r_1+r_1 r_2 r_\alpha)+\frac{4r_1r_2r_\alpha({r_1}^2+{r_2}^2)}{r^6}\right) \\
&\quad=\frac{1}{(4\pi\eta)^2}\left(-\frac{16{r_1}^2{r_2}^2 r_\alpha}{r^8}\right).
\end{aligned}
\tag{B.2.4}
$$

Here we use

$$
\frac{\partial^2 G_{\alpha 1}}{\partial r_2 \partial r_\delta}+\frac{\partial^2 G_{\alpha 2}}{\partial r_1 \partial r_\delta}=\frac{4}{4\pi\eta}\left(-\frac{1}{r^4}(r_\alpha r_1\delta_{2\delta}+r_\alpha r_2\delta_{1\delta}+r_1 r_2\delta_{\alpha\delta})+\frac{4r_1r_2r_\alpha r_\delta}{r^6}\right),
\tag{B.2.5}
$$

$$
\frac{\partial G_{\delta 1}}{\partial r_2}+\frac{\partial G_{\delta 2}}{\partial r_1}=\frac{1}{4\pi\eta}\left(-\frac{4r_1r_2r_\delta}{r^4}\right).
\tag{B.2.6}
$$

The third term in the integral vanishes, because

$$
\frac{\partial G_{\delta 1}}{\partial r_1}+\frac{\partial G_{\delta 2}}{\partial r_2}=0.
\tag{B.2.7}
$$

Thus, we have

$$
\begin{aligned}
V_\alpha(\boldsymbol{R})=&-\Lambda_{\beta\beta'\gamma\gamma'}\int\frac{\partial^2 G_{\alpha\beta}}{\partial r_\gamma \partial r_\delta}\frac{\partial G_{\delta\beta'}}{\partial r'_\gamma}S(\boldsymbol{R}+\boldsymbol{r})c(\boldsymbol{R}+\boldsymbol{r})d\boldsymbol{r} \\
=&\frac{1}{32\pi^2\eta^2}\int\frac{r_\alpha}{r^4}S(\boldsymbol{R}+\boldsymbol{r})c(\boldsymbol{R}+\boldsymbol{r})d\boldsymbol{r}.
\end{aligned}
\tag{B.2.8}
$$

The Kramers-Moyal coefficient of the second order is simplified in the following manner:

$$
\begin{aligned}
D(\boldsymbol{R})=-\frac{1}{8}\int\Bigg[&2\left(\frac{\partial^2 G_{\alpha 1}}{\partial r_1 \partial r_\delta}\frac{\partial G_{\delta 1}}{\partial r_1}+\frac{\partial^2 G_{\alpha 2}}{\partial r_2 \partial r_\delta}\frac{\partial G_{\delta 2}}{\partial r_2}\right)+\left(\frac{\partial^2 G_{\alpha 1}}{\partial r_2 \partial r_\delta}+\frac{\partial^2 G_{\alpha 2}}{\partial r_1 \partial r_\delta}\right)\left(\frac{\partial G_{\delta 1}}{\partial r_2}+\frac{\partial G_{\delta 2}}{\partial r_1}\right) \\
&+\left(\frac{\partial^2 G_{\alpha 1}}{\partial r_1 \partial r_\delta}+\frac{\partial^2 G_{\alpha 1}}{\partial r_2 \partial r_\delta}\right)\left(\frac{\partial G_{\delta 1}}{\partial r_1}+\frac{\partial G_{\delta 2}}{\partial r_2}\right)\Bigg]S(\boldsymbol{R}+\boldsymbol{r})c(\boldsymbol{R}+\boldsymbol{r})d\boldsymbol{r}.
\end{aligned}
\tag{B.2.9}
$$

The first term in the integral can be calculated as

$$
\begin{aligned}
&\frac{\partial G_{\alpha 1}}{\partial r_1}\frac{\partial G_{\alpha' 1}}{\partial r_1}+\frac{\partial G_{\alpha 2}}{\partial r_2}\frac{\partial G_{\alpha' 2}}{\partial r_2} \\
&\quad=\frac{1}{(4\pi\eta)^2}\left(\frac{r_\alpha}{r^2}-\frac{2{r_1}^2 r_\alpha}{r^4}\right)\left(\frac{r_{\alpha'}}{r^2}-\frac{2{r_1}^2 r_{\alpha'}}{r^4}\right)+\frac{1}{(4\pi\eta)^2}\left(\frac{r_\alpha}{r^2}-\frac{2{r_2}^2 r_\alpha}{r^4}\right)\left(\frac{r_{\alpha'}}{r^2}-\frac{2{r_2}^2 r_{\alpha'}}{r^4}\right) \\
&\quad=\frac{1}{(4\pi\eta)^2}\left(\frac{2r_\alpha r_{\alpha'}}{r^8}\left({r_1}^4+{r_2}^4-2{r_1}^2{r_2}^2\right)\right).
\end{aligned}
\tag{B.2.10}
$$

The second term is calculated as

$$
\left(\frac{\partial G_{\alpha 1}}{\partial r_2}+\frac{\partial G_{\alpha' 2}}{\partial r_1}\right)\left(\frac{\partial G_{\alpha' 1}}{\partial r_2}+\frac{\partial G_{\alpha' 2}}{\partial r_1}\right)=\frac{1}{(4\pi\eta)^2}\frac{16{r_1}^2{r_2}^2 r_\alpha r_{\alpha'}}{r^8},
\tag{B.2.11}
$$

since

$$\frac{\partial G_{\alpha 1}}{\partial r_2} + \frac{\partial G_{\alpha' 2}}{\partial r_1} = \frac{1}{4\pi\eta}\left(-\frac{4r_1 r_2 r_\alpha}{r^4}\right). \tag{B.2.12}$$

The third term in the integral vanishes since

$$\frac{\partial G_{\alpha 1}}{\partial r_1} + \frac{\partial G_{\alpha 2}}{\partial r_2} = 0. \tag{B.2.13}$$

Thus, the diffusion tensor originating from the active force dipole, ${D^A}_{\alpha\alpha'}$, can be represented as

$${D^A}_{\alpha\alpha'}(\boldsymbol{R}) = \int \frac{1}{2(4\pi\eta)^2}\frac{r_\alpha r_{\alpha'}}{r^4} S(\boldsymbol{R}+\boldsymbol{r})c(\boldsymbol{R}+\boldsymbol{r})d\boldsymbol{r}. \tag{B.2.14}$$

As an example of an actual system, we consider the case with constant concentration c_0 in the circular raft whose radius is R. Here, we regard $S(\boldsymbol{r})$ as a constant. Since the system is symmetric with regard to the center of the circular raft, we calculate in the case when $\boldsymbol{r} = (r, 0)$ without losing generality. Inside of the raft ($r < R - \ell_c$), $\boldsymbol{V}(\boldsymbol{r})$ and $D(\boldsymbol{r})$ are calculated as follows. We adopt the polar coordinates in which the origin corresponds to $\boldsymbol{r}$. The range of the integral of radial direction is $\left[0, -r\cos\theta + \sqrt{R^2 - r^2\sin^2\theta}\right]$. The upper limit of the integral is obtained by solving ${r_{max}}^2 + r^2 - 2r_{max} r\cos(\pi - \theta) = R^2$ with regard to r_{max}.

$$\begin{aligned}
\boldsymbol{V}(r\boldsymbol{e}_x) =& \frac{S}{32\pi^2\eta^2}\int \frac{1}{r'^4}\begin{pmatrix} r'_1 \\ r'_2 \end{pmatrix} c(\boldsymbol{r}+\boldsymbol{r}')d\boldsymbol{r}' \\
=& \frac{Sc_0}{32\pi^2\eta^2}\int_0^{2\pi}\int_0^{-r\cos\theta+\sqrt{R^2-r^2\sin^2\theta}} \frac{1}{r'^4}\begin{pmatrix} r'\cos\theta \\ r'\sin\theta \end{pmatrix} r'dr'd\theta \\
=& \frac{Sc_0}{32\pi^2\eta^2}\int_0^{2\pi}\left(\frac{-1}{-r\cos\theta+\sqrt{R^2-r^2\sin^2\theta}} - \frac{-1}{\ell_c}\right)\begin{pmatrix} \cos\theta \\ \sin\theta \end{pmatrix} d\theta \\
=& -\frac{Sc_0}{32\pi\eta^2}\begin{pmatrix} \dfrac{r}{R^2-r^2} \\ 0 \end{pmatrix},
\end{aligned} \tag{B.2.15}$$

$$\begin{aligned}
D^A(r\boldsymbol{e}_x) =& \frac{S}{32\pi^2\eta^2}\int \frac{1}{r'^4}\begin{pmatrix} {r'_1}^2 & r'_1 r'_2 \\ r'_1 r'_2 & {r'_2}^2 \end{pmatrix} c(\boldsymbol{r}+\boldsymbol{r}')d\boldsymbol{r}' \\
=& \frac{Sc_0}{32\pi^2\eta^2}\int_0^{2\pi}\int_0^{-r\cos\theta+\sqrt{R^2-r^2\sin^2\theta}} \frac{1}{r'^4}\begin{pmatrix} r'^2\cos^2\theta & r'^2\sin\theta\cos\theta \\ r'^2\sin\theta\cos\theta & r'^2\sin^2\theta \end{pmatrix} r'dr'd\theta \\
=& \frac{Sc_0}{32\pi^2\eta^2}\int_0^{2\pi}\left(\ln\left(-r\cos\theta+\sqrt{R^2-r^2\sin^2\theta}\right) - \ln\ell_c\right)\begin{pmatrix} \cos^2\theta & \sin\theta\cos\theta \\ \sin\theta\cos\theta & \sin^2\theta \end{pmatrix} d\theta \\
=& \frac{Sc_0}{32\pi\eta^2}\left\{\begin{pmatrix} \dfrac{\pi}{2}\ln\left(R^2-r^2\right) & 0 \\ 0 & \dfrac{\pi}{2}\ln\left(R^2-r^2\right) \end{pmatrix} + \ln\frac{1}{\ell_c}\begin{pmatrix} \pi & 0 \\ 0 & \pi \end{pmatrix}\right\} \\
=& \frac{Sc_0}{32\pi\eta^2}\ln\left(\frac{\sqrt{R^2-r^2}}{\ell_c}\right)\mathbb{1}.
\end{aligned} \tag{B.2.16}$$

Outside of the raft ($r > R + \ell_c$), $\boldsymbol{V}(\boldsymbol{r})$ and $D(\boldsymbol{r})$ are calculated as follows.

$$\begin{aligned}
\boldsymbol{V}(r\boldsymbol{e}_x) =& \frac{S}{32\pi^2\eta^2}\int \frac{1}{r'^4}\begin{pmatrix} r'_1 \\ r'_2 \end{pmatrix} c(\boldsymbol{r}+\boldsymbol{r}')d\boldsymbol{r}' \\
=& \frac{Sc_0}{32\pi^2\eta^2}\int_0^{2\pi}\int_0^R \frac{1}{(r'^2+r^2-2r'r\cos\theta)^2}\begin{pmatrix} r'\cos\theta - r \\ r'\sin\theta \end{pmatrix} r'dr'd\theta \\
=& \frac{Sc_0}{32\pi^2\eta^2}\int_0^R \begin{pmatrix} -\dfrac{2\pi r}{(R^2-r'^2)^2} \\ 0 \end{pmatrix} r'dr' \\
=& -\frac{Sc_0}{32\pi\eta^2}\begin{pmatrix} \dfrac{R^2}{r(r^2-R^2)} \\ 0 \end{pmatrix},
\end{aligned} \tag{B.2.17}$$

$$\begin{aligned}
&D^A(r\boldsymbol{e}_x) \\
&= \frac{S}{32\pi^2\eta^2}\int \frac{1}{r'^4}\begin{pmatrix} {r'_1}^2 & r'_1r'_2 \\ r'_1r'_2 & {r'_2}^2 \end{pmatrix} c(\boldsymbol{r}+\boldsymbol{r}')d\boldsymbol{r}' \\
&= \frac{Sc_0}{32\pi^2\eta^2}\int_0^{2\pi}\int_0^R \frac{1}{(r'^2+r^2-2r'r\cos\theta)^2}\begin{pmatrix} (r'\cos\theta-r)^2 & r'\sin\theta(r'\cos\theta-r) \\ r'\sin\theta(r'\cos\theta-r) & r'^2\sin^2\theta \end{pmatrix} r'dr'd\theta \\
&= \frac{Sc_0}{32\pi^2\eta^2}\int_0^R \begin{pmatrix} \dfrac{\pi(2r^2-r'^2)}{r^2(r^2-r'^2)} & 0 \\ 0 & \dfrac{\pi r'^2}{r^2(r^2-r'^2)} \end{pmatrix} r'dr' \\
&= \frac{Sc_0}{32\pi\eta^2}\begin{pmatrix} \dfrac{R^2}{2r^2} + \ln\dfrac{r}{\sqrt{r^2-R^2}} & 0 \\ 0 & -\dfrac{R^2}{2r^2} + \ln\dfrac{r}{\sqrt{r^2-R^2}} \end{pmatrix} \\
&= \frac{Sc_0}{32\pi\eta^2}\left\{\ln\left(\frac{r}{\sqrt{r^2-R^2}}\right)\mathbb{1} + \frac{R^2}{2r^2}\begin{pmatrix} 1 & 0 \\ 0 & -1 \end{pmatrix}\right\}.
\end{aligned} \tag{B.2.18}$$

By introducing the rotation tensor $\mathcal{R}(\theta)$ as

$$\mathcal{R}(\theta) = \begin{pmatrix} \cos\theta & -\sin\theta \\ \sin\theta & \cos\theta \end{pmatrix}, \tag{B.2.19}$$

$\boldsymbol{V}(\boldsymbol{r})$ and $D(\boldsymbol{r})$ are expressed as follows:

$$\boldsymbol{V}(\boldsymbol{r}) = \boldsymbol{V}(r,\theta) = \boldsymbol{V}(r\boldsymbol{e}_x)\mathcal{R}(\theta), \tag{B.2.20}$$

$$D(\boldsymbol{r}) = D(r,\theta) = \mathcal{R}(\theta)D(r\boldsymbol{e}_x)\mathcal{R}(-\theta), \tag{B.2.21}$$

where

$$\boldsymbol{V}(\boldsymbol{r}) = -\frac{Sc_0}{32\pi\eta^2}\begin{cases} \begin{pmatrix} \dfrac{r}{R^2-r^2} \\ 0 \end{pmatrix}, & (r < R - \ell_c), \\ \begin{pmatrix} \dfrac{R^2}{r(r^2-R^2)} \\ 0 \end{pmatrix}, & (r > R + \ell_c), \end{cases} \tag{B.2.22}$$

$$D(\boldsymbol{r}) = \frac{Sc_0}{32\pi\eta^2}\begin{cases} \ln\left(\dfrac{\sqrt{R^2-r^2}}{\ell_c}\right)\mathbb{1}, & (r < R-\ell_c), \\ \ln\left(\dfrac{r}{\sqrt{r^2-R^2}}\right)\mathbb{1} + \dfrac{R^2}{2r^2}\begin{pmatrix}1 & 0\\ 0 & -1\end{pmatrix}, & (r > R+\ell_c). \end{cases} \tag{B.2.23}$$

For the periphery of the raft $R-\ell_c < r < R+\ell_c$, the calculation is more complex.

B.2.2 Derivation of Eqs. (3.3.21) and (3.3.22)

According to the definition of the Kramers-Moyal coefficients of the first and second orders in Eqs. (3.2.22) and (3.2.23) and the Oseen tensor in Eq. (B.1.23), we have

$$\begin{aligned} &V(\boldsymbol{R}) \\ &= \frac{1}{15}\int\left[2\left(\frac{\partial G_{\alpha1}}{\partial r_1}\frac{\partial G_{\alpha'1}}{\partial r_1} + \frac{\partial G_{\alpha2}}{\partial r_2}\frac{\partial G_{\alpha'2}}{\partial r_2} + \frac{\partial G_{\alpha3}}{\partial r_3}\frac{\partial G_{\alpha'3}}{\partial r_3}\right)\right. \\ &\qquad + \left(\frac{\partial G_{\alpha1}}{\partial r_2} + \frac{\partial G_{\alpha'2}}{\partial r_1}\right)\left(\frac{\partial G_{\alpha'1}}{\partial r_2} + \frac{\partial G_{\alpha'2}}{\partial r_1}\right) + \left(\frac{\partial G_{\alpha2}}{\partial r_3} + \frac{\partial G_{\alpha'3}}{\partial r_2}\right)\left(\frac{\partial G_{\alpha'1}}{\partial r_2} + \frac{\partial G_{\alpha'2}}{\partial r_1}\right) \\ &\qquad + \left(\frac{\partial G_{\alpha1}}{\partial r_2} + \frac{\partial G_{\alpha'2}}{\partial r_1}\right)\left(\frac{\partial G_{\alpha'1}}{\partial r_2} + \frac{\partial G_{\alpha'2}}{\partial r_1}\right) \\ &\qquad \left. + \left(\frac{\partial G_{\alpha1}}{\partial r_1} + \frac{\partial G_{\alpha2}}{\partial r_2} + \frac{\partial G_{\alpha3}}{\partial r_3} + \frac{\partial G_{\alpha1}}{\partial r_1}\right)\left(\frac{\partial G_{\alpha'1}}{\partial r_1} + \frac{\partial G_{\alpha'2}}{\partial r_2} + \frac{\partial G_{\alpha'3}}{\partial r_3}\right)\right] S(\boldsymbol{R}+\boldsymbol{r})c(\boldsymbol{R}+\boldsymbol{r})d\boldsymbol{r}. \end{aligned} \tag{B.2.24}$$

Here, we used

$$\begin{aligned} \Lambda_{\beta\beta'\gamma\gamma'} &= \frac{1}{4\pi}\int_0^{2\pi}\int_0^{\pi} e_\beta e_{\beta'} e_\gamma e_{\gamma'} \sin\theta d\theta d\phi \\ &= \frac{1}{15}\left(\delta_{\beta\beta'}\delta_{\gamma\gamma'} + \delta_{\beta\gamma}\delta_{\beta'\gamma'} + \delta_{\beta\gamma'}\delta_{\beta'\gamma}\right) \\ &= \begin{cases} \frac{1}{5}, & (\beta,\beta',\gamma,\gamma') = (1,1,1,1),(2,2,2,2),(3,3,3,3), \\ \frac{1}{15}, & (\beta,\beta',\gamma,\gamma') = (1,1,2,2),(1,1,3,3),(1,2,1,2),(1,2,2,1),(1,3,1,3),(1,3,3,1), \\ & \qquad (2,1,1,2),(2,1,2,1),(2,2,1,1),(2,2,3,3),(2,3,2,3),(2,3,3,2), \\ & \qquad (3,1,1,3),(3,1,3,1),(3,3,1,1),(3,2,2,3),(3,2,3,2),(3,3,2,2), \\ 0, & \text{otherwise}, \end{cases} \end{aligned} \tag{B.2.25}$$

where e_1, e_2, and e_3 are first, second, and third components of a unit vector $\boldsymbol{e} = (\sin\theta\cos\phi, \sin\theta\sin\phi, \cos\theta)$, respectively. We also use the following relations.

$$\frac{\partial G_{\alpha1}}{\partial r_1}\frac{\partial G_{\alpha'1}}{\partial r_1} = \frac{r_\alpha r_{\alpha'}}{(8\pi\eta)^2 r^6}\left(1 - \frac{3{r_1}^2}{r^2}\right)^2, \tag{B.2.26}$$

$$\frac{\partial G_{\alpha1}}{\partial r_2}\frac{\partial G_{\alpha'2}}{\partial r_1} = -\frac{6r_\alpha r_1 r_2}{8\pi\eta r^5}, \tag{B.2.27}$$

$$\frac{\partial G_{\alpha1}}{\partial r_1} + \frac{\partial G_{\alpha2}}{\partial r_2} + \frac{\partial G_{\alpha3}}{\partial r_3} = 0. \tag{B.2.28}$$

Thus we have

$$V(\boldsymbol{R}) = \frac{1}{40\eta^2\pi^2}\int d\boldsymbol{r}\frac{r_\alpha}{r^6}S(\boldsymbol{R}+\boldsymbol{r})c(\boldsymbol{R}+\boldsymbol{r}). \tag{B.2.29}$$

The Kramers-Moyal coefficient of the second order is simplified in the following manner:

$$\begin{aligned} D(\boldsymbol{R}) = -\frac{1}{15}\int \Bigg[& 2\left(\frac{\partial^2 G_{\alpha 1}}{\partial r_1 \partial r_\delta}\frac{\partial G_{\delta 1}}{\partial r_1} + \frac{\partial^2 G_{\alpha 2}}{\partial r_2 \partial r_\delta}\frac{\partial G_{\delta 2}}{\partial r_2} + \frac{\partial^2 G_{\alpha 3}}{\partial r_3 \partial r_\delta}\frac{\partial G_{\delta 3}}{\partial r_3}\right) \\ & + \left(\frac{\partial^2 G_{\alpha 1}}{\partial r_2 \partial r_\delta} + \frac{\partial^2 G_{\alpha 2}}{\partial r_1 \partial r_\delta}\right)\left(\frac{\partial G_{\delta 1}}{\partial r_2} + \frac{\partial G_{\delta 2}}{\partial r_1}\right) + \left(\frac{\partial^2 G_{\alpha 2}}{\partial r_3 \partial r_\delta} + \frac{\partial^2 G_{\alpha 2}}{\partial r_3 \partial r_\delta}\right)\left(\frac{\partial G_{\delta 3}}{\partial r_1} + \frac{\partial G_{\delta 3}}{\partial r_1}\right) \\ & + \left(\frac{\partial^2 G_{\alpha 3}}{\partial r_1 \partial r_\delta} + \frac{\partial^2 G_{\alpha 1}}{\partial r_3 \partial r_\delta}\right)\left(\frac{\partial G_{\delta 3}}{\partial r_1} + \frac{\partial G_{\delta 1}}{\partial r_3}\right) \\ & + \left(\frac{\partial^2 G_{\alpha 1}}{\partial r_1 \partial r_\delta} + \frac{\partial^2 G_{\alpha 2}}{\partial r_2 \partial r_\delta} + \frac{\partial^2 G_{\alpha 3}}{\partial r_3 \partial r_\delta}\right)\left(\frac{\partial G_{\delta 1}}{\partial r_1} + \frac{\partial G_{\delta 2}}{\partial r_2} + \frac{\partial G_{\delta 3}}{\partial r_3}\right)\Bigg] S(\boldsymbol{R}+\boldsymbol{r})c(\boldsymbol{R}+\boldsymbol{r})d\boldsymbol{r}. \end{aligned} \tag{B.2.30}$$

Thus we have

$$D(\boldsymbol{R}) = \frac{1}{40\eta^2\pi^2}\int \frac{r_\alpha r_{\alpha'}}{r^6}S(\boldsymbol{R}+\boldsymbol{r})c(\boldsymbol{R}+\boldsymbol{r})d\boldsymbol{r}. \tag{B.2.31}$$

B.2.3 Derivation of Eqs. (3.4.1) and (3.4.2)

Here we consider the situation that the direction of active proteins are aligned in the angle $\theta = \theta_0$, i.e.,

$$\bar{N}^{(2)}_{\beta\gamma}\bar{N}^{(2)}_{\beta'\gamma'} = \begin{cases} \cos^4\theta_0, & (\beta,\gamma,\beta',\gamma') = (1,1,1,1), \\ \sin\theta_0\cos^3\theta_0, & (\beta,\gamma,\beta',\gamma') = (1,1,1,2),(1,1,2,1),(1,2,1,1),(2,1,1,1), \\ \sin^2\theta_0\cos^2\theta_0, & (\beta,\gamma,\beta',\gamma') = (1,1,2,2),(1,2,1,2),(1,2,2,1), \\ & \qquad (2,1,1,2),(2,1,2,1),(2,2,1,1), \\ \sin^3\theta_0\cos\theta_0, & (\beta,\gamma,\beta',\gamma') = (1,2,2,2),(2,1,2,2),(2,2,1,2),(2,2,2,1), \\ \sin^4\theta_0, & (\beta,\gamma,\beta',\gamma') = (2,2,2,2). \end{cases} \tag{B.2.32}$$

According to the definition of the Kramers-Moyal coefficients of the first and second orders in Eqs. (3.2.22) and (3.2.23) and the Oseen tensor in Eq. (B.1.18), we have

$$
\begin{aligned}
&V_\alpha(\boldsymbol{R})\\
&\quad= -\bar{N}^{(2)}_{\beta\gamma}\bar{N}^{(2)}_{\beta'\gamma'}\int \frac{\partial^2 G_{\alpha\beta}}{\partial r_\gamma \partial r_\delta}\frac{\partial G_{\delta\beta'}}{\partial r_{\gamma'}} S(\boldsymbol{R}+\boldsymbol{r})c(\boldsymbol{R}+\boldsymbol{r})d\boldsymbol{r}\\
&\quad= -\int \left[\frac{\partial^2 G_{\alpha 1}}{\partial r_1 \partial r_\delta}\frac{\partial G_{\delta 1}}{\partial r_1}\cos^4\theta_0\right.\\
&\qquad + \left\{\frac{\partial^2 G_{\alpha 1}}{\partial r_1 \partial r_\delta}\left(\frac{\partial G_{\delta 1}}{\partial r_2}+\frac{\partial G_{\delta 2}}{\partial r_1}\right)+\left(\frac{\partial^2 G_{\alpha 1}}{\partial r_2 \partial r_\delta}+\frac{\partial^2 G_{\alpha 2}}{\partial r_1 \partial r_\delta}\right)\frac{\partial G_{\delta 1}}{\partial r_1}\right\}\sin\theta_0\cos^3\theta_0\\
&\qquad + \left\{\left(\frac{\partial^2 G_{\alpha 1}}{\partial r_2 \partial r_\delta}+\frac{\partial^2 G_{\alpha 2}}{\partial r_1 \partial r_\delta}\right)\left(\frac{\partial G_{\delta 1}}{\partial r_2}+\frac{\partial G_{\delta 2}}{\partial r_1}\right)+\frac{\partial^2 G_{\alpha 1}}{\partial r_1 \partial r_\delta}\frac{\partial G_{\delta 2}}{\partial r_2}+\frac{\partial^2 G_{\alpha 2}}{\partial r_2 \partial r_\delta}\frac{\partial G_{\delta 1}}{\partial r_1}\right\}\sin^2\theta_0\cos^2\theta_0\\
&\qquad + \left\{\frac{\partial^2 G_{\alpha 2}}{\partial r_2 \partial r_\delta}\left(\frac{\partial G_{\delta 1}}{\partial r_2}+\frac{\partial G_{\delta 2}}{\partial r_1}\right)+\left(\frac{\partial^2 G_{\alpha 1}}{\partial r_2 \partial r_\delta}+\frac{\partial^2 G_{\alpha 2}}{\partial r_1 \partial r_\delta}\right)\frac{\partial G_{\delta 2}}{\partial r_2}\right\}\sin^3\theta_0\cos\theta_0\\
&\qquad \left.+\frac{\partial^2 G_{\alpha 2}}{\partial r_2 \partial r_\delta}\frac{\partial G_{\delta 2}}{\partial r_2}\sin^4\theta_0\right] S(\boldsymbol{R}+\boldsymbol{r})c(\boldsymbol{R}+\boldsymbol{r})d\boldsymbol{r}\\
&\quad= -\frac{1}{(4\pi\eta)^2}\int\left[\left(-\frac{({r_1}^2-{r_2}^2)^2 r_\alpha}{r^8}\right)\cos^4\theta_0+\left(-\frac{8r_1r_2({r_1}^2-{r_2}^2)r_\alpha}{r^8}\right)\sin\theta_0\cos^3\theta_0\right.\\
&\qquad\quad + \left(\frac{2({r_1}^2-{r_2}^2)^2 r_\alpha}{r^8}-\frac{16{r_1}^2{r_2}^2 r_\alpha}{r^8}\right)\sin^2\theta_0\cos^2\theta_0+\left(\frac{8r_1r_2({r_1}^2-{r_2}^2)r_\alpha}{r^8}\right)\sin^3\theta_0\cos\theta_0\\
&\qquad\quad \left.+\left(-\frac{({r_1}^2-{r_2}^2)^2 r_\alpha}{r^8}\right)\sin^4\theta_0\right] S(\boldsymbol{R}+\boldsymbol{r})c(\boldsymbol{R}+\boldsymbol{r})d\boldsymbol{r}\\
&\quad= \frac{1}{(4\pi\eta)^2}\int\left[\left(\frac{({r_1}^2-{r_2}^2)^2 r_\alpha}{r^8}\right)\cos^2 2\theta_0+\left(\frac{4r_1r_2({r_1}^2-{r_2}^2)r_\alpha}{r^8}\right)\sin 2\theta_0\cos 2\theta_0\right.\\
&\qquad \left.+\left(\frac{4{r_1}^2{r_2}^2 r_\alpha}{r^8}\right)\sin^2 2\theta_0\right] S(\boldsymbol{R}+\boldsymbol{r})c(\boldsymbol{R}+\boldsymbol{r})d\boldsymbol{r}\\
&\quad= \frac{1}{(4\pi\eta)^2}\int\left(({r_1}^2-{r_2}^2)\cos 2\theta_0+2r_1r_2\sin 2\theta_0\right)^2\frac{r_\alpha}{r^8}S(\boldsymbol{R}+\boldsymbol{r})c(\boldsymbol{R}+\boldsymbol{r})d\boldsymbol{r}. \qquad \text{(B.2.33)}
\end{aligned}
$$

By substituting $\boldsymbol{r} = r(\cos\theta\mathbf{e}_1+\sin\theta\mathbf{e}_2)$, we have

$$
V_\alpha(\boldsymbol{R}) = \frac{1}{(4\pi\eta)^2}\int\frac{r_\alpha}{r^4}\cos^2 2(\theta-\theta_0)S(\boldsymbol{R}+\boldsymbol{r})c(\boldsymbol{R}+\boldsymbol{r})d\boldsymbol{r}. \qquad \text{(B.2.34)}
$$

$$
\begin{aligned}
&D^A{}_{\alpha\alpha'}(\boldsymbol{R})\\
&\quad= \bar{N}^{(2)}_{\beta\gamma}\bar{N}^{(2)}_{\beta'\gamma'}\int \frac{\partial G_{\alpha\beta}}{\partial r_\gamma}\frac{\partial G_{\alpha'\beta'}}{\partial r'_\gamma} S(\boldsymbol{R}+\boldsymbol{r})c(\boldsymbol{R}+\boldsymbol{r})d\boldsymbol{r}\\
&\quad= \int \left[\frac{\partial G_{\alpha 1}}{\partial r_1}\frac{\partial G_{\alpha' 1}}{\partial r_1}\cos^4\theta_0\right.\\
&\qquad+\left\{\frac{\partial G_{\alpha 1}}{\partial r_1}\left(\frac{\partial G_{\alpha' 1}}{\partial r_2}+\frac{\partial G_{\alpha' 2}}{\partial r_1}\right)+\left(\frac{\partial G_{\alpha 1}}{\partial r_2}+\frac{\partial G_{\alpha 2}}{\partial r_1}\right)\frac{\partial G_{\alpha' 1}}{\partial r_1}\right\}\sin\theta_0\cos^3\theta_0\\
&\qquad+\left\{\left(\frac{\partial G_{\alpha 1}}{\partial r_2}+\frac{\partial G_{\alpha 2}}{\partial r_1}\right)\left(\frac{\partial G_{\alpha' 1}}{\partial r_2}+\frac{\partial G_{\alpha' 2}}{\partial r_1}\right)+\frac{\partial G_{\alpha 1}}{\partial r_1}\frac{\partial G_{\alpha' 2}}{\partial r_2}+\frac{\partial G_{\alpha 2}}{\partial r_2}\frac{\partial G_{\alpha' 1}}{\partial r_1}\right\}\sin^2\theta_0\cos^2\theta_0\\
&\qquad+\left\{\frac{\partial G_{\alpha 2}}{\partial r_2}\left(\frac{\partial G_{\alpha' 1}}{\partial r_2}+\frac{\partial G_{\alpha' 2}}{\partial r_1}\right)+\left(\frac{\partial G_{\alpha 1}}{\partial r_2}+\frac{\partial G_{\alpha 2}}{\partial r_1}\right)\frac{\partial G_{\alpha' 2}}{\partial r_2}\right\}\sin^3\theta_0\cos\theta_0\\
&\qquad\left.+\frac{\partial G_{\alpha 2}}{\partial r_2}\frac{\partial G_{\alpha' 2}}{\partial r_2}\sin^4\theta_0\right] S(\boldsymbol{R}+\boldsymbol{r})c(\boldsymbol{R}+\boldsymbol{r})d\boldsymbol{r}\\
&\quad= \frac{1}{(4\pi\eta)^2}\int\left[\frac{\left({r_1}^2-{r_2}^2\right)^2 r_\alpha r_{\alpha'}}{r^8}\cos^4\theta_0+\frac{8r_1r_2\left({r_1}^2-{r_2}^2\right)r_\alpha r_{\alpha'}}{r^8}\sin\theta_0\cos^3\theta_0\right.\\
&\qquad\qquad+\left(-\frac{2({r_1}^2-{r_2}^2)^2 r_\alpha r_{\alpha'}}{r^8}+\frac{16{r_1}^2{r_2}^2 r_\alpha r_{\alpha'}}{r^8}\right)\sin^2\theta_0\cos^2\theta_0\\
&\qquad\qquad+\left(-\frac{8r_1r_2\left({r_1}^2-{r_2}^2\right)r_\alpha r_{\alpha'}}{r^8}\right)\sin^3\theta_0\cos\theta_0\\
&\qquad\qquad\left.+\frac{\left({r_1}^2-{r_2}^2\right)^2 r_\alpha r_{\alpha'}}{r^8}\sin^4\theta_0\right] S(\boldsymbol{R}+\boldsymbol{r})c(\boldsymbol{R}+\boldsymbol{r})d\boldsymbol{r}\\
&\quad= \frac{1}{(4\pi\eta)^2}\int\left[\frac{\left({r_1}^2-{r_2}^2\right)^2 r_\alpha r_{\alpha'}}{r^8}\cos^2 2\theta_0+\frac{4r_1r_2\left({r_1}^2-{r_2}^2\right)r_\alpha r_{\alpha'}}{r^8}\sin 2\theta_0\cos 2\theta_0\right.\\
&\qquad\qquad\left.+\frac{4{r_1}^2{r_2}^2 r_\alpha r_{\alpha'}}{r^8}\sin^2 2\theta_0\right] S(\boldsymbol{R}+\boldsymbol{r})c(\boldsymbol{R}+\boldsymbol{r})d\boldsymbol{r}\\
&\quad= \frac{1}{(4\pi\eta)^2}\int\left(({r_1}^2-{r_2}^2)\cos 2\theta_0+2r_1r_2\sin 2\theta_0\right)^2\frac{r_\alpha r_{\alpha'}}{r^8} S(\boldsymbol{R}+\boldsymbol{r})c(\boldsymbol{R}+\boldsymbol{r})d\boldsymbol{r}.
\end{aligned}
\tag{B.2.35}
$$

By substituting $\boldsymbol{r} = r(\cos\theta\mathbf{e}_1 + \sin\theta\mathbf{e}_2)$, we have

$$
D_{\alpha\alpha'}(\boldsymbol{R}) = \frac{1}{(4\pi\eta)^2}\int \frac{r_\alpha r_{\alpha'}}{r^4}\cos^2 2(\theta-\theta_0) S(\boldsymbol{R}+\boldsymbol{r})c(\boldsymbol{R}+\boldsymbol{r})d\boldsymbol{r}. \tag{B.2.36}
$$

B.2.4 Derivation of Eqs. (3.4.4) and (3.4.5)

Here we consider the situation that the direction of active proteins are aligned in the angle $\theta = 0$, i.e., $\bar{N}^{(3)}_{33}\bar{N}^{(3)}_{33} = 1$ and otherwise 0. According to the definition of the Kramers-Moyal coefficients of the first and second orders in Eqs. (3.2.22) and (3.2.23) and the Oseen tensor in Eq. (B.1.23), we have

$$\begin{aligned}
V_\alpha(\boldsymbol{r}) =& - \bar{N}^{(3)}_{\beta\gamma}\bar{N}^{(3)}_{\beta'\gamma'}\int \frac{\partial^2 G_{\alpha\beta}}{\partial\rho_\gamma\partial\rho_\delta}\frac{\partial G_{\delta\beta'}}{\partial\rho_{\gamma'}}S(\boldsymbol{r}+\boldsymbol{\rho})c(\boldsymbol{r}+\boldsymbol{\rho})d\boldsymbol{\rho}\\
=& - \int \frac{\partial^2 G_{\alpha 3}}{\partial\rho_\delta\partial\rho_3}\frac{\partial G_{\delta 3}}{\partial\rho_3}S(\boldsymbol{r}+\boldsymbol{\rho})c(\boldsymbol{r}+\boldsymbol{\rho})d\boldsymbol{\rho}\\
=& - \frac{1}{(8\pi\eta)^2}\int \frac{\rho_\delta}{\rho^6}\left\{\delta_{\alpha\delta} - \frac{3}{\rho^2}\left(2\rho_\alpha\rho_3\delta_{3\delta} + \rho_\alpha\rho_\delta + {\rho_3}^2\delta_{\alpha\delta}\right) + \frac{15\rho_\alpha\rho_\delta{\rho_3}^2}{\rho^4}\right\}\\
&\qquad\qquad\qquad\qquad \times\left(1 - \frac{3{\rho_3}^2}{\rho^2}\right)S(\boldsymbol{r}+\boldsymbol{\rho})c(\boldsymbol{r}+\boldsymbol{\rho})d\boldsymbol{\rho}\\
=&\frac{1}{32\pi^2\eta^2}\int \frac{\rho_\alpha}{\rho^6}\left(1 - 6\cos^2\theta + 9\cos^4\theta\right)S(\boldsymbol{r}+\boldsymbol{\rho})c(\boldsymbol{r}+\boldsymbol{\rho})d\boldsymbol{\rho}\\
=&\frac{1}{8\pi^2\eta^2}\int \frac{\rho_\alpha}{\rho^6}P_2(\cos\theta)^2 S(\boldsymbol{r}+\boldsymbol{\rho})c(\boldsymbol{r}+\boldsymbol{\rho})d\boldsymbol{\rho},
\end{aligned} \tag{B.2.37}$$

where P_2 is Legendre polynomial of the second order. Here we used $\rho_3 = \rho\cos\theta$.

As for the diffusion enhancement, we have

$$\begin{aligned}
{D^A}_{\alpha\alpha'}(\boldsymbol{r}) =&\bar{N}^{(3)}_{\beta\gamma}\bar{N}^{(3)}_{\beta'\gamma'}\int \frac{\partial G_{\alpha\beta}}{\partial\rho_\gamma}\frac{\partial G_{\alpha'\beta'}}{\partial\rho'_\gamma}S(\boldsymbol{r}+\boldsymbol{\rho})c(\boldsymbol{r}+\boldsymbol{\rho})d\boldsymbol{\rho}\\
=&\int \frac{\partial G_{\alpha 3}}{\partial\rho_3}\frac{\partial G_{\alpha' 3}}{\partial\rho_3}S(\boldsymbol{r}+\boldsymbol{\rho})c(\boldsymbol{r}+\boldsymbol{\rho})d\boldsymbol{\rho}\\
=&\frac{1}{(8\pi\eta)^2}\int \frac{\rho_\alpha\rho_{\alpha'}}{\rho^6}\left(1 - \frac{3{\rho_3}^2}{\rho^2}\right)\left(1 - \frac{3{\rho_3}^2}{\rho^2}\right)S(\boldsymbol{r}+\boldsymbol{\rho})c(\boldsymbol{r}+\boldsymbol{\rho})d\boldsymbol{\rho}\\
=&\frac{1}{16\pi^2\eta^2}\int \frac{\rho_\alpha\rho_{\alpha'}}{\rho^6}P_2(\cos\theta)^2 S(\boldsymbol{r}+\boldsymbol{\rho})c(\boldsymbol{r}+\boldsymbol{\rho})d\boldsymbol{\rho}.
\end{aligned} \tag{B.2.38}$$

B.3 Derivation of the drift velocity $\boldsymbol{U}$

In this section, we simplify the drift velocity in Eq. (3.3.2).

B.3.1 Two-dimensional case without orientational order

According to the definition of the drift velocity in Eq. (3.3.2) and the simplified Kramers coefficients of the first and second orders in Eqs. (3.3.3) and (3.3.4), we have

$$\begin{aligned}
U_\alpha(\boldsymbol{r}) =&V_\alpha(\boldsymbol{r}) - \frac{\partial D_{\alpha\alpha'}(\boldsymbol{r})}{\partial r_{\alpha'}}\\
=&\frac{1}{32\pi^2\eta^2}\int\left(\frac{r'_\alpha}{r'^4} - \frac{r'_\alpha r'_{\alpha'}}{r'^4}\frac{\partial}{\partial r_{\alpha'}}\right)\left(S(\boldsymbol{r}+\boldsymbol{r}')c(\boldsymbol{r}+\boldsymbol{r}')\right)d\boldsymbol{r}'\\
=&\frac{1}{32\pi^2\eta^2}\int\left(\frac{r'_\alpha}{r'^4} + \left(\frac{\partial}{\partial r'_{\alpha'}}\frac{r'_\alpha r'_{\alpha'}}{r'^4}\right)\right)S(\boldsymbol{r}+\boldsymbol{r}')c(\boldsymbol{r}+\boldsymbol{r}')d\boldsymbol{r}'\\
&- \frac{1}{32\pi^2\eta^2}\int_\sigma \frac{r'_\alpha r'_{\alpha'}}{r'^4}S(\boldsymbol{r}+\boldsymbol{r}')c(\boldsymbol{r}+\boldsymbol{r}')ds'_{\alpha'},
\end{aligned} \tag{B.3.1}$$

where $\int_\sigma ds'_{\alpha'}$ is the integration along the periphery of the domain. Here, $\partial/\partial r_{\alpha'}$ can be regarded as $\partial/\partial r'_{\alpha'}$ and the partial integration is used. The derivative in the integrand is calculated as

$$\frac{\partial}{\partial r_{\alpha'}}\frac{r_\alpha r_{\alpha'}}{r^4} = \frac{\delta_{\alpha\alpha'} r_{\alpha'}}{r^4} + 2\frac{r_\alpha}{r^4} - 4\frac{r_\alpha r_{\alpha'}^2}{r^6} = -\frac{r_\alpha}{r^4}. \tag{B.3.2}$$

Thus, only the surface term remains

$$U_\alpha(\boldsymbol{r}) = -\frac{1}{32\pi^2\eta^2}\int_\sigma \frac{r'_\alpha r'_{\alpha'}}{r'^4} Q(\boldsymbol{r}+\boldsymbol{r}')ds'_{\alpha'}. \tag{B.3.3}$$

The integration is taken over the physical boundary σ_{outside} and the small cut-off surface σ_{inside} around $\boldsymbol{r}$. The integration taken over the physical boundary σ_{outside} becomes zero if $Q = 0$ at the boundary, as we always assume. As for the cut-off surface, we expand Q as

$$Q(\boldsymbol{r}+\boldsymbol{r}') = Q(\boldsymbol{r}) + r'_\alpha\frac{\partial Q(\boldsymbol{r})}{\partial r_\alpha} + \mathcal{O}(r'^2). \tag{B.3.4}$$

Then, the integral over the small cut-off surface is calculated as

$$\begin{aligned}
U_\alpha(\boldsymbol{r}) =& -\frac{1}{32\pi^2\eta^2}\int_\sigma \frac{r'_\alpha r'_{\alpha'}}{r'^4} Q(\boldsymbol{r}+\boldsymbol{r}')ds'_{\alpha'} \\
=& -\frac{1}{32\pi^2\eta^2}\int_0^{2\pi} \frac{\hat{r'}_\alpha \hat{r'}_{\alpha'}}{{\ell_c}^2}\left(Q(\boldsymbol{r}) + \ell_c\hat{r'}_\beta\frac{\partial Q(\boldsymbol{r})}{\partial r_\beta} + \mathcal{O}({\ell_c}^2)\right)(-\ell_c\hat{r'}_{\alpha'}d\phi') \\
=& \frac{1}{32\pi\eta^2}\frac{\partial Q(\boldsymbol{r})}{\partial r_\alpha} + \mathcal{O}(\ell_c),
\end{aligned} \tag{B.3.5}$$

where $\hat{r'}_\alpha$ is a unit vector which is parallel to r'_α, and $\hat{r'}_1 = \cos\phi'$ and $\hat{r'}_2 = \sin\phi'$. Here, we used $\hat{r'}_\alpha\hat{r'}_\alpha = 1$, and the integrations of $\hat{r}_\alpha$ and $\hat{r}_\alpha\hat{r}_{\alpha'}$ with regard to ϕ over $[0, 2\pi)$ are 0 and $\pi\delta_{\alpha\alpha'}$, respectively.

B.3.2 Three dimensional case without orientational order

According to the definition of the drift velocity in Eq. (3.3.2) and the simplified Kramers coefficients of the first and second orders in Eqs. (3.3.21) and (3.3.22), we have

$$\begin{aligned}
U_\alpha(\boldsymbol{r}) =& V_\alpha(\boldsymbol{r}) - \frac{\partial D_{\alpha\alpha'}(\boldsymbol{r})}{\partial r_{\alpha'}} \\
=& \frac{1}{40\pi^2\eta^2}\int \frac{r'_\alpha}{r'^6}Q(\boldsymbol{r}+\boldsymbol{r}')d\boldsymbol{r}' - \frac{1}{80\pi^2\eta^2}\int \frac{r'_\alpha r'_{\alpha'}}{r'^6}\frac{\partial Q(\boldsymbol{r}+\boldsymbol{r}')}{\partial r_{\alpha'}}d\boldsymbol{r}' \\
=& \frac{1}{40\pi^2\eta^2}\int \frac{r'_\alpha}{r'^6}Q(\boldsymbol{r}+\boldsymbol{r}')d\boldsymbol{r}' \\
&+ \frac{1}{80\pi^2\eta^2}\int \frac{\partial}{\partial r'_{\alpha'}}\left\{\frac{r'_\alpha r'_{\alpha'}}{r'^6}\right\}Q(\boldsymbol{r}+\boldsymbol{r}')d\boldsymbol{r}' - \frac{1}{80\pi^2\eta^2}\int_\sigma \frac{r'_\alpha r'_{\alpha'}}{r'^6}Q(\boldsymbol{r}+\boldsymbol{r}')ds_{\alpha'},
\end{aligned} \tag{B.3.6}$$

where $Q(\boldsymbol{r}) = S(\boldsymbol{r})c(\boldsymbol{r})$, and $\int_\sigma ds_{\alpha'}$ means the surface integral. Here $\partial/\partial r'_{\alpha'}$ can be regarded as $\partial/\partial r'_{\alpha'}$, and the partial integration is used.

$$\frac{\partial}{\partial r'_{\alpha'}}\left\{\frac{r'_\alpha r'_{\alpha'}}{r'^6}\right\} = \frac{r'_{\alpha'}\delta_{\alpha\alpha'}}{r'^6} + \frac{3r'_\alpha}{r'^6} - \frac{6r'_\alpha {r'_{\alpha'}}^2}{r'^8} = -2\frac{r'_\alpha}{r'^6}. \tag{B.3.7}$$

Thus, we obtain

$$U_\alpha(\boldsymbol{r}) = -\frac{1}{40\pi^2\eta^2}\int_\sigma \frac{r'_\alpha r'_{\alpha'}}{r'^6} Q(\boldsymbol{r}+\boldsymbol{r}')ds_{\alpha'}. \tag{B.3.8}$$

B.3.3 Two-dimensional case with orientational order

According to the definition of the drift velocity in Eq. (3.3.2) and the simplified Kramers coefficients of the first and second orders in Eqs. (3.4.1) and (3.4.2), we have

$$\begin{aligned}
U_\alpha(\boldsymbol{R}) =& V_\alpha(\boldsymbol{R}) - \frac{\partial D_{\alpha\alpha'}(\boldsymbol{R})}{\partial R_{\alpha'}} \\
=& \frac{1}{(4\pi\eta)^2}\int \left((r_1{}^2 - r_2{}^2)\cos 2\theta_0 + 2r_1r_2\sin 2\theta_0\right)^2 \frac{r_\alpha}{r^8} Q(\boldsymbol{R}+\boldsymbol{r})d\boldsymbol{r} \\
& - \frac{1}{(4\pi\eta)^2}\int \left((r_1{}^2 - r_2{}^2)\cos 2\theta_0 + 2r_1r_2\sin 2\theta_0\right)^2 \frac{r_\alpha r_{\alpha'}}{r^8} \frac{\partial Q(\boldsymbol{R}+\boldsymbol{r})}{\partial R_{\alpha'}} d\boldsymbol{r} \\
=& \frac{1}{(4\pi\eta)^2}\int \left((r_1{}^2 - r_2{}^2)\cos 2\theta_0 + 2r_1r_2\sin 2\theta_0\right)^2 \frac{r_\alpha}{r^8} Q(\boldsymbol{R}+\boldsymbol{r})d\boldsymbol{r} \\
& + \frac{1}{(4\pi\eta)^2}\int \frac{\partial}{\partial r_{\alpha'}}\left\{\left((r_1{}^2 - r_2{}^2)\cos 2\theta_0 + 2r_1r_2\sin 2\theta_0\right)^2 \frac{r_\alpha r_{\alpha'}}{r^8}\right\} Q(\boldsymbol{R}+\boldsymbol{r})d\boldsymbol{r} \\
& - \frac{1}{(4\pi\eta)^2}\int_\sigma \left((r_1{}^2 - r_2{}^2)\cos 2\theta_0 + 2r_1r_2\sin 2\theta_0\right)^2 \frac{r_\alpha r_{\alpha'}}{r^8} Q(\boldsymbol{R}+\boldsymbol{r})ds_{\alpha'},
\end{aligned} \tag{B.3.9}$$

where $Q(\boldsymbol{r}) = S(\boldsymbol{r})c(\boldsymbol{r})$. Here $\partial/\partial R_{\alpha'}$ can be regarded as $\partial/\partial r_{\alpha'}$ and the partial integration is used.

The derivatives in the integrands can be calculated as follows.

$$\begin{aligned}
& \frac{\partial}{\partial r_{\alpha'}}\left\{\left((r_1{}^2 - r_2{}^2)\cos 2\theta_0 + 2r_1r_2\sin 2\theta_0\right)^2 \frac{r_\alpha r_{\alpha'}}{r^8}\right\} \\
& \quad = 2\left\{r_1\left(2r_1\cos 2\theta_0 + 2r_2\sin 2\theta_0\right) - r_2\left(-2r_2\cos 2\theta_0 + 2r_1\sin 2\theta_0\right)\right\} \\
& \qquad \times \left((r_1{}^2 - r_2{}^2)\cos 2\theta_0 + 2r_1r_2\sin 2\theta_0\right)\frac{r_\alpha r_{\alpha'}}{r^8} \\
& \qquad \left((r_1{}^2 - r_2{}^2)\cos 2\theta_0 + 2r_1r_2\sin 2\theta_0\right)^2 \left\{\frac{\delta_{\alpha\alpha'} r_{\alpha'}}{r^8} + 2\frac{r_\alpha}{r^8} - 8\frac{r_\alpha r_{\alpha'}^2}{r^{10}}\right\} \\
& =(4+1+2-8)\left((r_1{}^2 - r_2{}^2)\cos 2\theta_0 + 2r_1r_2\sin 2\theta_0\right)^2 \frac{r_\alpha r_{\alpha'}}{r^8} \\
& = -\left((r_1{}^2 - r_2{}^2)\cos 2\theta_0 + 2r_1r_2\sin 2\theta_0\right)^2 \frac{r_\alpha r_{\alpha'}}{r^8}.
\end{aligned} \tag{B.3.10}$$

$$\begin{aligned}
& \frac{\partial}{\partial r_{\alpha'}}\left\{\left(((r_1{}^2 - r_2{}^2)^2 - 4r_1{}^2r_2{}^2)\cos 4\theta_0 + 4r_1r_2(r_1{}^2 - r_2{}^2)\sin 4\theta_0\right)\frac{r_\alpha r_{\alpha'}}{r^8}\right\} \\
& = r_1\left((4r_1(r_1{}^2 - r_2{}^2) - 8r_1r_2{}^2)\cos 4\theta_0 + (4r_2(r_1{}^2 - r_2{}^2) + 8r_1{}^2r_2)\sin 4\theta_0\right)\frac{r_\alpha r_{\alpha'}}{r^8} \\
& \quad + r_2\left((-4r_2(r_1{}^2 - r_2{}^2) - 8r_1{}^2r_2)\cos 4\theta_0 + (4r_1(r_1{}^2 - r_2{}^2) - 8r_1r_2{}^2)\sin 4\theta_0\right)\frac{r_\alpha r_{\alpha'}}{r^8} \\
& \quad + \left(((r_1{}^2 - r_2{}^2)^2 - 4r_1{}^2r_2{}^2)\cos 4\theta_0 + 4r_1r_2(r_1{}^2 - r_2{}^2)\sin 4\theta_0\right)\left\{\frac{\delta_{\alpha\alpha'} r_{\alpha'}}{r^8} + 2\frac{r_\alpha}{r^8} - 8\frac{r_\alpha r_{\alpha'}^2}{r^{10}}\right\} \\
& = (4+1+2-8)\left(((r_1{}^2 - r_2{}^2)^2 - 4r_1{}^2r_2{}^2)\cos 4\theta_0 + 4r_1r_2(r_1{}^2 - r_2{}^2)\sin 4\theta_0\right)\frac{r_\alpha r_{\alpha'}}{r^8} \\
& = -\left(((r_1{}^2 - r_2{}^2)^2 - 4r_1{}^2r_2{}^2)\cos 4\theta_0 + 4r_1r_2(r_1{}^2 - r_2{}^2)\sin 4\theta_0\right)\frac{r_\alpha r_{\alpha'}}{r^8}.
\end{aligned} \tag{B.3.11}$$

Thus, only surface terms remain as follows.

$$U_\alpha(\boldsymbol{R}) = -\frac{1}{(4\pi\eta)^2}\int_\sigma \left((r_1{}^2 - r_2{}^2)\cos 2\theta_0 + 2r_1r_2\sin 2\theta_0\right)^2 \frac{r_\alpha r_{\alpha'}}{r^8} Q(\boldsymbol{R}+\boldsymbol{r})ds_{\alpha'}. \tag{B.3.12}$$

The integration is taken over the physical boundary $\sigma_{\mathrm{outside}}$ and the small cut-off surface σ_{inside} around the $\boldsymbol{R}$. The integration taken over the physical boundary $\sigma_{\mathrm{outside}}$ becomes zero if $Q = 0$ at the boundary and so on. Here we consider the situation that $Q(\boldsymbol{R}+\boldsymbol{r})$ is given by $Q(\boldsymbol{R}+\boldsymbol{r}) = Q(\boldsymbol{r}) + r_\beta \partial Q(\boldsymbol{r})/\partial r_\beta$. Then the integral over the small cut-off surface can be calculated as

$$\begin{aligned} U_\alpha(\boldsymbol{R}) =& -\frac{1}{(4\pi\eta)^2}\int_0^{2\pi} \cos^2 2(\theta_0-\phi)\frac{\hat{r}_\alpha \hat{r}_{\alpha'}}{\ell_c{}^2}\left(Q_0 + \ell_c \hat{r}_\beta \frac{\partial Q(\boldsymbol{r})}{\partial r_\beta}\right)(-\ell_c \hat{r}_{\alpha'} d\phi) \\ =& \frac{\nabla Q}{32\pi\eta^2}. \end{aligned} \tag{B.3.13}$$

Here, we used the fact that the integration of $\cos^2 2(\theta_0-\phi)\cos\phi$, $\cos^2 2(\theta_0-\phi)\sin\phi$, $\cos^2 2(\theta_0 - \phi)\sin\phi\cos\phi$, $\cos 4(\theta_0-\phi)\cos\phi$, $\cos 4(\theta_0-\phi)\sin\phi$, $\cos 4(\theta_0-\phi)\cos^2\phi$, and $\cos 4(\theta_0-\phi)\sin\phi\cos\phi$ with regard ϕ over $[0, 2\pi)$ are zero, and only the integration of $\cos^2 2(\theta_0-\phi)\cos^2\phi$ and $\cos^2 2(\theta_0 - \phi)\sin^2\phi$ with regard to ϕ over $[0, 2\pi)$ is $\pi/2$ (the same value).

B.3.4 Three dimensional case with orientational order

According to the definition of the drift velocity in Eq. (3.3.2) and the simplified Kramers coefficients of the first and second orders in Eqs. (3.4.4) and (3.4.5), we have

$$\begin{aligned} &U_\alpha(\boldsymbol{r}) \\ &= V_\alpha(\boldsymbol{r}) - \frac{\partial D_{\alpha\alpha'}(\boldsymbol{r})}{\partial r_{\alpha'}} \\ &= \frac{1}{32\pi^2\eta^2}\int \frac{r'_\alpha}{r'^{10}}\left(r'^2 - 3r'_3{}^2\right)^2 Q(\boldsymbol{r}+\boldsymbol{r}')d\boldsymbol{r}' - \frac{1}{64\pi^2\eta^2}\int \frac{r'_\alpha r'_{\alpha'}}{r'^{10}}\left(r'^2 - 3r'_3{}^2\right)^2 \frac{\partial Q(\boldsymbol{r}+\boldsymbol{r}')}{\partial r_{\alpha'}} d\boldsymbol{r}' \\ &= \frac{1}{32\pi^2\eta^2}\int \frac{r'_\alpha}{r'^{10}}\left(r'^2 - 3r'_3{}^2\right)^2 Q(\boldsymbol{r}+\boldsymbol{r}')d\boldsymbol{r}' + \frac{1}{64\pi^2\eta^2}\int \frac{\partial}{\partial r_{\alpha'}}\left\{\frac{r'_\alpha r'_{\alpha'}}{r'^{10}}\left(r'^2 - 3r'_3{}^2\right)^2\right\} Q(\boldsymbol{r}+\boldsymbol{r}')d\boldsymbol{r}' \\ &\quad - \frac{1}{64\pi^2\eta^2}\int_\sigma \frac{r'_\alpha r'_{\alpha'}}{r'^{10}}\left(r'^2 - 3r'_3{}^2\right)^2 Q(\boldsymbol{r}+\boldsymbol{r}')ds_{\alpha'}, \end{aligned} \tag{B.3.14}$$

where $Q(\boldsymbol{r}) = S(\boldsymbol{r})c(\boldsymbol{r})$, and $\int_\sigma ds_{\alpha'}$ means the surface integral. Here $\partial/\partial r'_{\alpha'}$ can be regarded as $\partial/\partial r'_{\alpha'}$, and the partial integration is used.

$$\begin{aligned} &\frac{\partial}{\partial r_{\alpha'}}\left\{\frac{r'_\alpha r'_{\alpha'}}{r'^{10}}\left(r'^2 - 3r'_3{}^2\right)^2\right\} \\ &\quad = \left\{\frac{r'_{\alpha'}\delta_{\alpha\alpha'}}{r'^{10}} + \frac{3r'_\alpha}{r'^{10}} - \frac{10 r'_\alpha r'_{\alpha'}{}^2}{r'^{12}}\right\}\left(r'^2 - 3r'_3{}^2\right)^2 + 2\frac{r'_\alpha r'_{\alpha'}}{r'^{10}}(r'^2 - 3r'_3{}^2)(2r'_{\alpha'} - 6r'_3\delta_{3\alpha'}) \\ &\quad = -2\frac{r'_\alpha}{r'^{10}}\left(r'^2 - 3r'_3{}^2\right)^2. \end{aligned} \tag{B.3.15}$$

Thus, we obtain

$$U_\alpha(\boldsymbol{r}) = -\frac{1}{64\pi^2\eta^2}\int_\sigma \frac{r'_\alpha r'_{\alpha'}}{r'^{10}}\left(r'^2 - 3r'_3{}^2\right)^2 Q(\boldsymbol{r}+\boldsymbol{r}')ds_{\alpha'}. \tag{B.3.16}$$

As an example of an actual system, we consider the case with constant gradient of the activity of active proteins $Q(\boldsymbol{r}) = Q_0 + Q_1 \boldsymbol{a}\cdot\boldsymbol{r}$, where $Q(\boldsymbol{r}) = S(\boldsymbol{r})c(\boldsymbol{r})$.

$$\begin{aligned}
\boldsymbol{V}(\boldsymbol{r}) =& \frac{1}{32\pi^2\eta^2}\int \frac{r'_\alpha}{r'^6}(1-3\cos^2\theta)^2 Q(\boldsymbol{r}+\boldsymbol{r}')d\boldsymbol{r}' \\
=& \frac{Q_0+Q_1\boldsymbol{a}\cdot\boldsymbol{r}}{32\pi^2\eta^2}\int \frac{r'_\alpha}{r'^6}(1-3\cos^2\theta)^2 d\boldsymbol{r}' + \frac{Q_1}{32\pi^2\eta^2}\int \frac{r'_\alpha}{r'^6}(1-3\cos^2\theta)^2\left(\boldsymbol{a}\cdot\boldsymbol{r}'\right)d\boldsymbol{r}' \\
=& \frac{Q_0+Q_1\boldsymbol{a}\cdot\boldsymbol{r}}{32\pi^2\eta^2}\int_0^{2\pi}\int_0^{\pi}\int_{\ell_c}^{\infty}\frac{r'^2\sin\theta}{r'^6}(1-3\cos^2\theta)^2\begin{pmatrix} r'\sin\theta\cos\phi \\ r'\sin\theta\sin\phi \\ r'\cos\theta\end{pmatrix} dr'd\theta d\phi \qquad \text{(B.3.17)} \\
&+ \frac{Q_1}{32\pi^2\eta^2}\int_0^{2\pi}\int_0^{\pi}\int_{\ell_c}^{\infty}\frac{r'^2\sin\theta}{r'^6}(1-3\cos^2\theta)^2 \\
&\qquad \times\left(a_1 r'\sin\theta\cos\phi + a_2 r'\sin\theta\sin\phi + a_3 r'\cos\theta\right)\begin{pmatrix} r'\sin\theta\cos\phi \\ r'\sin\theta\sin\phi \\ r'\cos\theta\end{pmatrix} dr'd\theta d\phi \\
=& \frac{Q_0+Q_1\boldsymbol{a}\cdot\boldsymbol{r}}{32\pi^2\eta^2}\int_0^{\pi}\frac{1}{2{\ell_c}^2}\sin\theta(1-3\cos^2\theta)^2\begin{pmatrix} 0 \\ 0 \\ 2\pi\cos\theta\end{pmatrix} d\theta \\
&+ \frac{Q_1}{32\pi^2\eta^2}\int_0^{2\pi}\int_0^{\pi}\frac{1}{\ell_c}\sin\theta(1-3\cos^2\theta)^2 \\
&\qquad \times\left(a_1\sin\theta\cos\phi + a_2\sin\theta\sin\phi + a_3\cos\theta\right)\begin{pmatrix} \sin\theta\cos\phi \\ \sin\theta\sin\phi \\ \cos\theta\end{pmatrix} d\theta d\phi \\
=& \frac{Q_1}{32\pi^2\eta^2}\frac{1}{\ell_c}\begin{pmatrix} \frac{16\pi}{21}a_1 \\ \frac{16\pi}{21}a_2 \\ \frac{176\pi}{105}a_3\end{pmatrix} = \frac{Q_1}{14\pi\eta^2}\frac{1}{\ell_c}\begin{pmatrix} \frac{1}{3}a_1 \\ \frac{1}{3}a_2 \\ \frac{11}{15}a_3\end{pmatrix}, \qquad \text{(B.3.18)}
\end{aligned}$$

and

$$\begin{aligned}
D(\boldsymbol{r}) =& \frac{1}{64\pi^2\eta^2}\int \frac{r'_\alpha r'_{\alpha'}}{r'^6}(1-3\cos^2\theta)^2 Q(\boldsymbol{r}+\boldsymbol{r}')d\boldsymbol{r}' \\
=& \frac{Q_0+Q_1\boldsymbol{a}\cdot\boldsymbol{r}}{64\pi^2\eta^2}\int \frac{r'_\alpha r'_{\alpha'}}{r'^6}(1-3\cos^2\theta)^2 d\boldsymbol{r}' + \frac{Q_1}{64\pi^2\eta^2}\int \frac{r'_\alpha r'_{\alpha'}}{r'^6}(1-3\cos^2\theta)^2\left(\boldsymbol{a}\cdot\boldsymbol{r}'\right)d\boldsymbol{r}' \\
=& \frac{Q_0+Q_1\boldsymbol{a}\cdot\boldsymbol{r}}{64\pi^2\eta^2}\int_0^{2\pi}\int_0^{\pi}\int_{\ell_c}^{\infty}\frac{r'^2\sin\theta}{r'^6}(1-3\cos^2\theta)^2 \\
&\qquad \times\begin{pmatrix} r'^2\sin^2\theta\cos^2\phi & r'^2\sin^2\theta\sin\phi\cos\phi & r'^2\sin\theta\cos\theta\cos\phi \\ r'^2\sin^2\theta\sin\phi\cos\phi & r'^2\sin^2\theta\sin^2\phi & r'^2\sin\theta\cos\theta\sin\phi \\ r'^2\sin\theta\cos\theta\cos\phi & r'^2\sin\theta\cos\theta\sin\phi & r'^2\cos^2\theta\end{pmatrix} dr'd\theta d\phi \\
&+ \frac{Q_1}{64\pi^2\eta^2}\int_0^{2\pi}\int_0^{\pi}\int_{\ell_c}^{\infty}\frac{r'^2\sin\theta}{r'^6}(1-3\cos^2\theta)^2 \\
&\qquad \times\left(a_1 r'\sin\theta\cos\phi + a_2 r'\sin\theta\sin\phi + a_3 r'\cos\theta\right)
\end{aligned}$$

$$
\times \begin{pmatrix} r'^2 \sin^2\theta\cos^2\phi & r'^2\sin^2\theta\sin\phi\cos\phi & r'^2\sin\theta\cos\theta\cos\phi \\ r'^2\sin^2\theta\sin\phi\cos\phi & r'^2\sin^2\theta\sin^2\phi & r'^2\sin\theta\cos\theta\sin\phi \\ r'^2\sin\theta\cos\theta\cos\phi & r'^2\sin\theta\cos\theta\sin\phi & r'^2\cos^2\theta \end{pmatrix} dr' d\theta d\phi
$$

$$
\begin{aligned}
=&\frac{Q_0 + Q_1 \boldsymbol{a}\cdot\boldsymbol{r}}{64\pi^2\eta^2}\int_0^{2\pi}\int_0^{\pi}\frac{1}{\ell_c}\sin\theta(1-3\cos^2\theta)^2 \\
&\times \begin{pmatrix} \sin^2\theta\cos^2\phi & \sin^2\theta\sin\phi\cos\phi & \sin\theta\cos\theta\cos\phi \\ \sin^2\theta\sin\phi\cos\phi & \sin^2\theta\sin^2\phi & \sin\theta\cos\theta\sin\phi \\ \sin\theta\cos\theta\cos\phi & \sin\theta\cos\theta\sin\phi & \cos^2\theta \end{pmatrix} d\theta d\phi \\
&+ \frac{Q_1}{64\pi^2\eta^2}\int_{\ell_c}^{\infty}\frac{1}{r'}\begin{pmatrix} 0 & 0 & 0 \\ 0 & 0 & 0 \\ 0 & 0 & 0 \end{pmatrix} dr' \\
=&\frac{Q_0 + Q_1 \boldsymbol{a}\cdot\boldsymbol{r}}{64\pi^2\eta^2}\frac{1}{\ell_c}\begin{pmatrix} \frac{16\pi}{21} & 0 & 0 \\ 0 & \frac{16\pi}{21} & 0 \\ 0 & 0 & \frac{176\pi}{105} \end{pmatrix} = \frac{Q(\boldsymbol{r})}{28\pi\eta^2}\frac{1}{\ell_c}\begin{pmatrix} \frac{1}{3} & 0 & 0 \\ 0 & \frac{1}{3} & 0 \\ 0 & 0 & \frac{11}{15} \end{pmatrix}.
\end{aligned} \tag{B.3.19}
$$

It is noted that V_α and $(\partial D_{\alpha\alpha'})/(\partial r_{\alpha'})$ with constant gradient of Q still satisfy the equation $V_\alpha = 2(\partial D_{\alpha\alpha'})/(\partial r_{\alpha'})$, which is the same as the result in Ref. [39].

$$
\frac{\partial D_{\alpha\alpha'}(\boldsymbol{r})}{\partial \boldsymbol{r}} = \frac{Q_1}{28\pi\eta^2}\frac{1}{\ell_c}\begin{pmatrix} \frac{1}{3} & 0 & 0 \\ 0 & \frac{1}{3} & 0 \\ 0 & 0 & \frac{11}{15} \end{pmatrix}\begin{pmatrix} a_1 \\ a_2 \\ a_3 \end{pmatrix} = \frac{Q_1}{28\pi\eta^2}\frac{1}{\ell_c}\begin{pmatrix} \frac{1}{3}a_1 \\ \frac{1}{3}a_2 \\ \frac{11}{15}a_3 \end{pmatrix}, \tag{B.3.20}
$$

$$
\boldsymbol{U} = \boldsymbol{V} - \frac{\partial D(\boldsymbol{r})}{\partial \boldsymbol{r}} = \frac{Q_1}{28\pi\eta^2}\frac{1}{\ell_c}\begin{pmatrix} \frac{1}{3}a_1 \\ \frac{1}{3}a_2 \\ \frac{11}{15}a_3 \end{pmatrix}. \tag{B.3.21}
$$

Thus Eqs. (B.3.18) and (B.3.19) are obtained.